THE INVOLVEMENT OF P38GAMMA MAPK IN PATHOLOGICAL CARDIAC HYPERTROPHY

Clark, James; Loonat, Aminah Ahmed

Awarding institution:
King's College London

THE INVOLVEMENT OF P38GAMMA MAPK IN PATHOLOGICAL CARDIAC HYPERTROPHY

Aminah Ahmed Loonat

A Thesis submitted for the degree of Doctor of Philosophy

2015

King's College London
Cardiovascular Division
Rayne Institute, BHF Centre
4th Floor, Lambeth Wing
St Thomas' Hospital
London, SE1 7EH

ABSTRACT

p38-mitogen activated protein kinases (p38-MAPKs) are stress activated serine/threonine kinases that are activated during several different cardiac pathologies. Classically, studies have focused solely on p38α signaling in the heart. However, there is also high cardiac expression of the p38γ isoform but little is known about its cardiac function. The aim of this study was to elucidate the signaling pathway of p38γ, with a particular focus on its role in the progression of pathological cardiac hypertrophy. Comparisons of cardiac function and structure of wild type (WT) and p38γ knock out (KO) mice, in response to abdominal aortic banding, found that KO mice developed less ventricular hypertrophy than their corresponding WT controls, and have preserved cardiac function. Basal p38γ myocardial staining was primarily localised at the membranes and throughout the cytoplasm. Following aortic constriction, nuclear staining of p38γ increased, but no accumulation of p38α was observed. This suggests that the two isoforms play distinct roles in the heart.

To elucidate its signaling pathway, we generated an analogue sensitive p38γ, which is mutated at a gatekeeper residue, to specifically track and identify its endogenous substrates in the myocardium. The mutation allows only the mutant kinase, but not WT kinases, to utilise analogues of ATP that are expanded at the N^6 position and contain a detectable tag on the γ-phosphate. Transfer of this tag to substrates allows subsequent isolation and identification. Furthermore, unlike other p38-MAPKs, p38γ contains a C-terminal PDZ domain interacting motif. We have utilised this motif in co pull-down assays to identify interacting proteins of p38γ in the heart. Using these techniques we have identified, amongst other substrates, LDB3 and calpastatin as novel substrates of p38γ and we have determined the residues that are targeted for phosphorylation. Lastly we have shown that phosphorylation of calpastatin reduces its efficiency as a calpain inhibitor *in vitro*, hence proposing a mechanism by which p38γ may mediate its pro-hypertrophic role.

LIST OF PUBLICATIONS

Abstracts

British Society for Cardiovascular Research, Reading, 2014

A Loonat, F Hunt, S H Choi, E D Martin, N T Hertz, R Levin, K M Shokat, A L Burlingame, M S Marber and J E Clark. Elucidating the role of p38γ in pathological cardiac hypertrophy. *Heart* (2014)

British Society for Cardiovascular Research, London, 2014

M Thomas, S Uddin, A Loonat, M Marber, J Clark. P38γ mitogen-activated protein kinase is a mediator of pathological cardiac hypertrophy. *Heart* (2014)

The Biomedical Basis of Elite Performance, London, 2012

K. D. Tilgner, A. Loonat, M. Marber, J. E. Clark. Ablation of p38γ-MAPK reduces cardiac remodelling following pressure overload. *Proc Physiol Soc* (2012)

ACKNOWLEDGEMENTS

This PhD has been a truly remarkable journey. I set out looking for growth and adventure. I have gained that and so much more. I have encountered many wonderful people along the way, who have helped immeasurably throughout this project. My appreciation begins where my journey began. Thank you to my first supervisor, Dr James Clark, for giving me this opportunity and for your continuous guidance and support throughout. I would also like to extend my gratitude to my second supervisor, Prof. Michael Marber. Thank you for welcoming me into your group and for keenly taking an interest in my project. I feel extremely fortunate to have received supervision from two outstanding scientists.

I have also had the pleasure of learning from many wonderful and knowledgeable mentors in the lab: Dr Denise Martin, Dr Asvi Francois, Dr Rekha Bassi, Dr Emma Smith, Dr Raymond Tyther and Dr Gian Felice de Nicola. Thank you for your advice, guidance, and patience and for equipping me with the necessary molecular biology and biochemistry skills to undertake this project. Thank you again to Dr James Clark, the physiology guru, for sharing his expertise and his resources, in the form of project students, who have contributed so much to this research.

Special thanks go to all of my friends at the Rayne Institute, without whom this journey would have been somewhat tedious. I am thankful for the Scooter café sessions. The giggles, gossip and endless (but never pointless) discussions maintained my sanity on those trying days. Thank you to 'Jaloos' for much amusement and words of wisdom shared over copious cups of chai. In particular I would like to thank Pelin Arabacilar. I am so glad that we were able to undertake this journey together. Your energy and enthusiasm are infectious. Even through challenging times, you take everything in your stride. I have learnt so much from you, I admire you and I am so proud of you.

Last but not least, I would like to thank my amazing family. M.Ali, my hero! You took me under your wing when I moved to London and for that I am so thankful. Thank you to my siblings for your love, continuous support and encouragement. Thank you also to all my little nephews and nieces (10 at the current count). Their sweet little voices on the other end of the line on a Friday evening, asking me if I'm coming home, always made me smile, even after a disappointing week. My greatest appreciation is for my Mum and Dad. Thank you for your unconditional love. Your sacrifices, affection, kindness and spirituality underlie my achievements. I am so grateful for everything that you do.

TABLE OF CONTENTS

LIST OF FIGURES

LIST OF TABLES

Abbreviations

AKAP2	A-kinase associated protein 2
AMC	7-Amino-4-Methylcoumarin
Amp	Ampicillin
AngII	Angiotensin II
ANP	Atrial natriuretic peptide
AS	Analogue sensitive
ASK1	Apoptosis signal-regulating kinase 1
ATF2	Activating transcription factor 2
ATP	Adenosine triphosphate
BNP	B-type natriuretic peptide
BSA	Bovine serum albumin
BW	Body weight
CaMKII	Calcium/calmodulin kinase II
cAMP	3'-5'-cyclic adenosine monophosphate
cDNA	Complimentary DNA
cGMP	Cyclic guanosine monophosphate
CHF	Congestive heart failure
CID	Collision induced dissociation
CS	Calpastatin

CT-1	Cardiotropin-1
DAG	Diacylglycerol
DAPC	Dystrophin-associated protein complex
DAPI	4',6-diamidino-2-phenylindole
DLG1	Drosophila disc large tumour suppressor
DMEM	Dulbecco's modified eagle medium
DMSO	Dimethyl sulfoxide
DNA	Deoxyribonucleic acid
dNTP	Deoxynucleotide
DTT	Dithiothreitol
ECG	Electrocardiogram
ECL	Enhanced chemiluminescence
ECM	Extracellular matrix
EDTA	Ethylenediaminetetraacetic acid
EGTA	Ethylene glycol tetraacetic acid
EKV	ECG-gated Kilo-Hertz visualisation
ERK	Extracellular signal regulated kinase
ET-1	Endothelin I
ETD	Electron transfer dissociation
FAC	Focal adhesion complex
FAC	Fractional area change

FBS	Foetal bovine serum
GK	Guanylate kinase
GKAP	Guanylate kinase-associated protein
GPCR	G-protein coupled receptors
GST	Glutathione S-transferase
GTP	Guanosine-5'-triphosphate
HDAC	Histone deacetylases
HEK	Human embryonic kidney
HEPES	4-(2-hydroxyethyl)-1-piperazineethanesulfonic acid
HPLC	High performance liquid chromatography
HW	Heart weight
IEC	Ion exchange chromatography
IGF-1	Insulin like growth factor-1
IL-6	Interleukin 6
IPTG	Isopropyl β-D-1-thiogalactopyranoside
IVK	In vitro kinase assay
IκBα	Inhibitor of nuclear factor-κB
JNK	c-Jun N-terminal kinase
KO	Knock out
LB	Luria-Bertani
LC	Liquid chromatography

LC-MS	Liquid chromatography-Mass spectrometry
LDB3	Lim domain binding protein 3
LDS	Lithium dodecyl sulfate
LIF	Leukaemia inhibitory factor
LIM	Acronym: Lin11, Isl-1 and Mec-3
LTCC	L-type calcium channel
LV	Left ventricle
LVID;s	LV internal dimension at systole
MAP4	Microtubule associated protein 4
MAPK	Mitogen activated protein kinase
MBP	Myelin basic protein
MEK	Mitogen-activated protein kinase kinase
MI	Myocardial infarction
MMP	Metalloproteinases
mRNA	Messenger ribonucleic acid
NADH	Nicotinamide adenine dinucleotide (reduced)
NFAT	Nuclear factor of activated T-cells
NF-κB	Nuclear factor-κB
Ni-NTA	Nickel-nitriloacetoic acid
NMDA	N-methyl-D-aspartate
nNOS	Neuronal nitric oxide synthase

NO	Nitric oxide
NOS-1	Nitric oxide synthase-1
OCT	Optimal cutting temperature
ORF	Open reading frame
PBS	Phosphate buffered saline
PCR	Polymerase chain reaction
PDLIM5	PDZ and LIM domain 5
PDZ	Acronym: PSD-95, DLG1 and ZO-1
PEI	Polyethylenimine
PERE	Phenylephrine response element
PFD	Pirfenidone
PH	Pleckstrin homology
PIP2	Phosphatidylinositol 4,5-bisphosphate
PKA	Protein kinase A
PKC	Protein kinase C
PLC	Phospholipase C
PMCA	Plasma membrane calcium ATPase
PMSF	Phenylmethylsulfonyl fluoride
PNBM	p-Nitrobenzyl mesylate
PSD-95	Post synaptic density protein 95
PSF	Polypyrimidine tract-binding protein-associated splicing factor

PTPH1	Protein tyrosine phosphatase H1
PVDF	Polyvinylidene difluoride
RNA	Ribonucleic acid
SAP90	Synapse associated protein 90
SAP97	Synapse associated protein 97
SAPK	Stress activated protein kinase
SDS	Sodium dodecyl sulfate
SDS-PAGE	SDS polyacrylamide gel electrophoresis
SFM	Serum free media
SH3	Src homology 3
SOC	Super optimal broth with catabolite repression
SPEG	Striated muscle specific serine/threonine kinase
STZ	Streptozotocin
SU	Synthrophin unique
TAB1	TAK1 binding protein
TAE	Tris-Acetate-EDTA
TAK1	TGF-β activated protein kinase 1
TAO1/2	Thousand and one amino acid protein kinase 1/2
TBS	Tris buffered saline
TEV	Tobacco Etch Virus nuclear-inclusion-a endopeptidase
TFA	Trifluoroacetic acid

TGF-β	Transforming growth factor-β
UV	Ultraviolet
WGA	Wheat germ agglutinin
WT	Wild type
ZASP	Z-line alternatively spliced protein
Zfp260	Zinc finger protein 260
ZO-1	Zonula occludents-1
β-MHC	β-myosin heavy chain

1 INTRODUCTION

1.1 Heart Failure

Heart failure is defined as the inability of the heart to function as a pump to support the circulation in the normal physiological range. In the UK, around 800,000 people are estimated to suffer from heart failure (The National Heart Failure Audit 2012/2013). However with an ageing population and better treatments to manage the disease this number is only set to increase, resulting in the need for improved strategies to prevent the onset of disease.

The term ‘heart failure’ is actually an umbrella term used to describe the consequence of many different cardiac pathologies/diseases. It is therefore complex and encompasses the manifestation of many underlying conditions such as hypertension, ischaemia associated with coronary artery disease, valvular heart disease and cardiomyopathies. Whilst the cause of each condition is different, the heart responds to stress in a consistent manner, undergoing a process of remodelling, in an initial attempt to offset the stress and maintain cardiac output. This involves an increase in cardiac mass, cardiomyocyte hypertrophy and changes in left ventricular geometry. However, over time and with prolonged stress, cardiac remodelling becomes pathological. The heart becomes dilated and loses its elliptical shape. Thinning of the left ventricular wall, ventricular dilatation and increased stiffness ensue, causing diminished contractility and hindering the ability of the heart to pump efficiently. This predisposes the patient to progressive heart failure and/or to sudden dysrhythmic death.

Whilst we can visualise the changes in the shape, dimension and mass of the heart during the progression of disease, little is known about how these changes are implemented biochemically. Understanding the process of cardiac remodelling and the signalling pathways involved in its initiation are, therefore, key goals of scientific research. Insight into these pathways will hopefully yield

new therapeutic targets to prevent pathological remodelling and the subsequent mortality that occurs as a result of heart failure.

1.2 Cardiac Hypertrophy

Cardiac remodelling is often accompanied by the development of cardiac hypertrophy. Cardiac hypertrophy is characterised by an increase in the mass of the heart. As cardiomyocyte turnover is very low, the heart grows in size due to an increase of myocyte size (hypertrophy), rather than an increase in myocyte number (hyperplasia) (Soonpaa, Field 1994). Like the phases of remodelling, it begins as an adaptive response to reduce ventricular and septal wall stress and to maintain cardiac output. However with prolonged stimulus, it becomes pathological and contributes to the progression of heart failure. Whilst cardiac hypertrophy will be discussed here in the context of pathology, it must be noted that hypertrophy is not synonymous to pathological remodelling but can also be reversibly induced in physiological contexts such as exercise, pregnancy and postnatal growth (Hill, Olsen 2008). Unlike pathological hypertrophy, physiological hypertrophy appears to be a beneficial and reversible process. It maintains or increases cardiac function and does not feature the detrimental features of pathological hypertrophy such as fibrosis or apoptosis (Hill, Olson 2008).

Hypertrophy can occur by two different methods, depending on the type of stress applied to the myocardium. *Concentric* hypertrophy is an increase in left ventricular wall thickness and typically occurs in response to chronic pressure overload. At the cellular level, myocytes increase in size in width, due to addition of sarcomeres in parallel. In contrast *eccentric* hypertrophy is characterised by dilatation and thinning of the left ventricular wall and usually occurs due to volume overload. This occurs as myocytes increase in size longitudinally, by addition of sarcomeres in series (Mihl, Dassen & Kuipers 2008).

At the cellular level, myocytes display changes in gene expression and protein synthesis. Widely reported is the re-activation of the *foetal gene program*,

resulting in expression of genes that are expressed in development, but usually repressed in the adult heart (Kehat, Molkentin 2010, Barry, Davidson & Townsend 2008). This includes enhanced expression of genes encoding atrial natriuretic peptide (ANP) and b-type natriuretic peptide (BNP) (Gardner 2003), two commonly used markers of cardiac hypertrophy. These cellular changes are accompanied by accumulation of types I and III fibrillar collagen in the interstitium and death of cardiac myocytes by apoptosis or necrosis (Kehat, Molkentin 2010).

Biochemically, it is not clear exactly how hypertrophy occurs. It is evident that it is a multifaceted process that involves an integrated and orchestrated signalling response consisting of multiple signalling pathways. Numerous biochemical and neurohumoral stimuli have been reported to be involved such as catecholamines (noradrenaline and adrenaline), angiotensin II (AngII), endothelin I (ET-1), insulin like growth factor-1 (IGF-1) and cytokines such as interleukin 6 (IL-6), leukaemia inhibitory factor (LIF) and cardiotropin-1 (CT-1). Hypertrophic stimuli act on a variety of cell surface receptors that are G-protein coupled receptors (GPCR), receptors with intracellular tyrosine kinase domains or serine/threonine kinase domains and gp130-linked receptors (Heineke, Molkentin 2006).

Receptor stimulus leads to activation of intracellular signalling pathways that involve a plethora of signal transducers and converge on the nucleus to alter gene expression. For example, agonists such as noradrenaline, adrenaline, AngII and ET-1 bind to $G_{q/11}$ coupled receptors leading to activation of phospholipase C (PLC). PLC hydrolyses phosphatidylinositol 4,5-bisphosphate (PIP_2) to second messengers inositol 1,4,5-trisphosphate (IP_3) and diacyl glycerol (DAG). IP_3 binds to the IP_3 receptor located in the endoplasmic reticulum, causing an increase in the cytoplasmic calcium concentration. Rises in the intracellular concentration of calcium in turn mediates signalling via other pro-hypertrophic transducers such as calcineurin and Ca^{2+}/calmodulin kinase II (CaMKII) (Kehat, Molkentin 2010).

Elevated calcium concentration within the myocyte leads to direct activation of serine/threonine-specific phosphatase, calcineurin. Once activated calcineurin dephosphorylates nuclear factor of activated T-cells (NFAT), which is then able to translocate from the cytoplasm to the nucleus to mediate pro-hypertrophic gene transcription (Kehat, Molkentin 2010). CaMKII is also a calcium dependent pro-hypertrophic signalling transducer. Although its signalling pathway is not fully understood, it has been shown that its expression level and activity increases in a mouse model of cardiac hypertrophy (Colomer et al. 2003). CaMKII has many reported phosphorylation targets that have been implicated in cardiomyocyte hypertrophy such as transcription factors and histone deacetylases (HDACs) (Kreusser, Backs 2014).

Rises in intracellular calcium during hypertrophy and remodelling can alone, or coupled with oxidative stress, lead to upregulation and/or activation of proteolytic enzymes: metalloproteinases (MMPs), cathepsins, calpains and caspases. MMPs are a family of calcium and zinc-dependent proteases that have shown to be increasingly active during the progression of heart failure (Spinale et al. 2000). MMPs are implemented in pathological remodelling via degradation of extracellular matrix (ECM) components such as collagen and elastin (Wilson, Spinale 2001). Maintaining the integrity of the ECM is crucial for cardiac function. The collagen network provides structural support for myocytes and is essential in maintaining spatial alignment of myocytes and synchrony during the cardiac cycle (Muller, Dhalla 2012). Whilst the composition of the ECM is dynamically regulated by synthesis and degradation of its components, increased activity of MMPs contributes adversely during remodelling. Similarly cysteinyl cathepsin proteases have also been shown to be up regulated in hypertrophic and failing myocardium and like MMPs target ECM components, sharing several targets (Cheng et al. 2012). Therefore it is likely that MMPs and cathepsins cooperate activity to mediate ECM degradation during cardiac remodelling.

In contrast, calpains are calcium-dependent cysteine proteases that contribute to hypertrophy by targeting intracellular proteins. One such target of calpains is the serine/threonine-specific phosphatase, calcineurin. In addition to elevated

calcium, cleavage of the auto-inhibitory domain of calcineurin, by calpain, also results in activation of calcineurin (Burkard et al. 2005). As discussed above, this leads to the activation of pro-hypertrophic transcription factor, NFAT. The last family of proteolytic enzymes, caspases, are widely known for their role in apoptosis. Activation of caspases contributes to cardiac remodelling by executing programmed cell death of cardiomyocytes. Death of cardiomyocytes leads to replacement of myocytes with fibrous tissue, causing increased stiffness of the ventricle and diminished contractility (Dorn 2009).

Stimuli such as IGF-1 (acting via receptors with intracellular tyrosine kinase domain) and CT-1 (acting via the gp130-linked receptor) lead to activation of mitogen activated protein kinase (MAPK) signalling cascades. There are three types of MAPKs; p38, c-Jun N-terminal kinases (JNK) and extracellular-signal-regulated kinases (ERK). Whilst MAPKs are regarded as important regulators of cardiomyocyte growth, understanding of MAPK signalling in the context of cardiac hypertrophy is limited. ERK1 and ERK2 activation via the Ras-Raf1-MEK1/5 pathway is associated with the development of concentric hypertrophy without the hallmark features of pathological hypertrophy such as fibrosis or sudden death in MEK1 transgenic mice (Bueno et al. 2000). In contrast, activation of p38 and JNK has been reported to result in development of heart failure or cardiomyopathy in juveniles but without the development of cardiac hypertrophy (Heineke, Molkentin 2006, Wang 2007). This lends further credence to the idea that the development of hypertrophy involves the activation of multiple pathways, at different stages of the process, that are responsible for specific aspects of the multifaceted response we observe.

In addition to signalling events that are initiated by ligand mediated activation of receptors, signalling cascades described above can be initiated by direct detection of stretch by the cardiomyocyte. Studies have shown that stretch can be detected by integrins, cytoskeletal and sarcolemmal proteins (Ruwhof, van der Laarse 2000). Integrins are trans-membrane proteins that were thought to only mediate attachment of the intracellular cytoskeleton to the ECM. However, integrins are now recognised as ‘true’ receptors that sense stretch and transmit signals into the cell. Integrins cluster at focal adhesion sites on the cell surface

and recruit signalling proteins with their substrates into 'focal adhesion complexes' (FAC) to facilitate signal transduction. Signalling proteins associated with focal adhesion complexes include non-receptor kinases FAK and Src, cytoskeletal proteins and signal transducing molecules such as small GTPase Ras, ERKs and SAPKs. Furthermore, activation of integrins can also cause direct rearrangement of the actin cytoskeleton and this in turn may be a manner of transducing the stress signal to cells, resulting in activation of pathways involved in the hypertrophic response (Ruwhof, van der Laarse 2000, Barry, Davidson & Townsend 2008).

1.3 p38- MAPKs

p38-MAPKs are stress activated serine/threonine kinases that are activated during several different cardiac pathologies (Martin et al. 2012). The p38-MAPK family consists of four family members, p38α, p38β, p38γ and p38δ (see Table 1.1 for summary). Together they form one of the four main limbs of the classical MAPK family (other limbs of the family are ERK1/2, JNK and ERK3/4). The p38-MAPK isoforms have a high degree of sequence similarity; p38α and p38β are 75% identical and both are inhibited by pyridinyl imidazole molecules (such as SB203580). In contrast, p38γ and p38δ have a slightly lower degree of similarity to p38α (~60%), but share a higher degree of similarity to each other (~70%) and are not subject to inhibition by pyridinyl imidazole molecules (Kumar et al. 1997). The four isoforms also vary in terms of their tissue expression. Whilst p38α is ubiquitously expressed in most tissue types, the other p38 isoforms show more specific tissue expression. For instance, p38β is highly expressed in the brain, p38γ expression is highest in skeletal muscle and p38δ is highly expressed in the endocrine glands (Cuadrado, Nebreda 2010).

Table 1.1 The p38-MAPK isoforms

p38-MAPK isoform	Other names	Chromo-some	Amino acid length	Mw kDa	Identity to p38α	Expression
α	SAPK2α MAPK14	6p21.3-p21.2	360	38	100%	Ubiquitous
β	SAPK2β MAPK11	22q13.33	364	38	75%	Brain
γ	SAPK3 ERK6 MAPK12	22q13.33	367	46	62%	Skeletal muscle, Cardiac
δ	SAPK4 MAPK13	6p21.31	365	38	61%	Endocrine glands

All four isoforms of the p38 family are expressed in the myocardium, but p38α and p38γ have been reported to be the two most abundantly expressed isoforms (Dingar et al. 2010). As the founding member of the p38-MAPK family and with its ubiquitous tissue expression pattern, p38α is the most widely studied isoform of the family and studies on this kinase have greatly been aided by the use of pyridinyl imidazole inhibitor molecules. This is also true in the context of the heart and any functional roles of the other abundant isoform, p38γ, have been largely overlooked.

Recent work from our laboratory has investigated the role of the different p38-MAPK isoforms in the murine heart and has assessed the functional contribution of each isoform in the context of clinically relevant stimuli such as myocardial ischaemia and ischaemia-reperfusion injury. Our data shows a high degree of p38-MAPK activation in response to 10 min of ischaemia in both wild type (WT) and p38γ/δ knock out (KO) mice hearts compared to controls, but no difference in the level of phosphorylation between WT and KO mice. When stimulated with 30 min of ischaemia followed by 120 min of reperfusion, the same response was observed in both WT and KO mice (Sarafraz N. PhD Thesis, University of London). Whilst there was a significant reduction in left ventricular developed pressure (a surrogate of myocardial function) in both groups, there were no significant differences in the functional parameters measured between the KO and WT mice. As both cohorts responded to the

stimuli to the same extent, it suggests that the involvement of p38γ and p38δ isoforms, at least in the acute response of these stimuli is unlikely. It is well established that the isoform activated during these stimuli is p38α (Saurin et al. 2000, Martin et al. 2001, Tanno et al. 2003, Sicard et al. 2010). Examination of the roles of the p38γ and p38δ isoforms in non-cardiac tissue (described below in detail for p38γ), may hint at their function in the myocardium.

1.3.1 Structural features of p38-MAPKs

Structurally all MAPKs, including p38-MAPKs are similar. They all have a bi-lobal structure formed from a small amino-terminal lobe consisting of mainly β strands and a larger carboxy-terminal lobe formed by α helices, connected by a hinging residue. There is a deep cleft situated at the interface of the two domains and this forms the catalytic site and the binding site for ATP and Mg^{2+}. The conserved Thr-X-Tyr dual phosphorylation MAPK activation motif (TXY, X= glycine in p38-MAPKs, proline in ERKs and glutamic acid in JNKs) is located within the carboxy-terminal lobe. In the non-phosphorylated, inactive conformation, the activation loop is thought to reside in the peptide-binding channel that lies in a cleft between the N' and C' lobes of the kinase. During activation, the activation loop becomes dually phosphorylated and global conformational changes take place that relieve steric inhibition of the kinase, causing rearrangement of the activation loop out of the peptide binding cleft and allowing access to substrates for catalysis to occur. See Figure 1.1 for a cartoon representation of the structure of p38γ.

Despite their similarity there are key structural differences between the different p38-MAPK isoforms. One such difference between the p38α/β and p38γ/δ isoforms dictates sensitivity to pyridinyl imidazole molecules. Pyridinyl imidazole molecules such as SB203580 bind at the highly conserved ATP binding pocket of p38-MAPKs (Young et al. 1997) yet, remarkably, the molecules are able to display isoform selectivity. The selectivity of SB203580 to inhibit only the α/β isoforms, but not the γ/δ isoforms, is due to a difference in a single amino acid residue in the peptide sequence of the ATP binding pocket.

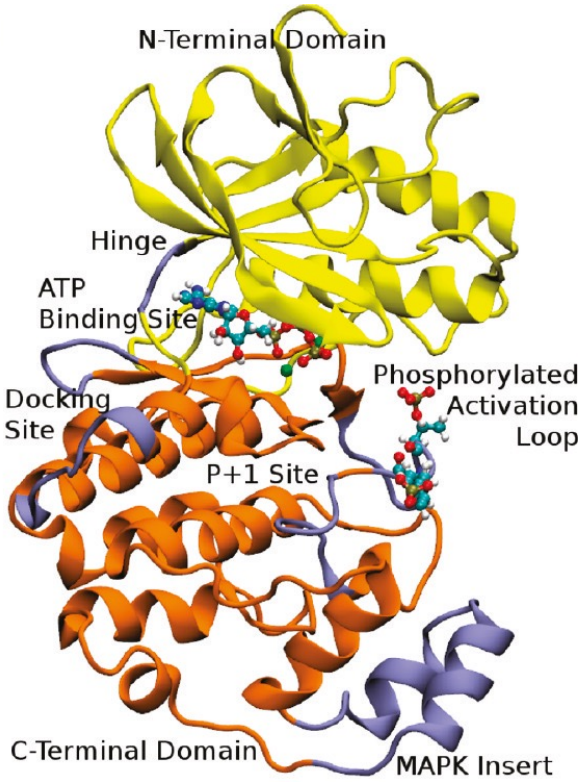

Figure 1.1 Structure of activated p38γ

Cartoon representation of the structure of activated p38γ. ATP and phosphorylated residues are shown in ball and stick representation. Yellow depicts the N- terminal domain and orange depicts the C-terminal domain. Purple regions highlight important motifs in the structure and are annotated on the diagram. Taken from Limardo et al. 2011.

A change from threonine in p38α/β to a bulkier methionine in p38γ/δ renders the p38γ/δ isoforms insensitive to SB203580. Conversely, mutation of methionine to a smaller amino acid in these typically insensitive isoforms can alter their sensitivity to these compounds (Eyers et al. 1998). The use of pyridinyl imidazole molecules has greatly aided research into elucidating the functional role of the p38α/β isoforms. The diaryl urea compound BIRB 796 is able to inhibit all p38-MAPK isoforms, but more potently inhibits the p38α/β isoforms. It exerts its action by stabilising the kinase in an inactive conformation that is unable to bind ATP (Bain et al. 2007). A lack of specific inhibitors of p38γ/δ has, in part, hindered research into the function of these isoforms.

1.3.1.1 A unique structural feature of p38γ

A key structural difference and a feature unique only to the p38γ isoform is the PDZ consensus sequence in the carboxy-terminal of this kinase (Hasegawa et al. 1999). PDZ domains are protein-protein interaction domains named after the first three proteins in which these domains were identified: **p**ost-synaptic density protein 95 (**P**SD-95), **D**rosophilia disc large tumour suppressor (**D**lg1) and **z**onula occludens-1 (**Z**O-1). The short amino acid sequence KETAL in the C' of p38γ can directly dock to PDZ domains of proteins and therefore adds a unique dimension to p38γ signalling. Several studies have utilised the presence of this sequence as 'bait' to search for potential p38γ substrates or interacting partners. Examples of proteins that have been found to interact with p38γ in this manner include α1-syntrophin (Hasegawa et al. 1999), PSD-95 (Sabio et al. 2004), synapse associated protein 97 (SAP97) (Sabio et al. 2005) and protein tyrosine phosphatase H1 (PTPH1) (Hou et al. 2010).

1.3.2 Signal transduction

Activation of p38-MAPKs occurs via the classical three-tiered MAPK signalling cascade (Figure 1.2) and involves sequential activation of two upstream kinases. In response to stress stimuli such as environmental stresses and inflammatory cytokines, p38-MAPKs become dually phosphorylated by upstream dual specificity MAPK kinases (MAPKK/MKK/MEK) at the TGY motif in their activation loop as described previously. Once activated p38-MAPKs phosphorylate target proteins at serine/threonine residues that are followed by a proline residue in the sequence.

There are several MKKs that are responsible for the phosphorylation of the different MAPKs. The specificity of activation of MAPKs by MKKs is determined by interactions between the N-terminal region of the MKK, docking sites present on the MAPK and by the structure of the MAPK activation loop that contains the TGY dual phosphorylation activation motif (Cuenda, Rousseau 2007). MKK6 is able to phosphorylate all p38-MAPK isoforms and MKK3 phosphorylates all p38-MAPK isoforms excluding p38β. Whilst MKK3 and MKK6 are specific activators of p38 type MAPKs, other MKKs such as MKK4 can phosphorylate

both p38α and JNK MAPKs and this may allow cross talk between different signalling pathways (Cuadrado, Nebreda 2010).

In order to dual phosphorylate and activate p38-MAPKs, MKKs must themselves become phosphorylated and activated. This is the responsibility of upstream MAPKK kinases (MAPKKK/MEKK), which phosphorylate MKKs on two conserved serine and threonine residues in their activation loops. The cellular pathway leading to p38-MAPK activation and the different kinases involved in p38-MAPK activation, under different stress conditions, is not yet fully understood. Numerous MAPKKKs have been implicated in activation of the p38-MAPK pathway and these include ASK1, TAK1, TAO1/2 and MEKK3/4. The magnitude and duration of p38-MAPK signalling depends on the activity of protein phosphatases that reverse the dual phosphorylation on the TGY motif to return the kinase to the inactive state. For p38α at least, several different types of phosphatases appear to be involved (protein phosphatases, protein tyrosine phosphatases and dual specificity phosphatases). Less is known regarding the regulation of the other p38 MAPK isoforms (Cuadrado, Nebreda 2010).

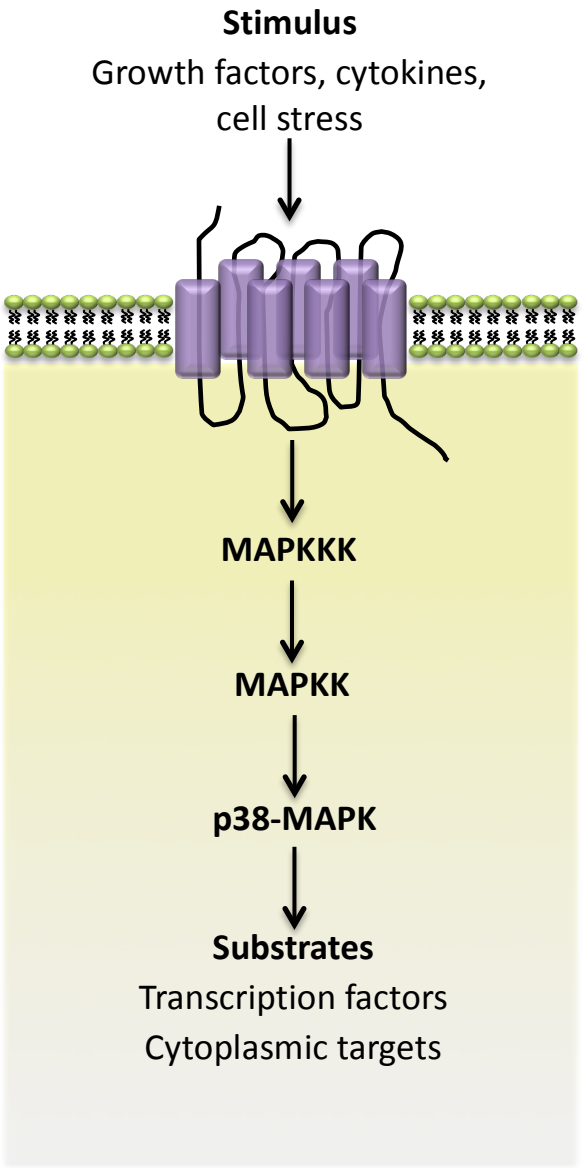

Figure 1.2 p38-MAPK signalling pathway

Activation of p38-MAPK consists of sequential activation of a series of protein kinases.

1.4 p38γ isoform

The p38γ isoform was independently identified in 1996 by three different groups as a serine/threonine kinase found to be highly enriched in skeletal muscle (Lechner et al. 1996, Li et al. 1996, Mertens, Craxton & Goedert 1996). However subsequent analysis of the isoform found that it is also highly and preferentially expressed in the myocardium (Dingar et al. 2010). Despite this, little is currently known about the role, if any, this isoform plays in the heart and studies have largely focused on the role of p38γ in skeletal muscle. Below is a brief outline of some of the physiological and pathophysiological roles that have been described for this isoform so far.

1.4.1 Physiological and pathophysiological roles of p38γ

1.4.1.1 Myoblast differentiation

A role of p38γ in skeletal muscle was first proposed in the conversion of myoblasts to differentiated myotubes (Lechner et al. 1996). p38γ mRNA expression was found to be induced in differentiated C2C12 cells in comparison to their undifferentiated counterparts, suggesting a role of p38γ in myogenic differentiation. Furthermore, when C2C12 myoblasts were transfected with WT p38γ, there was a significant enhancement in the rate of multinucleate myotube formation, in comparison to control-transfected cells. In addition, cells transfected with a dominant negative form of the enzyme showed no formation of myotubes and instead maintained the cells in a proliferative state.

The proposed role of p38γ in myoblast differentiation is further supported in subsequent studies. In both C2C12 and So18 muscle cells, p38γ mRNA was largely detected only in the differentiation phase of the muscle cells and very minimally at the myoblast stage. This was also reflected at the protein level, as the level of p38γ protein was found to be increased during differentiation (Tortorella, Lin & Pilch 2003). Furthermore, an examination of the roles of all p38 MAPK isoforms in myogenesis found that whilst myoblasts lacking p38α (but not those lacking p38β or p38δ) are unable to differentiate and form multinucleated myotubes, p38γ-deficient myoblasts exhibit an attenuated fusion

capacity (Perdiguero et al. 2007). This suggests a crucial role of p38γ in mediating muscle growth and development.

1.4.1.2 Other skeletal muscle roles

Several other aspects of p38γ signalling in skeletal muscle have also been examined. For example, an increase in p38γ phosphorylation and activity has been observed immediately after prolonged and strenuous running exercise in human subjects (Boppart et al. 2000), developmental regulation of p38γ expression has been observed in rat skeletal muscle (Tortorella, Lin & Pilch 2003), p38γ has been shown to been involved in regulation of GLUT1 expression and basal glucose uptake in adult skeletal muscle (Ho et al. 2004) and its activity has been shown to be involved in maintenance of slow skeletal muscle size (Foster, Tidball & Wang 2012). However, despite the range of studies examining the role of this isoform in skeletal muscle, key components of its signalling paradigm remain to be determined.

1.4.1.3 Oncogenesis

In addition to myoblast differentiation, another cell transformation process p38γ is implicated in is malignant transformation. Several studies have examined the role of p38γ in Ras mediated cell transformation and oncogenesis. The Ras family of proteins are critical in the control of normal and malignant cell growth. Mutations in *ras* genes that cause constitutively active Ras are commonly found to be the cause of many human cancers. Interestingly, a phosphorylation independent role of p38γ has been implicated in K-Ras malignant transformation. p38γ protein expression was found to be elevated in Ras transformed cells with no associated increase in p38γ phosphorylation (Tang et al. 2005). It has been proposed that the carboxy-terminal PDZ interacting motif of p38γ mediates its role in Ras transformation as C terminal truncated mutants of the kinase were unable to increase Ras transformation (Hou et al. 2010). Additionally, silencing of p38γ expression led to reversal of the morphological transformation and moreover, increased expression of p38γ was found in human tumour tissues, in comparison to matched normal tissues (Hou et al.

2010). This suggests a significant role of p38γ in oncogenesis and whilst the molecular mechanism remains to be fully elucidated, it is evident that a non-kinase role of p38γ is key to its pro-oncogenic activity.

1.4.1.4 Tumour suppression

In contrast to its pro-oncogenic role, tumour suppressive roles of p38γ have also been described. p38γ has been implicated in tumour suppression by mediating oncogene induced senescence (Kwong et al. 2009). Oncogene induced senescence is a defence mechanism against tumour development that is triggered in response to activation of oncogenes such as *ras* and is a common phenomenon that has been detected *in vivo*. A study of the role of the different p38 MAPK isoforms showed that p38α and p38γ mediated senescence via different molecular mechanisms. p38γ contributed to senescence by increasing the transcriptional activity of an inhibitor of cell proliferation, p53, by phosphorylating it at Ser^{33} and p38α mediated senescence by increasing the expression of $p16^{INK4A}$, a key effector of senescence. This further adds to the role of p38γ in regulation of cell processes and cell fate decisions and also highlights differential regulation mechanisms of the two p38 MAPK isoforms.

1.4.1.5 Cytoskeleton regulation

The PDZ interacting motif of p38γ has been shown to be involved in regulation of the cell cytoskeleton. Under osmotic stress conditions p38γ undergoes activation, resulting in the phosphorylation of SAP97/hDlg in HEK293 cells (Sabio et al. 2005). The phosphorylation of SAP97 was dependent on the interaction of the carboxy-terminal of p38γ with two PDZ domains of SAP97. SAP97 is a scaffold protein that forms multi-protein complexes to facilitate signal transduction. One such complex formed is with guanylate kinase-associated protein (GKAP), which localises SAP97 to the cytoskeleton. When SAP97 is phosphorylated by p38γ, it dissociates from GKAP and is released from the cell cytoskeleton. Whilst the significance of this dissociation is unclear, it is proposed that it may regulate the morphology of cells as an adaptive mechanism to changes in the environment such as osmotic stress.

1.4.1.6 mRNA processing and gene transcription

Further work into the regulation of hDlg (SAP97) by p38γ suggests that p38γ may play a role in regulation of mRNA processing and gene transcription (Sabio et al. 2010). In addition to forming protein complexes with cytoskeletal elements, under resting conditions hDlg has been shown to form protein complexes in the nucleus and interacts with nucleic acid binding proteins polypyrimidine tract-binding protein-associated splicing factor (PSF) and a related protein, $p54^{nrb}$. Unlike regulation of the hDlg-GKAP complex by phosphorylation following osmotic stress, p38γ regulates hDlg-PSF interaction via a kinase independent mechanism. Cell exposure to osmotic stress causes dissociation of hDlg-PSF and dissociation of the complex from RNA. Interestingly this dissociation event does not occur in cells lacking p38γ but was still observed in cells expressing inactive p38γ. Although the full details of the mechanism by which p38γ regulates hDlg-PSF complex dissociation are not fully understood, it is thought that p38γ accumulation in the nucleus after osmotic shock causes dissociation of the complex by competing for the same PDZ binding site as PSF on hDlg. This is supported by the observation that, under stress conditions, hDlg-PSF dissociation increases and hDlg-p38γ associations increase (Sabio et al. 2010). The findings of these studies demonstrates the critical role of the carboxy-terminal PDZ binding domain of p38γ in allowing it fulfil its regulatory roles.

1.4.2 Cardiac functions of p38γ

The cardiac functions of p38γ have yet to be elucidated. Initial characterisation studies of cardiac p38γ confirmed protein expression of p38γ in murine skeletal muscle but also found significant and restricted expression in the heart, lung, thymus and testes (Court et al. 2002 and Sarafraz N. PhD Thesis, University of London). Furthermore expression is conserved across species but not up-regulated in disease as analysis of normal and diseased hearts of different species (human, mouse, rat, dog and pig) shows constant expression of p38γ. Similarly, stimulation with hypertrophic agents of rat neonatal cardiac myocytes did not alter the expression of p38γ. However, immunofluorescence of

unstimulated myocytes found the pattern of p38γ staining to be distinct to that that of p38α. Whilst p38α staining was observed all throughout the cell, p38γ staining showed a more punctate pattern, only in the cell cytoplasm (Court et al. 2002), therefore reflecting a specialised role of p38γ in the myocardium.

A further study examining the roles of the different p38-MAPK isoforms also supports this notion and confirms the findings described above. For example, evaluation of mRNA levels of each p38-MAPK isoform shows that p38γ mRNA levels are comparable to those of p38α and this was also reflected at the protein level (Dingar et al. 2010 and Sarafraz N. PhD Thesis, University of London). More interestingly, the study also examined the effects of chronic pressure overload on the expression, activation and cellular location of different p38-MAPK isoforms. Whilst chronic pressure overload caused some changes in mRNA levels of the different isoforms this was not reflected at the protein level within the time frame studied. An increase in the phosphorylation signal of p38 was observed, which peaked at 3 days after overload and remained elevated in comparison to controls. Lastly, examination of the cellular localisation of p38α and p38γ, in hearts of pressure overload subjected mice, revealed an increase in the nuclear staining of p38γ but no nuclear accumulation of p38α following transverse aortic constriction (Dingar et al. 2010). Again, the differential localisation of the two dominant isoforms in the heart, suggests a differential response of the two isoforms. It is likely that they mediate their effects via different pathways and targets within the cell and therefore promote different functional effects.

Preliminary data from our lab obtained from WT mice and double knock out mice lacking the p38γ and p38δ isoforms (p38γ/$\delta^{-/-}$) also supports a role of p38γ in the development of pressure overload cardiac hypertrophy and dysfunction. Following abdominal aortic banding, p38γ/$\delta^{-/-}$ mice show markedly reduced cardiac dysfunction and develop less left ventricular hypertrophy, in comparison to their corresponding WT controls (Tilgner et al. 2012). Although it is difficult to attribute this phenotype specifically to the p38γ isoform, as the mice are double knock out, the phenotype observed is most likely to be as a result of p38γ knock down. This is because previous studies are in agreement that p38α and p38γ

are the two abundant isoforms in the myocardium, whilst the abundance of p38β and p38δ isoforms is relatively low. This, taken together with published data regarding the role of p38γ in the heart and the role it plays in other tissues, forms the basis for our hypothesis that p38γ may be crucially involved in transformation signalling processes within the heart during hypertrophy and remodelling.

1.5 Elucidating the signalling pathway of p38γ in the heart

An obvious starting point for elucidating the signalling pathway of p38γ is to examine substrates of the kinase in the heart. Unfortunately it is a difficult task to specifically attribute phosphorylation of a residue of a substrate to a given kinase. Despite the variety of kinases available within a cell, all kinases mediate phosphorylation via the same mechanism: by transfer of the γ-phosphate of ATP to a serine, threonine or tyrosine residue. Therefore it is not surprising that there is a high degree of homology in the structure and active site of most kinases. In turn this translates to a lack of kinase specific inhibitors that are available, particularly within a kinase family.

p38-MAPK isoforms are activated by an overlapping array of stimuli and the upstream signalling network that leads to kinase activation is not linear and segregated for each family member, further complicating this task. Looking downstream of the kinase also offers little ability to differentiate, as all members of the kinase family phosphorylate their substrates on a serine or threonine residue followed by a proline residue. For p38γ, the carboxy-terminal PDZ domain interacting sequence has aided the search for substrates and many studies have identified substrates of the kinase by an initial search for interacting proteins of the kinase (Table 1.2 summarises reported substrates of p38γ). However it is likely that there are substrates of p38γ that are not PDZ mediated. Fortunately, recent progress in scientific methodologies and the development of a powerful chemical genetic approach has made it possible to identify novel substrates of kinases in a specific manner.

Table 1.2 p38γ substrates

Substrate	KETAL-PDZ interaction?	Reference
MBP	None reported	Lechner et al. 1996
Tau	None reported	Goedert et al. 1997
ATF2	None reported	Cuenda et al. 1997
α1-syntrophin	Interaction of carboxy-terminal KETAL sequence of p38γ and PDZ domain of α1-syntrophin a prerequisite for phosphorylation	Hasegawa et al. 1999
Sab	Phosphorylation of Sab not dependent on the carboxy-terminal KETAL sequence of p38γ but dependent on the KIM1 sequence in Sab	Court et al. 2004
SAP90/PSD-95	Interaction of carboxy-terminal KETAL sequence of p38γ and PDZ domain of SAP90/PSD-95 a prerequisite for phosphorylation	Sabio et al. 2004
SAP97/hDlg	Interaction of carboxy-terminal KETAL sequence of p38γ and PDZ domain of SAP97/hDlg a prerequisite for phosphorylation	Sabio et al. 2005
MyoD	None reported	Gillespie et al. 2009
p53	None reported	Kwong et al. 2009
Topoisomerase IIα	None reported	Qi et al. 2011
PTPH1	Interaction of carboxy-terminal KETAL sequence of p38γ and PDZ domain of PTPH1 a prerequisite for phosphorylation	Hou et al. 2012

1.5.1 A chemical genetic approach for finding substrates of p38γ

A unique method that allows individual kinase substrates to be traced amongst cellular components has been developed by Shokat et al. (Figure 1.3). Specific kinase-substrate identification firstly involves the generation of 'analogue sensitive' (AS) versions of kinases that can utilise ATP analogues to transfer labelled phosphates to their target proteins. For the generation of such kinases, the kinase of interest is mutated at a 'gatekeeper' residue in the ATP binding pocket of the kinase. Mutation of the bulky gatekeeper residue to an amino acid with a smaller side chain, such as alanine or glycine, yields an enlarged ATP binding pocket by opening up a small hydrophobic pocket, usually shielded by the gatekeeper residue. As a result, the modified kinase is able to utilise analogues of ATP that are expanded in the corresponding N^6 position, whilst endogenous wild type (WT) kinases cannot. This method was first demonstrated in the modification of V-Src (Shah et al. 1997) and has since been successfully applied to several kinases and resulted in the successful identification of their substrates (Elphick et al. 2007). Importantly as the gatekeeper residue is buried deep within the ATP binding site, it is far away from the regions of the kinase that are involved in substrate-regulatory interactions and the AS kinases exhibit the same protein target specificity as WT kinases. Additionally some AS kinases have been shown to be catalytically efficient in using ATP analogues to phosphorylate their substrates, at a rate similar to WT kinase utilisation of ATP (Shah et al. 1997, Allen et al. 2007).

For specific substrate identification a further modification to the ATP analogue is required. A label can be introduced into the γ-phosphate of the ATP analogue to track phosphorylation of substrates. One such modification is substitution of a thiol group in place of the hydroxyl in the γ-phosphate of the ATP analogue. The introduction of this modification is advantageous over the use of other tracking modifications such as radiolabelling, as the resulting thiophosphorylated protein is resistant to dephosphorylation by phosphatases and therefore stabilises the labelled substrate. Once thiophosphorylation has occurred, the thiophosphate is converted into an affinity handle to allow detection, separation and subsequent identification of the substrate. This is achieved by alkylation of the

thiophosphate with *p*-Nitrobenzyl mesylate (PNBM) and yields thiophosphate esters, which can specifically be detected and recognised by thiophosphate ester antibodies (Allen et al. 2007, Allen, Lazerwith & Shokat 2005).

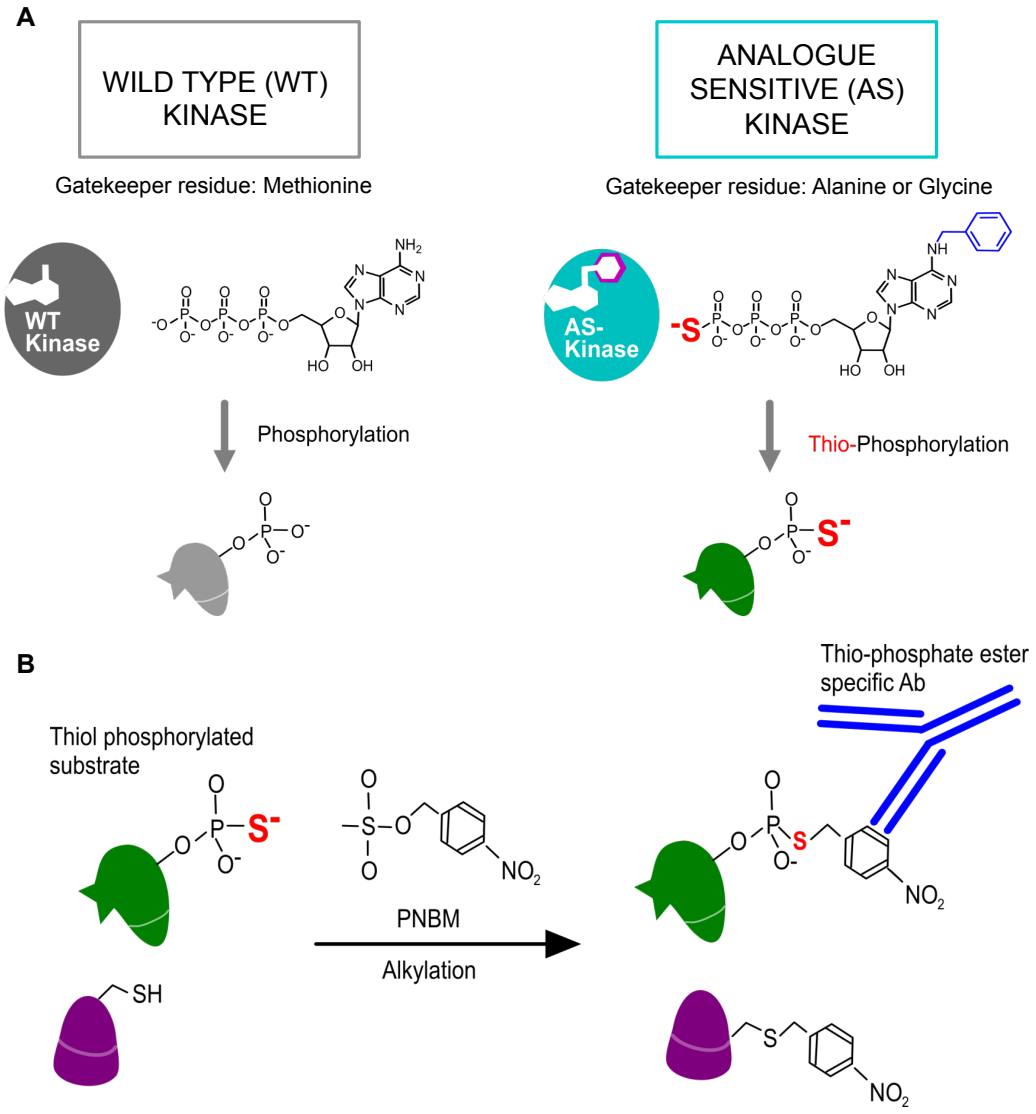

Figure 1.3 Shokat methodology for identification of kinase substrates

A, AS kinases are generated by a gatekeeper mutation to an amino acid with a small side chain such as alanine or glycine. This results in larger active site (in purple) that can accommodate enlarged ATP analogues (enlargement in blue) at the corresponding position. ATP analogues are also modified at the γ-phosphate to contain a thiol group. As a result, substrates undergo thiophosphorylation. ***B,*** Alkylation of thiophosphorylated substrates by PNBM results in thiophosphate esters, which are specifically detected by a commercially available antibody. The antibody does not recognise thioethers, which result from alkylation of free thiols. Images adapted by Dr James Clark (King's College London) from Blethrow et al. 2008 and Epitomics.com.

1.6 Aims of the project

Given the findings from the preliminary experiments conducted in our laboratory, the aims of this project are:

- To identify the endogenous substrates of the p38γ isoform in the myocardium.
- To identify any interacting proteins of p38γ via its carboxy-terminal PDZ interacting domain in the heart.
- To elucidate the signalling pathway in which p38γ is integrated in the heart.
- To determine the involvement of p38γ in the development of pathological cardiac hypertrophy.

1.7 Hypothesis

It is hypothesised that the p38γ isoform is pro-hypertrophic and that its signalling in the myocardium contributes to the development of pathological cardiac hypertrophy.

2 MATERIALS AND METHODS

Methodology relevant to more than one results chapter is provided here. Additional specific methodology is also provided in relevant results chapters.

All analytic-grade laboratory reagents were purchased from Sigma-Aldrich Chemical Co. (Poole, UK) unless otherwise stated.

2.1 Human Embryonic Kidney cell culture

Human embryonic kidney (HEK) cells were grown in culture for overexpression of various proteins. Cell lysates, containing overexpressed protein, were directly used in *in vitro* kinase assays or used to purify recombinant proteins.

2.1.1 Adherent HEK293 cells

HEK293 (American Type Culture Collection, Manassas, VA USA) were grown in Dulbecco's Modified Eagle Medium (DMEM) (PAA Laboratories) containing L-glutamine (584 mg/l) and supplemented with 10% (v/v) foetal bovine serum (FBS) (PAA Laboratories) and antibiotics (1% v/v streptomycin/penicillin) (PAA Laboratories). Cells were grown in a humidified 5% CO_2 incubator and maintained at 37°C. Once visually assessed to be 80% confluent, flasks of cells were washed twice with phosphate buffered saline (PBS) and harvested with 0.25% (w/v) trypsin, 0.02% (w/v) EDTA. Cells were centrifuged (390 x g for 3 min) and re-suspended into a suitable volume of fresh medium. For experiments, cells were seeded on to multi-well plates in medium composed as above.

2.1.1.1 Adherent HEK293 cell transfection

Cells were considered ready for transfection when 50- 80% confluent. For DNA transfection of cells, media in multiwell plates was replaced with serum free medium (SFM) (PAA Laboratories) with antibiotics (1% v/v streptomycin/penicillin) prior to transfection. For each well to be transfected, 1

µg of DNA was pre-incubated with 100 µL of Optimem (Gibco) and 2 µl of Turbofect (Thermo Scientific) in 1.5 mL microcentrifuge tubes at room temperature for 20 min. After incubation, Optimem up to 1 mL was added to each tube. Media was aspirated from wells and cells were washed with PBS. The DNA-Optimem mixtures were then added to corresponding wells in a drop wise fashion. Cells were then incubated in a humidified 5% CO_2 incubator and maintained at 37°C for 24 h. The following day cells were harvested as described below or used for further experimentation.

2.1.2 Suspension HEK cells

FreeStyle™ 293-F cells (Life Technologies) were grown in FreeStyle™ 293 expression medium (Life Technologies) containing Glutamax™-I. Cells were grown on an orbital shaker platform (135 rpm) in a humidified 8% CO_2 incubator and maintained at 37°C. Cells typically reached a density of 1 - 2 x 10^6 viable cells/mL every 2 -3 days at which point cells were passaged to a density of 2 x 10^5 viable cells/mL in fresh media following determination of cell viability and total count.

2.1.2.1 Suspension HEK cell transfection

For efficient transfection, cultures were stably maintained for at least 5 passages prior to transfection. In preparation for transfection, culture size of suspension HEK cells was scaled up to 300 mL. 24 h prior to transfection cells were seeded at a density of 1 x 10^6 viable cells/mL. On the day of transfection cells were counted to ensure that a density of 2 x 10^6 viable cells/mL and cell viability of 98% was achieved. Cells were collected by centrifugation at 3000 x g for 5 min and re-suspended in 150 mL of fresh FreeStyle™ 293 expression medium by briefly vortexing. Stock DNA prepared in media to give a final concentration of 3 µg/mL was pipetted into the cells and the flask was returned to the incubator for 5 min. Polyethylenimine (PEI) transfection reagent prepared in media to give a final concentration of 9 µg/mL was then added to the cells and cells were incubated for 24 h. The following day transfected cultures were diluted 1:1 with FreeStyle™ 293 expression medium. 2.2 mM valproic acid was

added to the cells and the flask returned to the incubator for a further 3 - 5 days. Cells were harvested in pre-weighed centrifuge tubes by centrifugation at 3000 x g for 5 min, media removed and washed in PBS. PBS was removed by centrifugation at 3000 x g for 5 min, pellets weighed and stored at -80°C.

2.1.3 Determining cell count and viability

To determine cell count and viability a 1:1 dilution of cells was prepared with Trypan Blue stain in a microcentrifuge tube. 10 µL of this mixture was mounted onto a haemocytometer (VWR) and viewed under a light microscope. The total number of cells and dead cells within a grid of the cytometer were counted and cell count and viability determined.

2.2 Cell sample preparation

To harvest cells, cells were washed in cold PBS and harvested in 2 x Laemmli sample buffer (120 mM Tris, pH 6.8, 6% w/v SDS, 20% v/v glycerol, 10% β-mercaptoethanol and 0.01% bromophenol blue) (Laemmli 1970) for sodium dodecyl sulfate polyacrylamide gel electrophoresis (SDS-PAGE) or lysis buffer (20 mM Hepes, pH 7.4, 150 mM NaCl, 1 mM EDTA, 1 mM EGTA, 1 mM Na_2VO_4, 50 mM NaF, 1 mM DTT and 0.5% (v/v) Triton X-100 and 1 x Protease Inhibitor Tablet (Roche)/ 50 mL buffer) for further experimentation.

2.3 DNA isolation and purification

2.3.1 Mini Prep

Isolation of plasmid DNA from bacterial cells, for subsequent cloning or sequencing reactions, was carried out using the NucleoSpin® Plasmid kit from Macherey-Nagel. The kit supplies all the buffers required for plasmid DNA isolation and all steps were carried out at room temperature. Briefly, 1 - 5 mL of saturated bacterial culture was centrifuged at 11,000 x g for 30 s to pellet cells. The supernatant was discarded and the pellet was re-suspended in 250 µL of Buffer A1. After ensuring thorough re-suspension of cells, 250 µL of Buffer A2 was added and gently mixed by tube inversion. Samples were incubated for 5

min at room temperature, after which 300 μL of Buffer A3 was added. Samples were again mixed by gentle tube inversion. Lysates were then clarified by centrifugation at 11,000 x g for 5 min, pellets discarded and supernatants transferred to NucleoSpin® Plasmid Columns supplied within the kit. Columns were centrifuged at 11,000 x g for 1 min and flowthrough discarded. To wash DNA retained on the silica membrane of the column, 600 μL of Buffer A4 was added and again centrifuged at 11,000 x g for 1 min. The flowthrough was discarded and the membrane dried by centrifugation at 11,000 x g for 2 min. To elute DNA, 50 μL of Buffer AE was added to the column, incubated for 1 min and DNA was eluted into a fresh collection tube by centrifugation at 11,000 x g for 1 min.

2.3.2 Maxi Prep

To isolate larger quantities of plasmid DNA from bacterial cells, for transfection of cells or sequencing, purification was carried out using QIAGEN HiSpeed® Plasmid Purification Kit according to manufacturer's instructions. The kit supplies all the buffers required for plasmid DNA isolation and all steps were carried out at room temperature unless otherwise stated. Briefly, 100 - 250 mL of saturated bacterial culture was centrifuged at 6000 x g for 15 min at 4°C. The supernatant was discarded and the pellet was re-suspended in 10 mL of Buffer P1. After ensuring thorough re-suspension of cells by vortexing up and down, 10 mL of Buffer P2 was added and mixed by gentle tube inversion. Samples were incubated for 5 min, after which 10 mL of pre-chilled Buffer P3 was added. Samples were again mixed by gentle tube inversion. Precipitated lysate was transferred into the barrel of a QIAfilter Cartridge and incubated for 10 min. During the incubation HiSpeed Maxi Tips were equilibrated with 10 mL of Buffer QBT. After incubation, precipitated lysate was filtered using the QIAfilter Cartridge into the equilibrated HiSpeed Maxi Tip and allowed to enter the resin by gravity flow. HiSpeed Tips were then washed with 60 mL of Buffer QC. Next, DNA was eluted from the tip into a 50 mL centrifuge tube with 15 mL of Buffer QF. DNA was precipitated by addition of 10.5 mL of isopropanol and incubated for 5 min. During this incubation QIAprecipitator Maxi Module filters were

attached onto the outlet nozzle of 30 mL syringes. Precipitated DNA was transferred into the syringe and mixture filtered through the QIAprecipitator using constant pressure. Next, DNA retained in the filter was washed with 2 mL of 70% ethanol and filters dried by passing air through the filter using an empty syringe under constant pressure. The QIAprecipitator was then transferred to the outlet nozzle of a 5 mL syringe and DNA eluted into a 1.5 mL microcentrifuge tube using 1 mL of TE Buffer.

2.3.3 Agarose gel purification

Isolation of PCR products from amplification reactions, electrophoresed on agarose gels, was carried out using the High Pure PCR Product Purification Kit from Roche Diagnostics. The kit supplies all the buffers required for DNA purification and unless stated, all steps were carried out at room temperature. Briefly the desired DNA band from an electrophoresed agarose gel was excised using an ethanol-cleaned scalpel. The gel slice was placed in a pre-weighed 1.5 mL microcentrifuge tube and mass determined. For every 100 mg of agarose gel slice, 300 μL of Binding Buffer was added to the microcentrifuge tube and vortexed in order to release the DNA. To completely dissolve the agarose, the suspension was incubated at 56°C for 10 min. Once dissolved, 150 μL of isopropanol per 100 mg of agarose gel slice was added to the suspension and thoroughly vortexed. The suspension was then transferred to the upper reservoir of a High Pure Filter Tube provided within the kit. The High Pure Filter Tube was centrifuged at maximum speed for 30 s and flowthrough discarded. A wash of retained DNA was performed by application of 500 μL of Wash Buffer to the upper reservoir of the Filter Tube and centrifuged at maximum speed for 1 min. Flowthough was discarded and a further wash of 200 μL was repeated in the same manner. Lastly, DNA was eluted into fresh collection tubes by addition of 50 μL of Elution Buffer to the upper reservoir of the Filter Tube and centrifugation at maximum speed for 1 min.

2.4 Site directed mutagenesis

To introduce mutations into DNA of kinases and substrates, site directed mutagenesis was performed using the QuickChange II Site-Directed Mutagenesis Kit (Agilent), according to manufacturer's instructions. Briefly PCR reactions were set up in reaction buffer using *PfuUltra* HF DNA polymerase, dNTPs, template DNA and two complimentary oligonucleotides containing the desired mutation. Specific details of primers and PCR conditions used can be found in relevant methods sections. Following PCR, reactions were placed on ice for 2 min, after which parental template DNA was digested using 1 µL of *Dpn* I restriction enzyme for 1 h at 37°C. Following digestion, DNA was transformed into bacterial cells as described in Section 2.7.1

2.5 Determination of DNA concentration and purity

DNA concentration was assessed by measuring the absorbance of UV at 260 nm, in an Eppendorf BioPhotometer Spectrophotometer. Using the relationship that one measurement of optical density at 260 nm equals 50 µg/mL of pure dsDNA, the concentration of DNA could be calculated. Using this absorbance method DNA quality could also be determined. Protein contaminants absorb UV at 280 nm, therefore the ratio of A_{260}/A_{280} is a common calculation used to determine purity. Furthermore, organic compounds or chaotropic salts contaminants present in the sample were also taken into account by determining the ratio A_{260}/A_{230}.

2.6 DNA electrophoresis

DNA samples were prepared for agarose gel electrophoresis by addition of 6 x Blue/Orange Loading Dya (Promega) to give a 1 X final. Samples were separated by hand cast 0.5 to 2% agarose gels in Tris-Acetate-EDTA (TAE; 40 mM Tris pH 7.6, 20 mM acetic acid, 1 mM ETDA) buffer supplemented with 0.01% (v/v) Gel Red stain (Biotium). Gels were electrophoresed in TAE buffer at 100 V for approximately 1 h. After electrophoresis gels were viewed and photographed using a UV transilluminator (Syngene, GeneSnap).

2.7 Bacterial Culture

One litre of Luria-Bertani (LB) broth, used for culture of bacterial cells, was composed of 10 g Tryptone, 5 g Yeast Extract and 10 g NaCl. Broth was prepared in deionised water when needed and autoclaved before use. Appropriate antibiotic was added on day of use. LB Agar plates were prepared by dissolving 5 g Tryptone, 2.5 g Yeast Extract, 5 g NaCl and 7.5 g Agar in 500 mL of deionised water. The solution was autoclaved and allowed to cool before addition of appropriate antibiotic. Approximately 30 mL of LB Agar was poured into 82 mm Petri dishes and allowed to set at room temperature. Once set, plates were stored at 4°C.

2.7.1 Bacterial cell transformation

Chemically competant bacterial cells were incubated with 100 ng or 2-3 µL of plasmid DNA on ice for 30 min. Cells were briefly heat shocked at 42°C for 45 s, before a further 2 min incubation on ice. 300 µL of Super Optimal broth with Catabolite repression (SOC, Promega) was added to cells and cells were incubated at 37°C, 220 rpm for 1 hr. 350 µL of transformed cells were inoculated onto LB-Amp (100 µg/mL) agar plates by streaking and incubated overnight at 37°C.

2.8 Heart Homogenisation

Snap frozen hearts were removed from -80°C and thawed on ice in lysis buffer (20 mM Hepes, pH 7.4, 150 mM NaCl, 1 mM EDTA, 1 mM EGTA, 1 mM Na_2VO_4, 5 mM NaF, 1 mM DTT, 0.5% (v/v) Triton X-100 and 1 x Protease Inhibitor Tablet (Roche)/50 mL buffer). For every 100 mg of heart tissue, 1 mL of lysis buffer was added. Heart tissue was cut up into small pieces and transferred to 1 mL mortar (Fisher Scientific) on ice. Tissue was completely homogenised by shearing forces generated at the interface of the mortar and pestle (glass/glass homogeniser). Homogenate was then transferred to 1.5 mL microcentrifuge tube and centrifuged at 11,000 rpm for 3 min at 4°C. The supernatants were collected for use in further experimentation, mixed with 2 x

Laemmli sample buffer for SDS-PAGE or stored at -80°C. Pellets containing insoluble material were discarded.

2.9 *In vitro* Kinase (IVK) assays

Phosphorylation of substrates was performed *in vitro* in kinase buffer (25 mM Tris, pH 7.5, 5 mM β-glycerophosphate, 2 mM DTT, 0.2 mM Na_3VO_4 and 10 mM $MgCl_2$) and contained 200 ng of kinase, 1 mM ATP or N^6 expanded ATP analogues and 1 ug of substrate. Reactions were set up on ice and briefly mixed before incubation at 30°C for 30 - 60 min. Where phospho-antibodies are available, the reactions were stopped by addition of 2 x Laemmli sample buffer and boiling for 5 min at 100°C. For detection of thiophosphorylated substrates, kinase reactions were stopped with 20 mM EDTA and alkylated with 5 mM *p*-Nitrobenzyl mesylate (PNBM) or vehicle for 1 -2 h at room temperature before addition of 2 x Laemmli sample buffer.

2.10 Determination of Protein Concentration

2.10.1 Absorbance at 280 nm

Protein concentration of purified proteins was determined by measuring the absorbance of proteins at 280 nm using a Nanodrop 2000c spectrophotometer (Thermoscientific). Protein concentration was calculated using Beer's law ($A = \varepsilon lc$, where A is absorbance at 280 nm, ε is the molar extinction coefficient, l is the path length of the spectrophotometer and c is the concentration of the protein in mols).

2.10.2 Bradford Assay

Protein concentration was measured by assay of Bradford (Bradford 1976) using the Pierce™ Coomassie (Bradford) Protein Assay Kit from Life Technologies, according to manufacturer's instructions. An albumin standard curve was generated by performing serial dilutions of stock albumin, in the same diluent as samples (0-2 mg/mL). The assay was performed in 96 well microplates in triplicate. 250 µL of coomassie assay reagent was added to 5 µL

of protein standard or sample and incubated for 10 min at room temp. Absorbance of standards and samples was then measured at 595 nm using a microplate reader (BioTek EL808). All 595 nm measurements were averaged and blank-corrected. An albumin standard curve was generated by plotting albumin concentration against absorbance at 595 nm. The curve was used to determine protein concentration of samples.

2.11 SDS-PAGE

Proteins samples were separated by size by SDS-PAGE. Samples were added to 2 x Laemmli sample buffer to give a 1 X final concentration of buffer. Samples were boiled at ~100°C for 5 min and centrifuged at 10,000 rpm for 2 min. Samples were separated by pre-cast gradient or hand-cast (various: 6 to 12%) Tris-Glycine SDS-PAGE mini gels, with a 4% stacking gel. Gels were electrophoresed at 90 V through the stacking gel (approx. 20 min) and 120 V through the resolving gel (approx. 100 min). Following electrophoresis, gels were further processed as described below.

2.12 Phos-tag™ SDS-PAGE

Phos-tag™ SDS-PAGE is a variation of the traditional SDS-PAGE analysis whereby resolving gels are supplemented with an alkoxide-bridged dinuclear metal ion complex that serves as a phosphate binding tag (Phos-tag™). The Phos-tag™ reagent captures phosphomonoester dianions bound to serine, threonine and tyrosine residues of proteins. This results in a mobility shift of phosphorylated proteins with the bound tag in SDS-PAGE. Therefore phosphorylated proteins in the gel are visualised as slower migration bands compared to corresponding non-phosphorylated bands (Kinoshita et al. 2006).

2.12.1 Tris-Glycine SDS-PAGE

For Phos-tag™ gel analysis of p38γ proteins, resolving gel solution was prepared as above but was supplemented with Phos-tag™ acrylamide (Wako chemicals, Germany) and $MnCl_2$ to a final concentration of 40 µM and gels were electrophoresed at a lower constant voltage of 90 V.

2.12.2 Bis-Tris PAGE

For Phos-tag™ gel analysis of higher molecular weight proteins such as calpastatin and LDB3, a bis-tris-buffered neutral-pH gel system was adopted. For this system, samples were added to 2 x Lithium Dodecyl Sulfate (LDS) loading buffer (282 mM Tris Base, 212 mM Tris HCl, pH 8.5, 20% Glycerol, 4% LDS, 200 µM DTT, 1 mM EDTA, 0.66 mM SERVA® Blue G250, 0.35 mM Phenol Red) to give a 1 X final. Samples were boiled at 70°C for 10 min and centrifuged at 10,000 rpm for 2 min. Samples were separated by hand-cast 8% bis-tris PAGE mini gels supplemented with 50 µM Phos-tag™ acrylamide and 100 µM $Zn(NO_3)_2$ with a 4% stacking gel. Gels were electrophoresed at 90 V through the stacking gel for approx. 20 min and 120 V through the resolving gel. Following electrophoresis, gels were further processed as described below.

2.13 Western Blot Analysis

Western blotting was carried out after SDS-PAGE to detect selected proteins using specific antibodies. Gels and methanol soaked PVDF membranes were equilibrated in transfer buffer (25 mM Tris, 19.2 mM glycine, 20% v/v methanol) for 5 min prior to transfer using a semi-dry transfer cell (Bio-Rad). Transfer was performed for 1 h at 24 V. Following transfer, non-specific binding sites on membranes were then blocked by incubation of the PVDF membrane in 1.2% non-fat milk powder, 0.3% bovine serum albumin (BSA) in TBS-T buffer (20 mM Tris, pH 7.4, 137 mM NaCl, 0.1% v/v Tween-20) for 1 h at room temperature. Membranes were subsequently incubated with primary antibody overnight at 4°C (Table 2.1). Blots were then washed with TBS-T for 5 min x 6 and incubated at room temperature for 1 h with the relevant secondary antibody. All HRP-conjugated secondary antibodies were obtained from GE Healthcare. Following this, blots were washed with TBS-T for 5 min x 8 and developed using ECL and exposure to HyperFilm.

2.13.1 Transfer of Phos-tag™ gels

For transfer of proteins from Phos-tag™ gels, gels were first washed in transfer buffer containing 1 mM EDTA for 15 min at room temperature on a shaking

platform. Phos-tag™ gels were then equilibrated in transfer buffer for a further 15 min prior to transfer. Transfer was carried out using a wet tank transfer cell (Bio-Rad) for 100 min at 90 V at 4°C. Following transfer, membranes were blocked and probed for proteins as described above.

2.14 Gel protein staining

2.14.1 Coomassie Blue staining

To visual proteins on electrophoresed gels, gels were stained with Coomassie Brilliant Blue R-250 staining solution (10% acetic acid, 50% methanol, 0.25% w/v Coomassie Brilliant Blue R-250) for 2 h to overnight at room temperature on a shaking platform. Following staining, gels were rinsed in destaining solution (10% acetic acid, 50% methanol) and incubated with fresh destaining solution for 2 h to overnight at room temperature on a shaking platform.

2.14.2 Silver staining

A more sensitive method to visualise proteins on electrophoresed gels is to stain proteins with silver. Silver staining was carried out using Modified PlusOne™ Staining Kit (GE Healthcare) according to manufacturer's instructions with the following modifications: 1) Gels were fixed overnight at room temperature; 2) both glutaraldehyde and formaldehyde were omitted from the silver solution and 3) 100 µl formaldehyde was used in the developing solution.

Table 2.1 Antibodies used for Western Blot analysis

Antibody	Blocking reagent	Primary antibody	Secondary antibody
p38γ (R&D Systems)	0.3% BSA 1.2% milk	1:8000 1% BSA	1:20 000 in TBS-0.1% Tween HRP-conjugated rabbit
pTyr (Santa Cruz)	0.3% BSA 1.2% milk	1:3000 5% milk	1:8000 in TBS-0.1% Tween HRP-conjugated rabbit
pThr (2B Scientific)	0.3% BSA 1.2% milk	1:10 000 5% milk	1:20 000 in TBS-0.1% Tween HRP-conjugated rabbit
p38T (Cell signalling)	0.3% BSA 1.2% milk	1:8000 1% BSA	1:20 000 in TBS-0.1% Tween HRP-conjugated rabbit
pp38 (Cell signalling)	0.3% BSA 1.2% milk	1:8000 1% BSA	1:20 000 in TBS-0.1% Tween HRP-conjugated rabbit
pATF2 (Cell signalling)	0.3% BSA 1.2% milk	1: 5000 1% BSA	1:8000 in TBS-0.1% Tween HRP-conjugated rabbit
T-ATF2 (Cell signalling)	0.3% BSA 1.2% milk	1:4000 1% BSA	1:8000 in TBS-0.1% Tween HRP-conjugated rabbit
MEK3/6 (Santa Cruz)	0.3% BSA 1.2% milk	1:2500 1% BSA	1:4000 in TBS-0.1% Tween HRP-conjugated rabbit
Thiophosphate (Abcam)	5% milk	1:8000 5% milk	1:16 000 in TBS-0.1% Tween HRP-conjugated rabbit
α1-syntrophin (Thermoscientific)	0.3% BSA 1.2% milk	1:8000 1% BSA	1:16 000 in TBS-0.1% Tween HRP-conjugated rabbit
α1-syntrophin (Abcam)	0.3% BSA 1.2% milk	1:2000 1% BSA	1:5000 in TBS-0.1% Tween HRP-conjugated rabbit
pTAB (Custom, Prof. Cohen. Dundee University)	0.3% BSA 1.2% milk	1:2000 1% BSA	1:4000 in TBS-0.1% Tween HRP-conjugate sheep
TAB (Santa Cruz)	0.3% BSA 1.2% milk	1:2000 1% BSA	1:4000 in TBS-0.1% Tween HRP-conjugate sheep
GST (Cell signalling)	0.3% BSA 1.2% milk	1:2000 1% BSA	1:4000 in TBS-0.1% Tween HRP-conjugate mouse
His (Cell signalling)	0.3% BSA 1.2% milk	1:1000 1% BSA	1:2000 in TBS-0.1% Tween HRP-conjugate rabbit

Antibody	Blocking reagent	Primary antibody	Secondary antibody
Zfp260 (Merck Millipore)	5% BSA	1:2000 5% BSA	1:4000 in TBS-0.1% Tween HRP-conjugate rabbit
PDLIM5 (LDB3) (Abnova)	5% milk	1:2000 5% milk	1:4000 in TBS-0.1% Tween HRP-conjugated mouse
PDLIM5 (LDB3) (Sigma)	5% milk	1:1000 1% BSA	1:4000 in TBS-0.1% Tween HRP-conjugated goat
pS98 LDB3 (Custom, CRB)	5% BSA	1:500 1% BSA	1:2000 in TBS-0.1% Tween HRP-conjugated rabbit
pS240 LDB3 (Custom, CRB)	5% BSA	1:500 1% BSA	1:2000 in TBS-0.1% Tween HRP-conjugated rabbit
Calpastatin (Cell signalling)	0.3% BSA 1.2% milk	1:2000 1% BSA	1: 4000 in TBS-0.1% Tween HRP-conjugated rabbit
pT197/S200 Calpastatin (Custom, CRB)	5% BSA	1:1000 1% BSA	1:2000 in TBS-0.1% Tween HRP-conjugated rabbit
pT448 Calpastatin (Custom, CRB)	5% BSA	1:1000 1% BSA	1:2000 in TBS-0.1% Tween HRP-conjugated rabbit

3 PURIFICATION AND ACTIVATION OF RECOMBINANT p38γ KINASES

3.1 Introduction

The purpose of the experiments contained in this chapter was to obtain pure, activated WT and mutant p38γ proteins. A total of four p38γ kinases were generated: WT, two AS mutant kinases and a carboxy-terminal PDZ consensus motif truncated p38γ. Generation of recombinant kinases forms the basis for many of the subsequent experiments described in this Thesis. For example, recombinant kinases obtained were needed to fulfill the *in vitro* chemical genetic approach for identifying substrates of p38γ. This entailed the addition or 'spiking' of recombinant AS p38γ into homogenised heart tissue. Additionally, recombinant kinases were spiked into heart homogenate to aid identification of interacting partners of p38γ in the myocardium. Kinases were ultimately used to validate substrates or interactions *in vitro*.

3.2 Specific Methods

3.2.1 Cloning of WT p38γ

E. coli expressing His-WT and AS p38γ kinases were previously prepared in the laboratory by Dr Eva Denise Martin as follows: The clone of the open reading frame (ORF) of murine *mapk12* (p38γ) was a kind gift from the Rudnicki Lab, University of Ottawa. A PCR reaction was then set up to amplify the region of plasmid encoding p38γ. Primers were designed to incorporate restriction enzyme sites for AscI (forward) and AflII (reverse). Primer sequences and conditions used for PCR are detailed in Table 3.1. PCR reactions were set up using Platinum® Pfx DNA Polymerase (Invitrogen) according to manufacturer's instructions.

Table 3.1 Primers and PCR conditions used for amplification of the ORF of *mapk12.* Primers were designed to incorporate restriction enzyme sites for AscI (forward) and AflII (reverse) for subsequent cloning into the pETDuet-1 expression vector.

Primer	Primer Sequence (5' to 3')
p38γ F	ATGAGCTCCCCGCCACCCGCCCGCAAGGGCTTTTACCGCC AGGAGGTGACCAAAACGGCCTGGGAGGTGCGCGCCGTGTAC CAAGACCTG
p38γ R	GACTTAAGTCACAGAGCCGTCTCCTTTGGAACTCTGGCTCC TAGCTGCCTAGG

PCR conditions

Step	Temperature	Time	Cycle
Initial Denaturation	94°C	5 min	1
Denaturation	94°C	30 s	30
Annealing	55°C	30 s	
Extension	68°C	1 min	
Final Extension	68°C	5 min	1

An 1191 bp PCR product corresponding to the expected size of p38γ's encoding region was electrophoresed and visualised on a 1% (w/v) agarose gel. The PCR product or 'insert' was gel purified using High Pure PCR Product Isolation Kit (Roche) according to manufacturer's instructions (Section 2.3.3). Insert DNA and target pETDuet-1 (Novagen) plasmid DNA were digested with AscI and AflII restriction enzymes (NEB, 1 hr, 37°C) according to manufacturer's instructions. Following double digestion of insert and plasmid DNA, DNA was electrophoresed on a 1% (w/v) agarose gel. DNA samples were gel purified and 10 µL ligations in 3:1 and 1:3 insert to vector ratios were set up using T4 DNA ligase (Promega) according to manufacturer's instructions. Ligations were incubated overnight at 4°C.

The following day 2 µL of each ligation reaction was used to transform α-Select Gold Competent Cells (Bioline) (Section 2.7.1). A selection of bacterial colonies were used to inoculate 5 mL LB cultures containing 100 µg/mL ampicillin. Following overnight incubation (220 rpm, 37°C), plasmid DNA purification was carried out as previously described (Section 2.3.1) and sent for sequencing (Eurofins MWG Operon). DNA from positive colonies was then used to transform *Escherichia coli (E.coli)* strain Rosetta BL21 DE3 (Bioline) (Section 2.7.1).

3.2.2 Cloning of Analogue Sensitive (AS) p38γ kinases

A site directed mutagenesis kit (Agilent) was used to engineer AS p38γ kinases according to manufacturer's instructions (Section 2.4). The gatekeeper methionine residue was substituted for glycine in AS1 p38γ and alanine in AS2 p38γ. In both AS p38γ kinases, additional rescue mutations were introduced to prevent loss of kinase activity. Primers and conditions used for PCR are detailed in Table 3.2. See Figure 3.1 for the amino acid sequence of the WT and mutated proteins. Following mutagenesis, DNA was transformed into bacterial cells and processed as described for above for WT p38γ.

Table 3.2 Primers and PCR conditions used for *mapk12* mutagenesis to generate two AS p38γ kinases (AS1 and AS2). PCR reactions for *mapk12* mutagenesis were performed using WT His-p38γ pETDuet-1 plasmid DNA as template. Each AS mutant was generated with two rescue mutations.

Primer	Primer Sequence (5' to 3')
AS1 F	CAGACTTCTACCTGGTGGGGCCATTCATGGGCACTG
AS1 R	CAGTGCCCATGAATGGCCCCACCAGGTAGAAGTCTG
AS2 F	CAGACTTCTACCTGGTGGCGCCATTCATGGGCACTG
AS2 R	CAGTGCCCATGAATGGCGCCACCAGGTAGAAGTCTG
Rescue 1 F	TGAAGCCTGGCAACCTGCTTGTGAATGAGGACTGTG
Rescue 1 R	CACAGTCCTCATTCACAAGCAGGTTGCCAGGCTTCA
Rescue 2 F	GACTGTGAGCTGAAGATCGCAGACTTTGGCCTTGCCAG
Rescue 2 R	CTGGCAAGGCCAAAGTCTGCGATCTTCAGCTCACAGTC

PCR conditions

Step	Temperature	Time	Cycle
Initial Denaturation	95°C	5 min	1
Denaturation	95°C	50 s	18
Annealing	60°C	50 s	
Extension	68°C	6.5 min	

```
WT      1    MGSSHHHHHHSQDPNSSSARRENLYFQSMSSPPPARKGFYRQEVTKTAWEVRAVYQDLQP  60
AS1     1    MGSSHHHHHHSQDPNSSSARRENLYFQSMSSPPPARKGFYRQEVTKTAWEVRAVYQDLQP  60
AS2     1    MGSSHHHHHHSQDPNSSSARRENLYFQSMSSPPPARKGFYRQEVTKTAWEVRAVYQDLQP  60

WT      61   VGSGAYGAVCSAVDSRTGNKVAIKKLYRPFQSELFAKRAYRELRLLKHMRHENVIGLLDV  120
AS1     61   VGSGAYGAVCSAVDSRTGNKVAIKKLYRPFQSELFAKRAYRELRLLKHMRHENVIGLLDV  120
AS1     61   VGSGAYGAVCSAVDSRTGNKVAIKKLYRPFQSELFAKRAYRELRLLKHMRHENVIGLLDV  120

WT      121  FTPDESLDDFTDFYLVMPFMGTDLGKLMKHETLSEDRIQFLVYQMLKGLKYIHAAGVIHR  180
AS1     121  FTPDESLDDFTDFYLVGPFMGTDLGKLMKHETLSEDRIQFLVYQMLKGLKYIHAAGVIHR  180
AS2     121  FTPDESLDDFTDFYLVAPFMGTDLGKLMKHETLSEDRIQFLVYQMLKGLKYIHAAGVIHR  180

WT      181  DLKPGNLAVNEDCELKILDFGLARQADSEMTGYVVTRWYRAPEVILNWMRYTQTVDIWSV  240
AS1     181  DLKPGNLLVNEDCELKIADFGLARQADSEMTGYVVTRWYRAPEVILNWMRYTQTVDIWSV  240
AS2     181  DLKPGNLLVNEDCELKIADFGLARQADSEMTGYVVTRWYRAPEVILNWMRYTQTVDIWSV  240

WT      241  GCIMAEMITGKILFKGNDHLDQLKEIMKITGTPPPEFVQKLQSAEAKNYMEGLPELEKKD  300
AS1     241  GCIMAEMITGKILFKGNDHLDQLKEIMKITGTPPPEFVQKLQSAEAKNYMEGLPELEKKD  300
AS2     241  GCIMAEMITGKILFKGNDHLDQLKEIMKITGTPPPEFVQKLQSAEAKNYMEGLPELEKKD  300

WT      301  FASVLTNASPQAVNLLERMLVLDAEQRVTAAEALTHPYFESLRDTEDEPKAQKYDDSFDD  360
AS1     301  FASVLTNASPQAVNLLERMLVLDAEQRVTAAEALTHPYFESLRDTEDEPKAQKYDDSFDD  360
AS2     301  FASVLTNASPQAVNLLERMLVLDAEQRVTAAEALTHPYFESLRDTEDEPKAQKYDDSFDD  360

WT      361  VDRTLEEWKRVTYKEVLSFKPPRQLGARVPKETAL  395
AS1     361  VDRTLEEWKRVTYKEVLSFKPPRQLGARVPKETAL  395
AS2     361  VDRTLEEWKRVTYKEVLSFKPPRQLGARVPKETAL  395
```

Figure 3.1 Aligned amino acid sequences of 6xHis-WT and AS p38γ proteins

Areas of interest annotated around sequence. 6xHis tag is underlined and TEV cleavage site is in green. Highlighted residues in yellow show location of point mutations. In pink is the TGY motif corresponding to the activation loop of the kinase. The 5 residues (red) of the PDZ consensus motif are truncated in the C' truncated mutant.

3.2.3 Cloning of Carboxy-terminal truncated p38γ

WT His-p38γ pETDuet-1 plasmid DNA was used as template to generate C' truncated p38γ. A stop codon was generated N terminal of p38γ's PDZ consensus motif. Mutagenesis was carried out as described in Section 2.4 but using KOD DNA polymerase (Toyobo) according to manufacturer's instructions. Primers and conditions used for PCR are detailed below. C' truncated p38γ lacks residues highlighted in red in Figure 3.1. Following mutagenesis, DNA was transformed into bacterial cells and processed as described for above for WT p38γ.

3.2.4 Protein Expression

To express protein, transformed Rosetta BL21 DE3 bacterial colonies were used to inoculate 15 ml standard LB broth medium containing 100 µg/mL ampicillin. After incubation overnight at 37°C, 220 rpm., cultures were used to inoculate 1L LB broth containing 100 µg/ml ampicillin. The cultures were grown at 37°C until the absorbance at 600 nm reached 0.5, at which point the temperature was lowered to 21°C. After 30 min at 21°C, expression of p38γ proteins was induced by addition of 1 mM isopropyl-thio-β-d-galactopyranoside (IPTG). Bacterial cells were grown for 5 h at 21°C and were then harvested by centrifuging at 5000 rpm at 4°C for 15 min. The expression level of recombinant p38γ proteins was monitored using SDS–PAGE and Western blot/staining analysis. The cell pellets were either immediately used or stored frozen at −80°C.

Table 3.3 Primers and PCR conditions used for *mapk12* mutagenesis to generate C' truncated p38γ. PCR reaction for *mapk12* mutagenesis was performed using WT His-p38γ pETDuet-1 plasmid DNA as template.

Primers	**Primer Sequence (5' to 3')**
p38γ trun F	GCTAGGAGCCAGAGTTCCATAGGAGACGGC
p38γ trun R	GCCGTCTCCTATGGAACTCTGGCTCCTAGC

PCR conditions

Step	**Temperature**	**Time**	**Cycle**
Initial Denaturation	95°C	2 min	1
Denaturation	95°C	20 s	25
Annealing	55°C	10 s	
Extension	70°C	3.5 min	

3.2.5 Purification of p38γ Proteins

3.2.5.1 Immobilised Metal Affinity Chromatography

Recombinant 6xHis-p38γ proteins were purified by metal affinity chromatography using nickel-nitriloacetic acid (Ni-NTA) agarose beads and a batch protocol as follows: Bacterial cell pellets were re-suspended in ice-cold lysis buffer (50 mM Tris, pH 7.4, 500 mM NaCl, 2 mM DTT and 10 mM imidazole, containing Roche protease inhibitor cocktail). Cell lysis was performed using a high intensity ultrasonic processor. Lysates were clarified by centrifugation at 10,000 rpm for 30 min at 4°C. Supernatants were filtered through 0.45 μM membrane filters before incubation with lysis buffer equilibrated Ni-NTA agarose beads for 1 h at 4°C on a rotator. Beads were pelleted by centrifugation at 3000 rpm for 5 min at 4°C and supernatant discarded. Beads were subsequently washed six times with 15 mL ice-cold wash buffer (50 mM Tris, pH 7.4, 500 mM NaCl, 2 mM DTT and 20 mM imidazole). p38γ proteins was eluted by applying 2 mL volumes of a 0.05–0.5 M imidazole gradient. p38γ peak fractions were pooled and extensively dialysed overnight at 4°C against 50 mM Tris, pH 7.4, 100 mM NaCl, 2 mM DTT buffer.

3.2.5.2 Ion Exchange Chromatography

p38γ proteins were further purified by ion exchange chromatography on a MonoQ 5/10 column (GE Healthcare) equilibrated in 50 mM Tris, pH 7.4, 100 mM NaCl and 2 mM DTT. p38γ proteins were eluted by applying 40 column volumes of a linear 0.1–0.6 M NaCl gradient. p38γ eluted at approximately 90 mM NaCl. All chromatographic steps were performed at 4°C. Fractions from each chromatographic step were analysed by SDS–PAGE, Phos-tag^{TM} SDS-PAGE and Western blot analysis. Fractions containing highly purified p38γ protein were pooled and used for subsequent biochemical studies. The enzyme were assayed for protein concentration and stored in aliquots at −80°C.

3.2.6 Activation of Non-active p38γ Proteins

Purified non-active p38γ proteins (0.2 mg/ml) were activated by incubating with constitutively active MBP-MKK6EE (0.02 mg/ml) in the presence of 0.1 mM ATP and 1 x kinase buffer (50 mM Tris, pH 7.5, 10 mM MgAc, 0.1 mM EGTA, 0.1% β-mercaptoethanol) for 1.5 h at 30°C without mixing. To separate MKK6EE from p38γ proteins, kinase reactions were incubated with amylose resin for 30 min at 4°C. Resin was pelleted by centrifugation at 3000 rpm for 5 min at 4°C and supernatant containing activated proteins was collected and analysed for phosphorylation by SDS–PAGE, Phos-tag™ SDS-PAGE and Western blot analysis. Activated proteins were dialysed into storage buffer (50 mM Tris, pH 7.5, 0.1 mM EGTA, 270 mM sucrose, 150 mM NaCl, 0.1% β-mercaptoethanol, 0.2 mM PMSF, 1 mM benzamidine) overnight at 4°C, assayed for protein concentration and stored in aliquots at -80°C.

3.3 Results

3.3.1 Purification of p38γ proteins

In order to elucidate the signalling pathway in which p38γ is integrated and its substrates and/or interacting partners, recombinant 6xHis tagged WT, two analogue sensitive and a carboxy-terminal PDZ consensus motif truncated (C' trun) p38γ recombinant proteins were firstly expressed and purified from *E. coli*. The polyhistidine tag encoded at the amino-terminal of the kinases enables purification of target protein by metal affinity capture. Metal affinity capture is based on the strong interaction of histidines, which form the tag, and a transition metal ion, in this case Ni^{2+}. Ni^{2+} immobilised on a matrix of agarose is used to isolate and purify tagged proteins. Following washing, proteins retained on the matrix are competitively eluted using the histidine analogue imidazole.

Figure 3.2 shows the outcome of purification of recombinant p38γ proteins. Firstly it can be seen that there is a sizable band in the *E. coli* lysate that shows high expression of recombinant p38γ proteins in *E. coli*. Secondly, it can be seen that for all proteins the Ni-NTA resin was successful at retaining the tagged proteins, although some impurities persisted. Impurities in the protein preparation occur due to non-specific binding of untagged *E. coli* proteins to the resin. Those eluents that contained a large amount of purified protein and little contaminating proteins were pooled and dialysed for subsequent experimentation.

3.3.1.1 Anion exchange chromatography

In order to enhance purity of the protein preparations, p38γ proteins purified by metal affinity capture, were then subjected to an additional polishing step by ion exchange chromatography (IEC). IEC allows separation of proteins based on charge. In anion exchange chromatography, negatively charged proteins are passed through a column composed of a positively charged solid support. Proteins bind to the column support due to ionic interactions between the oppositely charged ionic groups. Elution of protein from the column is performed

by either changing the pH of the buffer solution or by increasing the concentration of salt. For purification of p38γ proteins, a linear gradient of increasing salt concentration was applied, as described in materials and methods. The chromatogram obtained following IEC of WT-p38γ proteins is shown in Figure 3.3. Analysis of the chromatogram shows an increase in conductance during the application phase, when sample is injected into the column. This can be viewed as the flowthrough and represents proteins that do not bind to the column. As the linear salt gradient is applied to the column, a dominant large peak in absorbance is measured. At higher magnification (panel B of Figure 3.3) we observe there is a shoulder peak appended to the larger peak. Collection fractions corresponding to the dominant and shoulder peak were analysed by immunoblotting to confirm the purification of p38γ (panel C of Figure 3.3). To explore if the shoulder peak was a phosphorylated form of p38γ, samples were also probed using the phospho-p38 antibody. The results show that the shoulder peak fraction did contain p38γ, but did not correspond to a phosphorylated form of p38γ. As the identity of this species could not be elucidated, fractions corresponding to the shoulder were discarded. The remaining fractions were pooled and dialysed into storage buffer, as described in material and methods for subsequent experimentation. Consistent results were obtained following anion exchange chromatography of mutant p38γ proteins (Figure 3.4).

3.3.2 Activation and Validation of Kinase Activity of WT and AS p38γ

A key step in the production of recombinant proteins is to assess if proteins produced in bacteria are biologically active, particularly when a tag is added to a protein and/or if mutations are introduced. For kinases, an obvious assay is to assay kinase activity by measuring phosphorylation of a substrate. In order to validate the catalytic competency of recombinant p38γ kinases, kinases were first subject to phosphorylation and activation by upstream activating kinase, MKK6EE. A small sample of WT and AS p38γ kinases were tested for activation and subsequently for catalytic activity. Activation of p38γ proteins was inferred by Phos-tag^{TM} SDS-PAGE and Western blot analysis as shown in Figure 3.5.

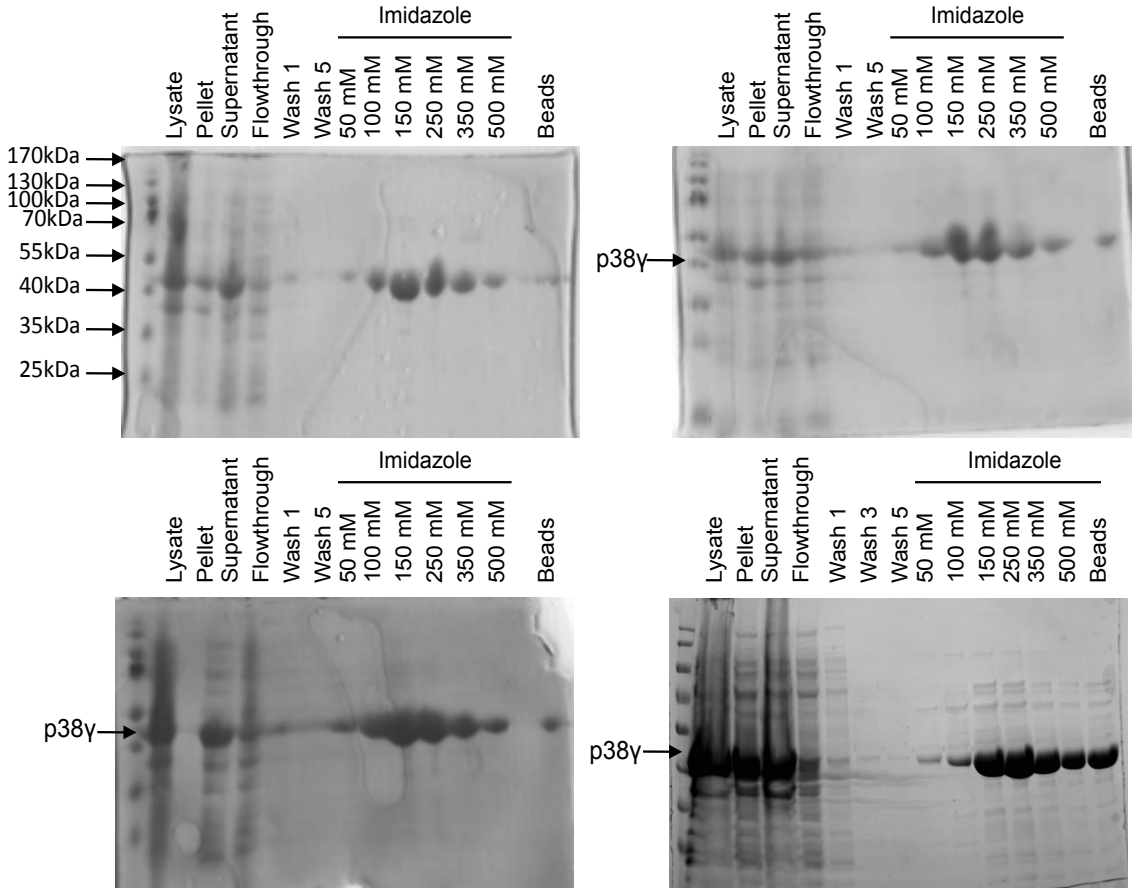

Figure 3.2 Purification of recombinant 6xHis-p38γ proteins (non-active) from *E.coli* by metal affinity capture

Samples were taken from each step of the purification process, prepared in 5 x sample buffer, resolved by 10% SDS-PAGE and stained with Coomassie as described in *Materials and Methods*. Gels show that there is high expression of p38γ proteins in *E.coli* and that the Ni-NTA agarose successfully retains the tagged proteins.

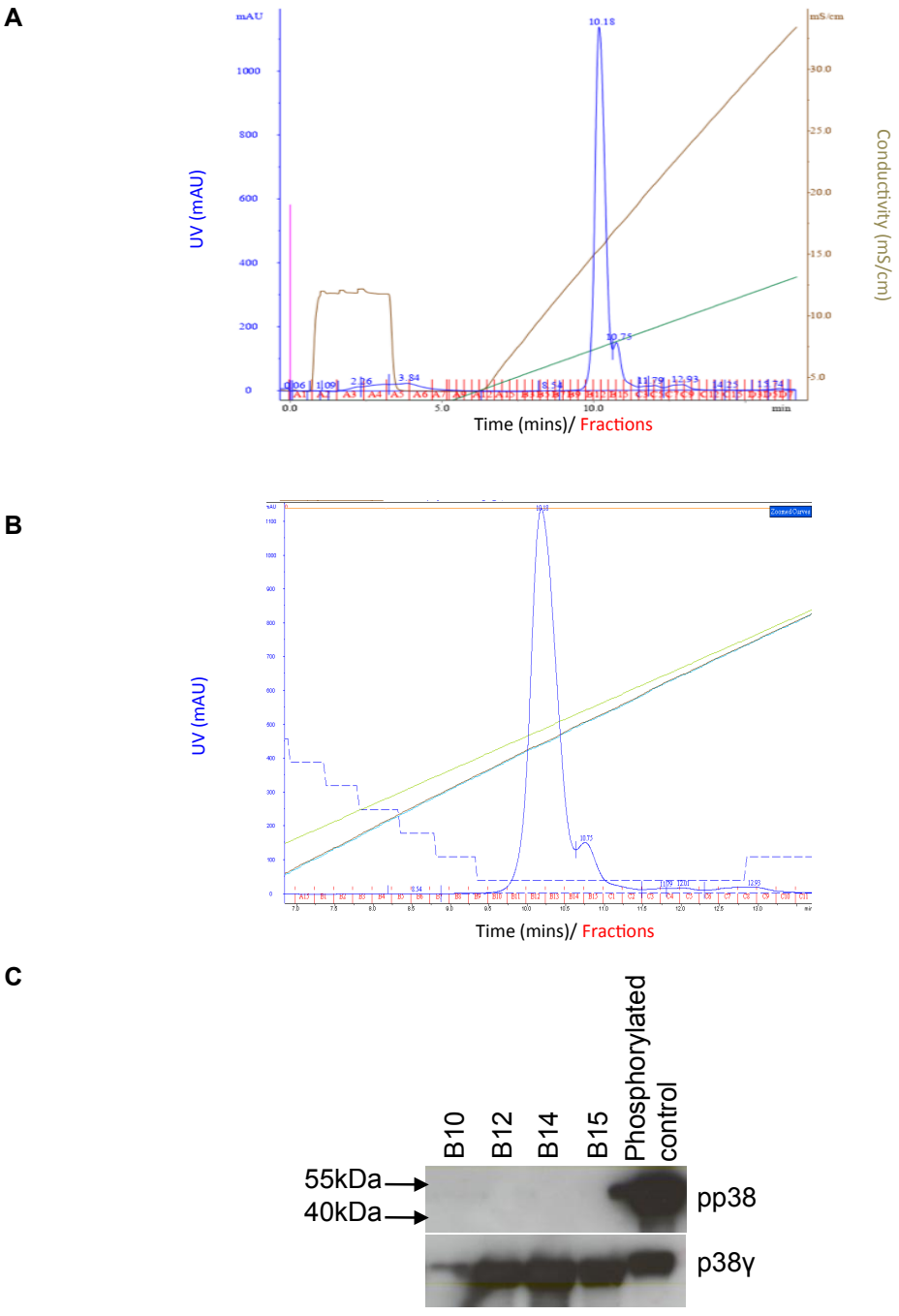

Figure 3.3 Anion exchange chromatography of 6xHis-WT-p38γ protein

Purity of WT p38γ obtained following metal affinity capture was refined by anion exchange chromatography as described in *Materials and Methods*. ***A,*** Chromatograph showing elution of WT p38γ. ***B,*** A higher magnification of the WT p38γ elution peak displays an appending shoulder peak. ***C,*** Immunoblot analysis of fractions corresponding to the peak (B10 – B14) and shoulder peak (B15) reveals that the protein eluted is p38γ and that the peak shoulder does not correspond to a phosphorylated form of p38γ.

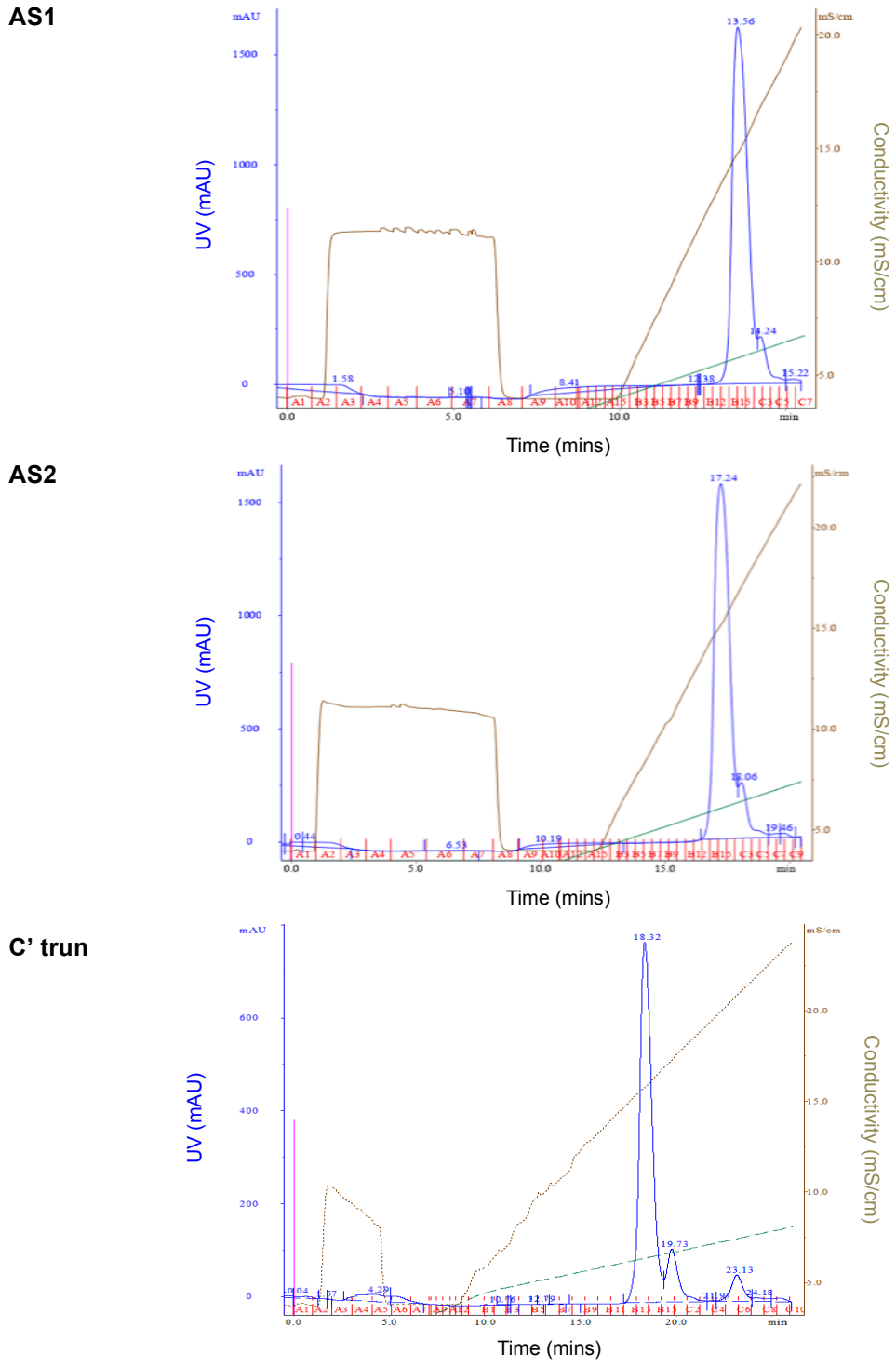

Figure 3.4 Anion exchange chromatography of 6xHis p38γ mutant proteins.

Purity of mutant p38γ proteins, obtained following metal affinity capture was refined by anion exchange chromatography, as described in *Materials and Methods.* Chromatographs obtained for AS and C' truncated p38γ proteins are consistent with the results obtained following anion exchange of WT p38γ.

To assess activation of p38γ proteins an antibody specific to the phosphorylated tyrosine 185 residue (pTyr), in the activation loop of p38γ, was used to probe membranes. As shown in Figure 3.5A, this antibody detects two bands when WT and AS p38γ proteins were activated by MKK6EE, whereas no bands are detected in the corresponding non-activated controls. The presence of two phospho bands suggested that maximal activation of p38γ may not have occurred during activation and that several phospho- species were present, perhaps a mono-phosphorylated and a dual-phosphorylated form of p38γ. Re-probe of the same membrane using a total p38 antibody detects the unphosphorylated protein in the non-activated group. Despite the unexplained presence of two phospho bands, the results suggests that activation of proteins was achieved by MKK6EE and this finding is mirrored in Figure 3.5B. Activated kinases from A were used in *in vitro* kinase assays to mediate phosphorylation of ATF2. WT and AS kinases were deemed catalytically competent, as phosphorylation of ATF2 was observed. Importantly, the mutations had no effect on the catalytic activity of the kinases and mediated phosphorylation of ATF2 to the same extent as WT p38γ.

Initial analysis of the Figure 3.5A suggested that maximal activation of p38γ had not occurred. This lead to the rationale that the reaction conditions used for activation were perhaps not optimal. To test this hypothesis and to optimise the activation of p38γ, the following changes were implemented: 1) increasing the concentration of MKK6EE, 2) increasing the concentration of ATP and lastly 3) increasing the activation reaction time. In the current activation reaction 20 ng/μL of MKK6EE was used to activate 250 ng/μL kinase (0.08:1). MKK6EE at this concentration had proven effective in maximally activating p38α in our laboratory (data not shown) but various different concentrations of MKK6EE have been reported in the literature to activate WT p38γ. The concentration of ATP was increased from 0.1 mM to 0.5 mM and the reaction was allowed to occur overnight as opposed to 30 min.

The outcome of these optimisations, to the activation reaction of WT p38γ, is shown in Figure 3.6. In addition to the pTyr antibody, samples in parallel were

also probed with a dual phosphorylated p38 antibody. The anti-pp38 antibody has previously been characterised in our laboratory to have a high affinity for the phosphorylated threonine in the activation loop and little affinity for phosphorylated tyrosine. Therefore in combination with the anti-pTyr antibody and total antibody, an attempt was made to deduce the composition of phospho-residues in each of the two bands previously detected by Phos-tag™ SDS-PAGE and Western blotting. Blots probed with phospho antibodies were stripped and re-probed with an antibody against p38γ to detect total protein.

Figure 3.6 reveals that, at the same ratio of p38γ to MKK6EE, increasing the concentration of ATP or the reaction time (lane 1) did not cause a deviation from the initial result observed in Figure 3.5. As before, two dominant bands are detected by the pTyr antibody (labelled 2 and 3 in red) and a fainter upper band is now also visible (labelled 1). Furthermore, an increase in the concentration of MKK6EE did not affect the outcome of the activation, as no changes in the banding pattern are observed. Probe of samples with the pp38 antibody, which has a propensity for the phosphorylated threonine of the activation loop, reveals a banding pattern similar to that of the pTyr antibody probe: a faint upper band (band 1) and two dominant lower molecular weight bands (bands 2 and 3). This suggests that a) p38γ has successfully been phosphorylated at the two crucial residues of the activation loop and b) within the pool of dual phosphorylated activated p38γ, phosphorylation is occurring at additional residues, outside the activation loop, resulting in the detection of multiple bands when probed with the phospho antibodies. However, a re-probe of membranes with the total p38γ antibody also reveals that some non-phosphorylated p38γ persists following activation (band 4).

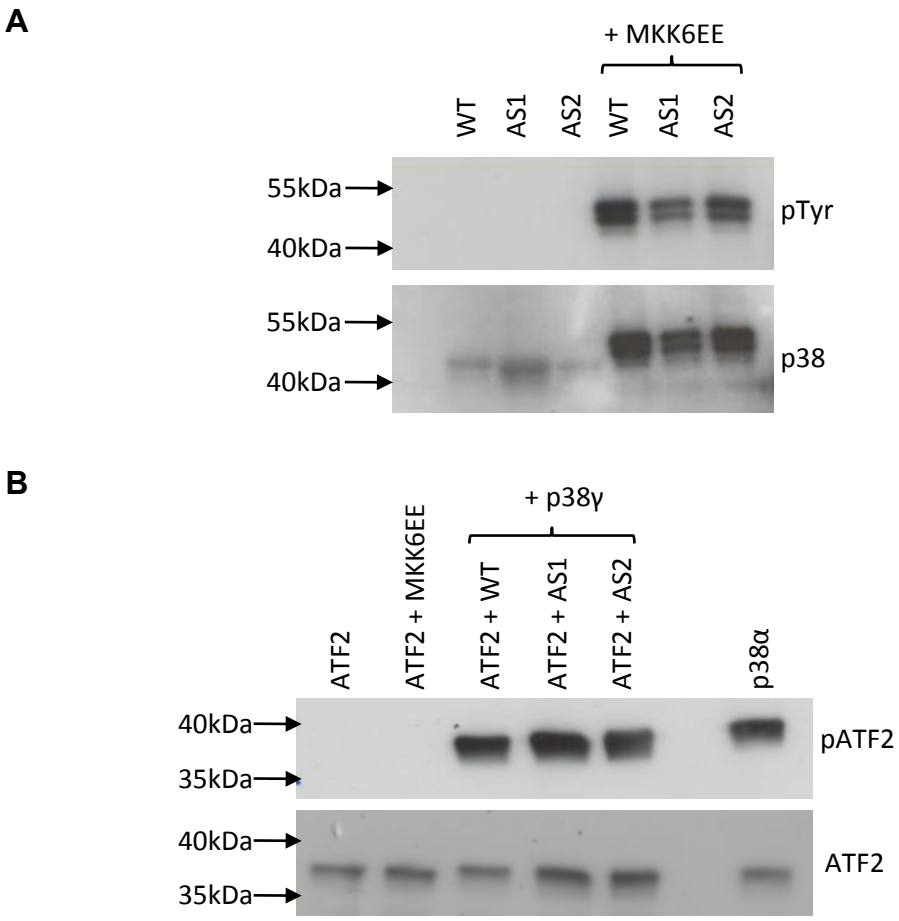

Figure 3.5 Small scale activation of purified 6xHis-p38γ proteins using MKK6EE and validation of kinase competency

A, Phos-tag™ SDS-PAGE and Western blot analysis of activated WT and AS p38γ proteins. Purified proteins were activated by MKK6EE *in vitro* and resolved by 10% Phos-tag™ SDS-PAGE, as described in *Materials and Methods*. ***B,*** Immunoblot analysis of ATF2 phosphorylation after *in vitro* exposure to activated WT and AS p38γ proteins. Samples were resolved by 10% SDS-PAGE, as described in *Materials and Methods*. All p38γ proteins successfully activated ATF2 *in vitro*.

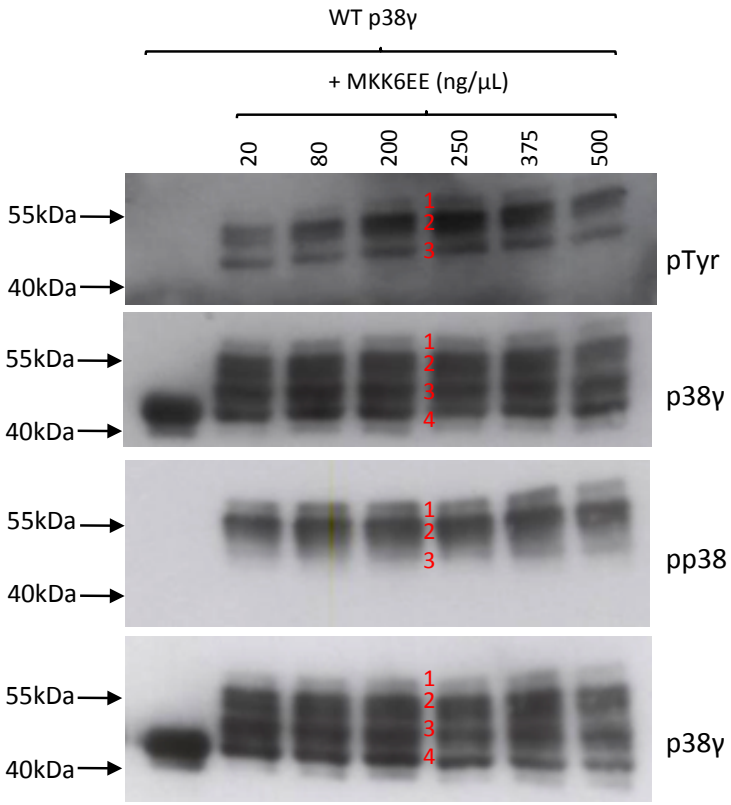

Figure 3.6 Optimising activation of 6xHis-p38γ protein (WT)

Phos-tag™ SDS-PAGE and Western blot analysis of activated WT p38γ. 250 ng/µL of purified protein was activated by different concentrations of MKK6EE *in vitro*, as described in *Materials and Methods*. Samples were resolved by 10% Phos-tag™ SDS-PAGE, as described in *Materials and Methods*. The anti-pTyr183 p38 and anti-pp38 antibodies detect multiple dual phosphorylated species (labelled 1, 2 and 3). Re-probe of membranes with the anti-p38γ antibody reveals that a non-phosphorylated species (labelled 4) also persists, despite optimisations to enhance activation.

As increasing the concentration of MKK6EE did not affect the activation of p38γ, it could be possible that the phosphorylation events observed are not MKK6EE mediated, but caused by auto-activation of p38γ. To test this possibility, additional controls were included in the experimental set up. However this was not the case, as phosphorylation was only detected in the presence of MKK6EE (Figure 3.7A). A review of similar, published, experiments all report MKK6 as the upstream activating kinase. However, MKK3 has also been reported to activate all isoforms of p38-MAPK excluding p38β. Therefore, activation of p38γ was also tested with constitutively active MKK3EE. It can be seen in Figure 3.7B that phosphorylation and activation of p38γ using MKK3EE was inferior compared to MKK6EE mediated activation.

Despite several different changes to the activation conditions, attempts to drive maximal activation of p38γ were largely unsuccessful and activation was consistently observed to the same submaximal extent. From the Phos-tag^{TM} SDS-PAGE and Western blotting analyses, we observe several bands that are immuno-reactive to both phospho antibodies tested and an additional band that appears upon total antibody probe. This suggests that there is a pool of dual activated p38γ, with some non-phosphorylated protein present. Although not maximally activated, all kinases were able to phosphorylate downstream substrate ATF2 (Figure 3.5B) and therefore this extent of activation was deemed satisfactory for subsequent experiments. Therefore, a large-scale activation of WT and AS kinases was carried out as per the original protocol, the outcome of which can be seen in Figure 3.8. As before, we observe the same banding pattern but importantly we observe uniform activation of WT and AS kinases. Following activation, kinase activity was comprehensively validated for catalytic activity (Figure 3.9), again by assessing phosphorylation of ATF2. Phosphorylation of ATF2 is only observed in the presence of active kinases, and when reactions are supplemented with ATP in the kinase reaction buffer. Again we observe that AS mutant kinases are able to mediate phosphorylation of ATF2 to the same extent as WT p38γ and lastly we observe that phosphorylation of ATF2 is not MKK6EE mediated.

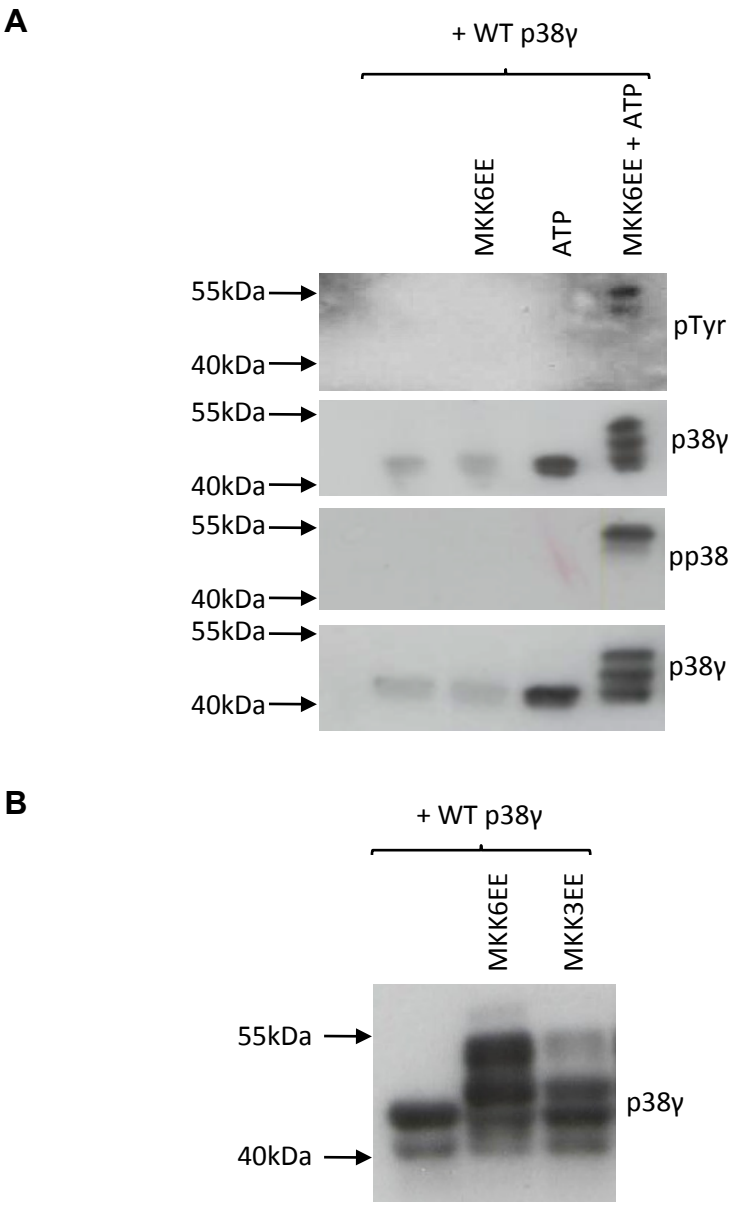

Figure 3.7 Further optimisations to p38γ activation reaction

Phos-tag™ SDS-PAGE and Western blot analysis of activated WT p38γ. Purified protein was activated by MKK6EE *in vitro*, as described in *Materials and Methods*. Samples were resolved by 10% Phos-tag™ SDS-PAGE, as described in *Materials and Methods*. ***A,*** Activation of WT p38γ is not auto-phosphorylation as phosphorylation is only detected in the presence of MKK6EE. ***B,*** MKK3EE mediated activation of WT p38γ is inferior to MKK6EE activation of p38γ.

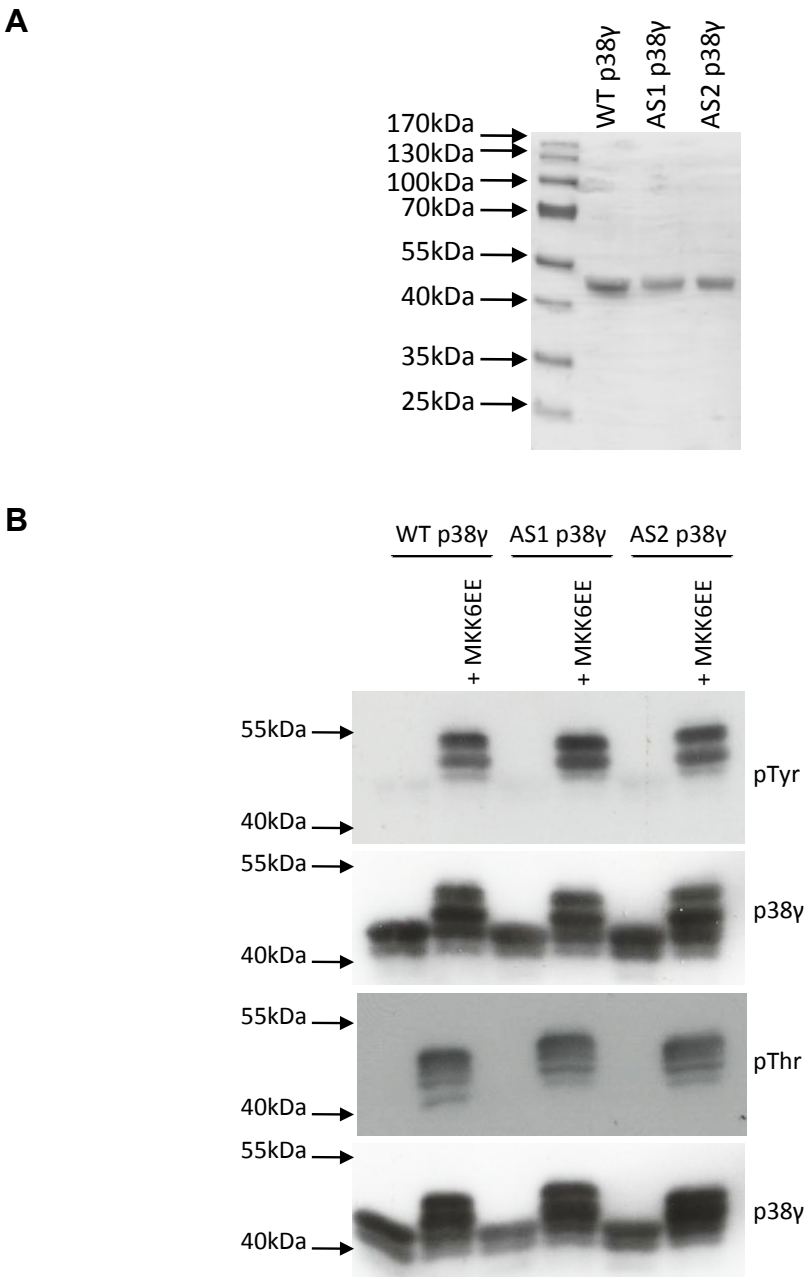

Figure 3.8 Final preparation of activated 6xHis-p38γ proteins

A, To assess purity of the final preparation of p38γ proteins, samples following activation and re-purification, were prepared in 5 x sample buffer, resolved by 10% SDS-PAGE and stained with Coomassie as described in *Materials and Methods*. ***B,*** Phos-tag™ SDS-PAGE and Western blot analysis of activated WT and AS p38γ proteins. Purified proteins were activated by MKK6EE *in vitro*, as described in *Materials and Methods*. Samples before and after activation with MKK6EE were resolved by 10% Phos-tag™ SDS-PAGE, as described in *Materials and Methods*. WT and AS p38γ kinases are phosphorylated to the same extent.

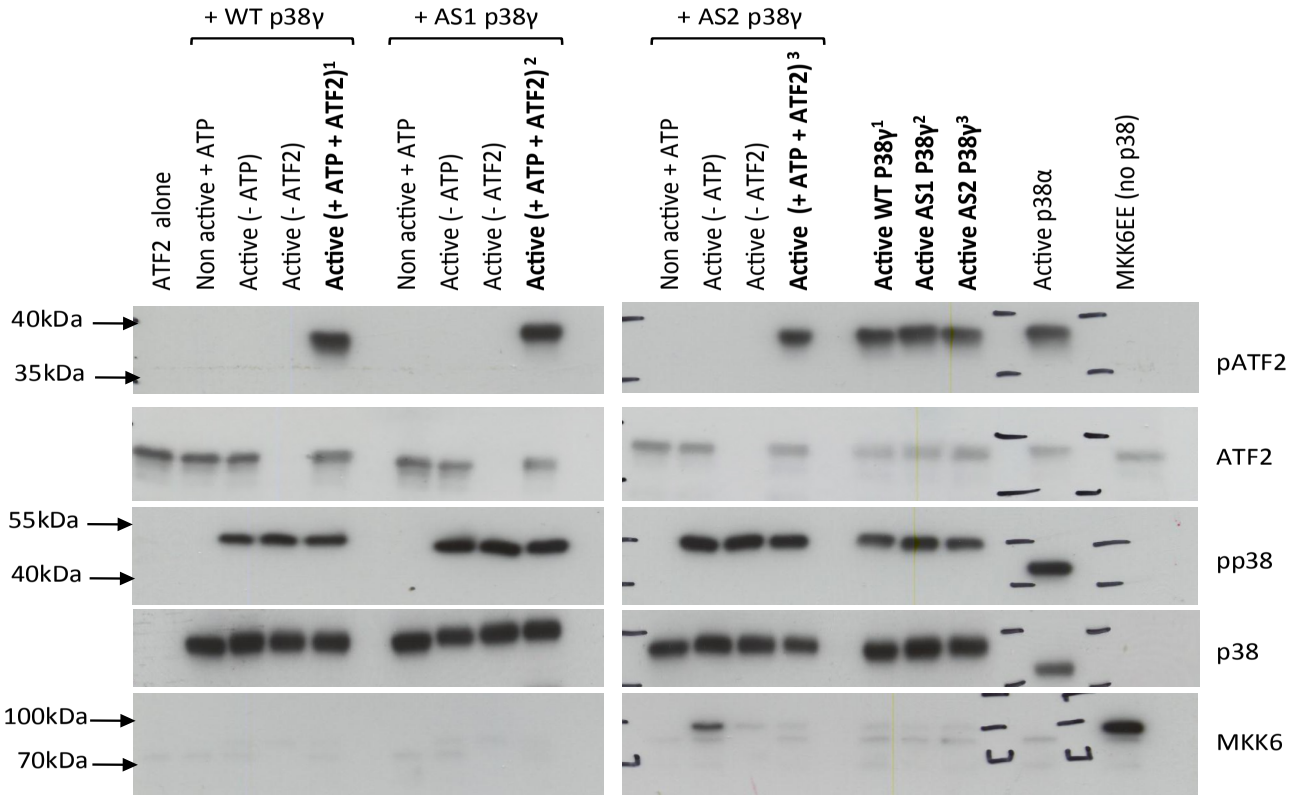

Figure 3.9 **Activated p38γ proteins phosphorylate ATF2 *in vitro***

Immunoblot analysis of ATF2 phosphorylation after *in vitro* exposure to non-active and MKK6EE- activated p38γ proteins as described in *Materials and Methods*. Samples were resolved by 10% SDS-PAGE, as described in *Materials and Methods*. Non-active p38γ proteins are unable to phosphorylate ATF2. MKK6EE activated p38γ proteins can only phosphorylate ATF2 in the presence of ATP. As loading is spread across two gels, loading of numbered samples is repeated on second gel to allow for comparison.

3.3.3 Activation and Validation of Kinase Activity of C' truncated p38γ

Following on from the findings of the experiments carried out using WT and AS kinases, carboxy-terminal truncated p38γ was activated in the same manner. Whilst included here alongside the generation of WT and AS kinases, this particular mutant was not produced in parallel to the preceding kinases. As such, knowledge gained from prior activation experiments was utilised and activation of this mutant was not as extensively characterised.

Therefore a basic assessment of phosphorylation was made, by comparing the extent of activation to previously activated WT p38γ. It can be seen in Figure 3.10A that the same banding pattern, and therefore the same extent of activation, is observed for both kinases. Activated carboxy-terminal truncated p38γ was also catalytically competent, as it was able to successfully mediate phosphorylation of ATF2 (Figure 3.10B).

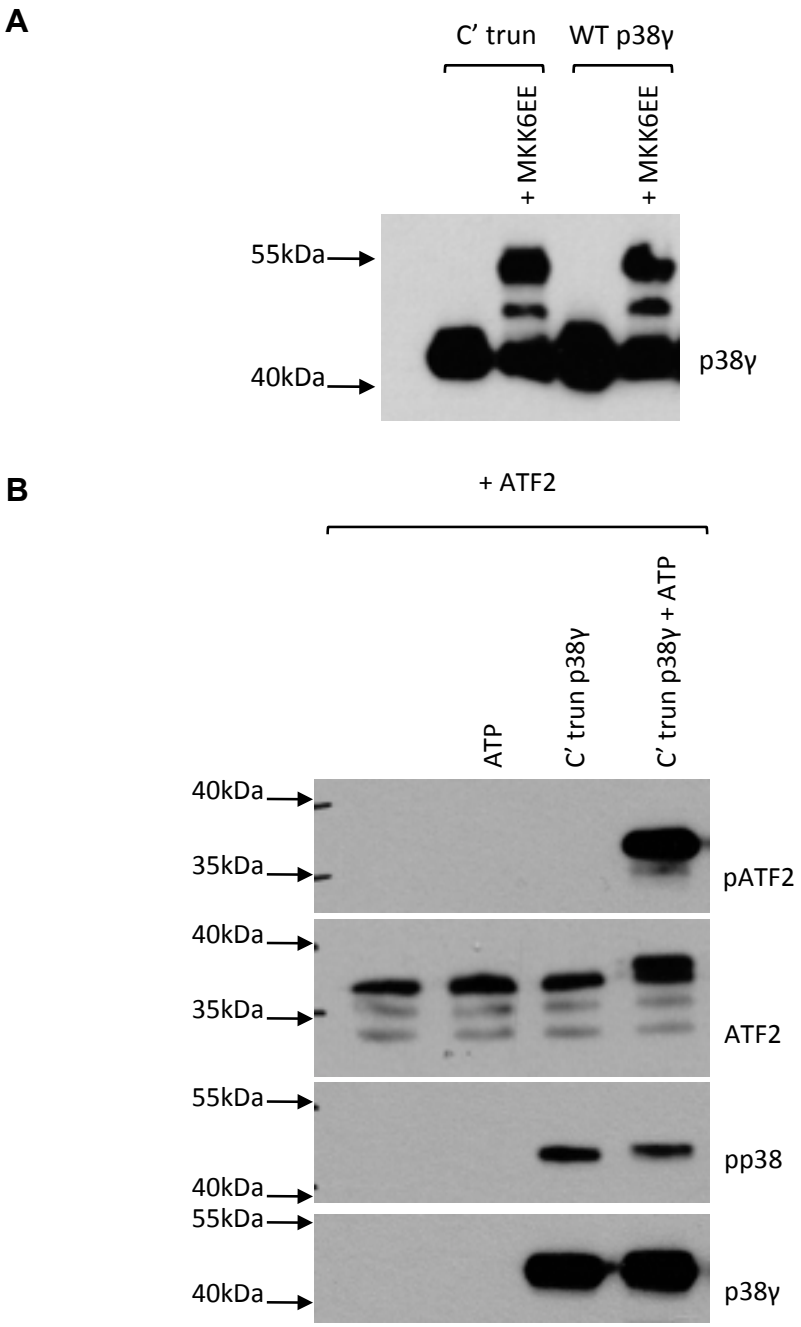

Figure 3.10 Activation of C' truncated p38γ and validation of kinase competency

A, Phos-tag™ SDS-PAGE and Western blot analysis of p38γ proteins. Purified proteins were activated by MKK6EE *in vitro*, as described in *Materials and Methods*. Samples before and after MKK6EE activation were resolved by 10% Phos-tag™ SDS-PAGE, as described in *Materials and Methods*. ***B,*** Immunoblot analysis of ATF2 phosphorylation after *in vitro* exposure to activated C' truncated p38γ. Samples were resolved by 10% SDS-PAGE, as described in *Materials and Methods*.

3.4 Discussion

3.4.1 Summary

To fulfil the proposed strategies for elucidating the signalling pathway of p38γ in the myocardium, an *E. coli* expression system has successfully been used to obtain recombinant WT and mutant p38γ proteins. Results in this chapter show that high yields of recombinant p38γ proteins were obtained following metal affinity purification. Anion exchange chromatography further refined the purity of the proteins obtained.

Following the two-step purification process, p38γ proteins were subject to activation by upstream activating kinase, MKK6EE. The resulting activation of proteins was assessed by Phos-tag^{TM} SDS-PAGE and Western blot analysis. The results obtained following activation show that obtaining maximal activation of isolated proteins presented a challenge. Measures taken to enhance activation did not improve activation. Although maximal activation could not be obtained, kinases displayed uniform activation. Importantly, purified activated proteins were catalytically competent, as all proteins were able to utilise ATP to phosphorylate ATF2 in *in vitro* kinase assays.

3.4.2 Activation of p38γ

3.4.2.1 MKK6 activation of p38γ

Upstream kinases MKK6 and MKK3 have been reported to activate p38γ *in vivo* and *in vitro.* In the same study, MKK4 is reported to activate p38γ in an *in vitro* setting only. However, the activation kinetics of p38γ activation by MKK4 are much slower in comparison to kinetics of MKK4 activation of p38α, under identical conditions (Cuenda et al. 1997). For this reason, MKK6EE was initially utilised in this study for activation of p38γ. Analysis of the activation of p38γ by MKK6EE by Phos-tag^{TM} SDS-PAGE and Western blot analysis using phospho-specific and pan-isoform antibodies revealed that a proportion of non-activated p38γ remained post activation. This was in contrast to the maximal activation of

p38α achieved under identical conditions in our laboratory in a parallel study (data not shown). Despite best efforts at optimising maximal activation of p38γ proteins, a proportion of non-active p38γ still persisted. Increasing the concentration of MKK6EE did not affect the activation status. Furthermore, a comparison between MKK6EE and MKK3EE mediated activation of p38γ revealed that MKK6EE was more effective at activating p38γ. Similarly, attempts at troubleshooting such as increasing the availability of ATP or increasing the reaction time, did not improve the activation status of the proteins.

There are few studies that can be found that report on the molecular events that determine the activation of p38-MAPKs. Further insight into this area of signalling may provide insight into how maximal activation of p38γ can be achieved. It is clear that activation of p38-MAPKs in cells is not an isolated signalling cascade, as it involves many different upstream signals that lead to p38 activation. One possibility is that maximal activation of p38γ can only be attained in such a cellular context, as it requires the contribution of unknown factors such as scaffold proteins or auxiliary kinases that are not present in an *in vitro* setting.

3.4.2.2 Post-translational modifications

Whilst expression of proteins in bacterial cells has the advantage of easily producing large quantities of protein, a limitation of using this system to express proteins is that bacterial cells cannot perform post-translational modifications that are required for required for mammalian protein function. Akin to phosphorylation of proteins, other post-translational modifications of proteins can also alter their function. Furthermore, post-translational modifications can determine the tertiary and quaternary structure of proteins and thus may affect signalling. However, it is unlikely that expression of p38γ proteins in bacteria has resulted in improper folding of p38γ proteins, as the proteins obtained are catalytically active and are able to successfully phosphorylate downstream

substrate ATF2. Furthermore, there are no known post-translational modifications of p38γ have been reported in the literature.

3.4.2.3 Assessing phosphorylation of proteins

Phos-tag™ SDS-PAGE with Western blot analysis is a relatively advanced tool used for assessing phosphorylation and, in this case, activation status of a kinase. This type of analysis has not previously been applied to assess the effectiveness of activation of p38γ by MKK6 in other published studies. Traditionally, activation of kinases has been inferred by use of phospho-specific antibodies specific to the kinase, by assessing phosphorylation of a substrate by phospho-directed antibodies or radioactively labelled phosphate incorporation. Other methods used in phospho-proteomics include mass spectrometry analysis of phosphorylated proteins to identify residues that undergo phosphorylation. Data obtained from this study has produced further information regarding the activation of p38γ by MKK6. It is possible that studies utilising p38γ activated *in vitro,* based on the standard protocol as described in *Materials and Methods,* also consist of a proportion of p38γ that remains non-activated following activation.

Using Phos-tag™ SDS-PAGE with Western blot analysis, a detailed analysis of p38γ phosphorylation and activation has been obtained through this study. Importantly, it shows that AS or C' truncation mutagenesis of p38γ does not affect phosphorylation and activation of the kinase. However, it is a time consuming and expensive method for such analysis. It may be necessary in cases where good phospho-specific antibodies are not available for a given protein. But for p38-MAPKs, a selection of phospho-specific antibodies, against residues of the activation loop, is commercially available. Therefore, for future experiments of this kind, it would be sufficient to assess phosphorylation by the use of the phospho-specific antibodies.

4 CHARACTERISATION OF p38γ KINASES AND SUBSTRATE IDENTIFICATION

4.1 Introduction

The *in vitro* chemical genetic or Shokat technique is a powerful method for identifying specific substrates of kinases. However, key questions arise regarding the behaviour of the mutant AS kinase with the use of an unnatural ATP analogue (Shah et al. 1997). In addition to substrate identification, this chapter also covers experiments that aim to characterise the activity of the AS p38γ kinases, in comparison to WT p38γ. A review of the literature covering the Shokat methodology, with a focus on its initial characterisation, is given below.

4.1.1 N^6 expanded ATP analogues

N^6 expanded ATP analogues used in this methodology are described as bio-orthogonal, in that they are silent or do not interact with the natural system, in contrast to its unmodified counterpart (Bishop et al. 2000a). Whilst we can assay if our WT kinase of interest is able to utilise ATP analogues, it is possible that other cellular kinases, with small gatekeeper residues, may also be able to utilise a larger ligand to mediate thiophosphorylation of proteins. This may cause a high background signal and complicate analysis. Fortunately, most kinases contain a bulky residue as the gatekeeper (Huang et al. 2010). Furthermore, this potential issue is offset by the slower kinetics of thiophosphorylation in contrast to phosphorylation (Parker et al. 2005).

The first reported AS kinase to be generated was v-Src (Shah et al. 1997). Quantitative comparison of WT and AS v-Src kinetics revealed that AS v-Src had a lower affinity for ATP and exhibited lower catalytic activity using ATP, in comparison to WT v-Src. However, AS v-Src was more efficient in utilising its orthogonal substrate [γ-^{32}P]*N*^{6}-cyclopentyl-ATP for phospho transfer, than ATP. This is beneficial, as in the presence of cellular ATP, AS kinases would preferentially use the ATP analogue. In addition, the mutant kinase utilises the

ATP analogue at a similar catalytic efficiency to WT v-Src utilisation of ATP. The K_{cat}/K_m of AS v-Src and the ATP analogue is only 50-fold lower than the K_{cat}/K_m of WT v-Src and ATP (Shah et al. 1997).

The kinetics described above do not take into account the second site modification of the N^6 expanded ATP analogues used in this study. Previously, target substrates were labelled with radioactivity donated from the ATP analogue. In this study, ATP analogues that are modified to contain a thiol group on the γ-phosphate are used. This is an additional factor that may alter the rate at which phospho transfer occurs. Analysis of the thiophosphorylation reaction has been performed using ATPγS. When tested with WT and AS versions of a varied selection of kinases (PKCδ, Cdc5 and JNK1), it was found that all kinases could successfully thiophosphorylate substrates using ATPγS (Allen et al. 2007). WT kinases could not utilise N^6 expanded-ATPγS analogues, but all AS kinases could utilise at least one of the N^6 expanded-ATPγS analogues tested. A quantitative analysis revealed that AS kinases had a lower K_{cat}/K_m for ATPγS (not N^6 expanded), in comparison to the respective WT kinase. This is to be expected given the findings from the previous study. As before, the K_{cat}/K_m increased when AS kinases used their preferred N^6 expanded-ATPγS analogue, although still reduced in comparison to WT kinases (Allen et al. 2007). Perhaps more interesting would be a comparison of thiophosphorylation and phosphorylation kinetics of AS and WT kinases.

4.1.2 Analogue Sensitive mutation

The introduction of a gatekeeper mutation to generate AS kinases has widely been reported and characterised (Shah et al. 1997). A key question when introducing any mutations in a protein is if mutations are functionally silent, and if not, how kinase activity and substrate recognition is affected. As discussed above, mutation of the gatekeeper residues in the above examples, results in a lower catalytic efficiency when using ATP as a phospho donor. However, no alterations in substrate selectivity or specificity have been reported for previously generated AS kinases, despite the proximity of the mutations to the substrate-binding site. For example, WT and AS v-Src displayed the same K_m

for substrate RR-Src, suggesting that mutations do not affect specificity (Shah et al. 1997). Selectivity between WT and AS v-Src was also consistent as both kinases phosphorylated an identical set of proteins when expressed in Sf9 insect cells (Shah et al. 1997). No differences in substrate or phosphorylation site specificity were observed between WT and AS cdk2 (Elphick et al. 2009). Data from this study (Figure 3.9) also demonstrates no change in substrate selectivity, as both WT and AS p38γ kinases were able to phosphorylate ATF2 to similar intensities.

4.1.3 Inhibitors

The Shokat methodology encompasses a third advantageous component. This is the ability to inhibit AS kinases with highly selective, cell permeable inhibitors that target the unique, enlarged ATP binding pocket (Bishop et al. 1998, Bishop et al. 2000a). Inhibitors 1-Napthyl-PP1 (Na-PP1) and 1-NapthylMethyl-PP1 (NM-PP1) are modified compounds of Src family kinase inhibitor, PP1. The derivatives are modified by the tethering of bulky chemical groups to a position corresponding to the enlarged pocket in the kinase active site. Therefore, they do not inhibit WT kinases, but selectively inhibit the mutant AS kinase. Whilst these inhibitors are modified compounds of PP1, which targets tyrosine kinases, they have also been shown to be potent inhibitors of serine/threonine AS kinases (Bishop et al. 2000b).

4.2 Specific Methods

4.2.1 Inhibitor IVKs

IVKs with inhibitors were performed as described in Section 2.9 but with the addition of the following inhibitors: 10 μM BIRB 796, 10 μM SB203580, 10 μM Na-PP1, 10 μM NM-PP1, 1 mM Staurosporine, and various concentrations of Pirfenidone. All inhibitors were added directly to kinase assays with the exception of BIRB 796 and Pirfenidone, which were pre-incubated with p38γ before addition of ATP and substrate. Pre-incubation of BIRB 796 with p38γ

was at room temperature for 30 min and Pirfenidone was pre-incubated for different time intervals at room temperature or at 30°C.

4.2.2 TAB1 IVK

To assess phosphorylation of TAB1 (Transforming Growth Factor-β (TGF-β) activated protein kinase 1 (TAK1) binding protein 1), IVKs were performed using HEK cell lysates overexpressing TAB1 proteins. 15 µL of HEK cell lysates were used per reaction and reactions were set up as described in Section 2.9.

4.2.3 Thiophosphorylation of heart proteins

To identity potential substrates of p38γ in the heart, IVKs were set up using homogenised heart tissue as a substrate source. Kinase reactions were set up in the same manner as described in Section 2.9 with some modifications. Kinase reactions were performed with 250 µg of heart homogenate, 100 ng of kinase, 0.5 mM PheEthγS, 0.2 mM ATP and 3 mM GTP. If subsequent isolation and capture of thiophosphorylated proteins was performed (section 4.2.4), then reactions were scaled up to 220 µL and contained 2 mg of heart homogenate, 20 µg of kinase, 1 mM PheEthγS, 0.4 mM ATP and 3 mM GTP.

4.2.4 Purification and Isolation of Thiophosphorylated Heart Peptides

4.2.4.1 Trypsin digestion

Following thiophosphorylation of heart proteins as described above, samples were processed by Dr Eva Denise Martin at University of California, San Francisco, with guidance from the Shokat laboratory. Comprehensive covalent capture methodology can be found in Hertz et al. 2010. Samples were mixed with denaturing buffer (100 mM NH_4HCO_3, 2 mM EDTA, 10 mM TCEP (tris(2-carboxyethyl)phosphine) and 6 M Urea) and incubated at 55°C for 1 h. Samples were cooled for 10 min at room temperature before samples were diluted 1:3 with 50 mM NH_4HCO_3 and TCEP concentration re-adjusted to 10 mM. 1 µg of Sequencing Grade Modified Trypsin (Promega) was then added per 20 µg of

heart lysate and pH of each sample adjusted to pH 8.0. Samples were incubated overnight on a rotating platform at 37°C.

4.2.4.2 Solid-phase extraction

The following morning samples were prepared for solid-phase extraction by adjusting the pH to pH 3.0 using 2.5% trifluoroacetic acid (TFA). Samples were desalted using Sep-Pak C18 Classic Cartridges (Waters). Cartridges were pre-equilibrated with 0.1% TFA, 50% acetonitrile solution followed by 0.1% TFA solution before addition of samples to cartridges. Samples were passed through the cartridges 5 times before cartridges were washed with 10 mL of 0.1% TFA. Peptides were then eluted from the resin using 1 mL of 0.1% TFA, 50% acetonitrile solution into microcentrifuge tubes and desalted peptides were concentrated to approximately 50 µL using a speed vacuum. 50% Acetonitrile and HEPES pH 7.3 was added to the samples to final concentration of 50 mM and pH adjusted using 5% NaOH to pH 7.0.

4.2.4.3 Covalent capture of thiophosphorylated peptides

Thiophosphorylated peptides were captured using iodoacetyl activated agarose beads (SulfoLink^{TM} Coupling Resin, Life Technologies). Beads were pre-equilibrated in 50 mm HEPES pH 7.0 before addition of peptides in the presence of 25 µg of BSA. Samples were incubated with beads overnight on a rotating platform at room temperature in the dark. The following morning beads were washed and peptides eluted by column chromatography. Columns were pre-washed with 50% acetonitrile and H_2O before loading of sample-bead mix into column. Beads were then sequentially washed with H_2O, 5 M NaCl, 50% acetonitrile and 5% formic acid. Beads were then incubated with 10 mM DTT for 10 min before peptides were eluted. 1 mg/mL oxone pH 4.0 was added to the column and incubated for 30 min to release peptides.

4.2.4.4 Desalting of phospho-peptides

Eluted phospho-peptides were immediately desalted and concentrated using ZipTip 0.6 µL C18 resin (Millipore). ZipTips were prewashed three times with 0.1% TFA, 50% acetonitrile solution followed by H_2O and three 0.1% TFA washes. Phospho-peptide samples were passed through the ZipTip five times after which ZipTips were washed twice with 0.1% TFA. Phospho-peptides were washed three times with 0.1% TFA, 50% acetonitrile solution. Lastly, peptides were concentrated to approximately 10 µL using a speed vacuum.

4.2.5 Liquid Chromatography-Mass Spectrometry/Mass Spectrometry (LC-MS/MS)

Analysis of phospho-peptides was carried out by the Bio-Organic Biomedical Mass Spectrometry Resource at UCSF (A.L. Burlingame, Director) using a Linear Trap Quadropole (LTQ) Orbitrap Velos ETD Mass Spectrometer (ThermoFisherScientific, UK). In brief, peptides were first separated by reverse-phase liquid chromatography (LC) using an Eksigent nano 1D HPLC (Eksigent) equipped with a 75 µM x 15 cm reverse phase C-18 column (LC Packings). A 3 – 32% acetonitrile gradient in 0.1% formic acid was applied (350 nL/min flow rate) to separate peptides. LC-MS/MS was achieved by coupling of the reverse phase column to an atmospheric pressure ionisation source in the mass spectrometer. Peptides were analysed in positive ion mode. The two most intense multiple charged peaks from each MS spectrum were selected for subsequent fragmentation with both collision-induced dissociation (CID) and electron transfer dissociation (ETD) mechanisms to generate fragmentation spectra. MS/MS spectra were searched against the Uniprot database using Protein Prospector software to identify proteins and phospho-sites.

4.3 Results

4.3.1 N^6 expanded ATP analogue screen

In the previous chapter it was concluded that all activated kinases were catalytically competent in phosphorylating ATF2 *in vitro,* using ATP as the phospho donor. The next stage was to identify an N^6 expanded analogue that mutant AS kinases can utilise for phospho transfer to substrates, but WT kinases cannot. To achieve this four different analogues were screened, against WT and AS kinases, in their ability to phosphorylate ATF2. Figure 4.1 depicts the structures of ATP and the candidate N^6 expanded analogues used in the screen. From Figure 4.2 it can be seen that both AS p38γ kinases could utilise ATP and all analogues tested to phosphorylate ATF2. In comparison, WT p38γ could not utilise the analogues to the same efficiency, as a signal for phosphorylated ATF2 could only be observed upon a longer exposure of film to membrane. From the longer exposure, it can be seen that WT p38γ can utilise 6-Bn-ATP (Bn) and 6-Fu-ATP (Fu) for phosphorylation of ATF2, but not 6-PhEt-ATP (PhEt) and 6-(1-MeBu)-ATP (MeBu), to the same extent. Therefore either of these analogues could be used in the Shokat approach.

To be able to specifically track substrates of p38γ amongst a multitude of cardiac proteins, the ATP analogue is also modified at the γ-phosphate. The modification, a thiol group in place of the hydroxyl group, is transferred to the substrate during thiophosphorylation. Therefore, the next step was to establish if the selected analogue, 6-PhEt-ATP, now also modified at the γ-phosphate (6-PhEt-ATPγS), could be utilised by AS p38γ kinases in thiophosphorylation of ATF2 (Figure 4.3). Whilst WT p38γ did not, both AS kinases successfully thiophosphorylated ATF2 using 6-PhEt-ATPγS. A stronger signal was observed for AS1 mediated thiophosphorylation of ATF2 than AS2.

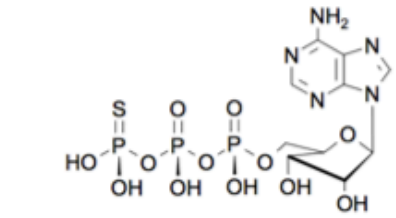

ATP

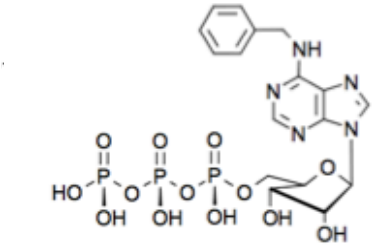

6-Bn-ATP

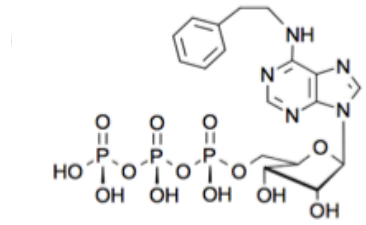

6-PhEt-ATP

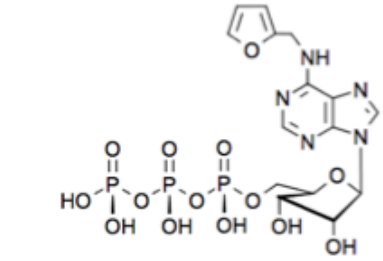

6-Fu-ATP

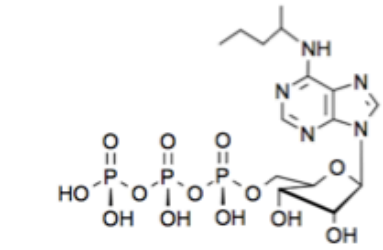

6-(1-MeBu)-ATP

Figure 4.1 Structures of ATP and N^6 expanded ATP analogues

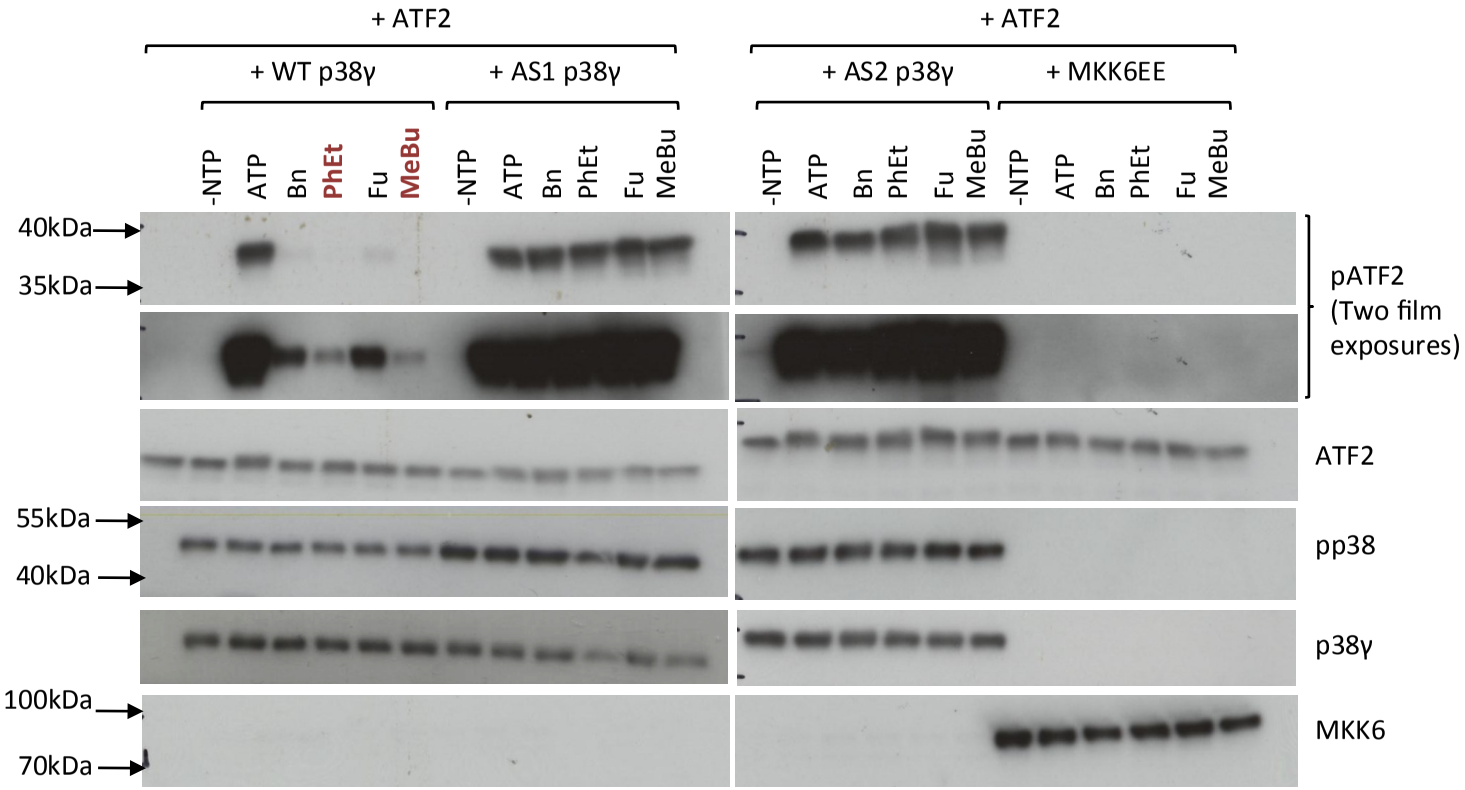

Figure 4.2 **Comparison between the ability of WT and AS p38γ kinases in phosphorylating ATF2 using ATP and N^6 expanded ATP analogues**

Immunoblot analysis of ATF2 phosphorylation after *in vitro* exposure to MKK6EE-activated p38γ proteins in the presence of various N^6 expanded ATP analogues (see Figure 4.1 for structures), as described in *Materials and Methods*. Samples were resolved by 10% SDS-PAGE, as described in *Materials and Methods*. AS p38γ kinases could utilise all analogues tested. WT p38γ was least efficient at utilising 6-PhEt-ATP and 6-(1-MeBu)-ATP for ATF2 phosphorylation.

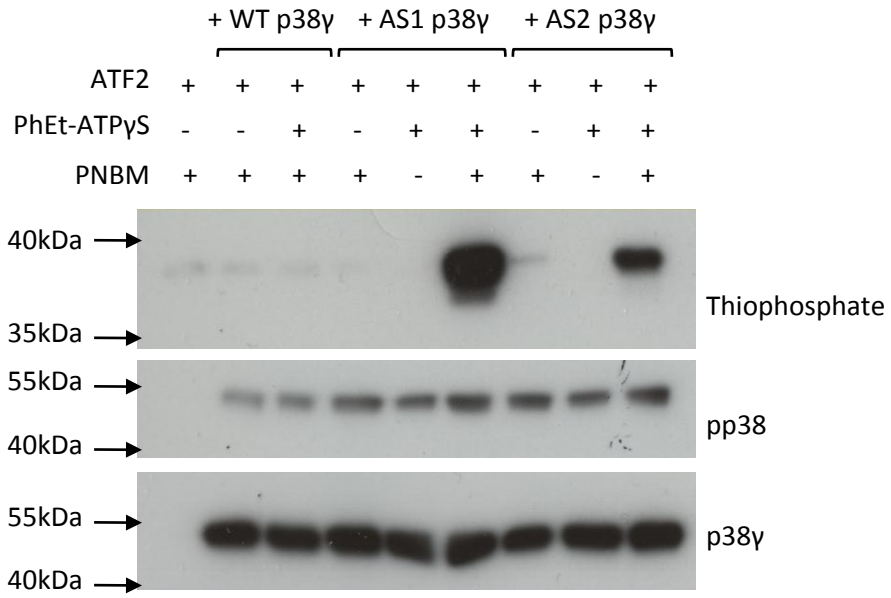

Figure 4.3 ***In*** **vitro kinase assay of ATF2 using p38γ kinases and 6-PhEt-ATPγS**

Immunoblot analysis of ATF2 thiophosphorylation after *in vitro* exposure to MKK6EE-activated p38γ proteins in the presence of 6-PhEt-ATPγS. Samples were resolved by 10% SDS-PAGE, as described in *Materials and Methods*. AS p38γ proteins successfully utilised 6-PhEt-ATPγS for ATF2 thiophosphorylation.

4.3.2 Inhibitor IVKs

Next, a series of inhibitors were tested for their ability to inhibit WT and both AS p38γ kinases. The diaryl urea compound BIRB 796 is a pan p38-MAPK inhibitor (Bain et al. 2007). Pre-incubation of 10 μM of BIRB 796 with WT and AS p38γ kinases, prior to ATF2 assays with ATP, results in complete inhibition of ATF2 phosphorylation by all kinases, as expected (Figure 4.4A). In contrast, pyridinyl imidazole molecules such as SB203580 are isoform selective and only inhibit the p38α and p38β isoforms (Eyers et al. 1998). However, AS p38γ kinases are mutated to contain a smaller gatekeeper residue, therefore should now undergo inhibition by SB203580. Incubation of kinase assays with 10 μM of SB203580 does not cause inhibition of WT p38γ, but results in complete inhibition of ATF2 phosphorylation by AS p38γ kinases (Figure 4.4B).

Na-PP1 and NM-PP1 are modified PP1 analogues that have been shown to specifically inhibit AS kinases. As expected neither analogue was able to inhibit WT p38γ (Figure 4.5). NM-PP1 was also unsuccessful at inhibiting AS kinases. In contrast, incubation with Na-PP1 resulted in complete inhibition of AS2 p38γ mediated ATF2 phosphorylation and almost complete inhibition of AS1 p38γ. Inhibition by staurosporine was also tested. Although staurosporine is generally a non-selective, ATP competitive, inhibitor of protein kinases, it has not been reported to inhibit p38-MAPKs. This is unusual given the high level of homology in the active sites of most kinases. It has been proposed that, kinases that are unsusceptible to staurosporine inhibition cannot accommodate the bulky staurosporine compound, due to the larger residues close to the active site (Meggio et al. 1995). Therefore, it was tested if AS p38γ kinases were susceptible to inhibition by staurosporine. However, under the conditions of the assay used, no inhibition of WT or AS p38γ kinases was observed by staurosporine (Figure 4.5).

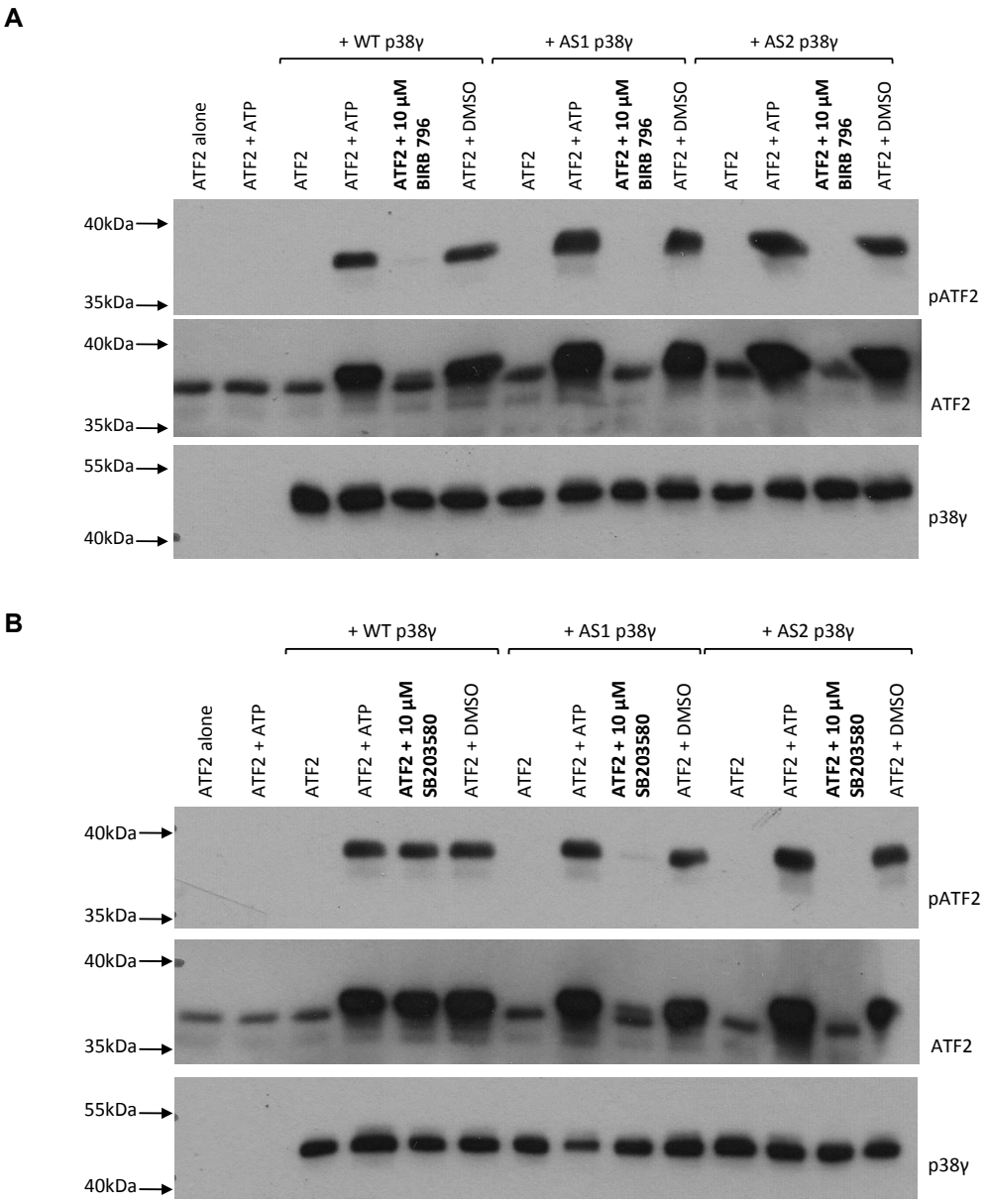

Figure 4.4 Inhibition of WT and AS p38γ kinase activity

Immunoblot analysis of ATF2 phosphorylation after *in vitro* exposure to MKK6EE-activated p38γ proteins in the presence of BIRB 796 (10 μM) (***A***) or SB203580 (10 μM) (***B***), as described in *Materials and Methods*. Samples were resolved by 10% SDS-PAGE, as described in *Materials and Methods*. BIRB 796 (10 μM) inhibits phosphorylation of ATF2 by all kinases tested. SB203580 (10 μM) inhibits phosphorylation of ATF2 by AS p38γ kinases but not WT p38γ.

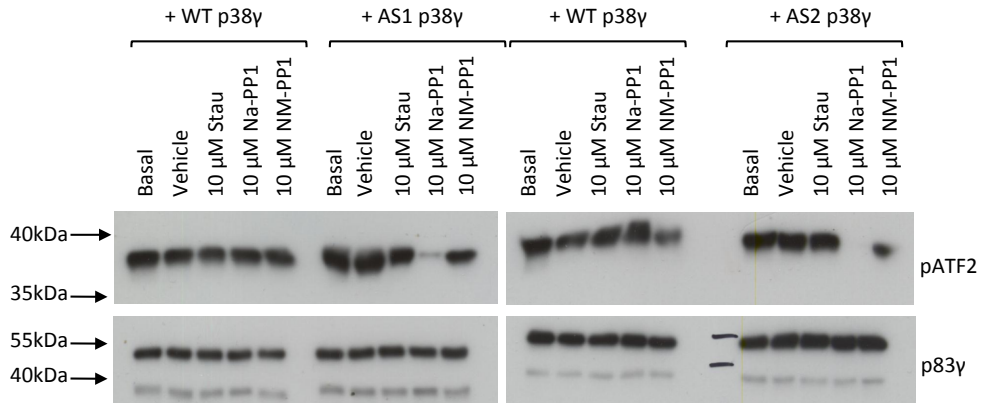

Figure 4.5 Inhibition of WT and AS p38γ kinase activity

Immunoblot analysis of ATF2 phosphorylation after *in vitro* exposure to activated MKK6EE-p38γ proteins in the presence of Staurosporine (10 μM), Na-PP1 (10 μM) and NM-PP1 (10 μM) as described in *Materials and Methods*. Vehicle is DMSO. Samples were resolved by 10% SDS-PAGE, as described in *Materials and Methods*. Staurosporine (10 μM) and NM-PP1 (10 μM) were unable to inhibit phosphorylation of ATF2 by all kinases tested. Na-PP1 (10 μM) partially and completely abolishes phosphorylation of ATF2 by AS1 and AS2 p38γ kinases, respectively, but not WT p38γ mediated phosphorylation.

There is some evidence in the literature to suggest that pirfenidone (PFD) is a specific inhibitor of p38γ (Blatt, Ozes 2005). Therefore, the effect of PFD on the inhibition of WT p38γ was firstly tested. From Figure 4.6A it can be seen that whilst 10 μM BIRB 796 successfully inhibited WT p38γ, no inhibition of WT p38γ was observed following pre-incubation with PFD, at any of the concentrations tested. Different assay conditions were also tested to investigate PFD inhibition further. Both the temperature and time scale of PFD pre-incubation with WT p38γ was altered and short five minute IVKs performed (Figure 4.6B). Despite this, no inhibition of WT p38γ with PFD was observed, although consistent inhibition was observed with BIRB 796.

4.3.3 Isoform substrate selectivity

α1-syntrophin is a known substrate of p38γ. Its phosphorylation has been shown to be dependent on the interaction of its PDZ domain with the C' binding motif of p38γ (Hasegawa et al. 1999). To test this, IVK assays of α1-syntrophin were conducted with AS p38γ and AS p38α isoforms. As p38α lacks the C' PDZ interacting motif, theoretically no thiophosphorylation of α1-syntrophin should occur. However, from Figure 4.7 it can be seen that both isoforms can thiophosphorylate α1-syntrophin and this can be inhibited by Na-PP1.

In contrast, TAB1 is a substrate of p38α that also facilitates its auto-activation. TAB1 interaction with p38α occurs at a bipartite docking site. The C' terminal of TAB1 binds to a canonical upper site, which overlaps with the binding surface used by other proteins that interact with p38α. The N' terminal of TAB1 in contrast binds to a lower non-canonical site, that so far, is TAB1 specific (De Nicola et al. 2013). Therefore to investigate if TAB1 could also undergo phosphorylation by p38γ, HEK cell lysates containing overexpressed WT or mutant TAB1 were subject to IVKs with p38α and p38γ. The mutant TAB1 is 'canonically mutated' in that it cannot interact with p38α at the upper canonical site. From Figure 4.8 it can be seen that incubation with p38α enhances phosphorylation of WT and mutant TAB1 from basal, but no increase in WT or mutant TAB1 phosphorylation is observed with p38γ. Therefore TAB1 is not a substrate of p38γ.

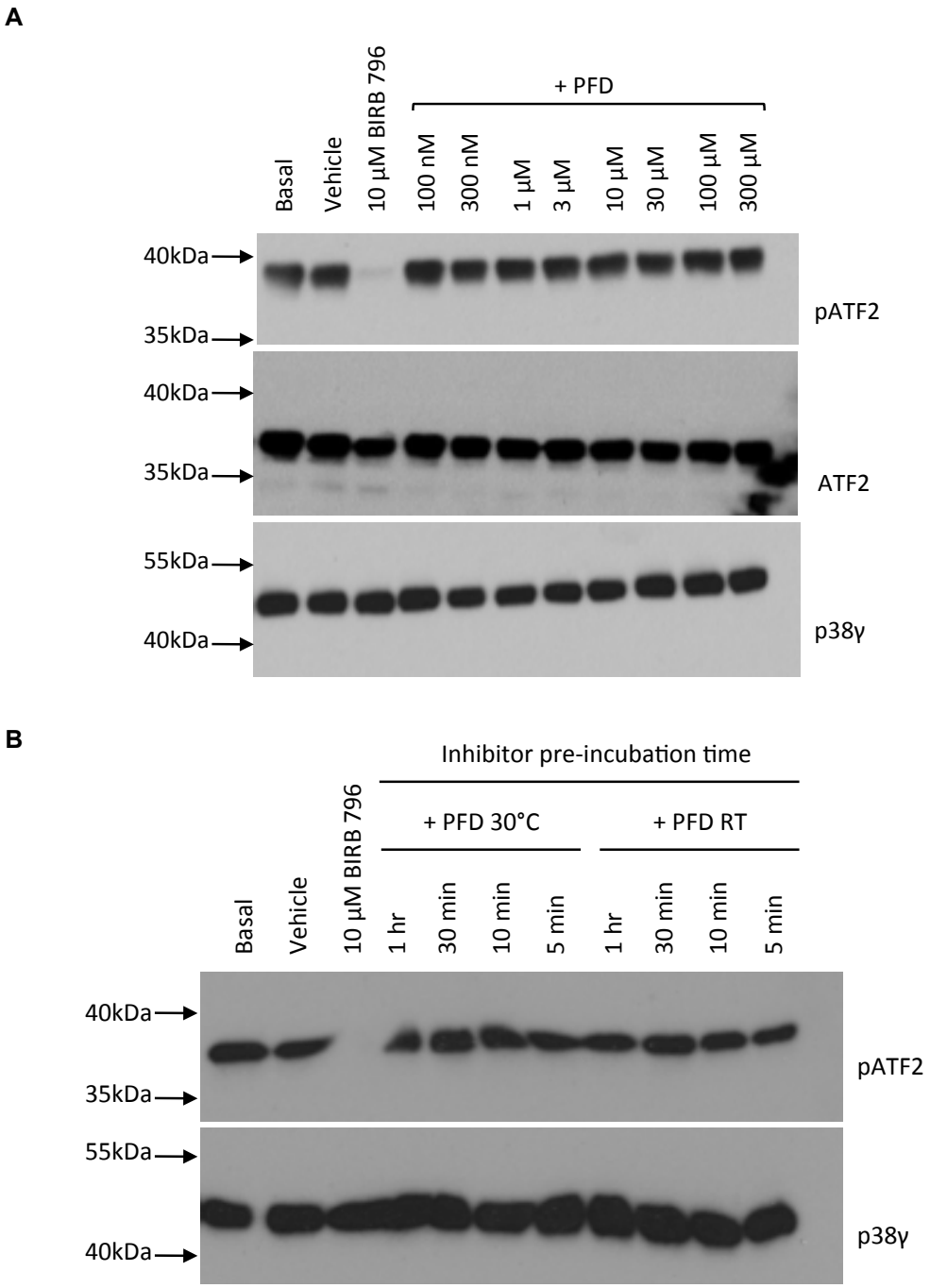

Figure 4.6 Inhibition of WT p38γ kinase activity by pirfenidone.

Immunoblot analysis of ATF2 phosphorylation after *in vitro* exposure to MKK6-activated WT p38γ, in the presence of pirfenidone (PFD). ***A,*** Samples pre-incubated with various concentrations of PFD 30 min before ATF2 IVK, as described in *Materials and Methods*. ***B,*** Samples were pre-incubated with 300 µM PFD for different time periods and at different temperatures before a short 5 min IVK with ATF2. Samples were resolved by 10% SDS-PAGE, as described in *Materials and Methods*. Vehicle is DMSO. No inhibition of ATF2 phosphorylation by PFD is observed under the conditions tested.

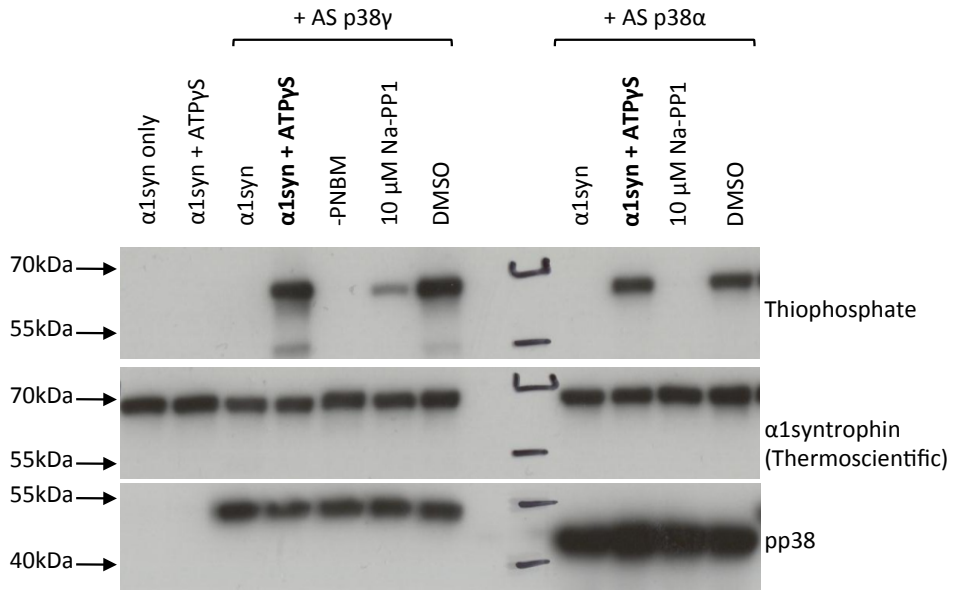

Figure 4.7 Differential substrates of p38γ and p38α isoforms.

Immunoblot analysis of α1-syntrophin phosphorylation after *in vitro* exposure to MKK6EE-activated p38 kinases, as described in *Materials and Methods*. Samples were resolved by 10% SDS-PAGE, as described in *Materials and Methods*. α1-syntrophin is a substrate of both p38γ and p38α. Na-PP1 completely abolishes α1-syntrophin phosphorylation by p38α but only partial inhibition is observed with p38γ.

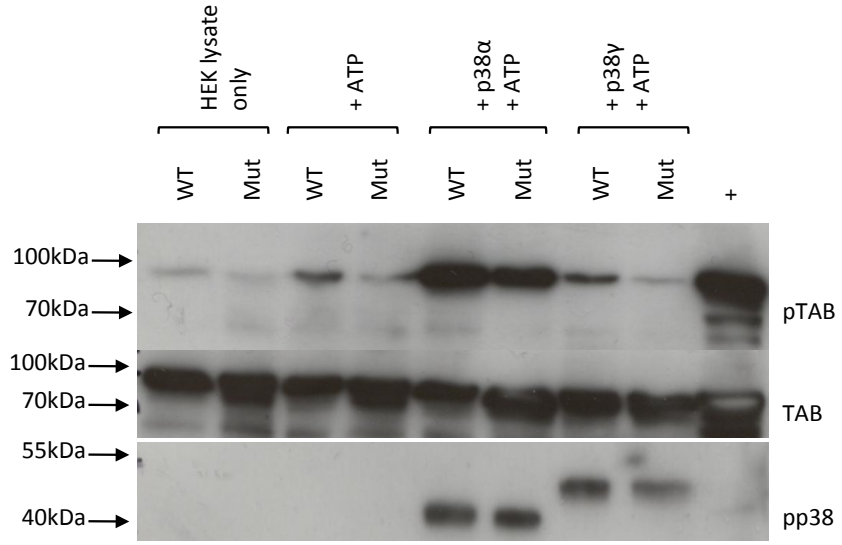

Figure 4.8 Differential substrates of p38γ and p38α isoforms.

Immunoblot analysis of TAB1 phosphorylation after *in vitro* exposure of HEK cell lysate to MKK6EE-activated p38 kinases, as described in *Materials and Methods*. Samples were resolved by 10% SDS-PAGE, as described in *Materials and Methods*. WT and mutant TAB1 is only phosphorylated by p38α, not p38γ.

4.3.4 Thiophosphorylation of cardiac proteins

Following the characterisation of AS p38γ proteins, the crucial experiment was to label cardiac substrates of p38γ, the outcome of which is shown in Figure 4.9. Following IVKs, a small volume of each sample was removed and alkylated for analysis by Western blotting. The bulk of each sample was used to purify and isolate thiophosphorylated peptides. Incubation of heart homogenate with 6-PhEt-ATPγS produces some background thiophosphorylation signal. This is the thiophosphorylation mediated by endogenous kinases that can accommodate the bulky analogue. However, the addition of 0.2 mM ATP and 3 mM GTP to the assay reduces this background signal. ATP and GTP compete with PhEt-ATPγS for occupation of the active site of kinases. As previously discussed, AS kinases preferentially use their analogues. Therefore, the presence of ATP and GTP does not impact upon thiophosphorylation mediated by the mutant AS kinase. Incubation of heart proteins with PhEt-ATPγS together with AS1 p38γ causes thiophosphorylation of many cardiac proteins, in the presence of the competing nucleotides. This signal can only be detected when samples are alkylated with PNBM. ATF2 was also spiked into heart homogenate in parallel kinase assays as a control. The thiophosphorylated ATF2 band can clearly be detected amongst many thiophosphorylated cardiac proteins.

For subsequent purification, isolation and detection of thiophosphorylated peptides, heart homogenate IVKs in triplicate, with and without AS1 p38γ, were used (labelled with asterisks in Figure 4.9.). Each sample was individually processed and analysed by LC-MS/MS. Any proteins that were detected to undergo thiophosphorylation in any control samples were removed from the analysis. Details of the remaining putative p38γ substrates are given in Table 4.1.

The 86 proteins identified in the screen are varied in their cellular localisations and biological functions. Analysis of the proteins was attempted based on cellular localisation or biological function, guided by the current literature concerning p38γ function. For example, given that substrates of MAPKs are

often transcription factors and that p38γ has been shown to translocate to the nucleus under hypertrophic conditions (Dingar at al. 2010), of particular interest were nuclear proteins. At least five of the proteins identified were nuclear: COP9 signalosome complex subunit 1, lamin-B1, pre-lamin-A/C, protein lyric and zinc finger protein 260 (zfp260). Amongst these, zfp260 was the only transcription factor detected.

P38γ has been shown to co-localise with Mitotracker in cardiac myocytes and HEK293 cells (Court et al. 2004). Interestingly, a large subset of proteins identified in this screen were of mitochondrial origin. Sab is the only known mitochondrial substrate of p38γ reported so far (Court et al. 2004). Mitochondrial substrates identified in this list were: 28S ribosomal protein S31, 40S ribosomal protein S20, ATP dependent RNA helicase, coiled-coil-helix-coiled-coil-helix domain-containing protein 2, cytochrome c oxidase copper chaperone**,** malonate-semialdehyde dehydrogenase [acylating], mimitin, mitochondrial antiviral signalling protein, tom22, mitochondrial inner membrane protein and NADH dehydrogenase flavoprotein 1. Whilst sab is phosphorylated by p38γ *in vitro* (Court et al. 2004), it was not identified as a substrate in the current study.

Given the function of p38γ described in non-cardiac tissue, in cytoskeletal regulation, it was anticipated that cytoskeletal protein substrates would be identified. Known cytoskeletal substrates of p38γ; SAP90, SAP97 and α1-syntrophin, were not detected in this screen. Novel cytoskeletal substrates identified were Akap2, Akap12, adenylyl cyclase-associated protein 2, band 4.1-like protein 1, lim domain binding protein 3, myristoylated alanine-rich C-kinase substrate, nebulin-related-anchoring protein and telethonin. Microtubule associated protein tau is one of the early reported substrates of p38γ (Goedert et al. 1997). It was detected as a substrate in the current screen. Alongside tau, several other microtubule-associated proteins were also detected to undergo phosphorylation. Stathmin and microtubule-associated protein 4, known substrates of p38-MAPKs (Parker et al. 1998 and Hu et al. 2010), were identified and previously unreported microtubule-associated protein substrates;

MAP7 domain-containing protein 1 and microtubule associated protein 1b, were also identified as putative substrates of p38γ.

The LC-MS/MS list also contained kinases of the MAPK cascade. Upstream kinases; map2k2 and map2k4 and downstream p38α substrate, mapkapk2 (Engel et al. 1995), were detected as substrates. P38γ itself was also detected to be auto-phosphorylated, interestingly at Tyr^{185}, despite the fact that it is a serine/threonine kinase. Other kinases detected were serine/threonine protein kinase 10, myosin light chain kinase 3 and striated muscle-specific serine/threonine protein kinase. Interestingly, the latter two kinases both belong to the myosin light chain kinase family.

The remaining proteins in Table 4.1 exhibit a wide range or biological functions and do not fall into any obvious functional categories. In addition to the trend analysis described above, analysis of results was also performed to evaluate error that occurs in attributing a phosphorylation event to a specific residue from the fragment ion spectra. Each phospho residue of a peptide is assigned an 'Ascore' number (Beausoleil et al. 2006). The Ascore algorithm helps to determine the confidence in the assignment of a phosphorylation event to a specific residue. When a peptide has two residues in close proximity that could potentially be phosphorylated, then the phospho assignment is likely to carry error and therefore is assigned a lower Ascore.

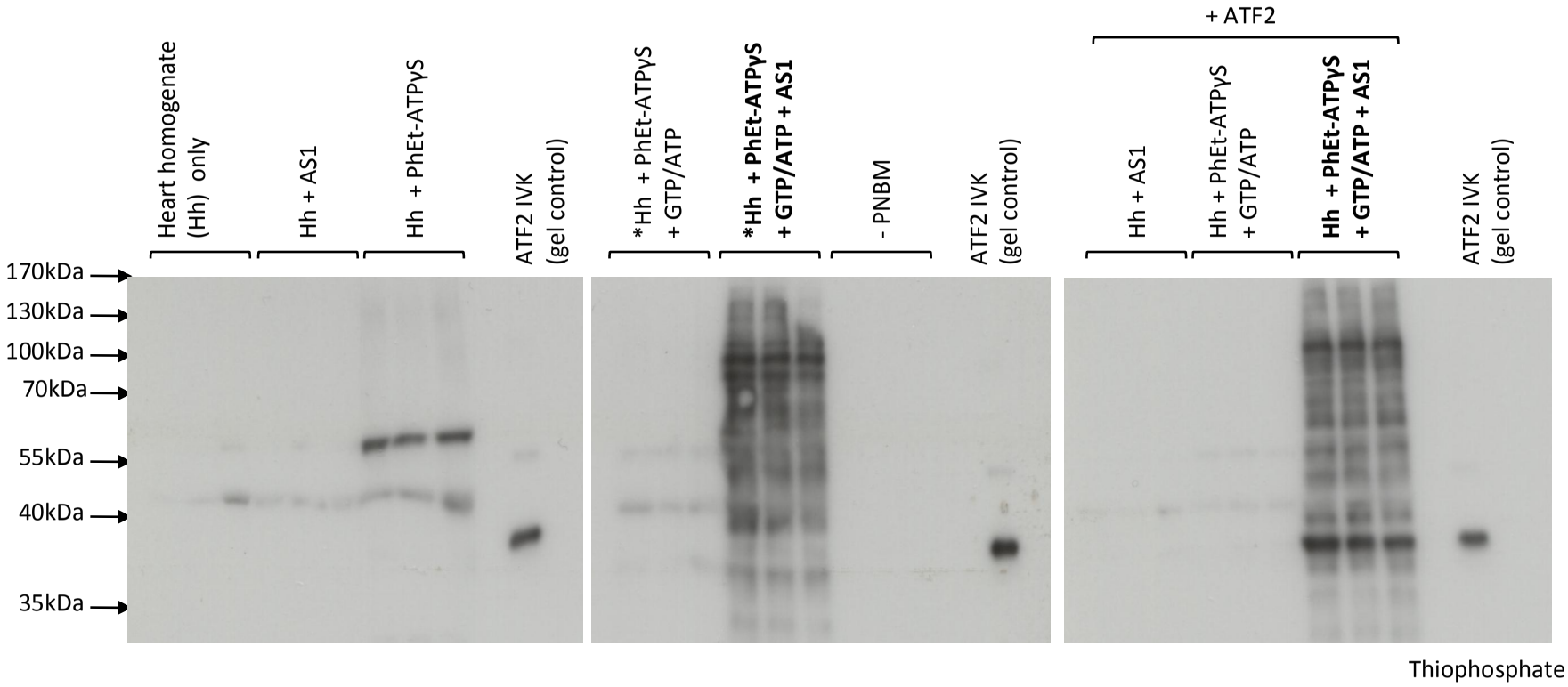

Figure 4.9 Thiophosphorylation of cardiac proteins by AS1 p38γ.

Immunoblot analysis of cardiac protein thiophosphorylation after *in vitro* exposure of heart homogenate to MKK6EE-activated AS1 p38γ and PhEt-ATPγS, as described in *Materials and Methods*. Whilst some endogenous kinases can mediate thiophosphorylation, this is reduced by competition with ATP and GTP. Many cardiac proteins are thiophosphorylated by AS1 p38γ (lanes labelled in bold). Samples were resolved by 10% SDS-PAGE, as described in *Materials and Methods*.

Table 4.1 Putative p38γ substrates identified following Shokat experiment

	GENE	UNIPROT ID	PROTEIN	SAMPLE	START	END	PEPTIDES	RESIDUE	Ascore	PROLINE DIRECTED SITE?
1	Mrps31	Q61733	28S ribosomal protein S31, mitochondrial	2	97	110	VDLSTANVK**T**PKPR	T106	47	Y
2	Rps20	P60867	40S ribosomal protein S20	2	5	19	DTGK**T**PVEPEVAIHR	T9	10	Y
				3	1	19	MAFKDTGK**T**PVEPEVAIHR	T9	10	Y
				3	5	19	DTGK**T**PVEPEVAIHR	T9	8	Y
3	Akap12	Q9WTQ5	A-kinase anchor protein 12	2	260	285	EKEPTKPLE**S**P**TS**PVSNETTSSFKK	S270, T272, S273	0	S270, S273
				2	260	284	EKEPTKPLESPT**S**PVSNETTSSFK	S273	11	Y
				2	1173	1202	QSQV**T**EEEAAAAQTEGPS**T**PSSFPAQEEHR	T1177, T1191	0	T1191
				3	261	285	EKEP**T**KPLE**S**P**TS**PVSNETTSSFKK	T265, S270, T272, S273	0	S270, S273
4	Akap2	O54931	A-kinase anchor protein 2	2	794	823	VKPPP**S**P**TT**EGP**S**LQPDLAPEEAAGTQRPK	S799, T801,T802, S806	0	S799
				2	12	23	SVPGVTS**T**PHSK	T19	7	Y
				3	12	23	SVPGVTS**T**PHSK	T19	10	Y
5	Cap2	Q9CYT6	Adenylyl cyclase-associated protein 2	2	294	313	AQGQIR**S**P**T**KTHTPSPTSPK	S300, T302	0	S300
				3	294	313	AQGQIR**S**P**T**KTHTPSPTSPK	S300, T302	0	S300
6	Apoa2	P09813	Apolipoprotein A-II	1	68	77	THEQL**T**PLVR	T73	10	Y
				2	68	77	**T**HEQL**T**PLVR	T68, T73	0	T73
				2	68	77	THEQL**T**PLVR	T73	36	T73
				3	68	77	THEQL**T**PLVR	T73	17	T73
7	Supv3l1	Q80YD1	ATP-dependent RNA helicase SUPV3L1, mitochondrial	1	665	678	ELDAIIQEGVHNI**T**KLIK	T674	INF	N
				1	720	736	ATEPL**S**PSDKELPLASR	S725	11	Y
				2	720	736	ATEPL**S**PSDKELPLASR	S725	12	Y
				3	720	736	ATEPL**S**PSDKELPLASR	S725	18	Y
				3	720	736	ATEPL**S**P**S**DKELPLASR	S725, S727	0	S725
8	Epb41l1	Q9Z2H5	Band 4.1-like protein 1	2	465	478	RSEAEEGEVR**T**PTK	T475	27	Y

	GENE	UNIPROT ID	PROTEIN	SAMPLE	START	END	PEPTIDES	RESIDUE	Ascore	PROLINE DIRECTED SITE?
9	Cast	P51125	Calpastatin	1	209	231	KKEQKPFT**T**PA**S**PVQSTPSKPSDK	T216, S219	0	Y
				1	211	231	EQKPFTPA**S**PVQSTPSKPSDK	S219	17	Y
				1	209	231	KKEQKPFTPA**S**PVQSTPSKPSDK	S219	23	Y
				2	211	231	EQKPFTPA**S**PVQSTPSKPSDK	S219	17	Y
				2	209	231	KKEQKPFTPA**S**PVQSTPSKPSDK	S219	23	Y
				2	459	471	STYQDKP**ST**PAEK	S466, T467	0	T467
				3	211	231	EQKPFTPA**S**PVQSTPSKPSDK	S219	19	Y
				3	209	231	KKEQKPFTPA**S**PVQSTPSKPSDK	S219	23	Y
				3	459	471	**ST**YQDKP**ST**PAEK	S459, T460, S466, T467	0	T467
10	Comt	O88587	Catechol O-methyltransferase	2	253	265	AVYQGPG**SS**PVKS	S260, S261	0	S261
11	Chchd2	Q9D1L0	Coiled-coil-helix-coiled-coil-helix domain-containing protein 2, mitochondrial	1	28	51	RAPAAQPPAAAAPSAVG**S**PAAAPR	S45	11	Y
				2	28	51	RAPAAQPPAAAAPSAVG**S**PAAAPR	S45	24	Y
				3	28	51	RAPAAQPPAAAAPSAVG**S**PAAAPR	S45	11	Y
12	Gps1	Q99LD4	COP9 signalosome complex subunit 1	2	459	466	EGSQGEL**T**PANSQSR	T459	15	Y
				3	459	466	EGSQGEL**T**PANSQSR	T459	12	Y
13	Cobll1	Q3UMF0	Cordon-bleu protein-like 1	1	296	309	EQTASAPA**T**PLVSK	T304	20	Y
				2	296	309	EQTASAPA**T**PLVSK	T304	33	Y
				2	294	309	KREQTASAPA**T**PLVSK	T304	17	Y
				3	296	309	EQTASAPA**T**PLVSK	T304	23	Y
				3	294	309	KREQTASAPA**T**PLVSK	T304	23	Y
14	Cxadr	P97792	Coxsackievirus and adenovirus receptor homolog	2	329	339	APQ**S**PTLAPAK	S332	26	Y
				3	329	339	APQ**S**PTLAPAK	S332	23	Y
15	Cfdp1	O88271	Craniofacial development protein 1	2	195	215	EKPQALVTSPA**T**PLPAGSGIK	T206	22	Y
16	Cox17	P56394	Cytochrome c oxidase copper chaperone	2	1	17	MPGLAAA**S**PAPPEAQEK	S8	INF	Y
17	Dync1i2	O88487	Cytoplasmic dynein 1 intermediate chain 2	2	144	165	EDEEEEDDVA**T**PKPPVEPEEEK	T154	INF	Y
				2	133	143	ETQ**T**PVTAQPK	T136	8	Y
				3	133	143	E**T**Q**T**PVTAQPK	T134, T136	0	Y

	GENE	UNIPROT ID	PROTEIN	SAMPLE	START	END	PEPTIDES	RESIDUE	Ascore	PROLINE DIRECTED SITE?
18	Dync1li1	Q8R1Q8	Cytoplasmic dynein 1 light intermediate chain 1	2	505	523	KPASVSPTTPT**S**PTEGEAS	S516	8	Y
				2	505	523	KPASV**S**P**TT**PTSPTEGEAS	S510, T512, T513	0	S510
				3	505	523	KPASVSPTTPT**S**PTEGEAS	S516	7	Y
				3	505	523	KPASV**S**P**TT**PTSPTEGEAS	S510, T512, T513	0	S510
				1	505	523	KPASVSPTTP**TS**PTEGEAS	T515, S516	0	S516
19	Dpysl3	Q62188	Dihydropyrimidinase-related protein 3	1	521	531	G**S**PTRPNPPVR	S522	23	Y
				2	521	531	G**S**PTRPNPPVR	S522	11	Y
				2	512	531	GGTPAG**ST**RG**S**PTRPNPPVR	S518, T519, S522	0	S522
				3	521	531	G**S**PTRPNPPVR	S522	26	Y
				3	512	531	GGTPAG**ST**RG**S**PTRPNPPVR	S518, T519, S522	0	S522
20	Map2k2	Q63932	Dual specificity mitogen-activated protein kinase kinase 2	2	390	398	LKQPS**T**PTR	T395	7	Y
21	Map2k4	P47809	Dual specificity mitogen-activated protein kinase kinase 4	2	1	38	MAAP**S**P**S**GGGG**S**GGGGG**T**PGPIGPPASGHPAVSSMQGK	S5, S7, S12, T18	0	S5, T18
22	Eea1	Q8BL66	Early endosome antigen 1	2	1389	1400	NAL**T**PSSKKPVR	T1392	34	Y
23	Efhd2	Q9D8Y0	EF-hand domain-containing protein D2	2	63	77	ADLNQGIGEPQ**S**PSR	S74	11	Y
				2	62	78	RADLNQGIGEPQ**S**P**S**RR	S74, S76	0	S74
				2	62	77	RADLNQGIGEPQ**S**PSR	S74	9	Y
				3	62	78	RADLNQGIGEPQ**S**P**S**RR	S74, S76	0	S74
				1	62	78	RADLNQGIGEPQ**S**P**S**RR	S74, S76	0	S74
24	Eif4h	Q9WUK2	Eukaryotic translation initiation factor 4H	2	217	239	TVA**T**PLNQVANPNSAIFGGARPR	T220	10	Y
				3	217	239	TVA**T**PLNQVANPNSAIFGGARPR	T220	10	Y
25	Fzd9	Q9R216	Frizzled-9	1	371	378	TIVVL**T**LR	T376	38	N
26	Lgalsla	Q8VED9	Galectin-related protein A	2	14	35	LDDGHLNNSLG**S**PVQADVYFPR	S25	9	Y
27	Gys1	Q9Z1E4	Glycogen [starch] synthase, muscle	2	709	738	SNSVDTGPSSSLSTPTEPL**S**PTSSLGEERN	S728	10	Y
				3	709	738	SNSVDTGPSSSLSTPTEPL**S**PTSSLGEERN	S728	8	Y
28	Gorasp2	Q99JX3	Golgi reassembly-stacing protein 2	3	407	430	ADA**SS**L**T**VDV**TS**PASKVPTTVEDR	S410, S411, T413, T417, S418	0	S418

	GENE	UNIPROT ID	PROTEIN	SAMPLE	START	END	PEPTIDES	RESIDUE	Ascore	PROLINE DIRECTED SITE?
29	Hspa4	Q61316	Heat shock 70 kDa protein 4	2	522	545	MQVDQEEPHTEEQQQQPQ**T**PAENK	T540	20	Y
				3	522	559	MQVDQEEPHTEEQQQQPQ**T**PAENKAESEEMETSQAGSK	T540	13	Y
				3	522	545	MQVDQEEPHTEEQQQQPQ**T**PAENK	T540	23	Y
30	Hspb2	Q99PR8	Heat shock protein beta-2	2	29	52	FGEGLLPEEIL**T**PTLYHGYYVRPR	T40	17	Y
31	Jph2	Q9ET78	Junctophilin-2	1	590	612	RSDSAPP**S**PVSATVPEEEPPAPR	S597	8	Y
				2	469	488	ETPQPEGGPP**S**PAG**T**PPQPK	S479, T483	13 (S479), 28 (T483)	Y
				2	590	612	RSDSAPP**S**PVSATVPEEEPPAPR	S597	6	Y
				3	469	488	ETPQPEGGPP**S**PAG**T**PPQPK	S479, T483	24 (S479), 48 (T483)	Y
				3	590	612	RSDSAPP**S**PVSATVPEEEPPAPR	S597	6	Y
32	Lmnb1	P14733	Lamin-B1	2	16	27	ASAPATPL**S**P**T**R	S24, T26	0	S24
				3	16	27	ASAPATPL**S**P**T**R	S24, T26	0	S24
33		Q9DB75	LITAF-like protein	3	22	30	SGAPL**T**PGR	T27	24	Y
34	Limch1	Q3UH68	LIM and calponin homology domains-containing protein 1	2	313	332	YGPR**T**PVSDDAESTSMFDMR	T317	19	Y
35	Ldb3	Q9JKS4	LIM domain-binding protein 3	2	85	107	RPIPISTTAPPIQ**S**PLPVIPHQK	S98	39	Y
				2	233	248	DLAVDSA**S**PVYQAVIK	S240	10	Y
				2	83	332	SKRPIPISTTAPPIQ**S**PLPVIPHQK	S98	15	Y
36	Map7d1	A2AJI0	MAP7 domain-containing protein 1	2	533	559	AAEEKEPAAPA**S**PAPSPVPSPTPAQPQK	S544	17	Y
37	Mapkapk2	P49138	MAP kinase-activated protein kinase 2	3	317	326	VPQ**T**PLHTSR	T320	37	Y
38	Aldh6a1	Q9EQ20	Methylmalonate-semialdehyde dehydrogenase [acylating], mitochondrial	1	518	535	EEDATL**SS**PAVVMPTMGR	S524, S525	0	S525
				2	511	535	TITSQWKEEDA**T**L**SS**PAVVMPTMGR	T522, S524, S525	0	S525
				2	518	535	EEDA**T**L**SS**PAVVMPTMGR	T522, S524, S525	0	S525
				2	518	535	EEDATL**SS**PAVVMPTMGR	S524, S525	0	S525
				3	518	535	EEDA**T**L**SS**PAVVMPTMGR	T522, S524, S525	0	S525
				3	518	535	EEDATLS**S**PAVVMPTMGR	S525	6	Y
39	Map1b	P14873	Microtubule-associated protein 1b	3	7178	7186	SDISPL**T**PR	T7184	19	Y

	GENE	UNIPROT ID	PROTEIN	SAMPLE	START	END	PEPTIDES	RESIDUE	Ascore	PROLINE DIRECTED SITE?
40	Map4	P27546	Microtubule-associated protein 4	2	845	861	NT**T**PTGAAPPAGMTSTR	T847	8	Y
				3	845	861	N**TT**PTGAAPPAGMTSTR	T846, T847	0	T847
				3	845	861	N**TT**P**T**GAAPPAGMTSTR	T846, T847, T849	0	T847
41	Mapt	P10637	Microtubule-associated protein tau	2	502	516	**S**R**T**PSLPTPPTREPK	S502, T504	0	T504
				3	502	516	**S**R**T**P**S**LPTPPTREPK	S502, T504, S506	0	T504
42	Ndufaf2	Q59J78	Mimitin, mitochondrial	2	114	129	ETSEELLP**S**PTATQVK	S122	11	Y
				3	114	129	ETSEELLP**S**PTATQVK	S122	10	Y
43	Mavs	Q8VCF0	Mitochondrial antiviral-signaling protein	2	192	230	EHQEQEPELGGAHAANVASVPIATYGPV**S**PTVSFQPLPR	S220	19	Y
44	Tomm22	Q9CPQ3	Mitochondrial import receptor subunit TOM22 homolog	1	1	22	MAAAVAAAGAGEPL**S**PEELLPK	S15	INF	Y
				2	1	22	MAAAVAAAGAGEPL**S**PEELLPK	S15	INF	Y
				3	1	22	MAAAVAAAGAGEPL**S**PEELLPK	S15	INF	Y
45	Immt	Q8CAQ8	Mitochondrial inner membrane protein	2	371	384	ELDSITPDI**T**PGWK	T380	30	Y
46	Mapk12	O08911	Mitogen-activated protein kinase 12	2	177	189	QADSEMTG**Y**VVTR	Y185	17	N
47	Murc	A2AMM0	Muscle-related coiled-coil protein	1	322	339	GGYSPQEGGDPP**T**PEPLK	T334	67	Y
				2	322	339	GGYSPQEGGDPP**T**PEPLK	T334	37	Y
				2	322	339	GGYSPQEGGDPP**T**PEPLK	T334	52	Y
				3	322	347	GGYSPQEGGDPP**T**PEPLKVTFKPQVR	T334	42	Y
				3	322	339	GGYSPQEGGDPP**T**PEPLK	T334	63	Y
48	Mbnl1	Q9JKP5	Muscleblind-like protein 1	2	1	12	MAVSV**T**PIRDTK	T6	23	Y
49	Marcks	P26645	Myristoylated alanine-rich C-kinase substrate	2	131	145	AEDGAAP**S**P**SS**E**T**PK	S138, S140, S141, T143	0	S138
50	Ndufv1	Q91YT0	NADH dehydrogenase [ubiquinone] flavoprotein 1,	2	82	98	TSGLRGRGGAGFP**T**GLK	T95	43	N
				3	82	98	TSGLRGRGGAGFP**T**GLK	T95	34	N
51	Nrap	Q80XB4	Nebulin-related-anchoring protein	2	199	213	VSTF**T**PVADTPELLR	T203	13	Y
				3	199	213	VSTF**T**PVADTPELLR	T203	13	Y
52	Nsfl1c	Q9CZ44	NSFL1 cofactor p47	3	137	156	VTK**S**PGETSKPRPFAGGGYR	S140	12	Y
53	Urb1	Q571H0	Nucleolar pre-ribosomal-associated protein 1	2	450	462	HSAL**S**LI**S**DILKR	S454, S457	0	N
54	Otud4	B2RRE7	OTU domain-containing protein 4	1	1009	1028	LQRPKEE**S**SEDENEVSNILR	S1016	22	N
				2	1009	1028	LQRPKEE**S**SEDENEVSNILR	S1016	21	N
				3	1009	1028	LQRPKEE**S**SEDENEVSNILR	S1016	22	N

	GENE	UNIPROT ID	PROTEIN	SAMPLE	START	END	PEPTIDES	RESIDUE	Ascore	PROLINE DIRECTED SITE?
55	Prdx6	O08709	Peroxiredoxin-6	1	163	182	VVDSLQLTGTKPVA**T**PVDWK	T177	18	Y
				1	163	183	VVDSLQLTGTKPVA**T**PVDWKK	T177	21	Y
				1	85	106	DINAYNGE**T**PTEKLPFPIIDDK	T93	9	Y
				1	85	97	DINAYNGE**T**P**T**EK	T93, T95	0	T93
				2	163	183	VVDSLQL**T**GT**K**PVA**T**PVDWKK	T170, T172, T177	0	T177
				2	163	183	VVDSLQLTGTKPVA**T**PVDWKK	T177	24	Y
				2	163	182	VVDSLQLTGTKPVA**T**PVDWK	T177	9	Y
				2	85	106	DINA**Y**NGE**T**P**T**EKLPFPIIDDK	Y89, T93, T95	0	T93
				2	85	97	DINAYNGE**T**PTEK	T93	14	Y
				2	85	108	DINAYNGE**T**P**T**EKLPFPIIDDKGR	T93, T95	0	T93
				2	85	108	DINAYNGE**T**P**T**EKLPFPIIDDKGR	T93, T95	0	T93
				3	163	183	VVDSLQLTGTKPVA**T**PVDWKK	T177	15	Y
				3	163	182	VVDSLQLTGTKPVA**T**PVDWK	T177	21	Y
				3	85	106	DINA**Y**NGE**T**P**T**EKLPFPIIDDK	Y89, T93, T95	0	T93
				3	85	108	DINAYNGE**T**P**T**EKLPFPIIDDKGR	T93, T95	0	T93
				3	85	97	DINAYNGE**T**P**T**EK	T93, T95	0	T93
56	Pcnp	Q6P8I4	PEST proteolytic signal-containing nuclear protein	1	134	150	NIGRD**T**PTSAGPNSFNK	T139	16	Y
				2	134	150	NIGRD**T**PTSAGPNSFNK	T139	34	Y
				3	134	150	NIGRD**T**PTSAGPNSFNK	T139	16	Y
57	Lmna	P48678	Prelamin-A/C	2	12	25	SGAQASSTPL**S**PTR	S22	10	Y
				3	12	25	SGAQASSTPL**S**PTR	S22	9	Y
58	Pnkd	Q69ZP3	Probable hydrolase PNKD	3	107	120	GHSK**T**QPRLFNGVK	T111	39	N
59	Pdcd6ip	Q9WU78	Programmed cell death 6-interacting protein	2	716	745	EPSAPSIPPPAYQSSPAAGHAAAPP**T**PAPR	T741	39	Y
				3	716	745	EPSAPSIPPPAYQSSPAAGHAAAPP**T**PAPR	T741	60	Y
60	Adrm1	Q9JKV1	Proteasomal ubiquitin receptor ADRM1	3	211	226	SQSAAV**T**PSSSTSSAR	T217	27	Y
61	Mtdh	Q80WJ7	Protein LYRIC	2	90	106	EEAAPP**T**PAPDDLAQLK	T96	INF	Y
				2	90	106	EEAAPP**T**PAPDDLAQLK	T96	INF	Y
62	Ppp1r3a	Q99MR9	Protein phosphatase 1 regulatory subunit 3A	2	578	596	EVGSGSNLEPGTSDL**SS**PR	S593, S594	0	S594
				3	578	596	EVGSGSNLEPGTSDL**SS**PR	S593, S594	0	S594
63	Tbrg4	Q91YM4	Protein TBRG4	2	58	76	EQVF**T**PYPEHQELDFLIEK	T62	18	Y
				3	58	76	EQVF**T**P**Y**PEHQELDFLIEK	T62, Y64	0	Y
64	Padi2	Q08642	Protein-arginine deiminase type-2	3	392	403	QLLGPDFG**Y**VTR	Y400	19	N

	GENE	UNIPROT ID	PROTEIN	SAMPLE	START	END	PEPTIDES	RESIDUE	Ascore	PROLINE DIRECTED SITE?
65	Mylk3	Q3UIZ8	Putative myosin light chain kinase 3	1	304	330	LSSGPLPQPLGPL**T**PDSDIHSGDALPR	T317	31	Y
				2	414	446	DETVGTTDLQQGIDPGAV**S**PEPGKDHAAQGPGR	S432	16	Y
				2	304	330	LSSGPLPQPLGPL**T**PDSDIHSGDALPR	T317	28	Y
66	Arhgef7	Q9ES28	Rho guanine nucleotide exchange factor 7	2	558	586	VTSVSNPTIKPHSVPSHTLPSHPL**T**PSSK	T582	11	Y
67	Las1l	A2BE28	Ribosomal biogenesis protein LAS1L	3	168	179	TYWSRQLEG**S**LK	S177	53	N
68	Rrbp1	Q99PL5	Ribosome-binding protein 1	3	102	131	VSAVAVAP**TS**VH**SS**VGH**T**PIATVPAMPQEK	T110, S111, S114, S115, T119	0	T119
69	Stk10	O55098	Serine/threonine-protein kinase 10	2	940	953	LSEEAEPRP**TT**PSK	T949, T950	0	T950
70	Tf	Q921I1	Serotransferrin	3	27	37	WCAV**S**EHENTK	S31	39	N
71	Snapin	Q9Z266	SNARE-associated protein Snapin	2	1	22	MAAAGSAAVSGAG**T**PVAGPTGR	T14	29	Y
				3	1	22	MAAAGSAAVSGAG**T**PVAGPTGR	T14	11	Y
72	Snx2	Q9CWK8	Sorting nexin-2	1	89	112	ELILSSEPSPAVTPV**T**PTTLIAPR	T104	11	Y
				2	89	112	ELILSSEPSPAVTPV**T**PTTLIAPR	T104	11	Y
				3	89	112	ELILSSEPSPAVTPV**T**PTTLIAPR	T104	9	Y
73	Stmn1	P54227	Stathmin	3	15	27	ASGQAFELIL**S**PR	S25	51	Y
74	Speg	Q62407	Striated muscle-specific serine/threonine-protein kinase	2	323	341	ALPGPSTQPPA**T**PTSPHRR	T334	15	Y
				2	364	387	SSGPSLAG**T**VE**S**RPQ**T**PLSEASGR	T372, S375, T379	0	T379
				3	364	387	SSGPSLAGTVE**S**RPQ**T**PLSEASGR	S375, T379	0	T379
				3	2773	2786	GTPD**S**PAQPAAAPR	S2777	8	Y
				3	323	341	ALPGPSTQPPA**T**PTSPHRR	T334	12	Y
75	Tom1	O88746	Target of MyB protein 1	1	453	478	AADRLPNLA**S**PSAEGPPRPSPGTAPR	S462	6	Y
				2	453	478	AADRLPNLA**S**PSAEGPPRPSPGTAPR	S462	14	Y
				3	453	478	AADRLPNLA**S**PSAEGPPRPSPGTAPR	S462	14	Y
76	Tecpr1	Q80VP0	Tectonin beta-propeller repeat-containing protein 1	1	925	954	LV**TS**GPWLEVAPI**T**L**S**DV**S**IIPESAHADGR	T927, S928, T938, S940, S943	0	N
77	Tcap	O70548	Telethonin	1	88	98	VLPLPIF**T**PTK	T95	10	Y
				2	88	98	VLPLPIF**T**P**T**K	T95, T97	0	T95
				3	88	98	VLPLPIF**T**P**T**K	T95, T97	0	T95
78	Tjp1	P39447	Tight junction protein ZO-1	2	340	357	SREEERMSKPGAI**ST**PVK	S353, T354	23 (S353), 23 (T536)	T354

	GENE	UNIPROT ID	PROTEIN	SAMPLE	START	END	PEPTIDES	RESIDUE	Ascore	PROLINE DIRECTED SITE?
79	Trak1	Q6PD31	Trafficking kinesin-binding protein 1	2	528	549	GELH**S**G**S**L**T**PTESIMSLGTHSR	S532, S534, T536	0	T536
80	Tmem55a	Q9CZX7	Transmembrane protein 55A	2	10	35	SPLLSASHSGNV**T**PTAPPYLQESSPR	T22	6	Y
				3	10	35	SPLLSASHSGNV**T**PTAPPYLQESSPR	T22	8	Y
81	Ubap2l	Q80X50	Ubiquitin-associated protein 2-like	2	428	441	SANDSTVH**S**PFTKR	S436	19	Y
82	Ubxn1	Q922Y1	UBX domain-containing protein 1	2	187	209	SSPPATDPGPVPS**S**PSQEPPTKR	S200	8	Y
				3	187	209	SSPPATDPGPVPS**S**PSQEPPTKR	S200	9	Y
83	Ugdh	O70475	UDP-glucose 6-dehydrogenase	2	470	480	RIPY**T**PGEIPK	T474	37	Y
84		Q149B8	Uncharacterized protein C1orf170 homolog	1	141	152	LLQGPAP**SS**PSK	S148, S149	0	S149
				2	295	335	ASKPQPDVALPKPASKPQSDIASSTHPF**T**PDVSLSTLAFK	T324	21	Y
				2	195	215	HSGSLDSAA**T**QM**SS**PQLTRPK	T204, S207, S208	0	S208
				2	141	152	LLQGPAP**SS**PSK	S148, S149	0	N
				3	141	152	LLQGPAP**SS**PSK	S148, S149	0	N
85	Vps28	Q9D1C8	Vacuolar protein sorting-associated protein 28 homolog	2	1	25	FHGIPA**T**PGVGAPGNKPELYEEVK	T8	91	Y
				3	1	25	FHGIPA**T**PGVGAPGNKPELYEEVK	T8	130	Y
86	Znf260	Q62513	Zinc finger protein 260	2	251	263	AFSGK**S**NL**T**EHEK	S256, T259	17 (S256), 31 (T259)	N

4.4 Discussion

4.4.1 Summary

The Shokat approach requires the use of an AS kinase in conjunction with a labelled ATP analogue. AS p38γ kinases have previously been shown to mediate phosphorylation of ATF2 using ATP. Experiments in this chapter show that AS p38γ kinases can utilise all ATP analogues tested to transfer phosphate to ATF2. Upon closer inspection, it was revealed that WT p38γ could also utilise some of the ATP analogues, albeit with lower efficiency. The analogue selected for the Shokat methodology was 6-PhEt-ATP, which was not well utilised by WT p38γ. When used in kinase assays with AS p38γ kinases in its labelled form (6-PhEt-ATPγS), both AS kinases successfully thiophosphorylated ATF2. AS1 p38γ mediated thiophosphorylation of ATF2 was stronger than AS2 p38γ and as such AS1 p38γ was chosen for the Shokat approach.

The introduction of mutations to the active site of a kinase also affects the selectivity of several inhibitors to the mutant AS kinase. Here a selection of compounds was tested for their ability to inhibit WT and AS p38γ kinases. BIRB 796 is a pan p38 isoform inhibitor. The mutation of the gatekeeper residue of AS p38γ kinases did not affect the ability of BIRB 796 to inhibit AS p38γ mediated phosphorylation. In contrast, SB203580 only inhibits the p38α and p38β isoforms. However, smaller gatekeeper residues in the AS p38γ kinases, renders them sensitive to SB203580 inhibition. Na-PP1 and NM-PP1 are modified PP1 analogues that have been shown to specifically and reversibly inhibit AS kinases. Both PP1 analogues were unsuccessful at inhibiting WT p38γ mediated ATF2 phosphorylation. Na-PP1 successfully inhibited both AS p38γ kinases, although some AS1 p38γ mediated ATF2 phosphorylation remained at the concentration tested. In comparison, NM-PP1 did not inhibit either AS p38γ kinase. As a positive control of NM-PP1 inhibition was not included, it is difficult to establish the reason for why NM-PP1 inhibition was not observed. If it truly does not show inhibition of AS p38γ kinases, it could be due to the reduced shape complementarity in the active site of the kinase due to the

extra methyl group present in the PP1 analogue. Given the larger active site of the mutant AS kinases, it was tested if the bulky staurosporine compound could now inhibit the AS p38γ kinases. No inhibition of WT or AS p38γ kinases was observed with staurosporine.

Pirfenidone, a reported specific inhibitor of p38γ, was also tested in kinase assays (Blatt, Ozes 2005). Pirfenidone is currently in clinical trials for the treatment of idiopathic pulmonary fibrosis and its supposed mechanism of action is blockage of TGF-beta-induced activation of p38γ and subsequent collagen synthesis (Blatt, Ozes 2005). Whilst this has been reported in brief scientific communications, conclusive data showing selective p38γ inhibition or the methodology used cannot be accessed. As such, a variety of conditions were tested in this study to establish inhibition of p38γ by pirfenidone. However, under the different conditions tested in this study, pirfenidone did not mediate inhibition of WT or AS p38γ kinases.

A distinguishing structural feature of p38γ is its carboxy-terminal PDZ interaction motif. It has been reported that p38γ phosphorylation of α1-syntrophin requires the interaction of the carboxy-terminal of p38γ with the PDZ domain of α1-syntrophin (Hasegawa et al. 1999). Despite the lack of the interacting motif in p38α, α1-syntrophin was successfully phosphorylated by p38α *in vitro*. Similarly, p38α contains a unique TAB1 docking site not known to be present in p38γ (De Nicola et al. 2013). However, whilst p38α could mediate phosphorylation of α1-syntrophin, p38γ does not phosphorylate TAB1.

Lastly and most importantly, this chapter concludes with the identification of 86 putative substrates of p38γ in the myocardium, following the Shokat approach. This is the first study of its kind to examine substrates of p38γ in the heart. The LC-MS/MS analysis of phosphorylated peptides also reveals potential target p38γ phosphorylation sites of a protein.

4.4.2 Shokat approach

The Shokat methodology is a powerful technique that overcomes many of the problems associated with identifying substrates of a kinase. Results from this chapter show that AS kinase function, with the labelled ATP analogue, reflects WT p38γ function with ATP. Substrate specificity is not altered, as ATF2 and α1-syntrophin are successfully thiophosphorylated by AS p38γ. An added advantage of the thiophosphate system is that upon alkylation, it enables assessment of phosphorylation of proteins where phospho-antibodies are not present, such as with α1-syntrophin.

Kinetically, AS kinases are not able to utilise ATP as efficiently as WT, but have been shown to utilise ATP analogues to comparable levels (Shah et al. 1997). This is beneficial in the presence of tissue homogenate, as it will preferentially use the ATP analogue over the high ATP pool already present in the tissue, or ATP that has been added to the system to reduce background thiophosphorylation by other WT kinases. In the case of AS1 p38γ, competition from supplementary ATP and GTP did not prevent AS1 p38γ mediated thiophosphorylation of cardiac proteins (Figure 4.9).

Whilst a comparison of phosphorylation by WT and AS kinases using ATP and ATP analogues has been made, the kinetics of thiophosphorylation in comparison to phosphorylation is not well characterised. It is however known that cellular ATPases are unable to utilise the γ-phosphorothioate of the analogue and that it is also resistant to dephosphorylation (Elphick et al. 2007). This is advantageous over the use of radiolabelled ATP analogues as the latter is subject to hydrolytic release of the labelled phosphate and incorporation into the cellular ATP pool. Furthermore, the phosphorothioate moiety of the target substrate can be alkylated, for use in visualisation, capture and identification of substrates. Following incubation of heart homogenate with AS1 p38γ and PhEt-ATPγS and subsequent alkylation, specific protein bands were detected that potentially represent substrates of p38γ.

In addition to substrate specificity of WT and AS p38γ kinases, another aspect examined in this study is inhibitor specificity. The introduction of mutations to the gatekeeper residue makes the AS kinases sensitive to inhibition by compounds that are traditionally ineffective towards the WT kinase. This is highly significant, as compounds that specifically modulate the activity of a kinase are powerful probes of signal transduction pathways. Importantly, the PP1 analogues are cell permeable inhibitors engineered to specifically inhibit AS kinases. They are modelled towards the enlarged active site surrounding the gatekeeper residue, akin to the expanded ATP analogue (Bishop et al. 2000a). Whilst an *in vitro* approach is taken in this study in the first instance, in future experiments the Na-PP1 inhibitor could be used in a cellular context to probe AS p38γ function and substrates within a cell.

There are limitations associated with the *in vitro* approach. Firstly, any substrates of p38γ already phosphorylated within the heart homogenate, will not be detected using this approach. This could explain why known substrates of p38γ were not identified by the Shokat experiment. In future experiments, this could potentially be overcome by pre-treatment of heart homogenate with phosphatases. A further reason for the lack of detection of known substrates is the difficulty in achieving high-stoichiometric phosphorylation in a whole heart homogenate. Full identification of substrates is therefore likely to require simplification of homogenate by fractionation or perhaps by increasing the size of the starting material.

A further limitation of this approach is that, as AS kinases are ‘spiked’ into heart homogenate, any spatial fidelity is lost. This could lead to the identification of false positives – proteins that do not physiologically undergo phosphorylation by p38γ. Whilst cells or an organism could be genetically modified to express AS kinases, the use of ATP analogues is problematic, owing to the lack of their cell permeability (Elphick et al. 2007). Despite the limitations of an *in vitro* approach, it overcomes many of the problems associated with identifying specific substrates of kinases, particularly when a specific inhibitor is unavailable. As such, it provides a useful starting point for the identification of p38γ substrates.

Proteins can then be validated as physiologically true substrates in subsequent experiments.

A requirement of LC-MS/MS identification of phosphorylated proteins and their phospho-sites is enrichment of phosphorylated peptides. Therefore, a covalent capture process was used to enrich thiophosphorylated peptides prior to mass spectrometry. A limitation of this part of the process is that peptides that bind non-specifically to the beads e.g. peptides that contain a cysteine, compromise sensitivity and block the capture of less prevalent thiophosphorylated peptides. Furthermore, any thiophosphorylated peptides that also contain a cysteine residue are not recoverable with this method. Thiophosphorylated peptides form a thiophosphate diester linkage with the iodoacetyl beads, which is susceptible to hydrolysis after oxidation of the sulphur, therefore allowing dissociation from the beads. In contrast, thioethers resulting from the capture of cysteine containing peptides remain attached to the resin as they are oxidised to stable sulfoxides (Hodgson, Schroder 2011). Phosphorylated peptides released from the beads are then subject to LC-MS/MS. As this method only aims to enrich and capture peptides that are phosphorylated, attribution of a phosphorylated peptide to a protein is often based on one unique peptide detected. This is a further limitation of the method, as the isoform identity of the protein cannot be specifically determined. Therefore this is a further aspect for consideration during validation of substrates.

4.4.3 Isoform substrate selectivity

Taking into account the physiological data regarding the function of p38γ in the myocardium so far, it is likely that it is playing a differential role to p38α. Therefore, a key question that arises when examining its signalling pathway and particularly its target substrates, is if they can also undergo phosphorylation by its sister kinase. This was examined for a known substrate of each kinase isoform *in vitro*. Despite the lack of a PDZ interacting motif, p38α phosphorylated α1-syntrophin, a known p38γ interacting protein and substrate. In contrast, TAB1 could not be phosphorylated by p38γ. This outcome may reflect the limitation of carrying out *in vitro* kinase assays. Assessing

phosphorylation in this manner is very rudimental. It does not take into account the cellular milieu, which no doubt contributes to the substrate specificity of different isoforms of a kinase. For instance, within a cell, α1-syntrophin may never be within close proximity to p38α to undergo phosphorylation by this isoform. The PDZ interaction is likely to be crucial in targeting α1-syntrophin for phosphorylation by p38γ. Co-localisation studies of substrate proteins and kinases may offer insight into the proximity of a substrate to a kinase. Also, depending on the availability of phospho-specific antibodies, the isoform selectivity of p38 MAPKs towards a substrate can be assessed in a physiological context by the parallel use of SB203580 and BIRB 796.

5 INTERACTING PROTEINS OF p38γ

5.1 Introduction

To investigate interacting partners of p38γ in the myocardium, a co pull-down study was performed. In contrast to a conventional immunoprecipitation approach, for this study recombinant WT p38γ (non-active and active) was firstly 'spiked' into heart homogenate. After a period of incubation, the polyhistidine tag of the recombinant proteins was then used to capture p38γ kinases and any interacting proteins that remained following a series of washes. Whilst the purpose of this study was to identify any specific interactions of p38γ in the myocardium, of particular interest were those proteins that contained a PDZ domain and therefore may interact with p38γ via its C' PDZ interacting motif (Hasegawa et al. 1999). Given below is an overview of PDZ domain signalling and known interactions of p38γ with PDZ domain containing proteins.

5.1.1 PDZ interactions

PDZ domains are the most abundant protein-protein interaction domains found in various species (Lee, Zheng 2010), yet their role in cardiac physiology has not been explored. PDZ domains are small modular domains of 80 to 100 amino acids, often found in scaffolding proteins, that recognise and bind to the extreme C' terminal peptide motif of target proteins. Furthermore, PDZ domain containing proteins often also consist of other interaction domains, forming multi-domain scaffolding proteins. Therefore the most obvious role of PDZ domains seems to be in the organisation and localisation of signalling complexes within a cell. Perhaps the most well characterised example of this occurs at the postsynaptic density of neuronal excitatory synapses, where a multitude of PDZ interactions take place for efficient glutamatergic signal transduction (Kim, Sheng 2004) (Figure 5.1). A multiple PDZ domain containing protein central to this process is PSD-95. It is the archetypal PDZ scaffold and its role at the synapse is well documented.

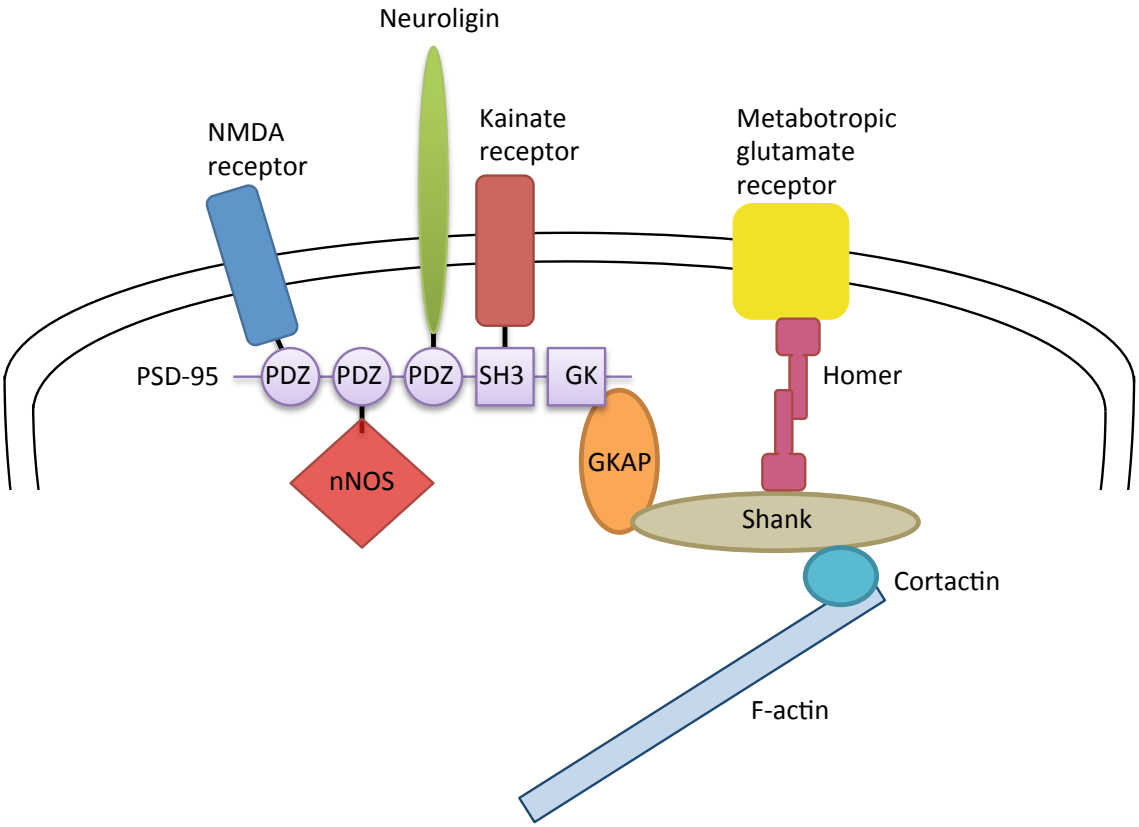

Figure 5.1 PSD-95 scaffolding at the postsynaptic density of excitatory synapses

Schematic diagram of protein-protein interactions at the postsynaptic density (PSD). PSD-95 interacts with the ionotropic glutamate receptor (NMDA) and the cell adhesion molecule neuroligin via PDZ interactions. The kainate glutamate receptor interacts with the SH3 domain of PSD-95. The GK domain of PSD-95 links it to the postsynaptic cytoskeletal matrix via binding of GKAP. GKAP binding to Shank is also PDZ mediated. Shank is another multiple protein-protein interaction domain containing protein. It links the PSD-95 complex to the metabotropic glutamate receptor via Homer protein dimers.

PSD-95 contains three PDZ domains, a Src Homology 3 (SH3) domain and a guanylate kinase like (GK) domain. It is localised to the synaptic membrane and forms interactions both with membrane proteins (glutamate receptors, ion channels and cell adhesion molecules) and intracellular signalling proteins. PSD-95 binding to membrane proteins has several different outcomes. It can affect factors such as surface delivery, endocytosis, subcellular localisation, subunit composition and in some cases even intrinsic functional properties of

ion channels (Kim, Sheng 2004). Furthermore as it is able to bind intracellular proteins such as neuronal nitric oxide synthase (nNOS), Ras and Rho GTPase-activating proteins, it also plays a role in facilitating postsynaptic signalling (Kim, Sheng 2004).

As reviewed earlier in Chapter 1 and further discussed here, PSD-95 has also been found to interact with and undergo phosphorylation by p38γ (Sabio et al. 2004). PSD-95 interacts with p38γ via its third PDZ domain and this interaction has shown to be a pre-requisite for PSD-95 phosphorylation. *In vitro* a C' truncated p38γ phosphorylated PSD-95 poorly compared to the full-length kinase. Cellular stress induced *in vivo* phosphorylation of PSD-95 (likely mediated by p38γ) was also reduced in the presence of a peptide corresponding to the C' terminal residues of p38γ (Sabio et al. 2004).

Like PSD-95, its family member SAP97 was subsequently shown to interact with p38γ via its PDZ domain. It was also shown to undergo phosphorylation by p38γ, again dependent on the PDZ interaction (Sabio et al. 2005). Functionally phosphorylation of SAP97 by p38γ, in response to hyperosmotic shock, was shown to affect binding of SAP97 to guanylate kinase-associated protein (GKAP). In its non-phosphorylated form binding of SAP97 to GKAP tethers it to the cytoskeleton. However upon phosphorylation by p38γ, SAP97 dissociates from the cytoskeleton. This suggests that p38γ forms a part of the regulatory response undertaken by cells, specifically in modulation of the cell cytoskeleton, in response to hyperosmotic stress. Further investigation of the SAP97-p38γ interaction also revealed a kinase independent modulatory role of p38γ. In this instance, p38γ was shown to cause dissociation of SAP97 from polypyrimidine tract-binding (PTB) protein-associated splicing factor (PSF) under osmotic stress conditions (Sabio et al. 2010). PSF is a RNA binding protein that regulates mRNA processing and gene transcription. Sorbitol treatment induces translocation of p38γ to the nucleus, resulting in displacement of PSF from SAP97 by p38γ, increased SAP97-p38γ association and also dissociation of PSF from RNA (Sabio et al. 2010). This mechanism therefore highlights an

additional role of p38γ in regulating transcriptional signalling events in response to stress.

Other known substrates that interact with p38γ via a PDZ interaction are α1-syntrophin (Hasegawa et al. 1999) and PTPH1 (Hou et al. 2010). α1-syntrophin is a cytoplasmic adaptor protein localised to the membrane periphery. Its role is to link cytoplasmic proteins to the dystrophin-associated protein complex (DAPC). Similar to PSD-95, it also consists of multiple protein-protein interaction domains, enabling it to bind simultaneously to multiple proteins and therefore fulfil its scaffolding role. α1-syntrophin contains an N' terminal PDZ domain, two pleckstrin homology (PH) domains and C' terminal syntrophin unique (SU) domain (Bhat, Adams & Khanday 2013). *In vitro* it has been shown to undergo phosphorylation by p38γ, an event that is dependent on the PDZ interaction. However the physiological significance of the p38γ and α1-syntrophin interaction and phosphorylation is not known.

The interaction of p38γ with PTPH1 via PDZ interaction is the only reported instance so far where the interacting protein is not a scaffold or adaptor protein. Earlier in the introductory chapter the pro-oncogenic role of p38γ was discussed and how its role in oncogenesis is mediated via a phosphorylation independent mechanism (Tang et al. 2005). Furthermore, it was shown that p38γ is dephosphorylated during Ras signalling, suggesting the involvement of a phosphatase. This was subsequently proposed to be PTPH1 (Hou et al. 2010). PTPH1 has been shown to dephosphorylate p38γ *in vivo*, an event that is dependent on PDZ interaction. Further investigation of the pro-oncogenic p38γ-PTPH1 interaction has also demonstrated that PTPH1 can itself undergo phosphorylation by p38γ, an event that is also dependent on the PDZ interaction (Hou et al. 2012).

5.2 Specific Methods

5.2.1 Tissue homogenisation

For initial co pull-down studies, heart and soleus tissue was homogenised as described in Section 2.8. However optimisation of the homogenisation buffer was required for the purpose of the co pull-down studies. The recipe of modified homogenisation buffer used here is as follows: 20 mM Hepes, pH 7.4, 300 mM NaCl, 1 mM Na_2VO_4, 5 mM NaF, 30 mM imidazole, 0.5% (v/v) Triton X-100 and 1 x Protease Inhibitor Tablet (Roche)/50 mL buffer.

5.2.2 Co pull-down

For initial co pull-down experiments 200 µL of heart or soleus homogenate was incubated with 100 µg of non-active or MKK6EE-actived p38γ kinases for 30 min at 30°C, before addition of 25 µL of 50% Ni-NTA agarose beads/lysis buffer slurry per reaction. Beads were incubated with spiked heart/soleus homogenate for 1 h at 4°C on a rotating platform. Beads were then pelleted by centrifugation at 3000 rpm for 1 min, supernatant collected and beads washed in wash buffer (lysis buffer without detergent) by gentle tube inversion. Beads were washed a further 4 times and washes collected. After the last wash 30 µL of 2 x Laemmli sample buffer was added to beads and samples were prepared for SDS-PAGE as described previously.

To reduce non-specific binding of heart proteins to Ni-NTA agarose beads the co pull-down approach was modified as follows: Following homogenisation of heart tissue, supernatants were first pre-cleared by addition of 25 µL of 50% Ni-NTA agarose beads/lysis buffer slurry per 200 µL heart homogenate for 1 hr at 4°C on a rotating platform. Beads were pelleted by centrifugation at 3000 rpm for 1 min and pre-cleared homogenate was assayed for protein concentration before use in subsequent steps.

100 µg of non-active and active p38γ kinases per sample were incubated with 25 µL of 50% Ni-NTA agarose beads/lysis buffer slurry for 1 hr at 4°C on a rotating platform. Beads were pelleted and washed three times in 1 mL wash

buffer (lysis buffer without detergent) by gentle tube inversion. Beads were collected by centrifugation at 3000 rpm for 1 min and all washes discarded. 200 µL of pre-cleared heart homogenate per sample was added to beads and allowed to incubate overnight at 4°C on a rotating platform. The following day beads were collected by centrifugation and 5 x 1 mL washes were performed in wash buffer. After removal of the final wash, beads were re-suspended in 30 µL of 2 x Laemmli sample buffer and samples prepared for SDS-PAGE as described previously.

5.2.3 Mass Spectrometry

Silver stained gel of co pull-down experiment was processed and analysed by Dr Steve Lynham at the core facility at King's College London as outlined below.

5.2.3.1 In-gel digestion of proteins

Bands of interest were excised and transferred to a microcentrifuge tube. Excised gel bands were washed in 100 mM NH_4HCO_3 for 5 min before washing with acetonitrile for 5 min. The supernatant was removed and gel pieces were rehydrated with further acetonitrile. Acetonitrile was removed and gel pieces were dehydrated using a speed vacuum. Gel pieces were rehydrated by incubating with 10 mM DTT at 56°C for 30 min. Supernatant was removed and 2 x 5 min acetonitrile washes were repeated as before with subsequent gel dehydration using a speed vacuum. 55 mM iodoacetamide was added to the samples and incubated at room temperature for 20 min in the dark. Supernatant was discarded and 2 x 5 min acetonitrile washes were carried out. For complete destaining of gels, gel pieces were incubated in a 1:1 solution of 100 mM NH_4HCO_3 and acetonitrile at 37°C for 30 min. The supernatant was removed and 2 x 5 min acetonitrile washes were carried out with subsequent gel dehydration using a speed vacuum. Sufficient volume of 13 ng/µL trypsin in 50 mM NH_4HCO_3 to cover gel pieces was added to samples and incubated at 4°C for 20 min. Unabsorbed trypsin was removed and gel pieces were incubated

with the minimal volume of 50 mM NH_4HCO_3 to cover gel pieces. Samples were incubated at 37°C for 2 h then overnight at room temperature.

The following morning supernatant from gel pieces was decanted and transferred to fresh microcentrifuge tubes. Gel pieces were washed with 50 mM NH_4HCO_3 at 37°C for 5 min and washed with acetonitrile at 37°C for 10 min. Supernatant from washes were pooled together with trypsin digest supernatant. Pooled samples were lyophilised using a speed vacuum and stored at -80°C until required.

5.2.3.2 LC-MS/MS

Each sample was resuspended in 10 µL of 50 mM NH_4HCO_3 prior to LC-MS/MS analysis. Peptides were first separated by reverse-phase LC using an EASY NanoLC system (ThermoFisherScientific, UK) equipped with a 75 µM x 15 cm reverse phase C-18 column. A three step linear gradient of acetonitrile in 0.1% formic acid was applied (300 nL/min flow rate over 180 min) to separate peptides. The eluent was ionised by electrospray ionisation using an Orbitrap Velos Pro (ThermoFisherScientific, UK) operating under Xcalibur v2.2. Peptides were analysed in positive ion mode. The instrument was programmed to acquire in automated data-dependent switching mode, selecting precursor ions based on their intensity for sequencing by CID fragmentation using a Top20 CID method. The MS/MS analyses were conducted using collision energy profiles that were chosen based on the mass-to-charge ratio (*m/z*) and the charge state of the peptide.

5.3 Results

To explore interactions of p38γ in the myocardium, a co pull-down approach was utilised. To test experimental conditions, parallel experiments were also established in skeletal muscle to co pull-down α1-syntrophin, a documented interacting partner of p38γ. Samples were taken from various stages of the co pull-down experiment for analysis, as shown in Figure 5.2. Under the initial experimental conditions, both non-active and MKK6EE-actived p38γ were successfully captured from spiked soleus or heart homogenate (lanes: Pull down 1 and 2). Little recombinant protein was lost in the flow through or during the washes. This suggests that the conditions used for the pull-down were suitable for the capture of p38γ. However, a high level of non-specific protein binding to beads was also encountered (beads + tissue control) and therefore little differences could be visualised between control and specific pull-down lanes. Therefore, some optimisation to the protocol, to reduce non-specific binding, was required.

A probe of samples against α1-syntrophin revealed the presence of α1-syntrophin in both inputs and enrichment of the protein with non-active or active p38γ, despite the occurrence of some non-specific binding to beads (Figure 5.3). Unfortunately, the α1-syntrophin antibody also detects a band in the ‘mock’ pull-down sample (beads with p38γ, without tissue). This is non-specific binding of the antibody to a contaminant *E.coli* protein remaining following p38γ purification. Given that the molecular weight of the contaminant protein is similar to that of α1-syntrophin, it interferes with analysis of the experiment. Therefore to counteract this, for subsequent co pull-downs a lower 6% SDS-PAGE gel was cast to enhance separation of the proteins and to clearly distinguish between the non-specifically detected band and the α1-syntrophin band.

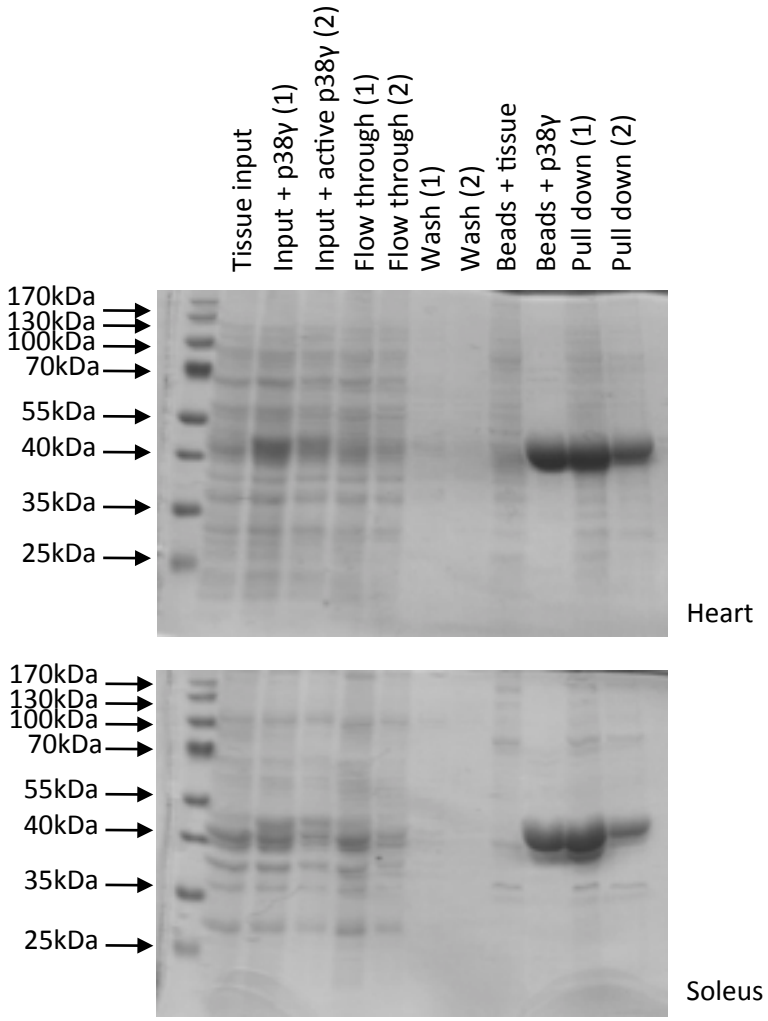

Figure 5.2 Heart and Soleus co pull-down analysis

Co pull-downs were performed in parallel with heart or soleus homogenate and p38γ (1) or MKK6EE-activated p38γ (2). Recombinant p38γ proteins were incubated with heart or soleus tissue prior to capture with Ni-NTA agarose beads, as described in *Materials and Methods*. Samples were resolved by 10% SDS-PAGE and Coomassie stained. Staining revealed successful capture of spiked p38γ proteins from tissue, but a high extent of non-specific binding of proteins to beads was also encountered.

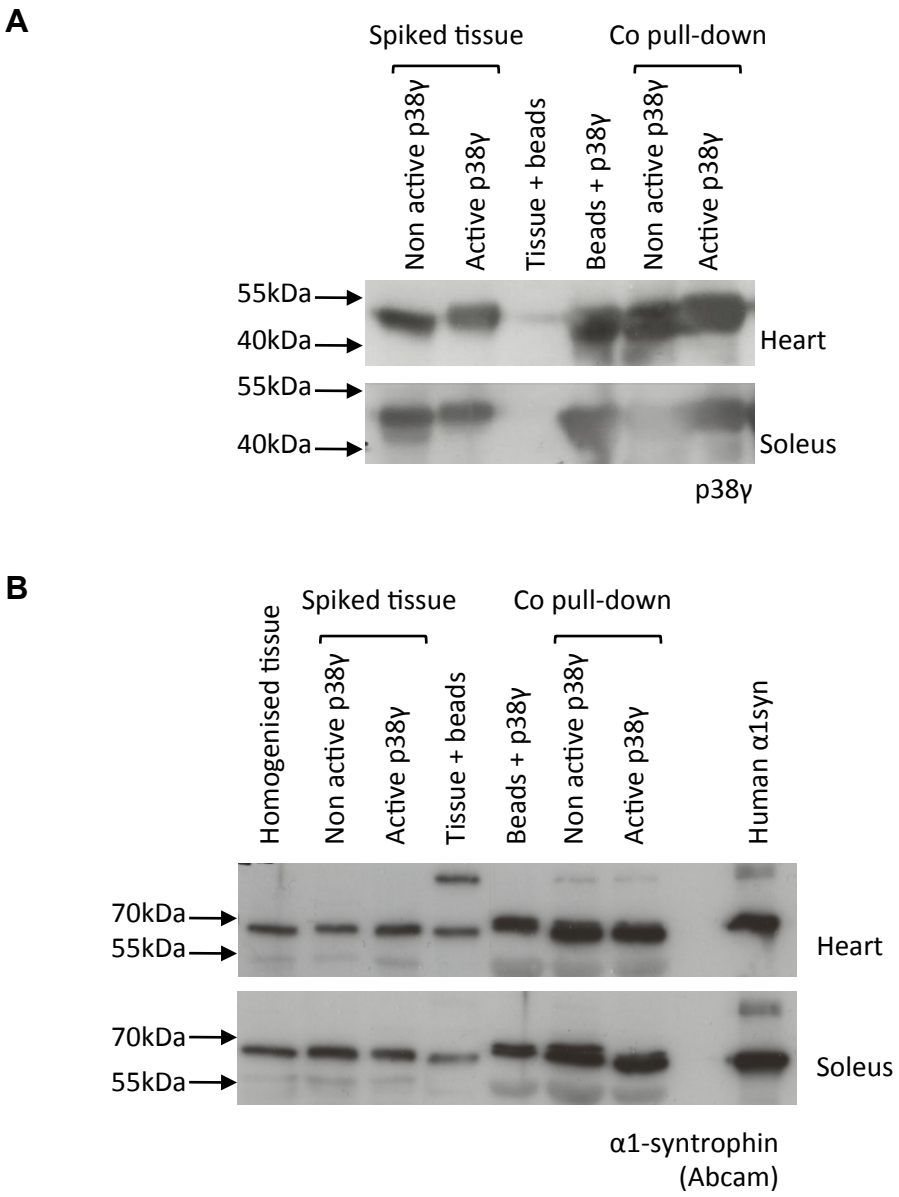

Figure 5.3 Immunoblot analyses of co pull-down

A, Immunoblot analysis of co pull-down samples for capture of p38γ from heart and soleus tissue. ***B,*** Immunoblot analysis of co pull-down samples for capture of α1-syntrophin from heart and soleus tissue. α1-syntrophin was successfully co-pulled down with both non-active and active p38γ. Some α1-syntrophin is pulled down non-specifically. Samples were resolved by 10% SDS-PAGE, as described in *Materials and Methods*.

To reduce the level of non-specific interactions of proteins with beads and to be able to visualise differences between control and pull-down samples, the following modifications to the protocol were made: 1) a higher concentration of salt (300 mM) was added to the tissue homogenisation buffer, 2) homogenisation buffer was supplemented with 20 mM imidazole and 3) the number and volume of washes were increased. As before, samples were taken from various stages of the co pull-down experiment for analysis as shown in Figure 5.4. The new optimisations did not affect the capture of the recombinant p38γ proteins. Increasing the concentration of imidazole or increasing the washing stringency did not cause loss of p38γ proteins in the flow through or during the washes. However the optimisations did not reduce the extent of non-specific binding, as there is no obvious differential banding pattern between control and pull-down samples. The immunoblot analysis of samples for α1-syntrophin in Figure 5.5 reveals that some non-specific binding of α1-syntrophin to the beads still persists, but binding of the contaminant *E.coli* protein is reduced.

As the previous modifications did not reduce the extent of non-specific binding of heart proteins to beads, an alternate approach to co pull-down was taken. In the previous experiments p38γ proteins were incubated with tissue homogenate for 30 min prior to incubation with beads for 1 h. In the current approach, p38γ proteins were first immobilised onto beads, before incubation with tissue homogenate. It was hoped that incubation of p38γ with beads would allow the recombinant proteins to occupy the binding sites on the surface of the beads before exposure to tissue proteins, therefore preventing non-specific interactions of proteins to beads. Furthermore, tissue homogenates were also pre-cleared with beads to remove any proteins that bound with high affinity non-specifically to the beads. A comparison of the two co pull-down approaches taken is shown in the schematic in Figure 5.6.

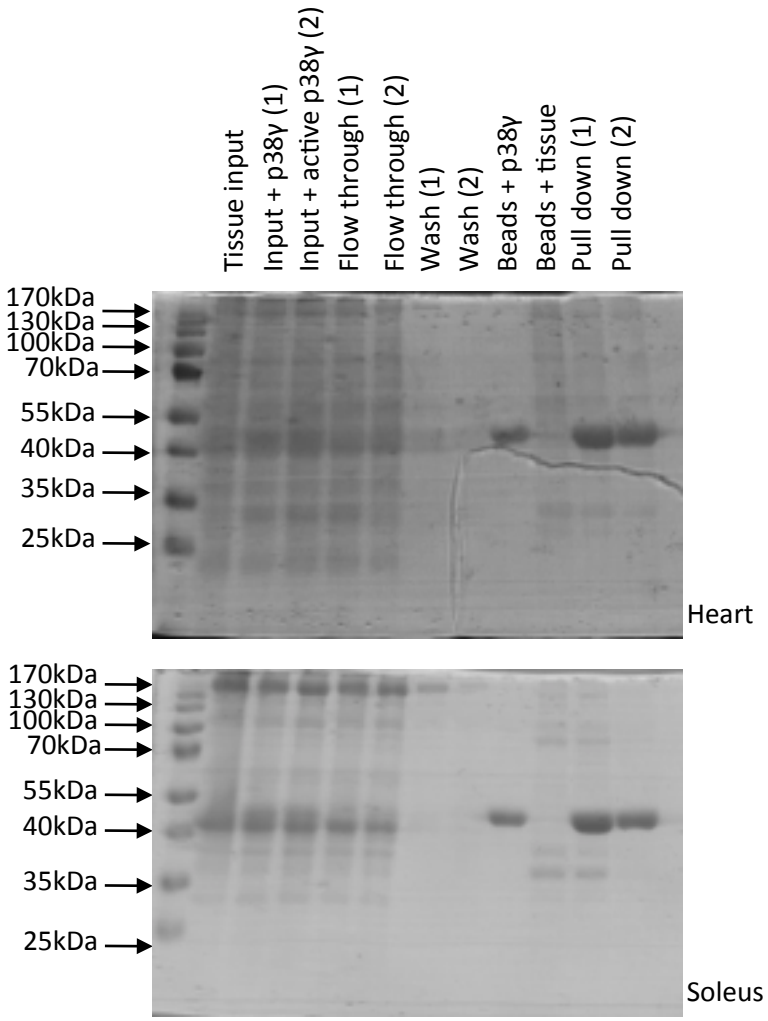

Figure 5.4 Heart and soleus co pull-down analysis following modifications to protocol

Co pull-downs were performed in parallel with heart or soleus homogenate and p38γ (1) or MKK6EE-activated p38γ (2). Recombinant p38γ proteins were incubated with heart or soleus tissue prior to capture with Ni-NTA agarose beads, as described in *Materials and Methods*. Samples were resolved by 10% SDS-PAGE and Coomassie stained. Modifications to the protocol did not cause a dramatic decrease in non-specific binding of proteins to the beads.

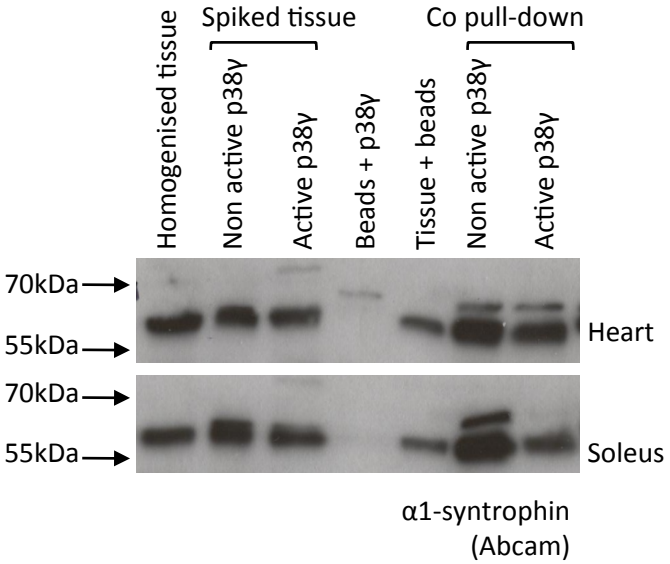

Figure 5.5 Immunoblot analysis of co pull-down

Immunoblot analysis of co pull-down samples, following modifications to the protocol, for capture of α1-syntrophin from heart and soleus tissue. Samples were resolved by 6% SDS-PAGE, as described in *Materials and Methods*. Non-specific binding of α1-syntrophin to the beads still persists, despite the modified protocol.

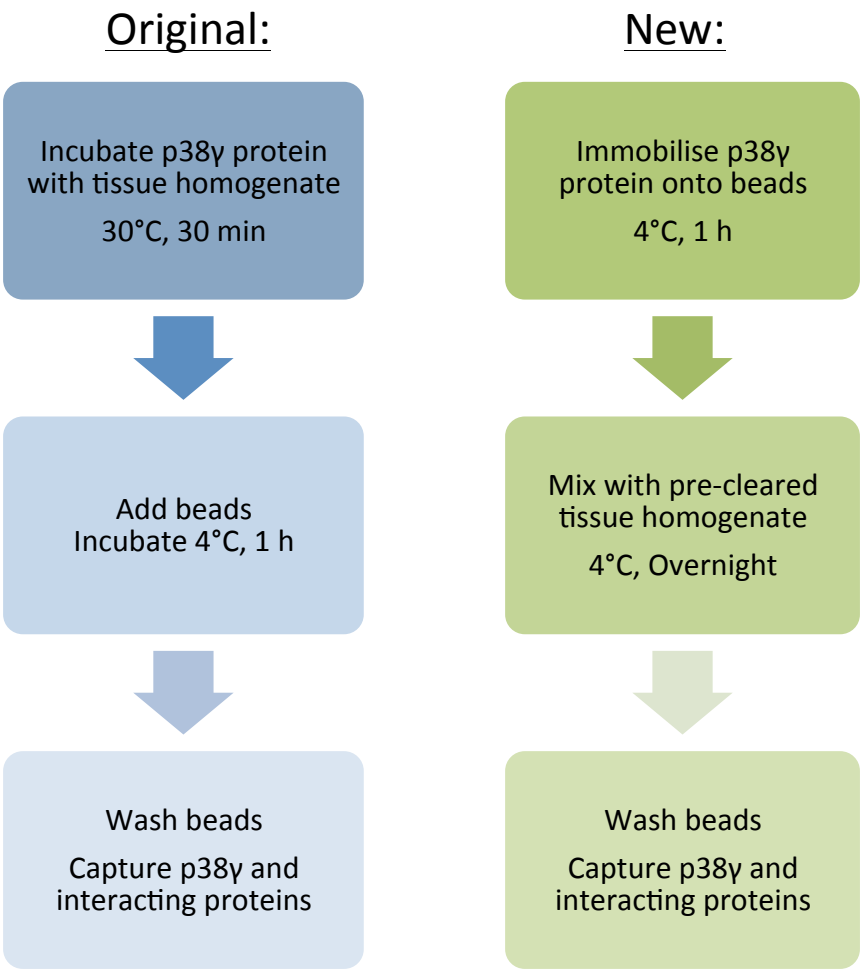

Figure 5.6 The two different approaches taken to identify interacting partners of p38γ

To reduce non-specific binding of cardiac proteins to beads, a modified co pull-down approach was devised.

Figure 5.7A shows the outcome of the new approach. A comparison is made between co pull-downs conducted with non pre-cleared and pre-cleared heart homogenate. To improve visualisation of protein bands, SDS-PAGE gels were stained with silver. In contrast to Coomassie stained gels, clearer and discreet bands are observed. As before, the new approach successfully captures p38γ proteins but pre-clearing the heart homogenate does not specifically reduce the extent of non-specific interactions. Furthermore the new approach and/or pre-clearing of tissue samples did not affect co-capture of α1-syntrophin but greatly reduced non-specific binding of α1-syntrophin to the beads (Figure 5.7B and C).

The interaction of α1-syntrophin with p38γ and subsequent phosphorylation, is mediated via the PDZ domain of α1-syntrophin and the C' interacting motif of p38γ. Therefore, co-capture of α1-syntrophin should not occur with p38α, which lacks the C' interacting motif. Whilst p38α can mediate *in vitro* phosphorylation of α1-syntrophin (Figure 4.7), α1-syntrophin co-capture with p38α is minimal in comparison to co-capture with p38γ (Figure 5.8).

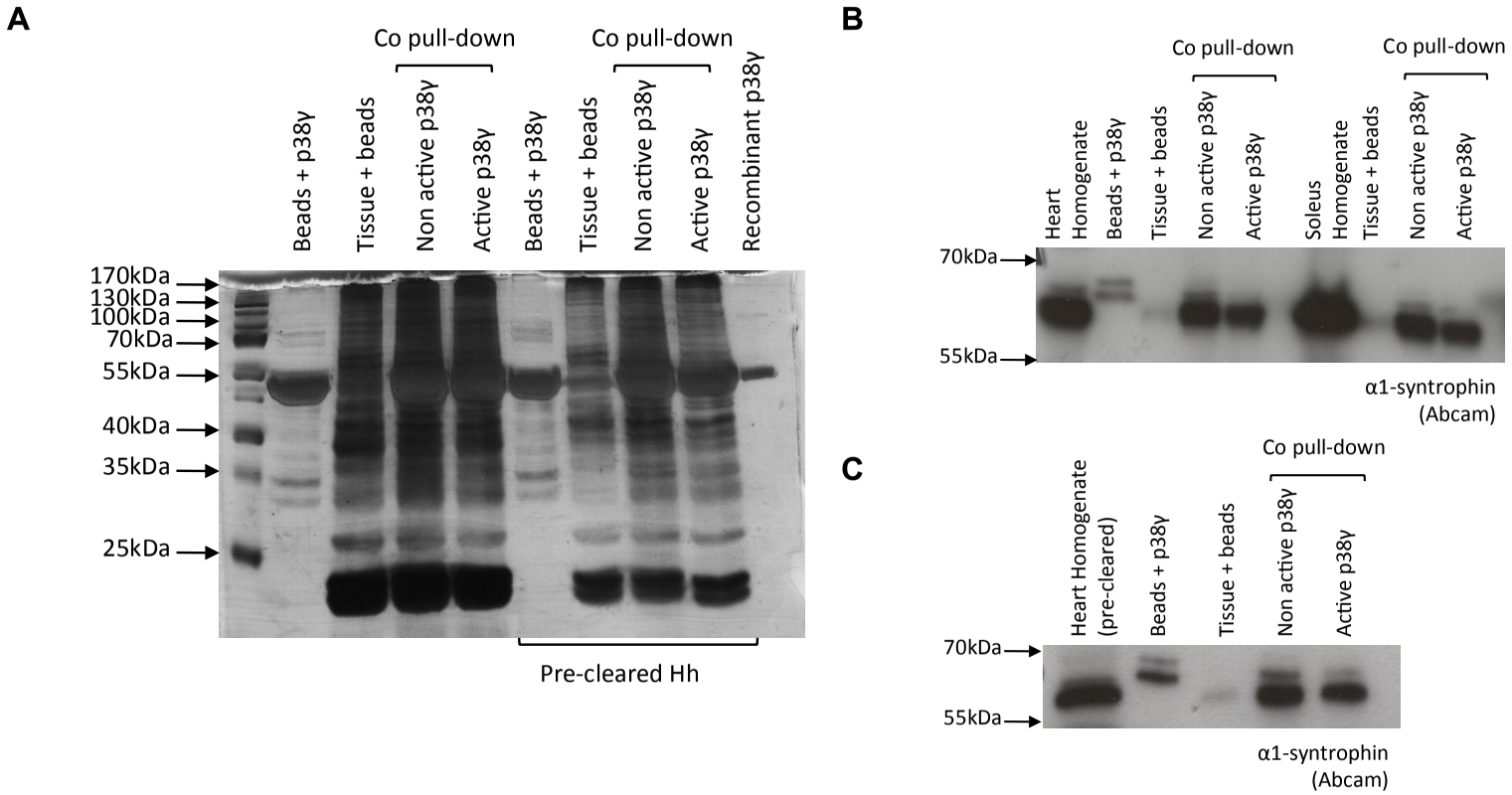

Figure 5.7 Analyses of the modified co pull-down approach

A, SDS-PAGE/silver staining analysis of proteins co-captured with p38γ from non pre-cleared and cleared heart homogenate. ***B,*** Immunoblot analysis of co pull-down samples, under the conditions of the new approach, for capture of α1-syntrophin from heart and soleus tissue. ***C,*** Immunoblot analysis of co pull-down samples, using pre-cleared heart homogenate, for capture of α1-syntrophin from heart tissue. Non-specific binding of α1-syntrophin is greatly reduced in the new approach. Samples were resolved by 6 or 10% SDS-PAGE and silver stained, as described in *Materials and Methods*.

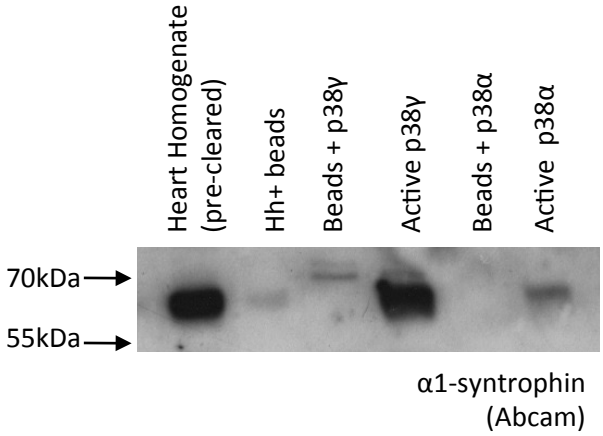

Figure 5.8 α1-syntrophin capture with p38γ and p38α.

Immunoblot analysis of co pull-down samples for capture of α1-syntrophin from heart tissue with p38γ and p38α. α1-syntrophin co-capture with p38α is minimal in comparison to co-capture with p38γ Samples were resolved by 6% SDS-PAGE, as described in *Materials and Methods*.

Despite the reduction in non-specific binding of α1-syntrophin to the beads under the new experimental approach, the optimisations carried out so far did not reduce the extent of non-specific binding of proteins to the beads. Therefore the type of resin used to pull-down p38γ was next examined. In addition to the co pull-downs with Ni-NTA agarose, cobalt resin co pull-downs with homogenised heart tissue were also carried out. Control, uncharged agarose was also incubated with heart homogenate to determine if the non-specific binding occurs due to the agarose matrix or the charged groups. From Figure 5.9 it can be seen that no proteins are detected when uncharged agarose alone is incubated with heart homogenate. This suggests that non-specific interactions occur with the charged groups on the agarose. Both nickel and cobalt agarose encountered non-specific interactions, but to a lesser extent with the cobalt beads. However, the overall binding efficiency of the cobalt resin appeared to be reduced compared to the nickel resin as less recombinant p38γ protein was also retained. As such, co-capture of α1-syntrophin was also reduced when cobalt resin is used in comparison to nickel. As expected, the uncharged control agarose did not bind any α1-syntrophin protein.

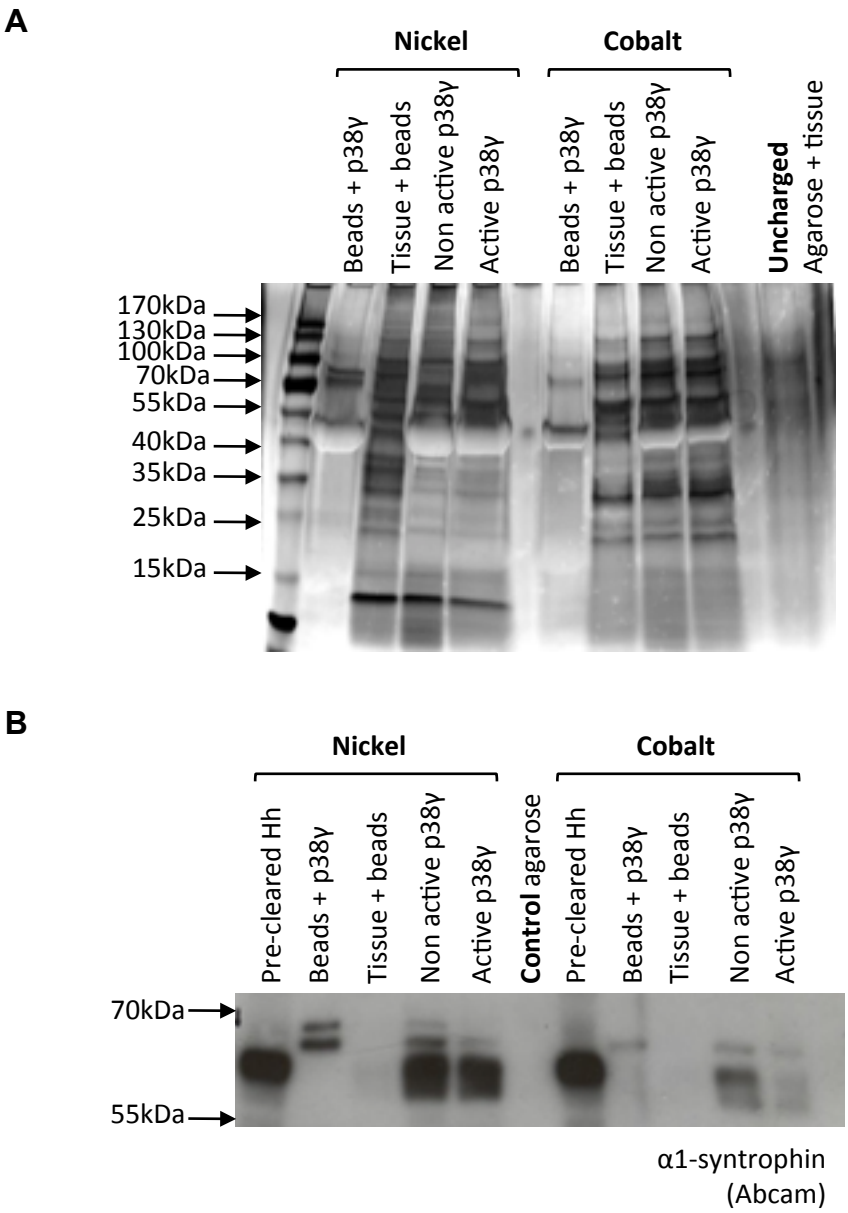

Figure 5.9 Heart co pull-down analysis

A, Comparison of co pull-downs using Ni-NTA and cobalt resin. The extent of non-specific binding of proteins to beads is reduced with cobalt resin, but it also retains less p38γ. Samples were resolved by 10% SDS-PAGE and silver stained, as described in *Materials and Methods*. ***B,*** Immunoblot analysis of co pull-down samples for capture of α1-syntrophin from heart tissue. Co-capture of α1-syntrophin was also reduced when cobalt resin is used in comparison to nickel. Samples were resolved by 6% SDS-PAGE, as described in *Materials and Methods*.

From the α1-syntrophin probes it can be seen that there is consistently little non-specific binding of α1-syntrophin to the beads and that it is only specifically pulled down in the presence of non-active or active p38γ. Yet, analysis of the stained proteins does not reveal any striking differences between the control and the co pull-down samples. For a more comprehensive analysis, co pull-down samples were further analysed by mass spectrometry. Co pull-downs for mass spectrometry were performed using nickel resin as before. Samples were resolved by SDS-PAGE and gels stained with silver as shown in Figure 5.10. Lanes marked with asterisks were individually processed and analysed by LC-MS/MS. Proteins identities were only accepted if they could be established at greater than 99.0% probability with at least two independent peptides.

A list of 20 proteins that were specifically pulled down with non-active or active p38γ is given in Table 5.1. A further list of 14 proteins, that were detected in control but had a higher frequency of peptides in the co pull-down sample, is given in Table 5.2. The proteins detected in the co pull-down study were also cross-referenced against the list of putative p38γ substrates detected by the Shokat approach. Proteins that appeared in both experiments are indicated in Table 5.1. and Table 5.2.

Additional overlapping proteins, that were bound non-specifically or did not meet the protein identify criteria, but appeared in both experiments are given Table 5.3.

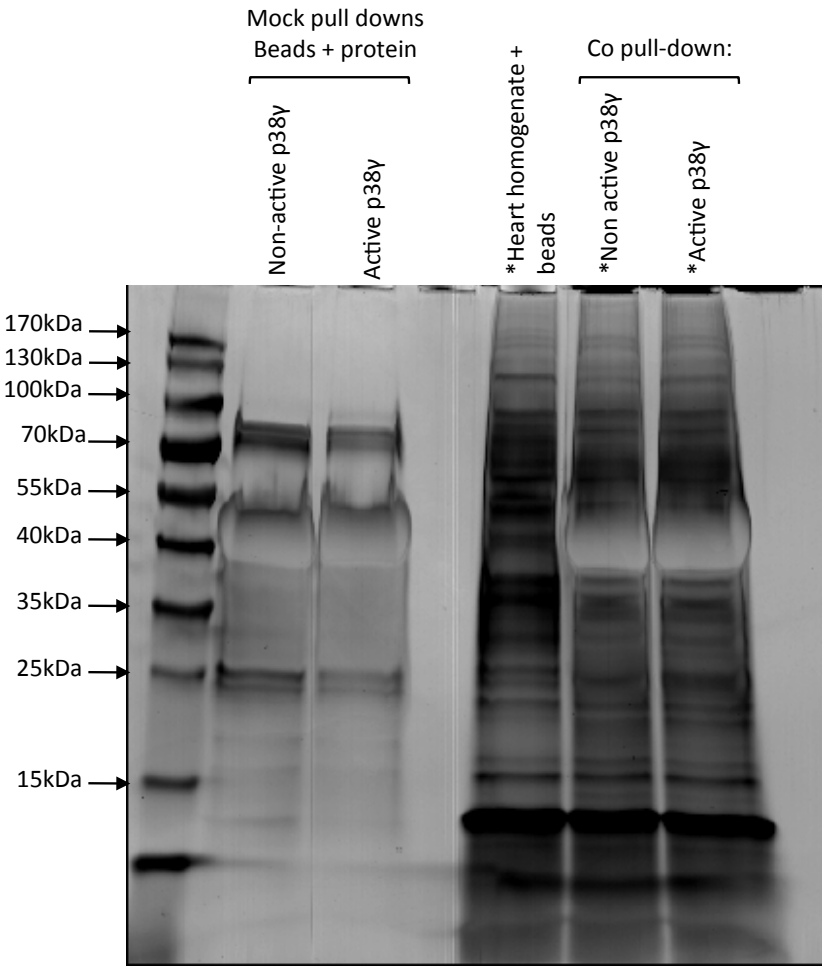

Figure 5.10 Preparation of co pull-down samples for mass spectrometry analysis

Co pull-down samples for LC-MS/MS analysis were prepared using Ni-NTA resin to capture p38γ and any interacting cardiac proteins. Samples were resolved by 10% SDS-PAGE and silver stained, as described in *Materials and Methods*. Entire lanes marked with asterisks were processed for LC-MS/MS analysis.

Table 5.1 Proteins specifically pulled down with p38γ

	UNIPROT ID	PROTEIN	SHOKAT	FUNCTION
1	Q9JHL1	Na(+)/H(+) exchange regulatory cofactor NHE-RF2		Scaffold
2	Q9D8T7	SRA stem-loop-interacting RNA-binding protein, mitochondrial		Nuclear receptor corepressor
3	Q80U72	Protein scribble homolog*		Scaffold
4	P27546	Microtubule-associated protein 4	✓	Microtubule protein
5	Q811D0	Disks large homolog 1*		Scaffold
6	O54931	A-kinase anchor protein 2	✓	Scaffold
7	Q60592	Microtubule-associated serine/threonine-protein kinase 2		Kinase
8	Q9JLV1	BAG family molecular chaperone regulator 3		Co-chaperone
9	P70670	Nascent polypeptide-associated complex subunit alpha, muscle-specific form		Transcription factor
10	O88492	Perilipin-4		Triacylglycerol packaging
11	Q62407	Striated muscle-specific serine/threonine-protein kinase	✓	Kinase
12	Q3UTJ2	Sorbin and SH3 domain-containing protein 2		Scaffold
13	Q9QWY8	Arf-GAP with SH3 domain, ANK repeat and PH domain-containing protein 1		GTPase-activating protein
14	P08122	Collagen alpha-2(IV) chain		Collagen type
15	P12382	6-phosphofructokinase, liver type		Glycolysis kinase
16	P60335	Poly(rC)-binding protein 1		Nucleic acid binding protein
17	Q921H8	3-ketoacyl-CoA thiolase A, peroxisomal		Fatty acid metabolism
18	P58252	Elongation factor 2		Translational elongation
19	Q91YE3	Egl nine homolog 1		Cellular oxygen sensor
20	Q69Z23	Dynein heavy chain 17, axonemal		Force generating protein of respiratory cilia

Key:

* **Known interactions**

PDZ domain

Table 5.2 p38γ interacting partners

Shown in the table below are proteins that were non-specifically pulled down but a higher frequency of peptides was detected in the co pull-down sample.

	UNIPROT ID	PROTEIN	SHOKAT	FUNCTION
1	Q9JKS4	LIM domain-binding protein 3	✓	Scaffold
2	Q9Z0U1	Tight junction protein ZO-2		Tight junction
3	P11531	Dystrophin		Anchors the extracellular matrix to the cytoskeleton
4	Q99KI0	Aconitate hydratase, mitochondrial		Isomerisation of citrate to isocitrate
5	Q8BWT1	3-ketoacyl-CoA thiolase, mitochondrial		Fatty acid metabolism
6	P50462	Cysteine and glycine-rich protein 3		Positive regulator of myogenesis.
7	P35486	Pyruvate dehydrogenase E1 component subunit alpha, somatic form, mitochondrial		Converts pyruvate to acetyl-CoA and CO2
8	Q8CGB6	Tensin-like C1 domain-containing phosphatase		Phosphatase
9	Q91VX2	Ubiquitin-associated protein 2		Ubiquitin–proteasome pathway
10	Q9ET54	Palladin		Cytoskeletal protein
11	Q8BTM8	Filamin-A		Scaffold
12	Q8CI51	PDZ and LIM domain protein 5		Scaffold
13	Q8QZT1	Acetyl-CoA acetyltransferase, mitochondrial		Ketone body metabolism
14	A2AQ25	Sickle tail protein		Developmental protein

Key:

* **Known interactions**

PDZ domain

Table 5.3 Proteins detected in both Shokat and co pull-down studies

Shown in the table below are proteins that were detected in both the Shokat and co pull-down studies but were bound non-specifically or did not meet the protein identify criteria.

	UNIPROT ID	PROTEIN
1	Q9ET78	Junctophilin-2
2	Q9EQ20	Methylmalonate-semialdehyde dehydrogenase [acylating], mitochondrial
3	Q9JKP5	Muscleblind-like protein 1
4	Q91YT0	NADH dehydrogenase [ubiquinone] flavoprotein 1, mitochondrial
5	Q80XB4	Nebulin-related-anchoring protein
6	B2RRE7	OTU domain-containing protein 4
7	O08709	Peroxiredoxin-6
8	P48678	Prelamin-A/C
9	Q9JKV1	Proteasomal ubiquitin receptor ADRM1
10	Q99MR9	Protein phosphatase 1 regulatory subunit 3A
11	Q9ES28	Rho guanine nucleotide exchange factor 7
12	P39447	Tight junction protein ZO-1

5.4 Discussion

5.4.1 Summary

A co pull-down study using recombinant 6xHis-WT p38γ was used to probe interacting partners of p38γ in the myocardium. For this Ni-NTA beads immobilised with 6xHis-WT p38γ were incubated with heart homogenate. After a series of washes, specific protein interactions were probed by SDS-PAGE followed by Western blotting or silver staining. Using this methodology endogenous α1-syntrophin was specifically pulled down with p38γ in soleus and heart tissue. Whilst the α1-syntrophin interaction with p38γ has previously been reported in skeletal muscle (Hasegawa et al. 1999), this is the first evidence of p38γ interacting with endogenous cardiac α1-syntrophin.

The aim of this study was to identify other novel interactions of p38γ in the myocardium. Due to the presence of its C' PDZ interacting motif, of particular interest were proteins that contained the complementary PDZ domain. Mass spectrometry analysis of p38γ co pull-down samples identified 20 proteins that were specifically pulled down with p38γ. Of these, 2 proteins have previously been reported as interacting partners of p38γ (protein scribble homolog and DLG1) and 4 proteins were identified to contain a PDZ domain. Interestingly, 3 proteins detected in this study were also identified as putative substrates by the Shokat screen. An additional 14 proteins were identified that were detected to be non-specifically bound to the Ni-NTA beads but a higher frequency of peptides, corresponding to the protein, were identified in the presence of p38γ. Within this second list, 3 proteins contain PDZ domains, 1 of which was also identified by the Shokat screen (LDB3).

5.4.2 6xHis co pull-down

A common strategy for assessing protein interactions of a protein of interest is co-immunoprecipitation. This utilises an antibody to precipitate the target protein and with it any interacting proteins. This strategy was initially employed to investigate interactions of p38γ in the myocardium (data not shown). A key

determinant of the success of this approach is the specificity of the antigen antibody and for p38γ little success was encountered. Another commonly encountered problem with the use of antibodies is the interference from the antibody light and heavy chains in the analysis of gels. Therefore, to overcome the limitations associated with co-immunoprecipitation, a 6xHis co pull-down approach was taken. In addition, conditions of 6xHis-WT p38γ binding to Ni-NTA were already well established from the purification of the protein earlier.

Co pull-down of endogenous α1-syntrophin with p38γ from soleus and heart tissue was used to assess success of the approach. Gratifyingly, in both settings, specific pull-down of α1-syntrophin with p38γ was observed without extensive optimisation of conditions. However, high levels of non-specific interactions were observed during gel analysis. As uncharged, control agarose did not retain proteins, much of the non-specific interactions of proteins were due to the charge present on the Ni-NTA or cobalt beads. A proportion of these non-specific interactions could be endogenous proteins that contain tandem histidine residues that mimic the 6xHis tag and therefore bind with high affinity to the charged agarose. A limitation of high non-specific binding is that it can obscure identification of proteins that are low abundance during mass spectrometry. Measures were taken to decrease the extent of non-specific interactions including the use of high stringency buffers and pre-clearing of heart homogenate with Ni-NTA agarose prior to co pull-downs. However this did not massively reduce the extent of non-specific interactions. In future co pull-down experiments, competitive elution could be employed to circumvent non-specific binding of proteins and clean up the analysis.

When examining interactions of a protein using this method, it is important to bear in mind that the proteins identified are not bona fide interacting proteins. This method is never physiological and as with many *in vitro* methods it does not take into account the cellular milieu, which determines the specificity of protein interactions. Therefore, a study of this kind is considered a complementary method to study protein interactions. In this instance it was used to complement the Shokat approach taken to identify substrates of p38γ.

A brief discussion of the proteins identified and the chosen substrates for further study is given below.

5.4.3 Putative substrates also identified as specific p38γ interacting proteins

Four putative Shokat substrates were identified as specific interacting proteins in this approach, none of which have previously been reported. The four proteins are microtubule associated protein 4 (MAP4), A-kinase anchoring protein 2 (AKAP2), striated muscle specific serine/threonine kinase (SPEG) and lim domain binding protein 3 (LDB3). An important consideration during the selection of candidate proteins for further study is the literature concerning their physiological or pathophysiological cardiac function. Given below is a brief overview of the functions of these proteins.

MAP4 is a known substrate of p38α (Parker et al. 1998) but this is the first report of MAP4 interaction with, and phosphorylation by p38γ. There is some evidence in the literature that implicates a role of MAP4 in cardiac hypertrophy. In severe pressure overload-induced cardiac hypertrophy densification of the microtubule network is observed. Densification of the microtubule network is proposed as one mechanism of contractile dysfunction. There is also transcriptional up regulation of MAP4 and extensive microtubule decoration by MAP4, which stabilises microtubules (Cheng et al. 2002 and Cheng et al. 2005). This is reported to have adverse effects on both contractile function and intracellular transport (Cheng et al. 2010). Phosphorylation of MAP4 prevents its function as a microtubule stabilising protein (Chang et al. 2001). Interestingly, the Shokat data found both MAP4 and stathmin to be substrates of p38γ. In contrast to MAP4, stathmin promotes destabilisation of microtubules and its phosphorylation prevents its destabilising function (Hu et al. 2010). Hence the role of p38γ in microtubule regulation is puzzling but interesting and warrants further investigation given the role of microtubules in cell growth and hypertrophy. Furthermore, several other microtubule proteins were also identified as putative substrates of p38γ (tau, MAP7 domain-containing protein

1 and microtubule associated protein 1b) suggesting that p38γ is likely involved in microtubule regulation.

AKAPs serve to compartmentalise and enhance PKA signalling within a cell. Fourteen different AKAPs are reported to be expressed in rodent and human hearts (Rababa'h et al. 2014). Different AKAPs are responsible for localising PKA to different subcellular locations. In the heart, AKAPs coordinate the regulation of many proteins, involved in excitation-contraction coupling, by PKA phosphorylation (Rababa'h et al. 2014). However, a review of the AKAP literature does not so far describe a role of AKAP2 in the heart. Therefore whilst the interaction with and phosphorylation of AKAP2 by p38γ is intriguing, as it raises the possibility of integration of two key signalling paradigms within the cell, to study the effect of the interaction/phosphorylation would require extensive initial characterisation of AKAP2 function in the heart.

The literature on SPEG function in the myocardium is again limited. However it could be considered an interesting candidate for further study. SPEG appears to be crucial for cardiac development and function as SPEG KO mice displayed a phenotype characteristic of dilated cardiomyopathy. SPEG KO mice had dilated atria and ventricles, with myofibril degeneration and reduced cardiac function by postnatal day 2. There was also increased neonatal mortality of SPEG KO mice in comparison to WT neonates (Liu et al. 2009). Despite this promising report, like with AKAP2, much work remains to be done to better understand SPEG function in the heart, in order to then assess the functional effect of p38γ interaction and phosphorylation.

LDB3 was found to be the most characterised protein in the heart from the 4 proteins detected in both approaches and an early favourite for further study. It is a cytoskeletal protein that has been associated with dilated cardiomyopathies (Zhou et al. 1999, Zheng et al. 2004). Additionally it also contains a PDZ domain, which is likely to be of significance to its function and interaction with p38γ. A more detailed account of LDB3 function is given the following chapter, which covers the characterisation of substrates chosen for further study.

5.4.4 Selection of proteins for further study

Despite the fact that MAP4, AKAP2 and SPEG are putative substrates that were also detected as p38γ interacting proteins, these proteins were not pursued any further. As discussed earlier, knowledge of AKAP2 and SPEG function in the heart is incomplete and therefore would require extensive characterisation of function before the functional effect of p38γ phosphorylation could be determined. The case of MAP4 is more interesting, given the known role of p38γ in cytoskeletal regulation in non-cardiac tissue and that cardiomyocyte hypertrophy involves expansion and reorganisation of the microtubule cytoskeleton (Fassett et al. 2009). However, as only 3 proteins were initially chosen for further study, it was considered that other substrates identified from the Shokat approach (but not interacting partners) were perhaps more worthy of selection. An example of this is zfp260. It was the only transcription factor identified in the Shokat screen and as reviewed in more detail in the following chapter, zfp260 is implicated in cardiac hypertrophy signalling. As p38γ translocates to the nucleus (Dingar at al. 2010) of particular interest were transcription factors. Therefore zfp260 was examined further as a substrate of p38γ. In addition to LDB3 and zfp260, calpastatin was the remaining protein chosen for further study. Calpastatin is the natural and endogenous inhibitor of calpain proteases. As outlined in Chapter 1, calpain proteases are activated during cardiac hypertrophy. A more detailed overview of calpastatin signalling in hypertrophy is also covered in the following chapter.

6 CHARACTERISATION OF NOVEL SUBSTRATES OF p38γ

6.1 Introduction

Following the Shokat and co pull-down approach, three proteins were selected for further study; zfp260, LDB3 and calpastatin. Below is an account of the relevance of each candidate protein in cardiac physiology.

6.1.1 Zinc finger protein 260

Biochemical signalling during the development of hypertrophy leads to the activation of several signalling pathways as described in Chapter 1. Many of these, including the p38-MAPK pathways, converge on the nucleus where they regulate the activity of nuclear transcriptional factors and consequently gene transcription. Therefore any transcription factors that were identified from the Shokat screen were of particular interest. Zfp260 is a transcription factor identified in the list of potential substrates of p38γ. Whilst the literature on zfp260 is limiting, interestingly it has been identified as a novel cardiac regulator and a nuclear effector of α1-adrenergic (Debrus et al. 2005) and ET-1 signalling (Komati et al. 2011), both key hypertrophic signalling pathways.

Zfp260 or PEX1 is a zinc dependent DNA-binding protein that is highly enriched in the heart. It was discovered as a 46 kDa protein that belongs to the *Krüppel* family of transcriptional regulators (Blottiere et al. 1999). It was then identified as a novel cardiac regulator during the search for phenylephrine response element (PERE) interacting proteins (Debrus et al. 2005). A PERE is a α1-adrenergic regulatory element found in the 5' flanking sequences of the atrial natriuretic factor (ANF) gene and is necessary for full transcriptional activation of the ANF gene in response to α1 adrenoceptor agonists. Zfp260 was found to bind the PERE element and activate the ANF promoter. Furthermore, an additional mode of zfp260 action is also suggested whereby it behaves as a GATA-4 cofactor (Debrus et al. 2005). GATA-4 is also a zinc finger protein

transcriptional factor and crucially a known hypertrophic nuclear effector (Liang, Molkentin 2002).

A subsequent study found zfp260 to also mediate nuclear ET-1 signalling (Komati et al. 2011). ET-1 stimulation of cardiomyocytes potentiated the zfp260 transcriptional activation of the ANF promoter, without an increase in mRNA or protein levels of zfp260. Therefore it was deduced that a post-translational modification might regulate its activity. It was found that PKCβ phosphorylates zfp260 to potentiate its transcriptional activity (Komati et al. 2011). Proteins are often shared targets of multiple kinases and phosphorylation of the same or different sites can lead to the same or different functional outcomes. For example phosphorylation of GATA-4 by ERK or p38-MAPK leads to its activation (Akazawa, Komuro 2003). Similarly, phosphorylation of zfp260 by pro-hypertrophic kinase p38γ, like PKCβ mediated phosphorylation, could also potentiate its activity and may explain the aggravated responses to pressure overload hypertrophy observed in WT mice in comparison p38γ/δ$^{-/-}$ mice (Figure 6.1).

Moreover, to illustrate the role of zfp260 in hypertrophy, zfp260 overexpression in cardiomyocytes or in an inducible cardiac specific transgenic mouse, induces genetic and phenotypic features of cardiac hypertrophy (Komati et al. 2011). However, it must be noted that whilst mice hearts overexpressing zfp260 showed a significant increase in left ventricular mass and an increase in myocyte size, there was no sign of fibrosis or abnormal remodelling and cardiac function was not significantly different. Thus suggesting that, whilst zfp260 is an important nuclear mediator of hypertrophic pathways, other factors are involved in the transition of the heart to a pathological state. Nevertheless, it is a protein worth validating as a p38γ substrate.

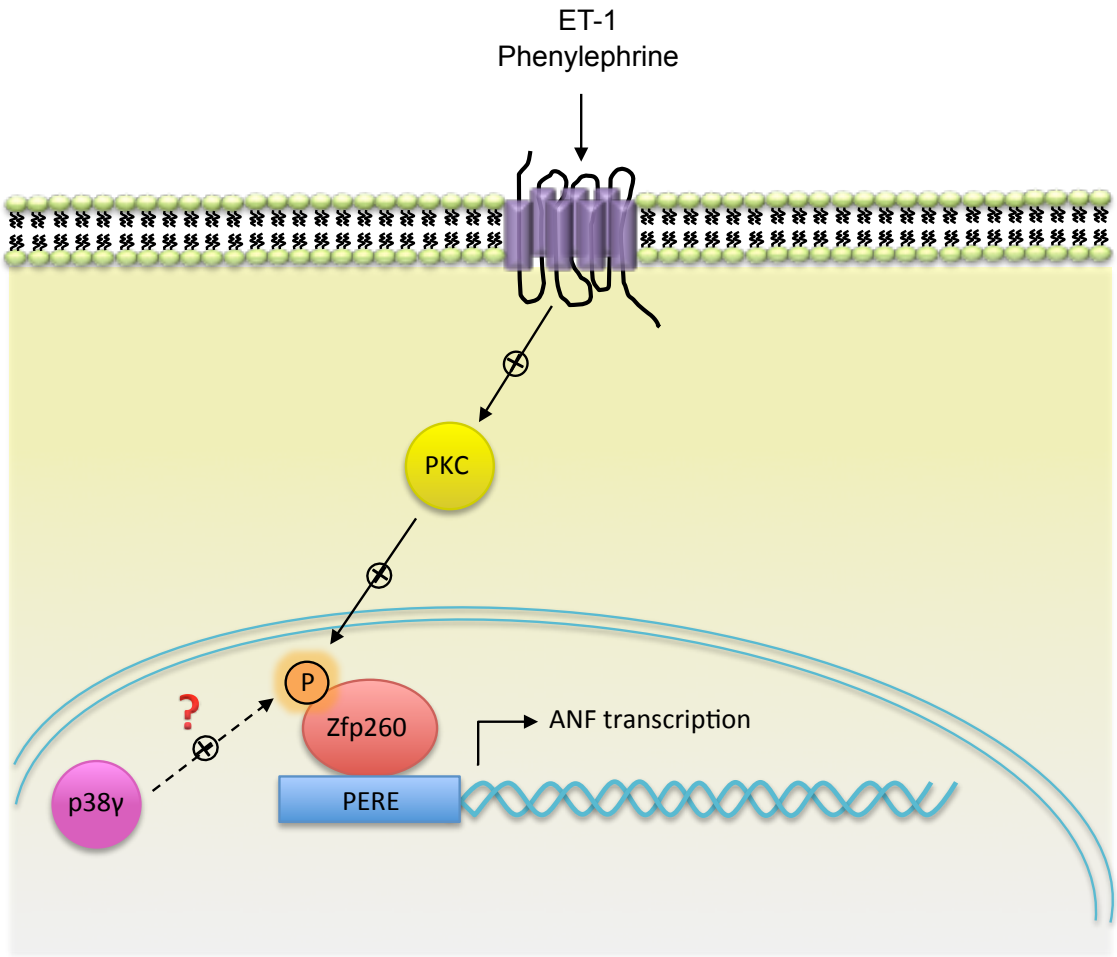

Figure 6.1 Zfp260 signalling in the myocardium

Zfp260 is a nuclear effector of α1-adrenergic (Debrus et al. 2005) and ET-1 signalling (Komati et al. 2011). Zfp260 binds to the PERE element in the 5' flanking sequence of the ANF gene. Phosphorylation of zfp260 by PKCβ potentiates its transcriptional activity. Similarly, phosphorylation by p38γ, which translocates to the nucleus during hypertrophy, could have the same effect.

6.1.2 Lim domain binding protein 3

LDB3 is a cytoskeletal protein that is highly and exclusively expressed in skeletal and cardiac muscle (Faulkner et al. 1999, Zhou et al. 1999). Also referred to as cypher or Z-line alternatively spliced protein (ZASP), it is localised to the Z-band and intercalated discs in striated muscle. Its precise function is not entirely clear but given its structure it is proposed to be a key cytoskeletal element involved in maintaining the integrity of the Z-line and for scaffolding of signalling proteins.

A study of cypher null mice reveals an essential role of cypher in maintaining the integrity of the Z-line (Zhou et al. 2001). In the first instance cypher null mice are not viable, with the majority of mice dying within 24 hrs of birth. Examination of heart tissue of neonatal WT and cypher KO mice reveals blood congestion and dilation of both ventricles in KO mice hearts. Additionally comparison of diaphragm muscle structure of WT and cypher KO mice shows highly disorganised and disrupted Z-lines in KO mice. However a comparison of diaphragm tissue during development (E17.5 - when the diaphragm is not yet active) reveals virtually indistinguishable diaphragms of WT and cypher KO mice. Therefore suggesting that cypher function is crucial for sustaining the Z-line during contraction, but not for Z disc assembly (Zhou et al. 2001). A follow up study using cardiac specific cypher KO and inducible cardiac specific cypher KO demonstrates that cypher plays a pivotal role in maintaining adult cardiac structure (Zheng et al. 2009). Both types of cypher KO mice had disrupted cardiomyocyte structure, decreased cardiac function and eventually developed a severe form of dilated cardiomyopathy followed by premature death (Zheng et al. 2009). Furthermore mutations in the *ZASP* gene have been associated with dilated cardiomyopathies (Lopez-Ayala et al. 2014) and left ventricular non compaction (Vatta et al. 2003, Lopez-Ayala et al. 2014) in humans, demonstrating the essential role of cypher in the heart.

The cypher sequence contains many protein-protein interaction domains that enable its scaffolding function (Figure 6.2). Firstly located at the amino-terminal of the protein is a classical PDZ domain, which has been shown to interact with

α-actinin, the key component of the Z-line (Zhou et al. 1999). Interestingly, p38γ contains a PDZ interaction consensus motif at its carboxy- terminal suggesting that cypher is likely to be substrate of this isoform and that the PDZ interaction could be a pre-requisite for phosphorylation. Data obtained from the co pull-down study supports this postulation. Whilst some cypher protein was non-specifically pulled down, there was an in increase in the number of cypher peptides detected in the presence of p38γ. Towards the middle of the cypher polypeptide chain there is a stretch of nine 5-8 amino acid repeats with minimum consensus sequence of Y(S/T)P(S/T). Currently it is not known what function this repetitive, polar sequence of amino acids confers to the function of cypher, but it has also been proposed to be a protein-protein interaction domain (Zhou et al. 1999). Lastly the carboxy-terminal of cypher contains three (**L**in11, **I**sl-1 and **M**ec-3) LIM protein-protein interaction domains, which have been shown to mediate the interaction of cypher with protein kinase C (PKC) (Zhou et al. 1999).

In addition to the many different protein-protein interactions available in cypher, it has also been proposed that a stretch of amino acids in cypher (200-217) could form an amphipathic helix (Lin et al. 2013). Interestingly, A-kinase anchoring proteins (AKAPs) bind to the regulatory subunits of protein kinase A (PKA) via an amphipathic helix (Carr et al. 1991). Therefore the ability of cypher to behave as an AKAP was tested. It was found that cypher could be specifically pulled down with the RIIα subunit of PKA from co-transfected HEK293 cells and that this interaction decreased when residues in the helix were mutated or the interaction was completely abolished when the helix region was deleted. Similarly, immunoprecipitation of cypher from mice heart tissue also co-immunoprecipitates the RIIα subunit (Lin et al. 2013). The functional significance of this interaction is also suggested. The PDZ domain of cypher interacts with the L-type calcium channel (LTCC) via its C' terminal PDZ interacting motif. Hence, cypher facilitates phosphorylation of LTCC by PKA, at least *in vitro* (Lin et al. 2013). Cypher therefore poses as an interesting target as it could be crucial in the scaffolding, integration and regulation of multiple signalling pathways within the cell (Figure 6.2).

There are also shorter, splice variant, isoforms of cypher present in cardiac muscle (Huang et al. 2003). Cypher 2 is also highly and exclusively expressed in skeletal and cardiac muscle. It is a ~30 kDa variant of cypher that does not feature the repetitive polar amino acid sequence or the carboxy-terminal LIM domains. Like canonical cypher it has an amino-terminal PDZ domain that interacts with α-actinin. A third variant, denoted cypher 3, is highly homologous to cypher 1 but lacks a stretch of 61 amino acids located after the PDZ domain and prior to the repetitive, polar amino acid sequences. Therefore it is slightly smaller with a molecular weight of ~70 kDa but still exhibits all the protein-protein interaction domains of full-length cypher. The putative phosphorylation sites (Ser^{98} and Ser^{240}) from the Shokat experiment are present in all splice variants of cypher. From the Shokat experiment we cannot be sure if the long or the short isoforms of cypher, or indeed all 3, are substrates of p38γ. Mass spectrometry analysis of the co pull-down experiment detects peptides exclusive to the longer isoforms of cypher (cypher 1 and 3), suggesting that the longer isoforms are likely substrates. It has been reported that cypher 1 is the predominant isoform expressed in the heart throughout development and into adulthood (Huang et al. 2003), therefore the sequence of the cypher recombinant protein used for subsequent validation experiments corresponds to the sequence of the cypher 1.

Whilst cypher can interact with PKC (Zhou et al. 1999) and PKA (Lin et al. 2013), regulation of cypher activity by phosphorylation, if any, is not well understood. Cypher can undergo phosphorylation by PKC but the functional significance of this phosphorylation event is not known (Zhou et al. 1999). Often phosphorylation of a scaffold protein at interacting domains alters its structure, thereby preventing interaction with binding partners. However analysis of the cypher sequence reveals that the putative p38γ sites (Ser^{98} and Ser^{240}) are not within any of the protein-protein interaction domains. Further examination of cypher function itself will be required to understand the consequence of its phosphorylation.

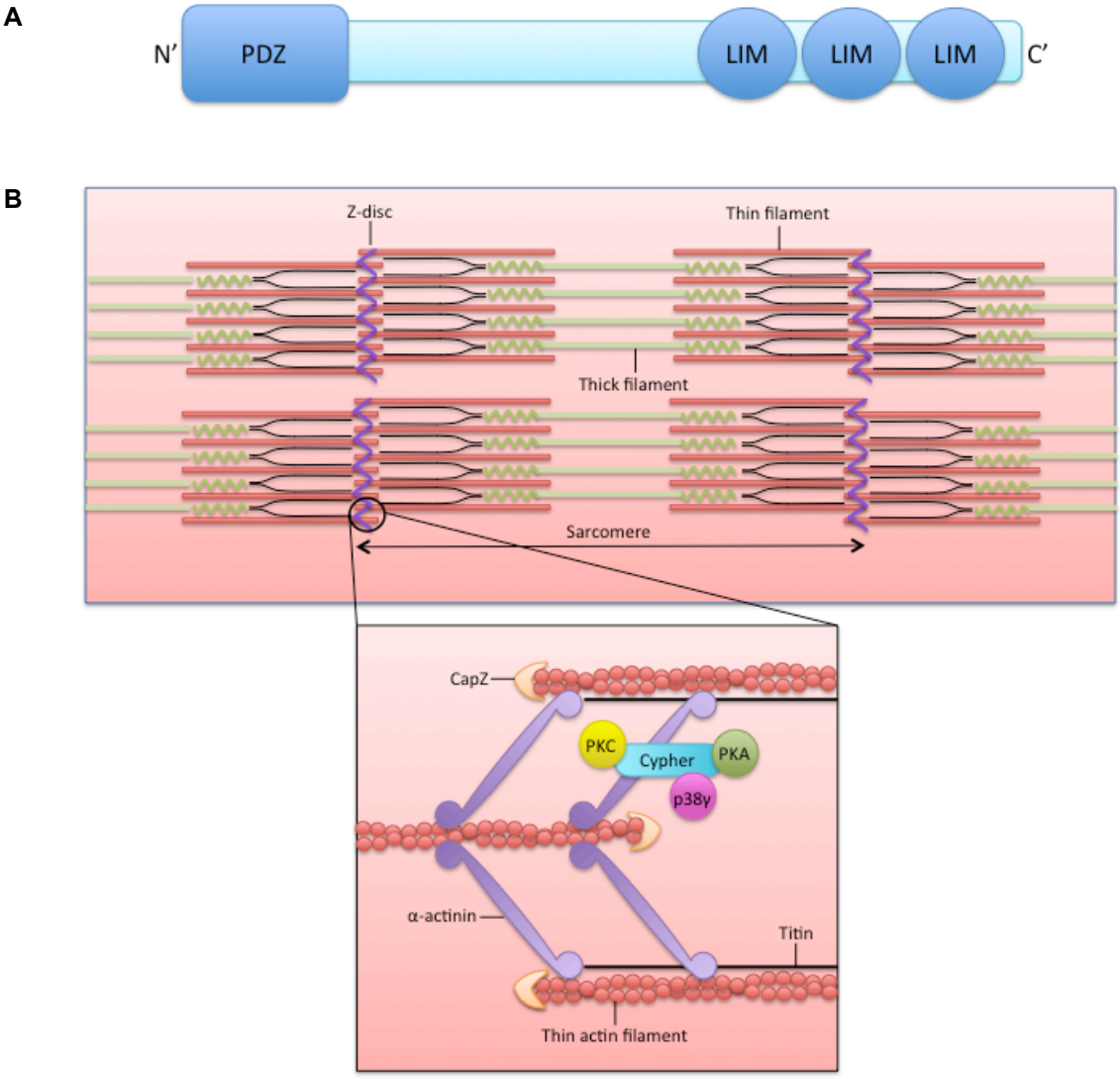

Figure 6.2 Scaffolding function of Cypher

A, The cypher protein structure exhibits many protein-protein interaction domains. ***B,*** Cypher is a scaffolding protein localised to the Z-disc (shown here) and intercalated disc of cardiomyocytes. It binds to α-actinin via its PDZ domain and PKC via its LIM domains. Cypher is also a putative p38γ interacting protein and substrate.

6.1.3 Calpastatin

Calpastatin is the natural and endogenous inhibitor of calpain proteases. As reviewed briefly in Chapter 1, calpain proteases become activated by increased intracellular calcium concentration during hypertrophy. To understand the rationale behind the selection of calpastatin for validation as a true p38γ substrate, a more in depth understanding of the calpain system and its signalling during hypertrophy is required. Thus, below is a summary of the calpain-calpastatin system, calpain biology pertaining to the heart and, importantly, regulation of calpastatin by phosphorylation.

Calpain proteases form an important regulatory mechanism within cells and as such calpains are ubiquitously expressed within all cells. The two conventional calpain isoforms, μ-calpain (calpain 1) and m-calpain (calpain 2), are named according to the concentration of calcium (micromolar or millimolar respectively) required for their activation. Both calpains are heterodimeric proteins, consisting of a large 80 kDa catalytic subunit and a small 28 kDa common regulatory subunit. In their non-active form, calpains are localised to the cytosol. Binding of calcium to the EF hands in calpain causes a conformational change and results in calpain activation (Goll et al. 2003). An example of calpain signaling during cardiac hypertrophy is depicted in Figure 6.3B. As discussed earlier, calpain proteases mediate degradation of calcinuerin, allowing subsequent dephosphorylation and activation of the pro-hypertrophic NFAT transcription factor (Burkard et al. 2005).

Calpastatin is also ubiquitously expressed and specifically inhibits both calpain proteases. It has an N' terminal L domain followed by four repetitive inhibitory (I-IV) domains that can each reversibly inhibit one calpain molecule (Figure 6.3A). In its calpain-unbound form, calpastatin is an intrinsically unstructured protein. It can only bind to active calpain and upon binding it adopts a defined structure (Mellgren 2008). Each inhibitory domain of calpastatin is further divided into three subdomains; A, B and C. Subdomain B is formed of a conserved stretch of 12 amino acids that are essential for calpain inhibition (Wendt, Thompson & Goll 2004). The resolved crystal structure of the calcium bound m-calpain in

complex with a single calpastatin inhibitory domain shows that subdomains A and C, of each inhibitory domain, form contacts with the EF hand domain regions of calpain. Binding of subdomains A and C then allows subdomain B to occupy the substrate binding cleft of calpain, preventing calpain proteolysis of substrates (Hanna, Campbell & Davies 2008, Mellgren 2008, Moldoveanu, Gehring & Green 2008).

Calpain activity during cardiovascular pathophysiological processes has been assessed in several studies examining different disease stimuli. Generally inhibition of calpain activity shows favourable improvements in cardiac function. For example, chronic infusion of Angiotensin II induces cardiac hypertrophy in mice, an effect that is blunted in transgenic mice overexpressing calpastatin (Letavernier et al. 2008). Similarly, short-term streptozotocin (STZ) induced type 1 diabetes in mice causes an increase in cardiomyocyte size and up regulation of ANP and β-MHC, indicative of cardiac hypertrophy. However the same changes are not observed in Capn4 KO mice following STZ injection. Capn4 KO mice lack the regulatory subunit of calpains, resulting in disruption of calpain 1 and 2 activities. Similar responses were also observed in transgenic mice overexpressing calpastatin following STZ injection (Li et al. 2011).

A more recent study has assessed calpain activity in myocardial remodelling following acute myocardial infarction (MI). Again, inhibition of calpain in transgenic mice overexpressing calpastatin shows a blunted response to acute MI (Ye et al. 2015). Calpastatin transgenics display significantly reduced infarct sizes, less ventricular hypertrophy and global myocardial fibrosis. Assessment of calpain expression and activity post-MI shows significant increases in protein expression of calpain 1 and 2 and calpain activity in WT mice and a significant decrease in calpastatin expression. Whilst the transgenic mice showed no change in baseline calpain expression or activity, post-MI calpain expression and activity was attenuated compared to WT mice (Ye et al. 2015). Data from patients with congestive heart failure (CHF) further supports calpain data from mouse models of cardiac remodelling. There is a significant increase in the protein levels of both calpain 1 and 2 in severe failing hearts compared to

hearts of healthy controls and concomitant increase in cleavage of calpain substrate cain/cabin 1 (Yang et al. 2010).

The studies discussed above highlight the involvement of the calpain system in cardiac hypertrophy and remodelling, thus presenting calpastatin as an attractive candidate for elucidation as a p38γ substrate. The question then arises: what is the functional significance of calpastatin phosphorylation? An obvious starting point is assessing if phosphorylation of calpastatin affects its ability to inhibit calpain and few laboratories have examined this so far. The matter is slightly complicated, as studies have examined calpastatin phosphorylation in different species. Generally phosphorylation of calpastatin is reported in the extreme N' terminal region of the inhibitor molecule, a region which is least conserved and subject to alternative splicing (Goll et al. 2003). In all examples given here the phosphorylation sites are not conserved in the murine calpastatin sequence. Nonetheless the findings offer insight into how potential phosphorylation of calpastatin by p38γ might regulate its activity.

Phosphorylation of calpastatin from rat skeletal muscle and brain has been most extensively studied. Isolation of calpastatin from various rat tissues (skeletal muscle, brain, kidney and heart) results in the purification of two calpastatin isoforms, distinguishable as two separate peaks following ion exchange chromatography (Pontremoli et al. 1992, Salamino et al. 1994). The two isoforms were termed calpastatin I and calpastatin II. Analysis of rat skeletal muscle calpastatins shows that calpastatin I is the most abundant form and shows maximal efficiency in inhibiting calpain I. In contrast calpastatin II is less abundant and exhibits higher inhibition of calpain 2. The difference between the two isoforms was subsequently attributed to a phosphorylation event of a single isoform by PKA. Calpastatin I undergoes reversible phosphorylation by PKA resulting in a switch in the inhibitory preference of the inhibitor (Pontremoli et al. 1992, Salamino et al. 1994). Isolated rat brain calpastatin II and recombinant phospho-calpastatin was found to undergo phosphorylation by PKA and PKC *in vitro* at a single serine residue in the N' terminal. In this instance phosphorylation renders the inhibitor less efficient in inhibiting both brain

calpains (Salamino et al. 1997, Averna et al. 1999). It was shown that phosphorylation changes the affinity of calpastatin for calpain, as a higher concentration of calcium is needed for interaction of phospho-calpastatin with calpain compared to non-phosphorylated calpastatin (Averna et al. 1999).

Immunoprecipitation of calpastatin from human hematopoietic HUT-102 cell line also results in isolation of non-phosphorylated and phosphorylated calpastatin (Adachi et al. 1991). Analysis of cellular localisation of the two calpastatin forms found that non-phosphorylated calpastatin was found mainly in the cytosolic fraction, whereas 30% of phosphorylated calpastatin was found in the membrane fraction (Adachi et al. 1991). Phosphorylation of calpastatin has also been shown to alter its localisation in human neuroblastoma LAN-5 cells visually. In its phosphorylated form calpastatin is localised in aggregates close to the nucleus. Increasing the intracellular calcium concentration results in dephosphorylation of calpastatin and its redistribution as a soluble inhibitor. Treatment with 3'-5'-cyclic adenosine monophosphate (cAMP) reverses its distribution into aggregates following phosphorylation (Averna et al. 2001). Taken together, these studies indicate many different aspects of calpastatin signalling (calpain specificity, inhibitory efficiency, calpain interaction affinity and cellular localisation) that phosphorylation could regulate.

The three putative p38γ proline directed phosphorylation sites from the Shokat screen are Thr^{216}, Ser^{219} and Thr^{467} in isoform 1 (or Thr^{197}, Ser^{200} and Thr^{448} in isoform 2). Analysis of the calpastatin sequence reveals that Thr^{216} and Ser^{219} are located N' terminal to the first inhibitory domain of calpastatin and Thr^{467} is located in the sequence linking inhibitory domains 2 and 3. Therefore the locations of the sites do not coincide with key regions of calpastatin known to be essential in mediating calpain interaction and/or inhibition. Despite this, given the functional effects calpastatin phosphorylation described above, if p38γ phosphorylation reduces the inhibitory efficiency of calpastatin (Figure 6.3B), this may explain the aggravated responses to pressure overload hypertrophy observed in WT mice in comparison p38γ/$\delta^{-/-}$ mice.

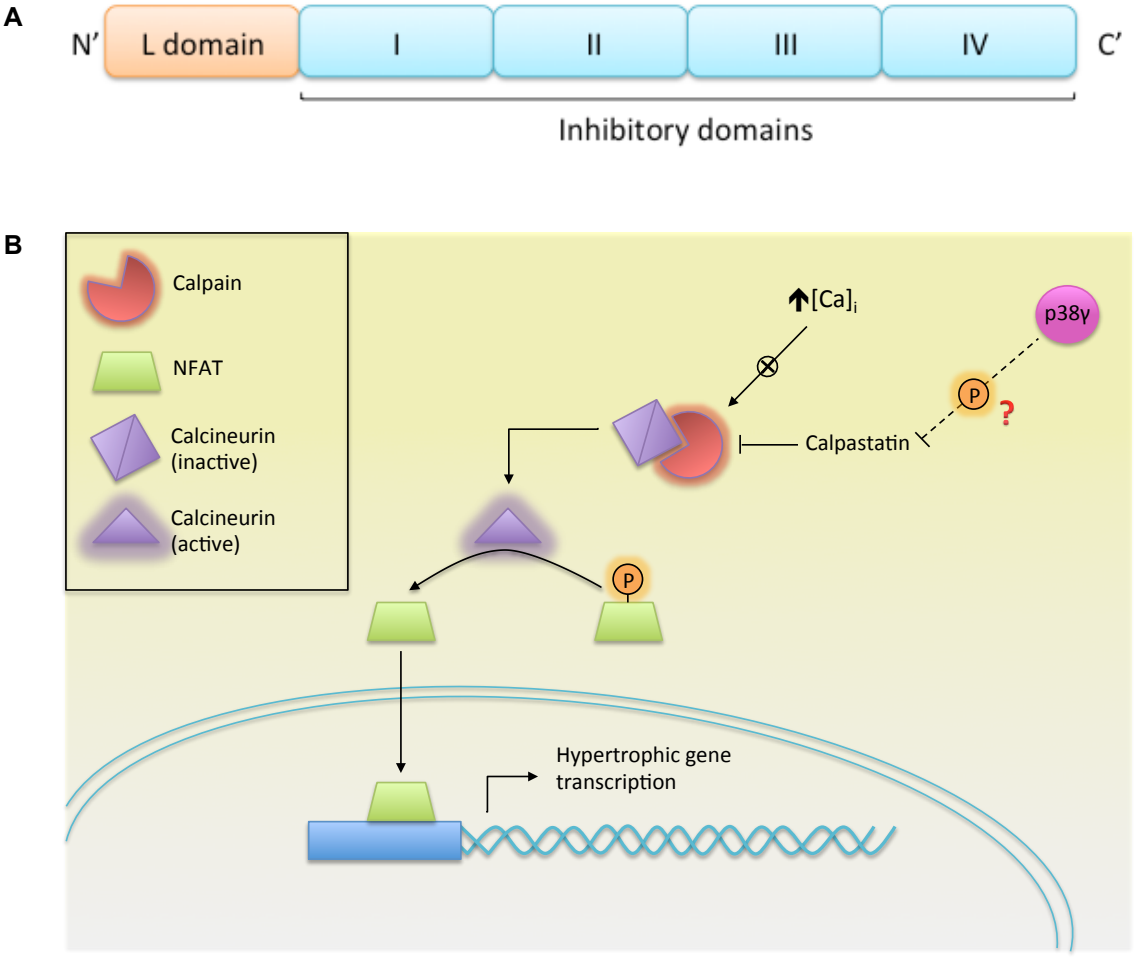

Figure 6.3 Calpastatin signalling in the myocardium

A, Calpastatin is multi-headed inhibitor molecule. ***B,*** A target of calpain is calcineurin. Activation of calpain by an increase in intracellular calcium concentration during hypertrophic signalling leads to proteolysis of the auto inhibitory domain of calcinuerin, leading to its activation. Once activated, calcineurin dephosphorylates NFAT, allowing translocation of NFAT to the nucleus and transcription of pro-hypertrophic genes. Calpain activity is regulated by calpastatin, which binds to active calpain to prevent its activity. However, phosphorylation of calpastatin by p38γ may reduce the efficiency of calpastatin to inhibit calpain and as a result lead to increased calcineurin activity.

6.2 Specific Methods

6.2.1 Cloning of *Znf260*

GST-zfp260 was generated by sub-cloning the ORF of murine *znf260* from the pYX-Asc vector (Source Bioscience) into the pGEX-3X GST expression vector (GE Lifesciences). See Figure 6.5 for amino acid sequence of GST-zfp260. Firstly to obtain purified donor plasmid, 5 mL LB broth medium containing 100 µg/mL ampicillin was inoculated with DH10B TonA host bacteria and incubated overnight, 220 rpm at 37°C. The following morning plasmid DNA was extracted from 2 mL of culture using NucleoSpin® Plasmid purification kit (Macherey-Nagel) as described in Section 2.3.1.

A PCR reaction was then set up to amplify the region of plasmid encoding *znf260*. Primers and conditions used for PCR are detailed in Table 6.1. Primers were designed to incorporate restriction enzyme sites for BamHI (forward) and SmaI (reverse). PCR reactions were set up using Platinum® Pfx DNA Polymerase (Invitrogen) according to manufacturer's instructions. A 1224 bp PCR product corresponding to the expected size of *znf260*'s encoding region was electrophoresed and visualised on a 1% (w/v) agarose gel (Figure 6.4).

The PCR product or 'insert' was gel purified using High Pure PCR Product Isolation Kit (Roche) according to manufacturer's instructions (Section 2.3.3). Insert DNA and target pGEX-3X plasmid DNA were sequentially digested with BamHI (NEB, 1 hr, 37°C) and SmaI restriction enzymes (NEB, 1 hr, 25°C) according to manufacturer's instructions. Agarose gels from cloning steps are shown in Figure 6.4. Following double digestion of insert and plasmid DNA, DNA was electrophoresed on a 1% (w/v) agarose gel. Both DNA samples were gel purified and 10 µL ligations in 3:1 and 1:3 ratios were set up using T4 DNA ligase (Promega) according to manufacturer's instructions. Ligations were incubated overnight at 4°C.

Table 6.1 Primers and PCR conditions used for amplification of *znf260* from the pYX-Asc vector. Primers were designed to incorporate restriction enzyme sites for BamHI (forward) and SmaI (reverse) for subsequent cloning into the pGEX-3X GST expression vector.

Primer	Primer Sequence (5' to 3')
Znf260 F	GCGGGATCCTTATGTTGGAGAGCCTTCAGCCT
Znf260 R	GTCCCGGGTTAATGAATGTGGATTCTCTGGT

PCR conditions

Step	Temperature	Time	Cycle
Initial Denaturation	94°C	5 min	1
Denaturation	94°C	15 s	35
Annealing	60°C	30 s	
Extension	68°C	3 min	
Final Extension	68°C	5 min	1

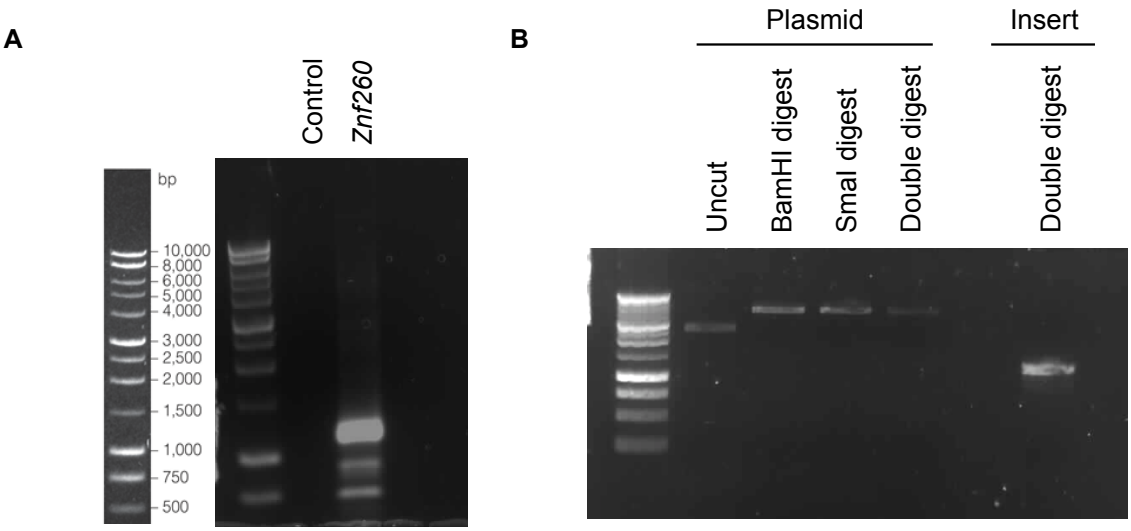

Figure 6.4 ***Znf260*** **cloning**

A, 1224 bp PCR product corresponding to the expected size of *znf260*'s coding region. DNA was electrophoresed and visualised on a 1% (w/v) agarose gel, as described in *Materials and Methods*. ***B,*** Sequential digestion of *znf260* and pGEX-3X plasmid DNA with BamHI and SmaI restriction enzymes.

The following day 2 µL of each ligation reaction was used to transform α-Select Gold Competent Cells (Bioline) (Section 2.7.1). A selection of bacterial colonies were used to inoculate 5 mL LB cultures containing 100 µg/mL ampicillin. Following overnight incubation (220 rpm, 37°C), plasmid DNA purification was carried out as previously described and sent for sequencing (Eurofins MWG Operon). DNA from positive colonies was then used to transform *E.coli* strain Rosetta BL21 DE3 (Bioline). Transformed bacterial colonies were used to set up cultures for protein expression as previously described for expression of His-p38γ proteins (Section 3.2.3) with the following variations: 1) 0.1 mM IPTG was used to induce expression of protein and 2) bacterial cells were grown at 37°C following induction.

6.2.1.1 Purification of GST-zfp260

Bacterial cells were re-suspended in ice cold lysis buffer (phosphate buffered saline, pH 7.4, 2 mM DTT and Roche protease inhibitor cocktail). Cell lysis was performed using a high intensity ultrasonic processor. Lysates were clarified by centrifugation at 4600 rpm for 40 min at 4°C. The supernatant was filtered

through a 0.45 μM membrane filter before incubation with lysis buffer equilibrated glutathione sepharose beads (GE Lifesciences), for 1 h at 4°C on a rotator. Beads were pelleted by centrifugation at 3000 rpm for 1 min at 4°C and supernatant discarded. Beads were subsequently washed with 10 mL ice-cold PBS for 2 min at room temperature on a rotator. Five further 10 mL washes were carried out. GST-zfp260 was eluted by applying 1.5 mL volumes of a 10 mM to 40 mM reduced glutathione gradient. Fractions containing GST-zfp260 were pooled and extensively dialysed overnight at 4°C against 50 mM Tris, pH 8.0, 50 mM NaCl, 2 mM DTT buffer. The following morning GST-zfp260 was removed from dialysis, assayed for protein concentration and stored in aliquots at −80°C.

```
Zfp260  1    MSPILGYWKIKGLVQPTRLLLEYLEEKYEEHLYERDEGDKWRNKKFELGLEFPNLPYYID  60
Zfp260  61   GDVKLTQSMAIIRYIADKHNMLGGCPKERAEISMLEGAVLDIRYGVSRIAYSKDFETLKV  120
Zfp260  121  DFLSKLPEMLKMFEDRLCHKTYLNGDHVTHPDFMLYDALDVVLYMDPMCLDAFPKLVCFK  180
Zfp260  181  KRIEAIPQIDKYLKSSKYIAWPLQGWQATFGGGDHPPKSDLIEGRGILMLESLQPESHLL  240
Zfp260  241  HDEPDPGESVYECNECKETFSLEQNFVEHKKTHSGEKSPECTGCGEESSQASSLTLHLRS  300
Zfp260  301  RPRRESYKCGECGKAFSQRGNFLSHQKQHTEERPSESKKTPVPMTTTVRNQRNTGNKPYA  360
Zfp260  361  CKECGKAFNGKSYLKEHEKIHTGEKPFECSQCGRAFSQKQYLIKHQNIHSGKKPFKCNEC  420
Zfp260  421  GKAFSQKENLIIHQRIHTGEKPYECKGCGKAFIQKSSLIRHQRSHTGEKPYTCKECGKAF  480
Zfp260  481  SGKSNLTEHEKIHIGEKPYKCNECGTIFRQKQYLIKHHNIHTGEKPYECNKCGKAFSRIT  540
Zfp260  541  SLIVHVRIHTGDKPYECKICGKAFCQSSSLTVHMRSHTGEKPYGCNECGKAFSQFSTLAL  600
Zfp260  601  HMRIHTGEKPYQCSECGKAFSQKSHHIRHQRIHIH  635
```

Figure 6.5 Amino acid sequence of GST-zfp260

The GST tag of the protein is at the amino terminal. Residues of the tag are underlined.

6.2.2 Cloning of LDB3 for bacterial expression

His-LB3 was generated by sub-cloning the ORF of murine *ldb3* from the pcR4-TOPO vector (Source Bioscience) into the pETDuet-1 expression vector (Novagen). Firstly to obtain purified donor plasmid, 5 mL LB broth medium containing 30 µg/mL kanamycin was inoculated with DH10B TonA host bacteria and incubated overnight, 220 rpm at 37°C. The following morning plasmid DNA was extracted from 2 mL of culture using NucleoSpin® Plasmid purification kit (Macherey-Nagel) as described in Section 2.3.1

A PCR reaction was then set up to amplify the region of plasmid encoding *ldb3*. Primers and conditions used for PCR are detailed in Table 6.2. Primers were designed to incorporate restriction enzyme sites for BamHI (forward) and HindIII (reverse). The reverse primer was designed to also incorporate a HA tag into the protein. PCR reactions were set up using Platinum® Pfx DNA Polymerase (Invitrogen) according to manufacturer's instructions. PCR reactions and subsequent digestions were performed by Dr Eva Denise Martin.

A 2206 bp PCR product corresponding to the expected size of *ldb3*'s coding region was electrophoresed and visualised on a 1% (w/v) agarose gel. The PCR product or 'insert' was gel purified using High Pure PCR Product Isolation Kit (Roche) according to manufacturer's instructions (Section 2.3.3). Insert DNA and target pETDuet-1 plasmid DNA were digested with BamHI and HindIII restriction enzymes (NEB, 1 hr, 37°C) according to manufacturer's instructions. Following double digestion of insert and plasmid DNA, DNA was electrophoresed on a 1% (w/v) agarose gel. Both DNA samples were gel purified and 10 µL ligations in 3:1 and 1:3 ratios were set up using T4 DNA ligase (Promega) according to manufacturer's instructions. Ligations were incubated overnight at 4°C.

Table 6.2 Primers and PCR conditions used for amplification of *ldb3* from the pcR4-TOPO vector. Primers were designed to incorporate restriction enzyme sites for BamHI (forward) and HindIII (reverse) for subsequent cloning into the pETDuet-1 expression vector.

Primer	Primer Sequence (5' to 3')
LDB3 F	TTGGATCCAATGTCTTACAGTGTGACTCTGACTGGGCCTGGGCCCTG
LDB3 R	TTAAGCTTTTATACCCATACGATGTTCCAGATTACGCTCACGTTGATGGCATGTGCGTG

PCR conditions

Step	Temperature	Time	Cycle
Initial Denaturation	94°C	5 min	1
Denaturation	94°C	30 s	30
Annealing	55°C	30 s	
Extension	68°C	2 min	
Final Extension	68°C	5 min	1

The following day 2 µL of each ligation reaction was used to transform α-Select Gold Competent Cells (Bioline) (Section 2.7.1). A selection of bacterial colonies were used to inoculate 15 mL LB cultures containing 100 µg/mL ampicillin. Following overnight incubation (220 rpm, 37°C), plasmid DNA purification was carried out as previously described and sent for sequencing (Eurofins MWG Operon). DNA from positive colonies was then used to transform *E.coli* strain Rosetta BL21 DE3 (Bioline). Transformed bacterial colonies were used to set up cultures for protein expression as previously described for expression of His-p38γ proteins (Section 3.2.3) except that bacteria were grown at 26°C following IPTG induction. Immobilised metal affinity purification of His-LDB3 was carried out as previously described for His-p38γ.

6.2.2.1 Mutagenesis of LDB3

PCR reactions for LDB3 mutagenesis were performed using WT His-LDB3 pETDuet-1 plasmid DNA as template. Two LDB3 mutants were generated: S98A and S240A LDB3. For generation of double mutant (S98A/S240A), S240A His-LDB3 pETDuet-1 plasmid DNA was used as template. KOD DNA polymerase (Toyobo) was used for mutagenesis and reactions were set up according to manufacturer's instructions. Primers and conditions used for PCR are detailed in Table 6.3.

Following PCR, parental template WT-LDB3 pETDuet-1 plasmid DNA was digested using 1 µL DpnI (Agilent) at 37°C for 1 h and 3 µL of each reaction was then used to transform α-Select Gold Competent Cells (Bioline) (Section 2.7.1). A selection of bacterial colonies were used to inoculate 15 mL LB cultures containing 100 µg/mL ampicillin. Following overnight incubation (220 rpm, 37°C), plasmid DNA purification was carried out as previously described and sent for sequencing (Eurofins MWG Operon). DNA from positive colonies was then used to transform *E.coli* strain Rosetta BL21 DE3 (Bioline). Transformed bacterial colonies were used to set up cultures for protein expression as described above for expression of WT His-LDB3. Immobilised metal affinity purification of His-LDB3 was carried out as described for His-p38γ.

Table 6.3 Primers and PCR conditions used for mutagenesis of *ldb3.* PCR reactions for LDB3 mutagenesis were performed using WT His-LDB3 pETDuet-1 plasmid DNA as template. Two serine mutants of LDB3 were generated: S98A and S240A.

Primer	Primer Sequence (5' to 3')
S98A F	CCTCCCATCCAGGCCCCGCTGCCAG
S98A R	CTGGCAGCGGGGCCTGGATGGGAGG
S240A F	GGTGGACAGCGCCGCTCCTGTGTACCA
S240A R	TGGTACACAGGAGCGGCGCTGTCCACC

PCR conditions

Step	Temperature	Time	Cycle
Initial Denaturation	95°C	2 min	1
Denaturation	95°C	20 s	25
Annealing	55°C	10 s	
Extension	70°C	3.5 min	

6.2.3 Cloning of LDB3 for mammalian expression

To express LDB3 in mammalian Human Embryonic Kidney (HEK) cells, a sub-cloning strategy was employed to generate mammalian expression pcDNA™3.1 vectors containing WT, S98A, S240A and DM LDB3 DNA. See Figure 6.6 for amino acid sequences of WT and mutant LDB3 proteins. Respective pETDuet-1 vectors of each protein were used as template DNA in PCR reactions to amplify the ORF of each gene. KOD DNA polymerase (Toyobo) was used for PCR and reactions were set up according to manufacturer's instructions. Primers and conditions used for PCR are detailed in Table 6.4.

A 2172 bp PCR product corresponding to the expected size of LDB3's coding region was electrophoresed and visualised on a 1% (w/v) agarose gel. The PCR products or 'inserts' were gel purified using High Pure PCR Product Isolation Kit (Roche) according to manufacturer's instructions. 10 ng of each insert was incubated with pcDNA™3.1 vector DNA according to manufacturer's instructions for 15 min at room temperature. 2 µL of each reaction was then used to transform α-Select Gold Competent Cells (Bioline) (Section 2.7.1). A selection of bacterial colonies were used to inoculate 15 mL LB cultures containing 100 µg/mL ampicillin. Following overnight incubation (220 rpm, 37°C), plasmid DNA purification was carried out as previously described and sent for sequencing (Eurofins MWG Operon). DNA from positive colonies was used to transfect HEK293 cells (Section 2.1).

Table 6.4 Primers and PCR conditions used for amplification of WT and mutant *ldb3* from the respective pETDuet-1 vectors of each protein.

Primer	Primer Sequence (5' to 3')
TOPO F	CACCATGTCTTACAGTGTGACTCTGACTGG
TOPO R	CACGTTGATGGCATGTGCGTGCTTCTTGCA

PCR conditions

Step	Temperature	Time	Cycle
Initial Denaturation	95°C	2 min	1
Denaturation	95°C	20 s	35
Annealing	68°C	10 s	
Extension	70°C	44 S	
Final Extension	70°C	10 min	1

```
WT           1    MSYSVTLTGPGPWGFRLQGGKDFNMPLTISRITPGSKAAQSQLSQGDLVVAIDGVNTDTM 60
S98A         1    MSYSVTLTGPGPWGFRLQGGKDFNMPLTISRITPGSKAAQSQLSQGDLVVAIDGVNTDTM 60
S98A/S240A   1    MSYSVTLTGPGPWGFRLQGGKDFNMPLTISRITPGSKAAQSQLSQGDLVVAIDGVNTDTM 60
S240A        1    MSYSVTLTGPGPWGFRLQGGKDFNMPLTISRITPGSKAAQSQLSQGDLVVAIDGVNTDTM 60

WT           61   THLEAQNKIKSASYNLSLTLQKSKRPIPISTTAPPIQSPLPVIPHQKDPALDTNGSLATP 120
S98A         61   THLEAQNKIKSASYNLSLTLQKSKRPIPISTTAPPIQAPLPVIPHQKDPALDTNGSLATP 120
S98A/S240A   61   THLEAQNKIKSASYNLSLTLQKSKRPIPISTTAPPIQAPLPVIPHQKDPALDTNGSLATP 120
S240A        61   THLEAQNKIKSASYNLSLTLQKSKRPIPISTTAPPIQSPLPVIPHQKDPALDTNGSLATP 120

WT           121  SPSPEARASPGALEFGDTFSSSFSQTSVCSPLMEASGPVLPLGSPVAKASSEGAQGSVSP 180
S98A         121  SPSPEARASPGALEFGDTFSSSFSQTSVCSPLMEASGPVLPLGSPVAKASSEGAQGSVSP 180
S98A/S240A   121  SPSPEARASPGALEFGDTFSSSFSQTSVCSPLMEASGPVLPLGSPVAKASSEGAQGSVSP 180
S240A        121  SPSPEARASPGALEFGDTFSSSFSQTSVCSPLMEASGPVLPLGSPVAKASSEGAQGSVSP 180

WT           181  KVLPGPSQPRQYNNPIGLYSAETLREMAQMYQMSLRGKASGAGLLGGSLPVKDLAVDSAS 240
S98A         181  KVLPGPSQPRQYNNPIGLYSAETLREMAQMYQMSLRGKASGAGLLGGSLPVKDLAVDSAS 240
S98A/S240A   181  KVLPGPSQPRQYNNPIGLYSAETLREMAQMYQMSLRGKASGAGLLGGSLPVKDLAVDSAA 240
S240A        181  KVLPGPSQPRQYNNPIGLYSAETLREMAQMYQMSLRGKASGAGLLGGSLPVKDLAVDSAA 240

WT           241  PVYQAVIKTQSKPEDEADEWARRSSNLQSRSFRILAQMTGTEYMQDPDEEALRRSSTPIE 300
S98A         241  PVYQAVIKTQSKPEDEADEWARRSSNLQSRSFRILAQMTGTEYMQDPDEEALRRSSTPIE 300
S98A/S240A   241  PVYQAVIKTQSKPEDEADEWARRSSNLQSRSFRILAQMTGTEYMQDPDEEALRRSSTPIE 300
S240A        241  PVYQAVIKTQSKPEDEADEWARRSSNLQSRSFRILAQMTGTEYMQDPDEEALRRSSTPIE 300

WT           301  HAPVCTSQATSPLLPASAQSPAAASPIAASPTLATAAATHAAAASAAGPAASPVENPRPQ 360
S98A         301  HAPVCTSQATSPLLPASAQSPAAASPIAASPTLATAAATHAAAASAAGPAASPVENPRPQ 360
S98A/S240A   301  HAPVCTSQATSPLLPASAQSPAAASPIAASPTLATAAATHAAAASAAGPAASPVENPRPQ 360
S240A        301  HAPVCTSQATSPLLPASAQSPAAASPIAASPTLATAAATHAAAASAAGPAASPVENPRPQ 360

WT           361  ASAYSPAAAASPAPSAHTSYSEGPAAPAPKPRVVTTASIRPSVYQPVPASSYSPSPGANY 420
S98A         361  ASAYSPAAAASPAPSAHTSYSEGPAAPAPKPRVVTTASIRPSVYQPVPASSYSPSPGANY 420
S98A/S240A   361  ASAYSPAAAASPAPSAHTSYSEGPAAPAPKPRVVTTASIRPSVYQPVPASSYSPSPGANY 420
S240A        361  ASAYSPAAAASPAPSAHTSYSEGPAAPAPKPRVVTTASIRPSVYQPVPASSYSPSPGANY 420
```

```
WT          421  SPTPYTPSPAPAYTPSPAPTYTPSPAPTYSPSPAPAYTPSPAPNYTPTPSAAYSGGPSES 480
S98A        421  SPTPYTPSPAPAYTPSPAPTYTPSPAPTYSPSPAPAYTPSPAPNYTPTPSAAYSGGPSES 480
S98A/S240A  421  SPTPYTPSPAPAYTPSPAPTYTPSPAPTYSPSPAPAYTPSPAPNYTPTPSAAYSGGPSES 480
S240A       421  SPTPYTPSPAPAYTPSPAPTYTPSPAPTYSPSPAPAYTPSPAPNYTPTPSAAYSGGPSES 480

WT          481  ASRPPWVTDDSFSQKFAPGKSTTTVSKQTLPRGAPAYNPTGPQVTPLARGTFQRAERFPA 540
S98A        481  ASRPPWVTDDSFSQKFAPGKSTTTVSKQTLPRGAPAYNPTGPQVTPLARGTFQRAERFPA 540
S98A/S240A  481  ASRPPWVTDDSFSQKFAPGKSTTTVSKQTLPRGAPAYNPTGPQVTPLARGTFQRAERFPA 540
S240A       481  ASRPPWVTDDSFSQKFAPGKSTTTVSKQTLPRGAPAYNPTGPQVTPLARGTFQRAERFPA 540

WT          541  SSRTPLCGHCNNVIRGPFLVAMGRSWHPEEFNCAYCKTSLADVCFVEEQNNVYCERCYEQ 600
S98A        541  SSRTPLCGHCNNVIRGPFLVAMGRSWHPEEFNCAYCKTSLADVCFVEEQNNVYCERCYEQ 600
S98A/S240A  541  SSRTPLCGHCNNVIRGPFLVAMGRSWHPEEFNCAYCKTSLADVCFVEEQNNVYCERCYEQ 600
S240A       541  SSRTPLCGHCNNVIRGPFLVAMGRSWHPEEFNCAYCKTSLADVCFVEEQNNVYCERCYEQ 600

WT          601  FFAPICAKCNTKIMGEVMHALRQTWHTTCFVCAACKKPFGNSLFHMEDGEPYCEKDYINL 660
S98A        601  FFAPICAKCNTKIMGEVMHALRQTWHTTCFVCAACKKPFGNSLFHMEDGEPYCEKDYINL 660
S98A/S240A  601  FFAPICAKCNTKIMGEVMHALRQTWHTTCFVCAACKKPFGNSLFHMEDGEPYCEKDYINL 660
S240A       601  FFAPICAKCNTKIMGEVMHALRQTWHTTCFVCAACKKPFGNSLFHMEDGEPYCEKDYINL 660

WT          661  FSTKCHGCDFPVEAGDKFIEALGHTWHDTCFICAVCHVNLEGQPFYSKKDKPLCKKHAHA 720
S98A        661  FSTKCHGCDFPVEAGDKFIEALGHTWHDTCFICAVCHVNLEGQPFYSKKDKPLCKKHAHA 720
S98A/S240A  661  FSTKCHGCDFPVEAGDKFIEALGHTWHDTCFICAVCHVNLEGQPFYSKKDKPLCKKHAHA 720
S240A       661  FSTKCHGCDFPVEAGDKFIEALGHTWHDTCFICAVCHVNLEGQPFYSKKDKPLCKKHAHA 720

WT          721  INVKGQDNSADIQHSGGRSSLEGPRFEGKPIPNPLLGLDSTRTGHHHHHH 770
S98A        721  INVKGQDNSADIQHSGGRSSLEGPRFEGKPIPNPLLGLDSTRTGHHHHHH 770
S98A/S240A  721  INVKGQDNSADIQHSGGRSSLEGPRFEGKPIPNPLLGLDSTRTGHHHHHH 770
S240A       721  INVKGQDNSADIQHSGGRSSLEGPRFEGKPIPNPLLGLDSTRTGHHHHHH 770
                                            ↑                ↑
                                          V5 tag    Polyhistidine tag
```

Figure 6.6 Aligned amino acid sequences of 6xHis-WT, S98A, S240A and S98A/S240A LDB3 proteins

Areas of interest are annotated around sequence. Both tags are located at the carboxy-terminal of the protein. Residues highlighted in yellow show location of point mutations.

6.2.4 Cloning of Calpastatin

6.2.4.1 RNA Extraction

RNA was extracted from WT mouse heart stored in RNAlater (Invitrogen) using RNeasy Fibrous Tissue Kit (Qiagen) according to manufacturer's instructions. Concentration and purity of RNA was assessed by measuring absorbance of RNA/DNA at 260 nm using a Nanodrop 2000c spectrophotometer (Thermoscientific). 28s/18s ratio and RNA integrity number (RIN) score to assess integrity of RNA was determined by FWB Genomics Facility (King's College London) using a 2100 Bioanalyser (Agilent). RNA obtained was stored in aliquots at -80°C.

6.2.4.2 Reverse Transcription and Calpastatin dsDNA Synthesis

To generate cDNA from heart mRNA first strand cDNA synthesis was carried out using Superscript III Reverse Transcriptase (Invitrogen) according to manufacturer's instructions. The resulting reaction containing RNA/cDNA hybrids was subsequently used to generate double stranded *cast* DNA. Platinum® Pfx DNA Polymerase (Invitrogen) was used to set up PCR according to manufacturer's instructions. Primers and conditions used for PCR are detailed in Table 6.5. Primers were designed against Isoform 1 of calpastatin and were designed to incorporate restriction enzyme sites for SmaI (forward) and EcoRI (reverse).

6.2.4.3 Calpastatin cloning

A 2313 bp PCR product corresponding to the expected size of *cast* was electrophoresed and visualised on a 1% (w/v) agarose gel. The PCR product or 'insert' was gel purified using High Pure PCR Product Isolation Kit (Roche) according to manufacturer's instructions (Section 2.3.3) and sent for sequencing (Eurofins MWG Operon). Sequencing revealed that DNA coding Isoform 2 of calpastatin was generated. Insert DNA and target pGEX-3X plasmid DNA were sequentially digested with SmaI (NEB, 1 hr, 25°C) and EcoRI restriction

enzymes (NEB, 1 hr, 37°C) according to manufacturer's instructions. Following double digestion of insert and plasmid DNA, DNA was electrophoresed on a 1% (w/v) agarose gel. Both DNA samples were gel purified and 10 µL ligations in 3:1 and 1:3 ratios were set up using T4 DNA ligase (Promega) according to manufacturer's instructions. Ligations were incubated overnight at 4°C.

The following day, 2 µL of each ligation reaction was used to transform α-Select Gold Competent Cells (Bioline) (Section 2.7.1). A selection of bacterial colonies were used to inoculate 15 mL LB cultures containing 100 µg/mL ampicillin. Following overnight incubation (220 rpm, 37°C), plasmid DNA purification was carried out as previously described and sent for sequencing (Eurofins MWG Operon). DNA from positive colonies was then used to transform *E.coli* strain Rosetta BL21 DE3 (Bioline). Transformed bacterial colonies were used to set up cultures for protein expression as previously described for expression of His-p38γ proteins (Section 3.2.3) with the following variations: 1) 0.1 mM IPTG was used to induce expression of protein and 2) bacterial cells were grown at 37°C following induction.

6.2.4.4 Mutagenesis of Calpastatin

PCR reactions for calpastatin mutagenesis were performed using WT GST-calpastatin pGEX-3X plasmid DNA as template. Two calpastatin mutants were generated: T197A/S200A and T448A calpastatin. See Figure 6.7 for amino acid sequences of WT and mutant calpastatin proteins. KOD DNA polymerase (Toyobo) was used for mutagenesis and reactions were set up according to manufacturer's instructions. Primers and conditions used for PCR are detailed in Table 6.6.

Following PCR, parental template WT GST-calpastatin pGEX-3X plasmid DNA was digested using 1 µL DpnI (Agilent) at 37°C for 1 h and 3 µL of each reaction was then used to transform α-Select Gold Competent Cells (Bioline) (Section 2.7.1). A selection of bacterial colonies where used to inoculate 15 mL LB cultures containing 100 µg/mL ampicillin. Following overnight incubation (220 rpm, 37°C), plasmid DNA purification was carried out as previously

described and sent for sequencing (Eurofins MWG Operon). DNA from positive colonies was then used to transform *E.coli* strain Rosetta BL21 DE3 (Bioline). Transformed bacterial colonies were used to set up cultures for protein expression as previously described for WT GST-calpastatin. Purification of mutant calpastatin proteins was carried out as previously described for purification of WT GST-calpastatin.

6.2.5 Mass Spectrometry

Silver stained gels of phosphorylated substrates were processed and analysed by Dr Steve Lynham at the core facility at King's College London as described in Section 5.2.3.

Table 6.5 Primers and PCR conditions used for the generation of ds *cast* DNA. Primers were designed to incorporate restriction enzyme sites for SmaI (forward) and EcoRI (reverse) for subsequent cloning into the pGEX-3X GST expression vector.

Primer	**Primer Sequence (5' to 3')**
Calpa F	TACCCGGGATGTCCCAGCCCGGCCCGAAGCCTGCCGCCTCT
Calpa R	TTGAATTCTTAACTGTGTCTTGCATCTTCTTTAGCCTTTGGCTT GGACAC

PCR conditions

Step	**Temperature**	**Time**	**Cycle**
Initial Denaturation	94°C	5 min	1
Denaturation	94°C	15 s	35
Annealing	60°C	30 s	
Extension	68°C	2.5 min	
Final Extension	68°C	10 min	1

Table 6.6 Primers and PCR conditions used for mutagenesis of *cast.* PCR reactions for *cast* mutagenesis were performed using WT GST-calpastatin pGEX-3X plasmid DNA as template. Two phosphorylation mutants of calpastatin were generated: T197A/S200A and T448A.

Primer	**Primer Sequence (5' to 3')**
T197A/S200A F	GAACAGAAACCATTCGCACCAGCTGCACCTGTGCAGTCCA
T197A/S200AR	TGGACTGCACAGGTGCAGCTGGTGCGAATGGTTTCTGTTC
T448A F	CGATCTACATATCAAGACAAACCATCTGCGCCAGCTGAAA AG
T448A R	CTTTTCAGCTGGCGCAGATGGTTTGTCTTGATATGTAGAT CG

PCR conditions

Step	**Temperature**	**Time**	**Cycle**
Initial Denaturation	95°C	2 min	1
Denaturation	95°C	20 s	25
Annealing	55°C	10 s	
Extension	70°C	3.5 min	

```
WT           1    MSPILGYWKIKGLVQPTRLLLEYLEEKYEEHLYERDEGDKWRNKKFELGLEFPNLPYYID 60
T448         1    MSPILGYWKIKGLVQPTRLLLEYLEEKYEEHLYERDEGDKWRNKKFELGLEFPNLPYYID 60
T197A/S200A  1    MSPILGYWKIKGLVQPTRLLLEYLEEKYEEHLYERDEGDKWRNKKFELGLEFPNLPYYID 60

WT           61   GDVKLTQSMAIIRYIADKHNMLGGCPKERAEISMLEGAVLDIRYGVSRIAYSKDFETLKV 120
T448         61   GDVKLTQSMAIIRYIADKHNMLGGCPKERAEISMLEGAVLDIRYGVSRIAYSKDFETLKV 120
T197A/S200A  61   GDVKLTQSMAIIRYIADKHNMLGGCPKERAEISMLEGAVLDIRYGVSRIAYSKDFETLKV 120

WT           121  DFLSKLPEMLKMFEDRLCHKTYLNGDHVTHPDFMLYDALDVVLYMDPMCLDAFPKLVCFK 180
T448         121  DFLSKLPEMLKMFEDRLCHKTYLNGDHVTHPDFMLYDALDVVLYMDPMCLDAFPKLVCFK 180
T197A/S200A  121  DFLSKLPEMLKMFEDRLCHKTYLNGDHVTHPDFMLYDALDVVLYMDPMCLDAFPKLVCFK 180

WT           181  KRIEAIPQIDKYLKSSKYIAWPLQGWQATFGGGDHPPKSDLIEGRGIPGMSQPGPKPAAS 240
T448         181  KRIEAIPQIDKYLKSSKYIAWPLQGWQATFGGGDHPPKSDLIEGRGIPGMSQPGPKPAAS 240
T197A/S200A  181  KRIEAIPQIDKYLKSSKYIAWPLQGWQATFGGGDHPPKSDLIEGRGIPGMSQPGPKPAAS 240

WT           241  PRPSRGAAARHTQEHVNEKNIGSSSKPGEKKGSDEKKAASLGSSQPSRPHVGEAATATKV 300
T448         241  PRPSRGAAARHTQEHVNEKNIGSSSKPGEKKGSDEKKAASLGSSQPSRPHVGEAATATKV 300
T197A/S200A  241  PRPSRGAAARHTQEHVNEKNIGSSSKPGEKKGSDEKKAASLGSSQPSRPHVGEAATATKV 300

WT           301  TASSAATSKSPSMSTTETKAVKTESKKPQSSEQPVVHEKKSKGGPKEGSEPKNLPKHTSS 360
T448         301  TASSAATSKSPSMSTTETKAVKTESKKPQSSEQPVVHEKKSKGGPKEGSEPKNLPKHTSS 360
T197A/S200A  301  TASSAATSKSPSMSTTETKAVKTESKKPQSSEQPVVHEKKSKGGPKEGSEPKNLPKHTSS 360

WT           361  TGSKHAHKEKALSRSNEQMVSEKPSESKTKFQDVPSAGGESVAGGGTVATALDKVVGKKK 420
T448         361  TGSKHAHKEKALSRSNEQMVSEKPSESKTKFQDVPSAGGESVAGGGTVATALDKVVGKKK 420
T197A/S200A  361  TGSKHAHKEKALSRSNEQMVSEKPSESKTKFQDVPSAGGESVAGGGTVATALDKVVGKKK 420

WT           421  EQKPFTPASPVQSTPSKPSDKSGMDAALDDLIDTLGGHEDTNRDDPPYTGPVVLDPMYST 480
T448         421  EQKPFTPASPVQSTPSKPSDKSGMDAALDDLIDTLGGHEDTNRDDPPYTGPVVLDPMYST 480
T197A/S200A  421  EQKPFAPAAPVQSTPSKPSDKSGMDAALDDLIDTLGGHEDTNRDDPPYTGPVVLDPMYST 480

WT           481  YLEALGIKEGTIPPEYRKLLEKNEGITQPLPDSPKPMGTDQAIDALSSDFTCSSPTGKQS 540
T448         481  YLEALGIKEGTIPPEYRKLLEKNEGITQPLPDSPKPMGTDQAIDALSSDFTCSSPTGKQS 540
T197A/S200A  481  YLEALGIKEGTIPPEYRKLLEKNEGITQPLPDSPKPMGTDQAIDALSSDFTCSSPTGKQS 540
```

```
WT           541  EKEKSTGEIFKAQSAGVTRSSVPPKEKKRKVEEEVINDQALQALSDSLGTRQPDPPSHVS 600
T448         541  EKEKSTGEIFKAQSAGVTRSSVPPKEKKRKVEEEVINDQALQALSDSLGTRQPDPPSHVS 600
T197A/S200A  541  EKEKSTGEIFKAQSAGVTRSSVPPKEKKRKVEEEVINDQALQALSDSLGTRQPDPPSHVS 600

WT           601  QAEQVKEAKAKEERQEKCGEDEDTVPAEYRLKPAKDKDGKPLLPEPEETSKSLSESELIG 660
T448         601  QAEQVKEAKAKEERQEKCGEDEDTVPAEYRLKPAKDKDGKPLLPEPEETSKSLSESELIG 660
T197A/S200A  601  QAEQVKEAKAKEERQEKCGEDEDTVPAEYRLKPAKDKDGKPLLPEPEETSKSLSESELIG 660

WT           661  ELSADFDRSTYQDKPSTPAEKKSNDTSQTPPGETVPRASMCSIRSAPPKLASLKGVVPED 720
T448         661  ELSADFDRSTYQDKPSAPAEKKSNDTSQTPPGETVPRASMCSIRSAPPKLASLKGVVPED 720
T197A/S200A  661  ELSADFDRSTYQDKPSTPAEKKSNDTSQTPPGETVPRASMCSIRSAPPKLASLKGVVPED 720

WT           721  AVETLAGSLGTREADPEHEKTVEDKVKEKAKEEEHEKLGEKEETVPPDYRLEEVKDKDGK 780
T448         721  AVETLAGSLGTREADPEHEKTVEDKVKEKAKEEEHEKLGEKEETVPPDYRLEEVKDKDGK 780
T197A/S200A  721  AVETLAGSLGTREADPEHEKTVEDKVKEKAKEEEHEKLGEKEETVPPDYRLEEVKDKDGK 780

WT           781  PLLPKESQEQLAPLSDDFLLDALSQDFSSPANISSLEFEDAKLSAAISEVVSQTPAPSTH 840
T448         781  PLLPKESQEQLAPLSDDFLLDALSQDFSSPANISSLEFEDAKLSAAISEVVSQTPAPSTH 840
T197A/S200A  781  PLLPKESQEQLAPLSDDFLLDALSQDFSSPANISSLEFEDAKLSAAISEVVSQTPAPSTH 840

WT           841  AAAPLPGTEQKDKELDDALDELSDSLGQRPPDPDENKPLDDKVKEKIKPEHSEKLGERDD 900
T448         841  AAAPLPGTEQKDKELDDALDELSDSLGQRPPDPDENKPLDDKVKEKIKPEHSEKLGERDD 900
T197A/S200A  841  AAAPLPGTEQKDKELDDALDELSDSLGQRPPDPDENKPLDDKVKEKIKPEHSEKLGERDD 900

WT           901  TIPPEYRHLLDNDGKDKPEKPPTKKTEKPDQDRDPIDALSEDLDSCPSTTETSKNTAKGK 960
T448         901  TIPPEYRHLLDNDGKDKPEKPPTKKTEKPDQDRDPIDALSEDLDSCPSTTETSKNTAKGK 960
T197A/S200A  901  TIPPEYRHLLDNDGKDKPEKPPTKKTEKPDQDRDPIDALSEDLDSCPSTTETSKNTAKGK 960

WT           961  SKKTSSSKASKDGEKTKDSSKKTEEVSKPKAKEDARHS 998
T448         961  SKKTSSSKASKDGEKTKDSSKKTEEVSKPKAKEDARHS 998
T197A/S200A  961  SKKTSSSKASKDGEKTKDSSKKTEEVSKPKAKEDARHS 998
```

Figure 6.7 Amino acid sequences of GST-WT, T197A/S200A and T448A mutant calpastatin proteins

Areas of interest are annotated around sequence. The GST tag (underlined) is located at the amino-terminal of each protein. Residues highlighted in yellow show location of point mutations.

6.2.6 Calpain Activity Assay

Measurement of calpain activity was carried out *in vitro* using purified native calpain I from porcine erythrocytes (Millipore) in buffer containing calcium (50 mM Tris HCl pH 7.8, 30 mM NaCl, 1 mM DTT and 3 mM CaCl) or buffer without calcium (50 mM Tris HCl pH 7.8, 30 mM NaCl, 1 mM DTT and 1 mM EGTA). All assays were in 100 µL total volume in 96 well format, in triplicate. Each reaction contained 1 µg of calpain I and 20 µM of synthetic Suc-Leu-Leu-Val-Tyr-7-Amino-4-Methylcoumarin (Suc-Leu-Leu-Val-Tyr-7-AMC) fluorescent substrate (Calbiochem) in appropriate buffer. Reactions were incubated for 10 min at 21°C before fluorescence readings were taken using the Gemini XS (Molecular Devices) plate reader for 1 h. Fluorophores were excited at 380 nM and emission of cleaved substrate was measured at 460 nm. See Figure 6.8 for schematic of assay. Inhibition of calpain by calpastatin was measured by addition of 0.2 µg to 4.5 µg of WT calpastatin. To assess the effect of phosphorylation of calpastatin on calpain inhibition, calpastatin was phosphorylated by p38γ as described in Section 2.9 prior to incubation in calpain reactions.

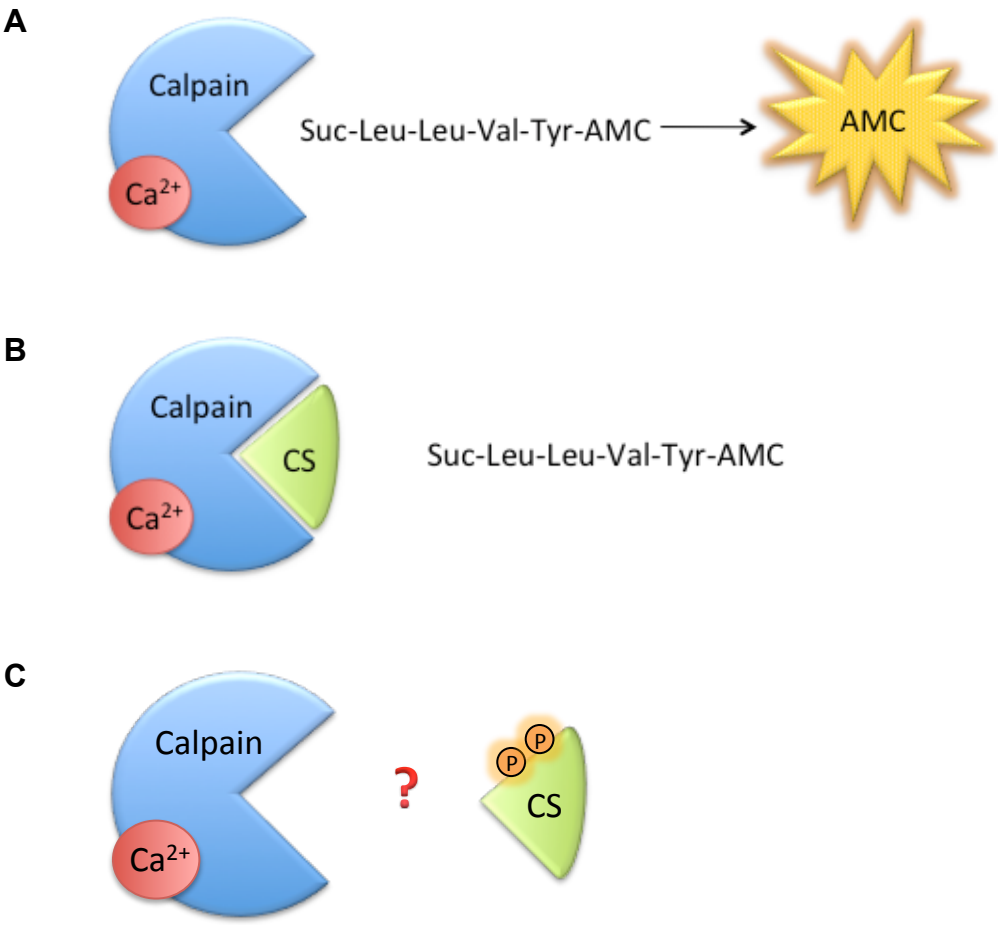

Figure 6.8 ***In vitro*** **calpain assay**

Fluorometric method for detecting *in vitro* calpain activity. Suc-leu-leu-val-Tyr-AMC is a synthetic fluorogenic peptide substrate of calpain proteases. ***A,*** Following cleavage by calpain, the 7-Amino-4-Methylcoumarin (AMC) fluorophore is generated and can be monitored at excitation/emission = 380/460 nm. ***B,*** Addition of calpastatin (CS) inhibits calpain and prevents the liberation of AMC fluorophore. ***C,*** It is not known what effect phosphorylation of CS by p38γ has on its ability to inhibit calpain.

6.3 Results

6.3.1 Zfp260

To validate zfp260 as a substrate of p38γ, recombinant GST-zfp260 was engineered for expression in *E.coli.* Successful expression of GST-zfp260 in the selected bacterial colony, following induction of a 5 mL culture with IPTG, can be observed in Figure 6.9A. Samples from the total lysate, the insoluble and soluble fractions following lysis were probed with the GST antibody. As expected the GST antibody detects a 26 kDa band corresponding to the GST tag in the control samples (colony expressing empty vector). In bacterial cells transfected with GST-zfp260 vector, the GST antibody detects a protein at the expected molecular weight of the GST-zfp260 (~70 kDa) and lower molecular weight bands likely to be degradation products of the recombinant protein. From this initial analysis, the expressed protein appears to be entirely insoluble. However, following a larger volume of bacterial culture and extensive lysis, GST-zfp260 is obtained in a soluble form. The outcome of purification of GST-zfp260 is shown in Figure 6.9B. A dominant band corresponding to the size of zfp260 cannot be observed in the *E.coli* cell lysate, suggesting low expression of the protein in host cells. Despite this, following purification with glutathione sepharose, there is successful retention of zfp260 protein and some contaminant proteins. Eluents were pooled and dialysed for subsequent experimentation.

For substrate validation, GST-zfp260 was subject to *in vitro* kinase assays with p38γ. As phospho-zfp260 antibodies are unavailable, kinase assays were performed with ATPγS and probed with the thiophosphate antibody. Unfortunately no thiophosphorylation of zfp260 was detected by p38γ or p38α, although p38γ successfully thiophosphorylated α1-syntrophin (Figure 6.10). The Phos-tag^{TM} SDS-PAGE analysis of zfp260 kinase assays was also attempted but phosphorylated species were not observed (data not shown). Lastly, the products of zfp260 kinase assays were also prepared for LC-MS/MS (Figure 6.11) but no phosphorylated peptides could be detected.

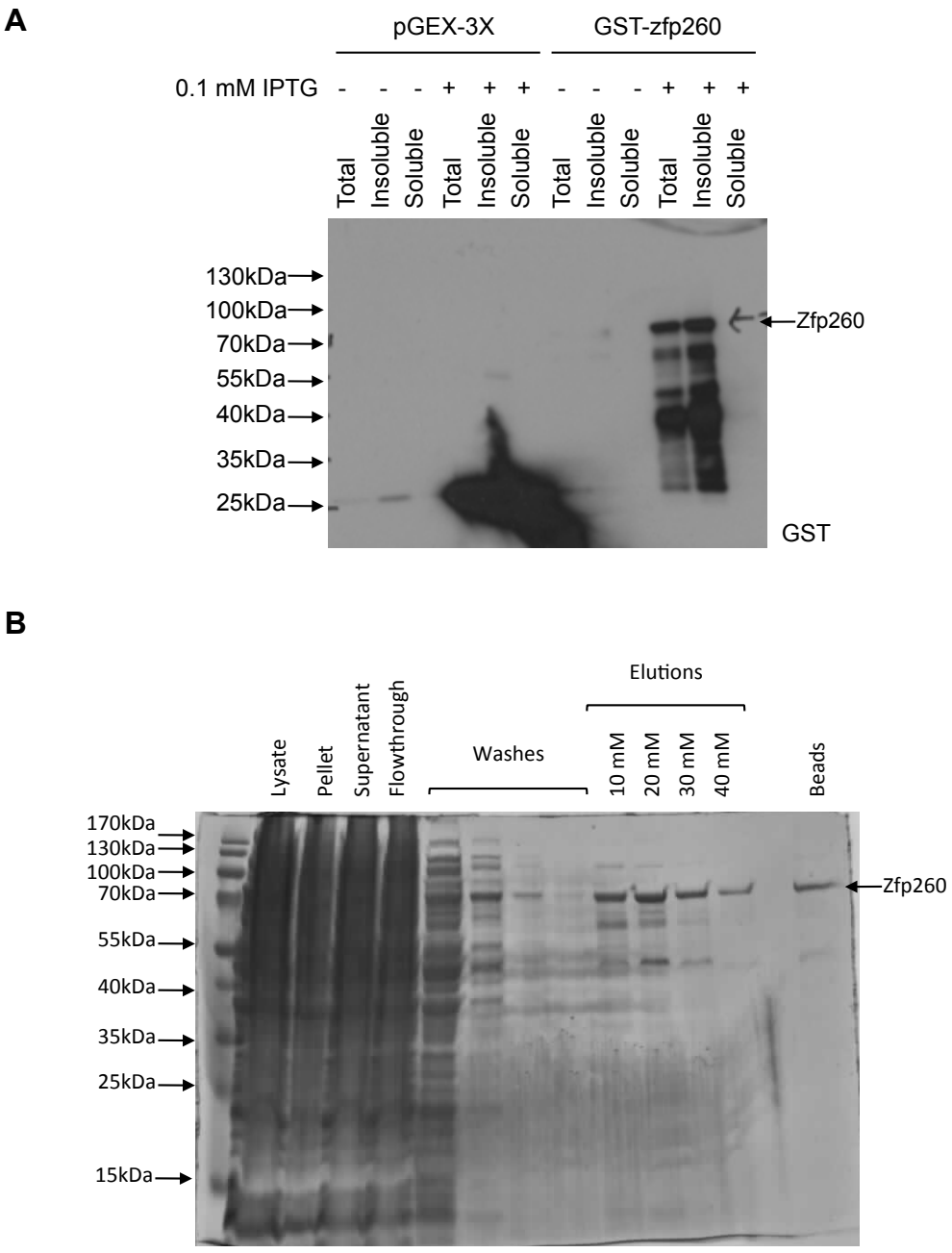

Figure 6.9 Expression and purification of recombinant GST-zfp260 from *E.coli* by glutathione sepharose chromatography

A, Immunoblot analysis of lysed (total lysate, soluble and insoluble fractions) *E.coli* cells transfected with empty host vector (pGEX-3X) or GST-zfp260. GST antibody detects recombinant GST-zfp260 at the correct molecular weight (~70 kDa) in the insoluble fraction of IPTG induced cells ***B,*** Purification of GST-zfp260 from *E.coli* by glutathione sepharose chromatography. Samples were taken from each step of the purification process, prepared in 5 x sample buffer and resolved by 10% SDS-PAGE and stained with Coomassie, as described in *Materials and Methods*. There is low expression of GST-zfp260, but it is successfully purified using glutathione sepharose.

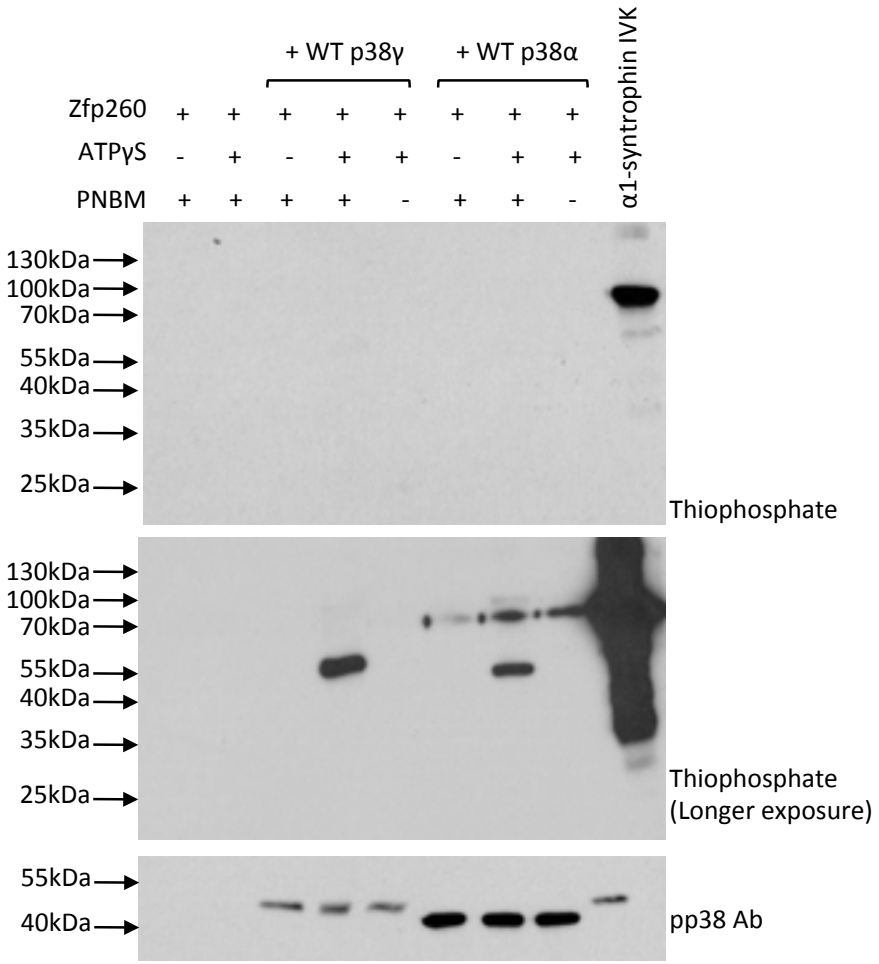

Figure 6.10 *In vitro* kinase assay of zfp260 using WT p38 and ATPγS

Immunoblot analysis of zfp260 thiophosphorylation after *in vitro* exposure to MKK6EE-activated p38 kinases. Samples were resolved by 10% SDS-PAGE, as described in *Materials and Methods*. Thiophosphorylation of zfp260 was not detected, even at a longer exposure of film, despite detection of α1-syntrophin thiophosphorylation.

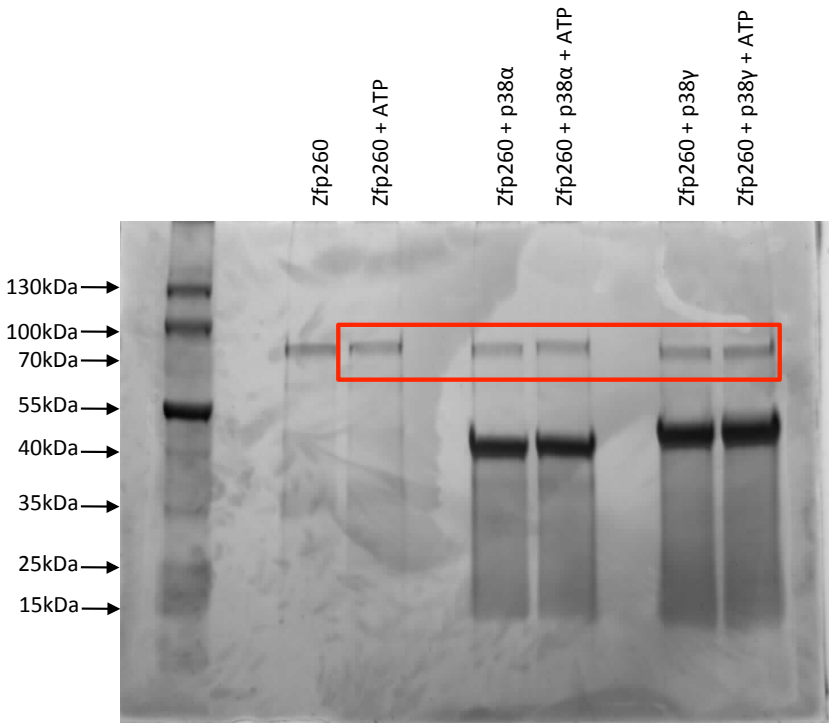

Figure 6.11 Preparation of zfp260 IVK samples for mass spectrometry analysis

Samples for LC-MS/MS analysis were resolved by 4-20% gradient SDS-PAGE and stained with silver as described in *Materials and Methods*. Boxed zfp260 protein bands were cut out and processed for analysis.

6.3.2 Lim domain binding protein 3

To confirm LDB3 as a substrate of p38γ, recombinant His-LDB3 was engineered for expression in *E.coli.* Once a colony successfully expressing the His-LDB3 protein was established, a large *E.coli* culture for protein expression was prepared. The outcome of purification of His-LDB3 is shown in Figure 6.12A. A dominant band corresponding to the size of His-LDB3 cannot be observed in the *E.coli* cell lysate, suggesting low expression of the protein in host cells. Despite this, following purification by metal affinity capture, there is successful retention of His-LDB3 protein and some contaminant proteins. Eluents from the two highest imidazole concentrations were pooled and dialysed for subsequent experimentation. Purification of His-LDB3 was confirmed by probing dialysed protein with His and LDB3 antibodies (Figure 6.12B). As expected, both antibodies detect a band corresponding to the molecular weight of His-LDB3 (110 kDa). The LDB3 antibody also detects lower molecular weight bands which is likely to be degraded LDB3 protein.

Next, purified His-LDB3 was subject to kinase assays with p38γ and ATPγS. As shown in Figure 6.13A, LDB3 successfully undergoes thiophosphorylation by both p38γ and p38α kinases. As LDB3 possesses a PDZ domain, it was tested if the interaction of the C' PDZ interacting motif of p38γ with the PDZ domain of LDB3 was needed for phosphorylation to occur. This was tested by using C' truncated p38γ in kinase assays with LDB3 for varying times. From Figure 6.13B, it can be seen that both WT and C' truncated p38γ phosphorylate LDB3 to the same extent, suggesting that, at least *in vitro,* the PDZ interaction is not needed for substrate phosphorylation.

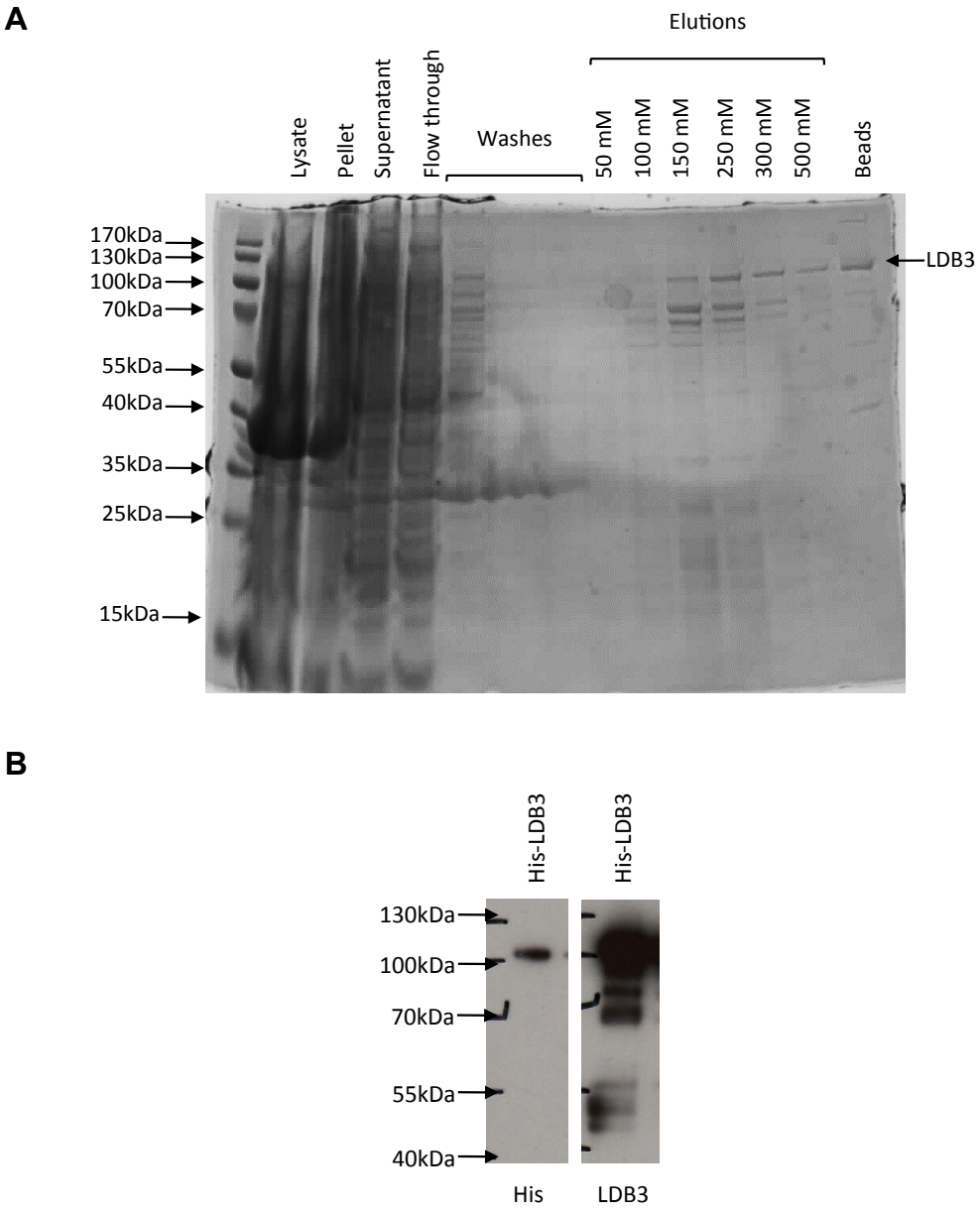

Figure 6.12 Purification of recombinant His-LDB3 from *E.coli* by metal affinity capture

A, Samples were taken from each step of the purification process, prepared in 5 x sample buffer and resolved by 10% SDS-PAGE and stained with Coomassie, as described in *Materials and Methods*. There is low expression of His-LDB3, but it is successfully purified using Ni-NTA agarose. ***B,*** Immunoblot analysis of His-LDB3 purification. His-LDB3 is detected at the correct molecular weight of 110 kDa. There appears to be some degradation of protein during purification as detected by the LDB3 antibody. Samples were resolved by 10% SDS-PAGE, as described in *Materials and Methods*.

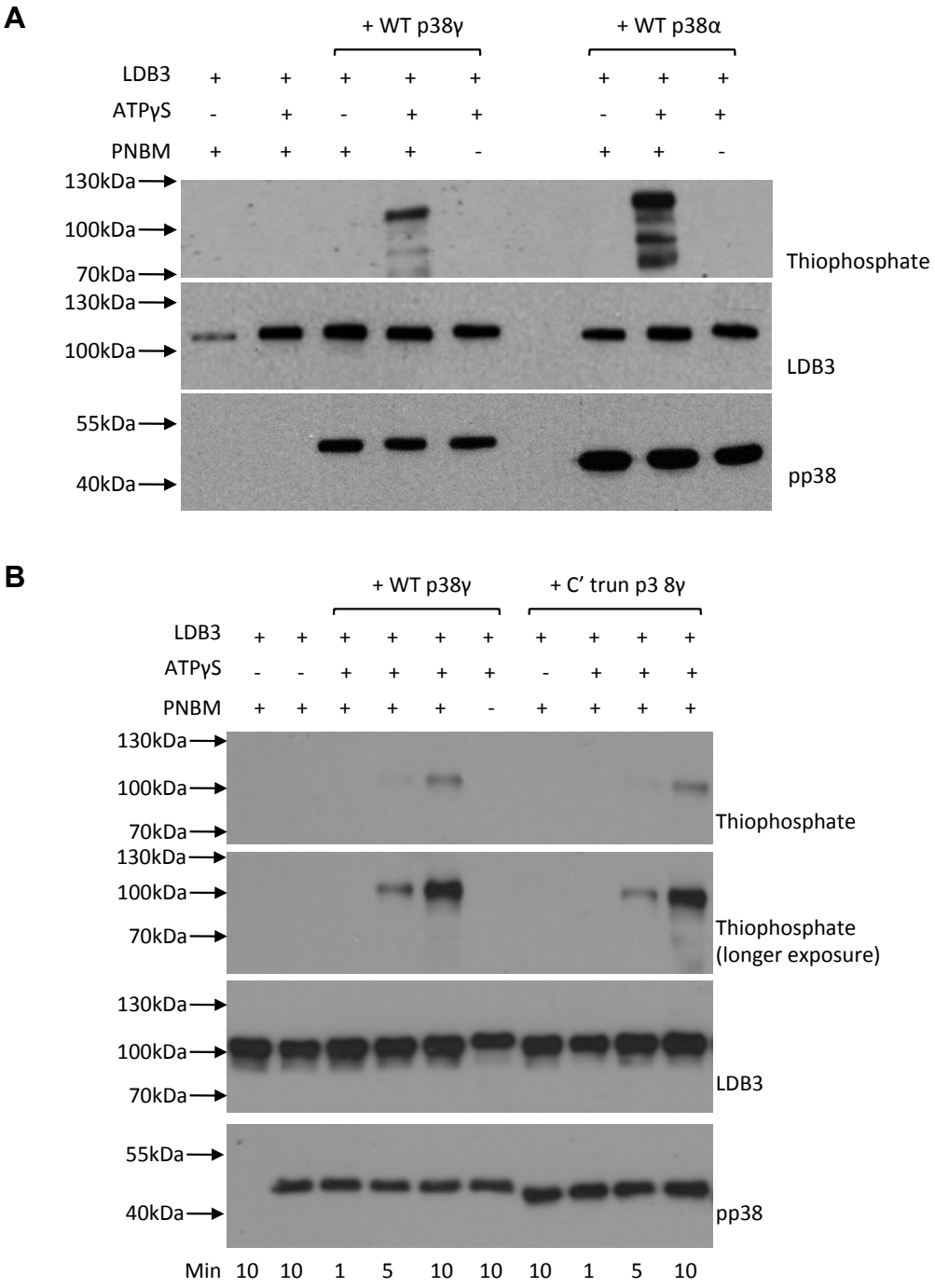

Figure 6.13 *In vitro* kinase assay of LDB3 using p38 and ATPγS

Immunoblot analysis of LDB3 thiophosphorylation after *in vitro* exposure to various MKK6EE-activated p38 kinases. Samples were resolved by 10% SDS-PAGE, as described in *Materials and Methods*. ***A,*** LDB3 can be thiophosphorylated by both WT p38α and p38γ ***B,*** Thiophosphorylation of LDB3 by WT and C' truncated p38γ. Truncation of p38γ C' PDZ interacting motif does not affect thiophosphorylation of LDB3 *in vitro*.

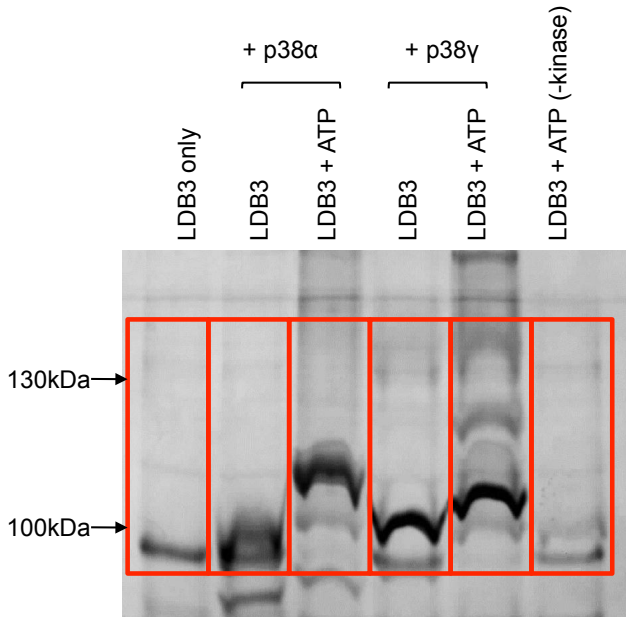

Figure 6.14 Phos-tag™ analysis of LDB3 *in vitro* kinase assay

Samples for LC-MS/MS analysis were resolved by Phos-tag™ SDS-PAGE and stained with silver as described in *Materials and Methods*. Boxed regions were cut out and individually processed for LC-MS/MS analysis per lane.

To determine target phospho-residues, His-LDB3 kinase assays were analysed by LC-MS/MS. For this samples were resolved by Phos-tag™ SDS-PAGE and stained with silver (Figure 6.14). The Phos-tag™ SDS-PAGE analysis of LDB3 phosphorylation reveals that multiple sites are phosphorylated by p38γ. This supports findings from the Shokat experiment, which detected Ser^{98} and Ser^{240} to undergo thiophosphorylation by p38γ. Furthermore, the Phos-tag™ suggests that LDB3 is phosphorylated to different extents by p38γ and p38α kinases. The LC-MS/MS analysis of LDB3 phosphorylation, given in Table 6.7 confirms this finding. Furthermore LC-MS/MS of the Phos-tag™ SDS-PAGE gel also confirms the phosphorylation sites detected from the Shokat experiment. Ser^{98} is detected to undergo phosphorylation by both isoforms. In contrast, although Ser^{240} phosphorylation is detected in the control sample (LDB3 with ATP), it is only detected to undergo phosphorylation by p38γ. In addition to the Shokat sites, Thr^{119} and Ser^{179} are phosphorylated by both isoforms and Ser^{121} is also phosphorylated by p38γ.

Table 6.7 LC-MS/MS analysis of LDB3 phosphorylation

		p38α		p38γ	
LDB3	**LDB3 + ATP**	**LDB3**	**LDB3 +ATP**	**LDB3**	**LDB3 +ATP**
				T92 (1)	
			S98 (2)		**S98 (4)**
T113 (1)					T113 (2)
	S116 (1)				S116 (1)
			T119 (1)		**T119 (1)**
					S121 (1)
			S179 (1)		**S179 (1)**
				S220 (1)	S220 (1)
S228 (1)	S228 (1)	S228 (1)		S228 (1)	S228 (1)
			S238 (2)	S238 (1)	
	S240 (1)				**S240 (2)**

(x) denotes number of peptides detected. Proline directed sites are given in bold.

As Ser^{98} and Ser^{240} were the only sites detected to undergo phosphorylation by p38γ by two independent experiments, LDB3 phosphorylation at these two sites was subsequently validated. To achieve this, phosphorylation deficient mutants of LDB3 at these sites (S98A, S240A and S98A/S240A double mutant) were engineered for expression in *E.coli.* Unfortunately, little or no expression of LDB3 mutants was encountered in the different strains of bacteria tested. Therefore, WT and mutant LDB3 genes were cloned into mammalian expression vector, for overexpression of proteins in HEK293 cells. Purification of all His-LDB3 proteins from HEK293 cells is shown in Figure 6.15. Although expression of proteins is suboptimal, sufficient protein was purified for subsequent assays. All His-LDB3 protein preparations encountered the same degree of contaminants and/or degraded proteins.

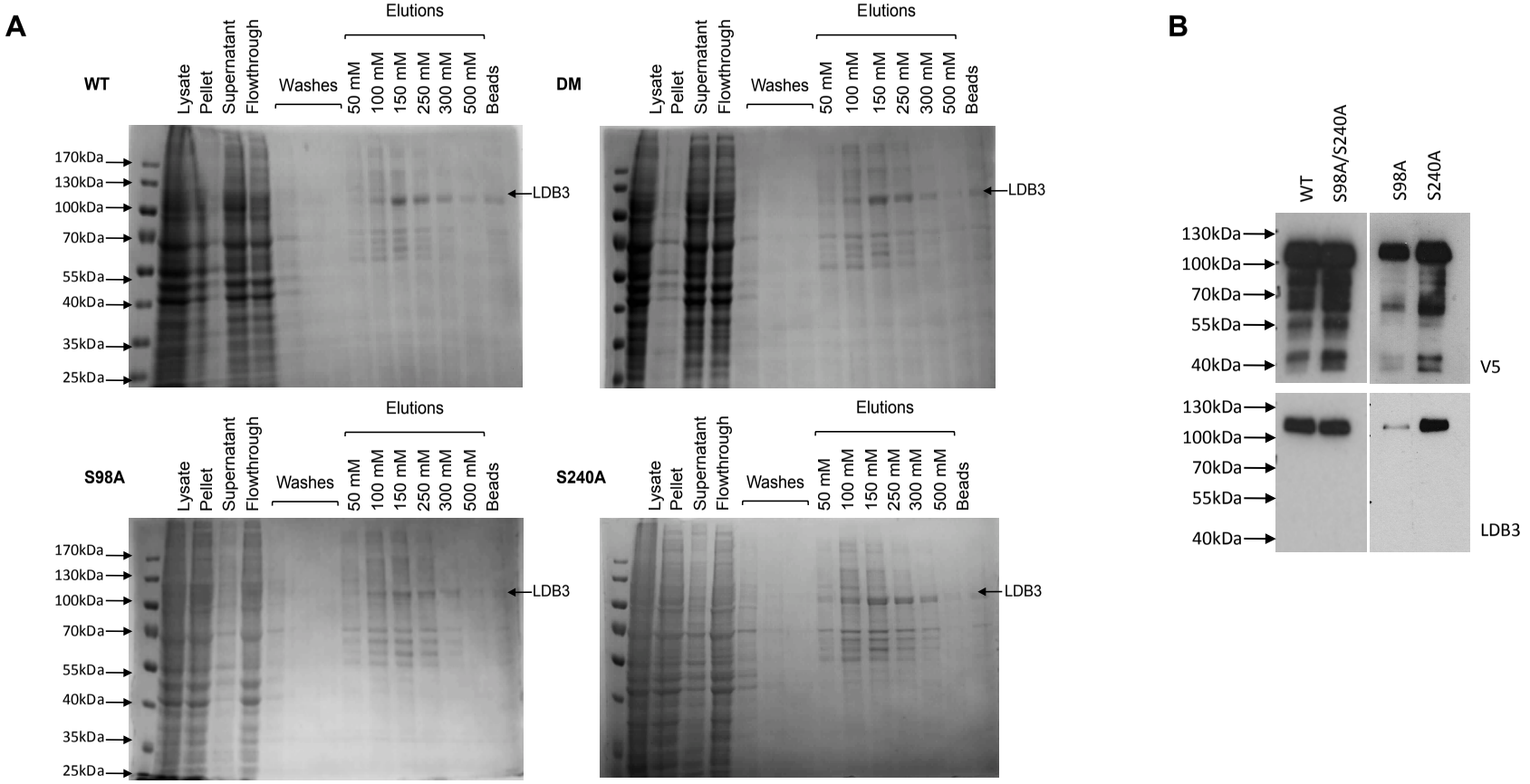

Figure 6.15 Purification of His-LDB3 proteins from HEK293 cells by metal affinity capture

A, Samples were taken from each step of the purification process, prepared in 5 x sample buffer, resolved by 10% SDS-PAGE and stained with Coomassie as described in *Materials and Methods*. Expression of His-LDB3 is suboptimal, but it is successfully purified using Ni-NTA agarose. ***B,*** Immunoblot analysis of His-LDB3 purification reveals degradation of protein during purification. Samples were resolved by 10% SDS-PAGE, as described in *Materials and Methods*.

Fractions that contained the most recombinant protein were pooled and purification of His-LDB3 was confirmed by Western blotting analysis. In this instance, samples were probed with an antibody against the V5 tag and the LDB3 antibody. The V5 antibody detects all His-LDB3 proteins and many lower molecular weight bands that are likely to be degraded proteins. In contrast the LDB3 antibody only detects the dominant LDB3 protein band at 110 kDa. Although the V5 antibody detects similar levels of WT and mutant proteins, this is not reflected in the LDB3 antibody probe. Interestingly, signal intensity of the S98A mutant, but not the double mutant is reduced with the LDB3 antibody, despite the fact the equal amounts of protein were loaded. And this is something that is also observed in subsequent experiments. Often introduction of a mutation can change the epitope of an antibody and therefore result in a reduced signal, but this is puzzling, as detection of the double mutant, which also contains the S98A mutation, is not perturbed.

To validate the phosphorylation sites, the next experiment was to examine if thiophosphorylation of LDB3 by p38γ is reduced or abolished in the mutant proteins. The result of this experiment is shown in Figure 6.16. As before, WT LDB3 is thiophosphorylated by p38γ. As anticipated, the single site S98A and S240A mutants also undergo thiophosphorylation. However, it was expected that thiophosphorylation in the double site LDB3 mutant would at least be reduced. This was not the case, as the signal intensity did not noticeably decrease. Hence, this is thiophosphorylation at the additional sites detected in the LC-MS/MS analysis of kinase reactions.

The thiophosphorylation kinase assay could not be used to validate Ser^{98} and Ser^{240} as p38γ target phosphorylation sites. Therefore, phospho-antibodies that specifically recognise these sites were generated and used to probe kinase assays. Kinase assays were set up with WT and mutant LDB3 proteins, p38γ and ATP. Firstly it can be seen in Figure 6.17 that the phospho-Ser^{98} antibody detects phosphorylation of WT LDB3 by p38γ, as expected. Secondly, the signal is abolished when this site is mutated in the single or the double LDB3 mutant. Thirdly, the phospho-Ser^{98} antibody is highly specific, as it does not detect any non-phosphorylated LDB3 protein. A concern of expressing protein

for purification in mammalian cells is that they may become basally phosphorylated and therefore complicate experimental analysis. In this case, LDB3 proteins were not basally phosphorylated. This can be concluded from the phospho-Ser^{98} antibody probe and the corresponding LDB3 antibody probe. When LDB3 is incubated with p38γ and ATP, the resultant phosphorylated protein presents at a slightly higher molecular weight than the corresponding non-phosphorylated control. Again, we observe a reduced signal intensity of the S98A mutant with the LDB3 antibody. But importantly, the results of these blots confirm that Ser^{98} is phosphorylated by p38γ *in vitro*.

The phospho-Ser^{240} antibody probe also validates Ser^{240} as a target site of p38γ *in vitro*. Although this phospho-antibody is non-specific, as it detects non-phosphorylated LDB3, a discernable band is observed with WT LDB3 that is abolished in the S240A or double mutant. As discussed above, the LDB3 antibody probe reveals that phosphorylated LDB3 presents at a slightly higher molecular weight than the corresponding non-phosphorylated control.

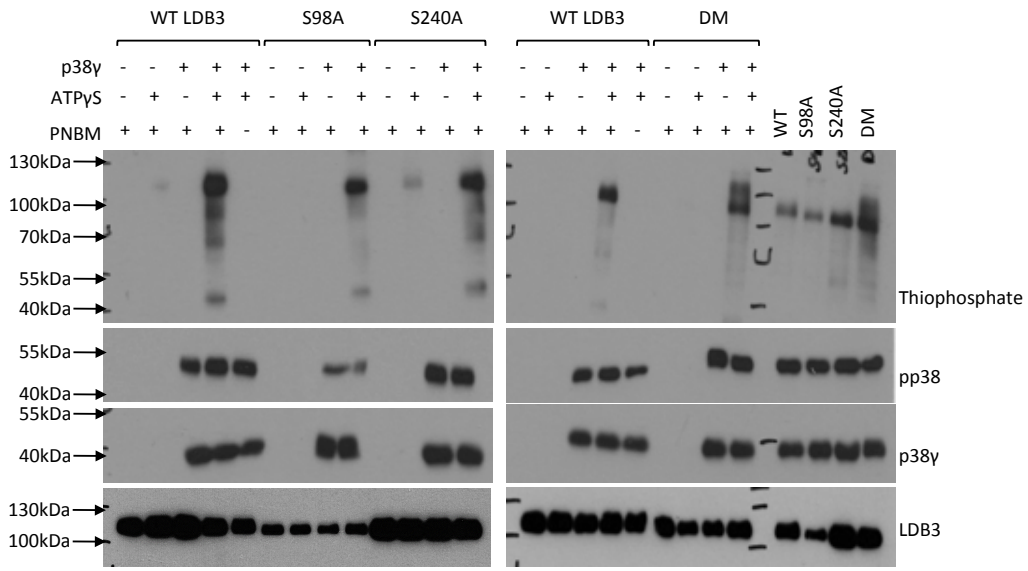

Figure 6.16 Thiophosphorylation of WT and mutant LDB3 by p38γ *in vitro*

Immunoblot analysis of WT and phospho-mutant LDB3 thiophosphorylation after *in vitro* exposure to p38γ. Mutation of residues did not noticeably decease thiophosphorylation signal. Samples were resolved by 10% SDS-PAGE, as described in *Materials and Methods*.

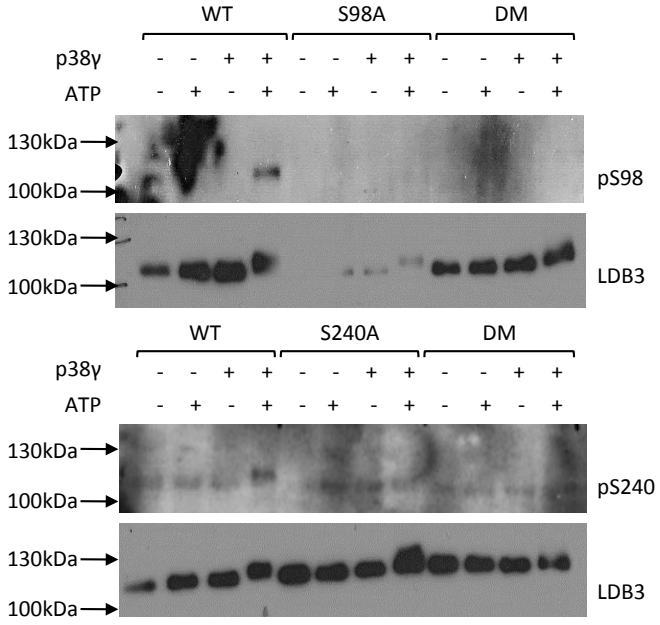

Figure 6.17 Phosphorylation of WT and mutant LDB3 by p38γ *in vitro*

Immunoblot analysis of WT and phospho-mutant LDB3 phosphorylation after *in vitro* exposure to p38γ. Phosphorylation is not detected by phospho antibodies with corresponding alanine mutant, validating Ser^{98} and Ser^{240} as p38γ target sites. Samples were resolved by 10% SDS-PAGE, as described in *Materials and Methods*.

6.3.3 Calpastatin

For validation of calpastatin as a substrate of p38γ, recombinant GST-calpastatin was engineered for expression in *E.coli.* As the ORF of murine calpastatin was commercially unavailable, calpastatin DNA was generated in house. The quality and the integrity of the RNA extracted from mouse heart is shown in Figure 6.18. The 28s:18s ribosomal RNA ratio calculated from the electropherogram is 2. This indicates that the purified RNA is of high quality. Another measure given from the electropherogram is the RNA integrity number. This was determined to be 7.8, which suggests that although some degradation is present, the extracted RNA is of a good quality. Extracted RNA was then used to generate double stranded calpastatin DNA. Sequencing of calpastatin DNA revealed that the generated DNA corresponded to the sequence of calpasatin isoform 2 (Figure 6.6).

Expression of GST-calpastatin in the selected bacterial colony, following induction of a 5 mL culture with IPTG, can be observed in Figure 6.19. Samples from the total lysate, the insoluble and soluble fractions following lysis were probed with the GST antibody. As expected the GST antibody detects a 25 kDa band corresponding to the GST tag in the control samples (colony expressing empty vector). In bacterial cells transfected with GST-calpastatin vector, the GST antibody detects a protein at the expected molecular weight of the GST-calpastatin (~120 kDa) and lower molecular weight bands likely to be degradation products of the recombinant protein. From this initial analysis, the expressed protein appears to be entirely insoluble. However, following a larger volume of bacterial culture and extensive lysis, GST-calpastatin is obtained in a soluble form. The outcome of purification of GST-calpastatin is shown in Figure 6.19B. A dominant band corresponding to the size of calpastatin can be observed in the *E.coli* cell lysate, suggesting good expression of the protein in host cells. During purification with glutathione sepharose, there is successful retention of the calpastatin protein, with some loss during washes. Some contaminant proteins are also present post purification. Eluents were pooled and dialysed for subsequent experimentation.

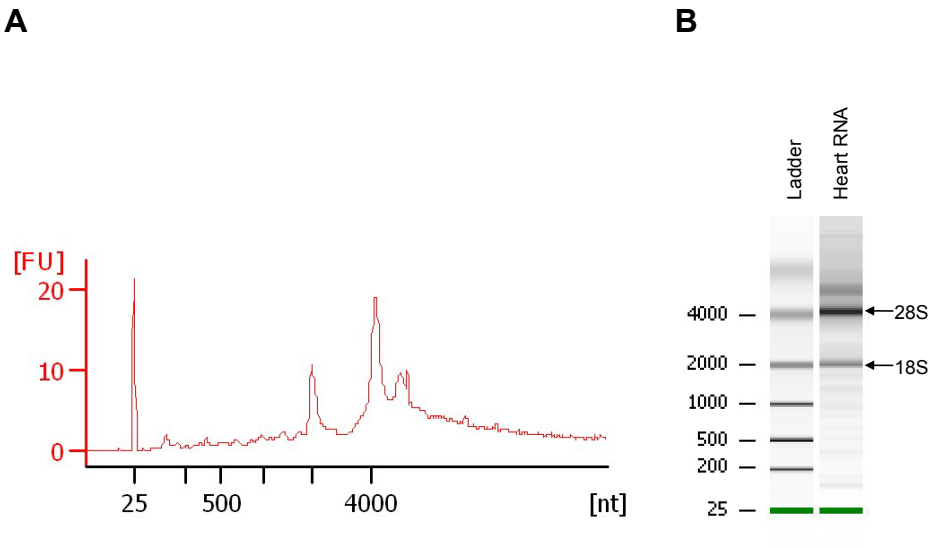

Figure 6.18 Assessment of RNA quality and integrity

A, Electropherogram of heart RNA sample. 18S (2000 nt) and 28S (4000 nt) peaks are clearly visible. ***B,*** Data from A is displayed as a gel-like image.

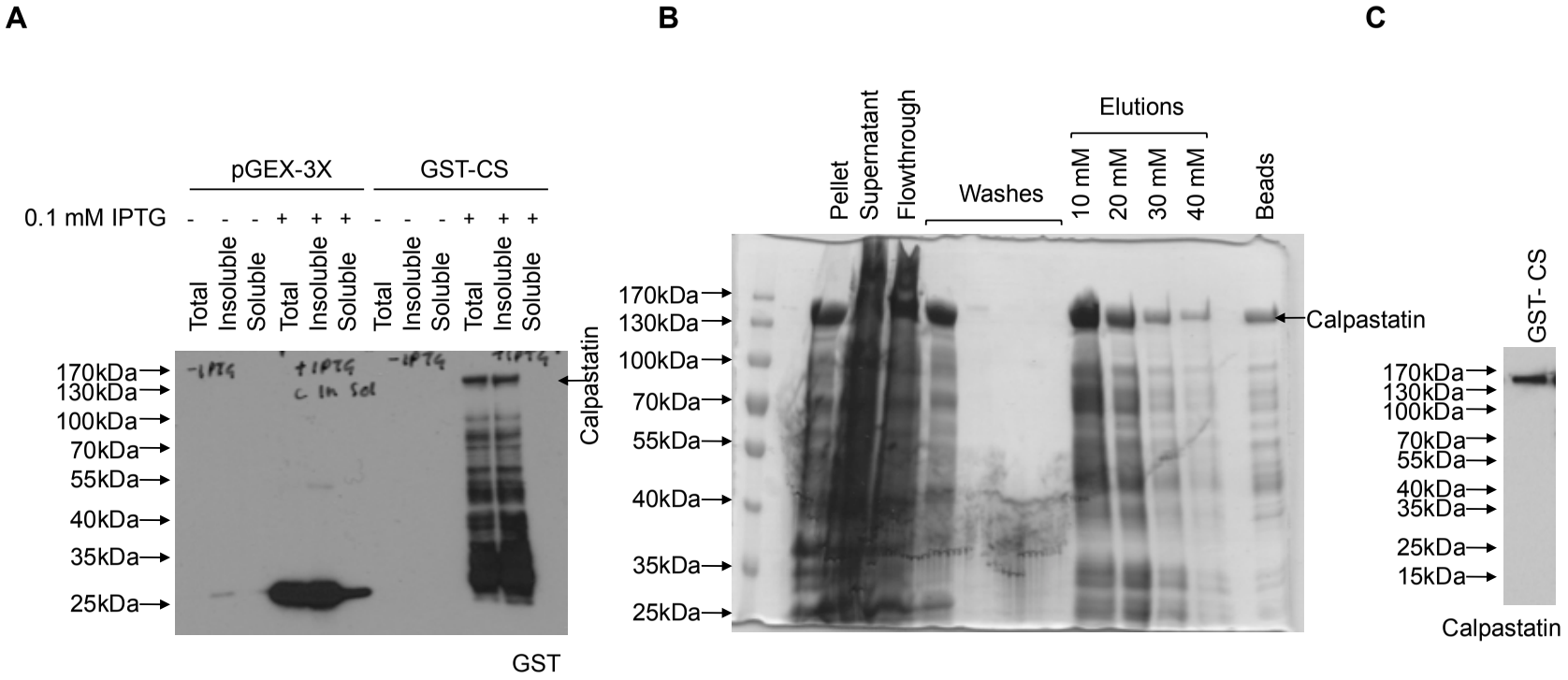

Figure 6.19 Purification of GST-calpastatin from *E.coli* by glutathione sepharose chromatography

A, Immunoblot analysis of lysed (total, soluble and insoluble fractions) *E.coli* cells transfected with empty host vector (pGEX-3X) or GST-CS (calpastatin). GST antibody detects recombinant GST-CS at the correct molecular weight in the insoluble fraction of IPTG induced cells. ***B,*** Purification of GST-CS from *E.coli* by glutathione sepharose chromatography. There is good expression of GST-CS and it is successfully purified using glutathione sepharore. Samples were taken from each step of the purification process, prepared in 5 x sample buffer and resolved by 10% SDS-PAGE and stained with Coomassie, as described in *Materials and Methods*. ***C,*** Immunoblot analysis of GST-CS purification.

Purified GST-calpastatin was subject to kinase assays with p38γ and ATPγS. As shown in Figure 6.20A, calpastatin successfully undergoes thiophosphorylation by both p38γ and p38α kinases. To determine target phospho-residues, GST-calpastatin kinase assays were analysed by LC-MS/MS. As before, samples for this were resolved by Phos-tag^{TM} SDS-PAGE and stained with silver (Figure 6.20B). The Phos-tag^{TM} SDS-PAGE analysis of calpastatin phosphorylation reveals that multiple sites are phosphorylated by p38γ, which mirrors the findings from the Shokat experiment. Furthermore, the Phos-tag^{TM} shows that a different pattern of phosphorylation by p38γ and p38α kinases. The LC-MS/MS analysis of calpastatin phosphorylation is given in Table 6.8. In this instance, p38α mediated phosphorylation of calpastatin was not analysed.

LC-MS/MS of the Phos-tag^{TM} SDS-PAGE gel confirms three out of the seven phosphorylation sites detected in the Shokat experiment: Thr^{216}, Ser^{219} and Thr^{467}. Interestingly, these sites are also the only sites detected in the Shokat experiment that are proline directed. In addition to the aforementioned sites, the present LC-MS/MS analysis also returned 21 additional phosphorylation sites, only three of which are proline directed (Ser^{81}, Thr^{479} and Thr^{624}). As before, only those sites that were detected by the two independent analyses were pursued further. The assigned phosphorylation sites from both mass spectrometry studies are given for isoform 1 of calpastatin. As the recombinant calpastatin used for this study is isoform 2, the Thr^{216}, Ser^{219} and Thr^{467} phosphorylation sites are Thr^{197}, Ser^{200} and Thr^{448} respectively.

To validate phosphorylation of calpastatin at the selected sites, phosphorylation deficient mutants of calpastatin were engineered for expression in *E.coli.* To aid design of mutant proteins, the peptide and available crystal structures of calpastatin were examined. Thr^{197} and Ser^{200} are located prior to the first inhibitory domain of the molecule, whereas Thr^{448} is located in between the second and third inhibitory domains. Therefore, a double T197A/S200A and a single T448A mutant were generated.

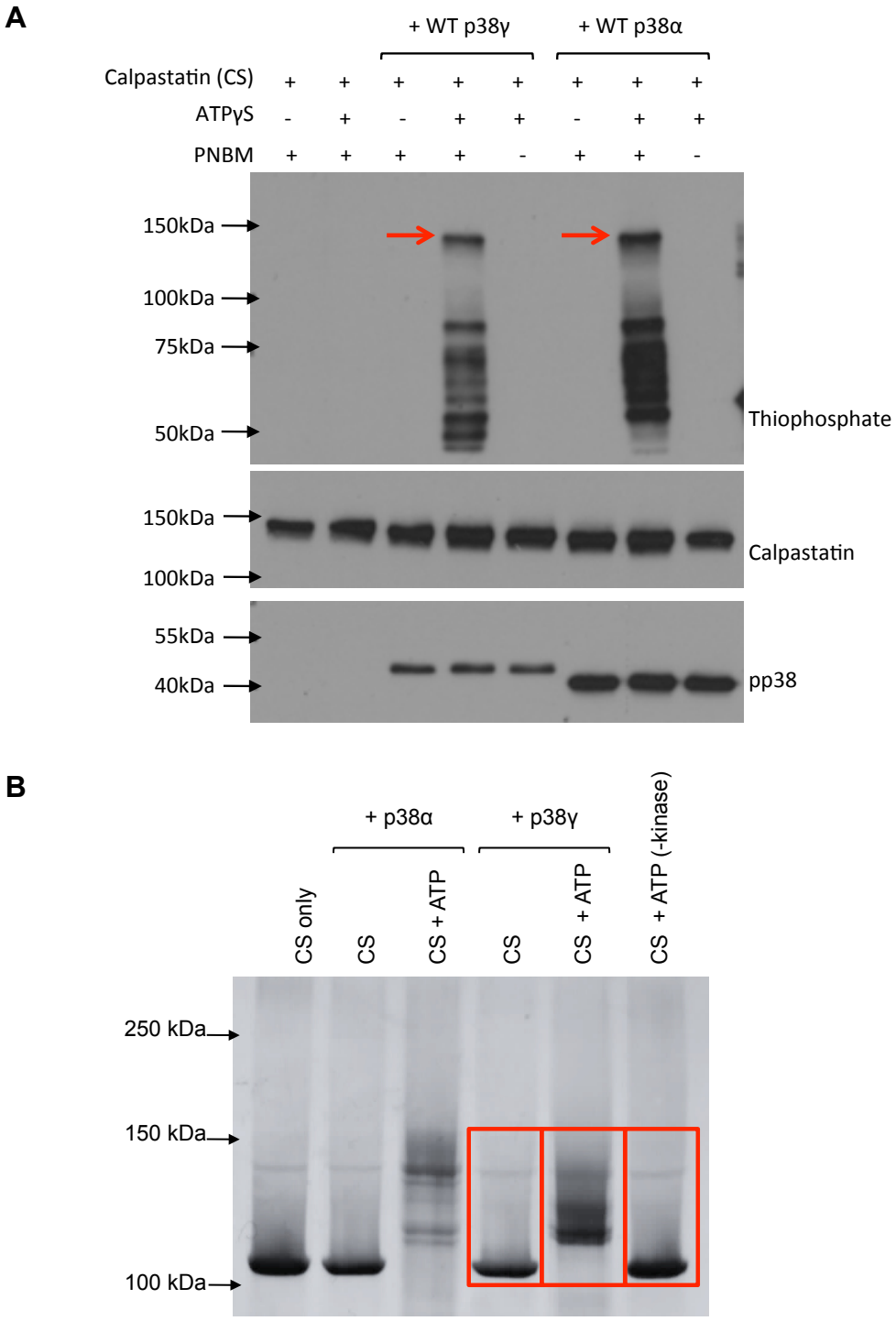

Figure 6.20 *In vitro* kinase assays of calpsatatin

A, Immunoblot analysis of calpastatin thiophosphorylation after *in vitro* exposure to MKK6EE-activated p38α or p38γ with ATPγS. CS can be phosphorylated by both isoforms. Samples were resolved by 10% SDS-PAGE, as described in *Materials and Methods*. ***B,*** Phos-tag™ analysis of calpastatin *in vitro* kinase assays. Samples for LC-MS/MS analysis were resolved by Phos-tag™ SDS-PAGE and stained with silver as described in *Materials and Methods*. Boxed regions were cut out and individually processed for analysis per lane.

Table 6.8 LC-MS/MS analysis of Calpastatin phosphorylation

	p38γ	
CS + ATP	**CS**	**CS + ATP**
	S11(1)	**S11 (1)**
		T78 (1)
S79 (1)	**S79 (1)**	**S79 (1)**
		S81 (1)
S158 (1)	S158 (1)	
	T160 (2)	
		S165 (1)
S167 (1)		
		T171 (1)
	T178 (1)	
		T179 (1)
T181 (1)	T181 (1)	
		S191 (1)
		T197 (1)
S210 (1)	S210 (1)	
		T216 (2)
		S219 (5)
		S223 (2)
		T224 (1)
		S229 (1)
S358 (1)	S358 (1)	
		S377 (1)
T420 (1)		
S421 (1)	S421 (1)	
S434 (1)	S434 (1)	
		T439 (1)
		S440 (1)
T441 (1)	T441(1)	
		S446 (1)
		S453 (1)
		T467 (1)
		T479 (2)
		T624 (1)
		S628 (1)
		S653 (2)
T697 (1)	T697 (1)	
		T716 (1)
		S735 (1)

(x) denotes number of peptides detected. Proline directed sites are given in bold.

Purification of mutant GST-calpastatin proteins is shown in Figure 6.21. As with WT calpastatin, there is good expression of recombinant proteins. Glutathione sepharose chromatography retains much of the overexpressed protein, although some loss occurs during the washes. In the eluents, a similar banding pattern of contaminant proteins is encountered as observed with WT calpastatin purification. The immunoblot analysis of WT and mutant proteins shows that mutation of protein does not affect the ability of the calpastatin antibody to recognise the epitope.

To see if mutation of calpastatin at phosphorylation sites had any effect on the thiophosphorylaiton signal, WT and mutant calpastatin proteins were subject to kinase assays with p38γ and ATPγS. From Figure 6.22 it can be seen that the thiophosphorylation signal is reduced with both mutant proteins compared to WT calpastastin thiophosphorylation and to a greater extent with the double mutant. To conclusively determine Thr^{197}/Ser^{200} and Thr^{448} as target p38γ phosphorylation sites, phospho-antibodies that specifically recognise these sites were generated and used to probe kinase assays. Kinase assays were set up with WT and mutant calpastatin proteins, p38γ and ATP. From Figure 6.23 it can be seen that both phospho-calpastatin antibodies detect phosphorylation of WT calpastatin, as expected. Both antibodies are phospho-specific as they do not detect the non-phosphorylated calpastatin protein. Importantly, the phospho-antibodies do not detect phosphorylation of the respective mutant protein. Therefore, the results of these blots confirm that Thr^{197} and/or Ser^{200}, and Thr^{448} are phosphorylated by p38γ *in vitro*.

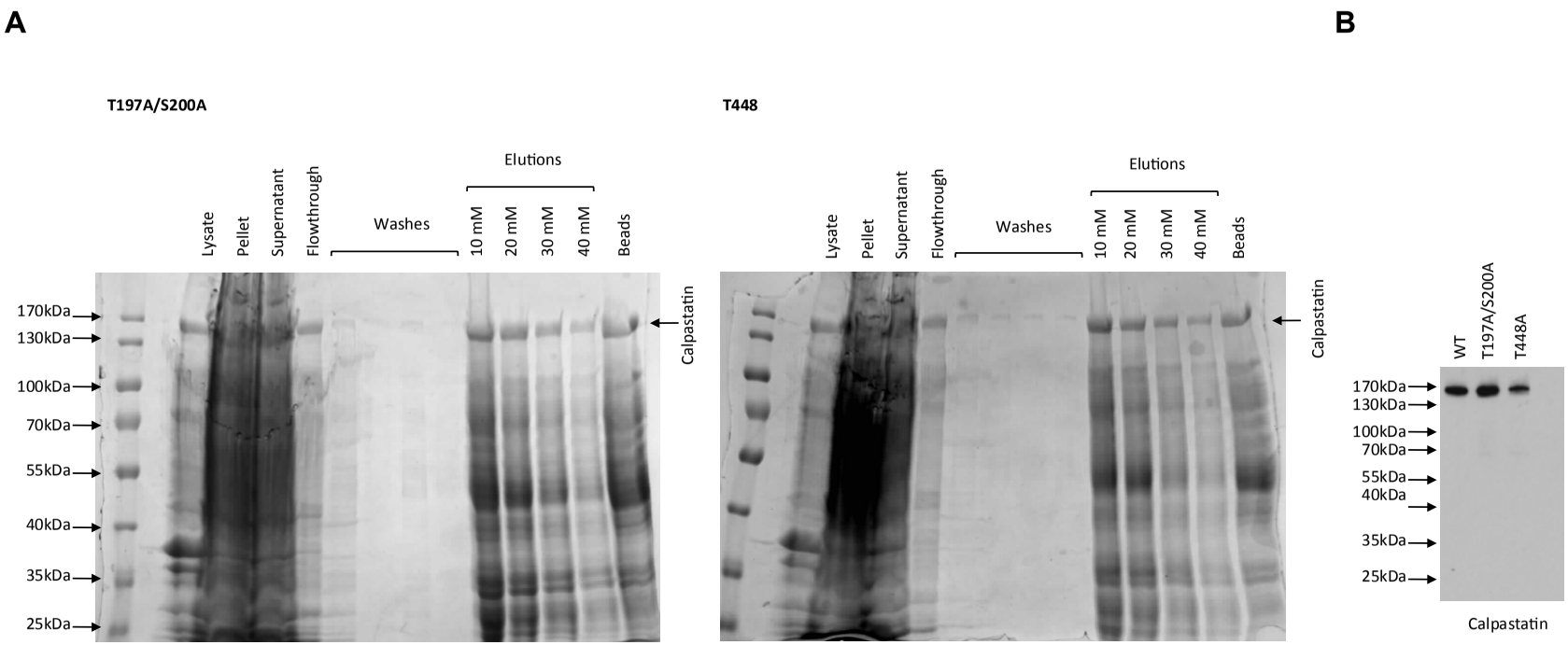

Figure 6.21 Purification of GST-calpastatin mutants from *E.coli* by glutathione sepharose chromatography

A, Samples were taken from each step of the purification process, prepared in 5 x sample buffer, resolved by 10% SDS-PAGE and stained with Coomassie, as described in *Materials and Methods*. There is good expression of GST-CS mutants and it is successfully purified with glutathione sepharose, although some contaminants persist. ***B,*** Immunoblot analysis of GST-CS mutant protein purification.

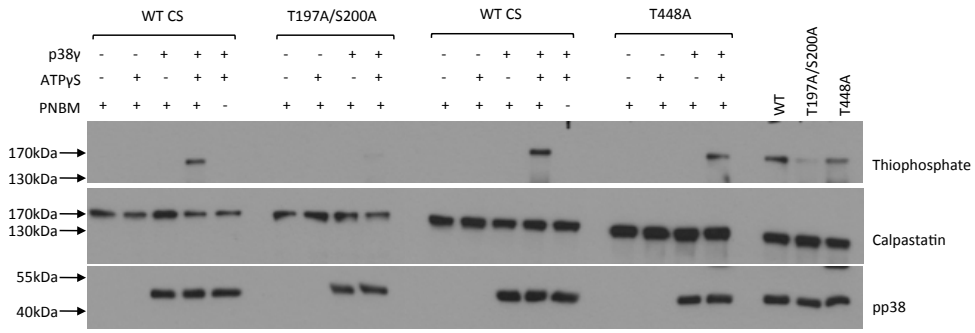

Figure 6.22 Thiophosphorylation of WT and mutant calpastatin by p38γ *in vitro*

Immunoblot analysis of WT and phospho-mutant calpastatin thiophosphorylation after *in vitro* exposure to p38γ. Thiophosphorylation signal is reduced with both mutant proteins in comparison to WT calpastastin thiophosphorylation and to a greater extent with the double mutant. Samples were resolved by 10% SDS-PAGE, as described in *Materials and Methods*.

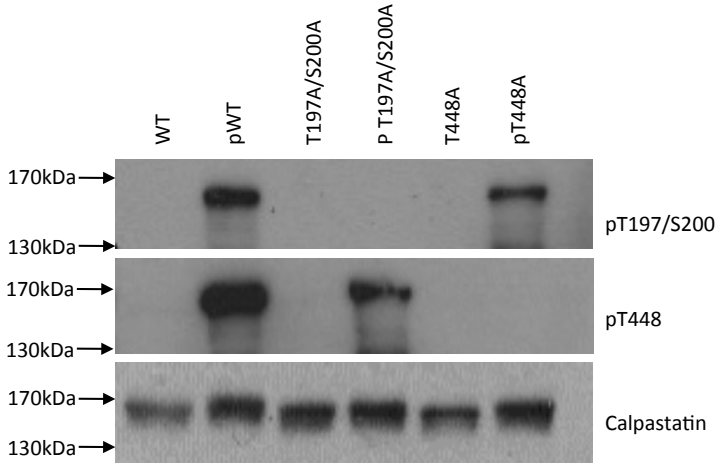

Figure 6.23 Phosphorylation of WT and mutant calpastatin by p38γ *in vitro*

Immunoblot analysis of WT and phospho-mutant calpastatin phosphorylation after *in vitro* exposure to p38γ. Phosphorylation is not detected by phospho antibodies with the corresponding alanine mutant CS protein, validating Thr^{197}/Ser^{200} and Thr^{448} as p38γ target sites. Samples were resolved by 10% SDS-PAGE, as described in *Materials and Methods*.

6.3.3.1 Functional effect of calpastatin phosphorylation

As calpastatin is the endogenous inhibitor of calpain proteases, an obvious assay to assess the functional significance of calpastatin phosphorylation, is to measure calpain activity in the presence of non-phosphorylated and phosphorylated calpastatin. Firstly the activity of calpain I was established *in vitro* against a synthetic substrate that fluoresces when cleaved. As expected, fluorescence is only observed in the presence of calcium, as calcium is required for calpain activity (Figure 6.24A). Next, non-phosphorylated WT calpastatin was added to calpain assays (Figure 6.24B and C). This caused a calpastatin dose dependent decrease in fluorescence, indicating dose dependent inhibition of calpain activity.

In order to assess the effect of p38γ phosphorylation on the ability of calpastatin to inhibit calpain, calpastatin was phosphorylated by p38γ prior to incubation with calpain. To control for kinase assay components, total calpain activity was measured in the presence of kinase assays components (without p38γ). To control for the addition of protein to the assay, calpastatin kinase assays were performed with both non-active and active p38γ. From Figure 6.25A it can be firstly be seen that fluorescence was still encountered in the presence of kinase assay components. Secondly, a significantly higher fluorescence signal was measured when calpastatin is in its phosphorylated state, in comparison to non-phosphorylated calpastatin (when calpastatin IVK was performed with non-active p38γ). This indicates that phosphorylation of calpastatin by p38γ significantly reduces the efficiency of calpastatin in inhibiting calpain *in vitro*. The phosphorylation status of calpastatin, following incubation with p38γ, was confirmed by SDS-PAGE and Western blotting using the phospho-specific antibodies, as shown in Figure 6.25.

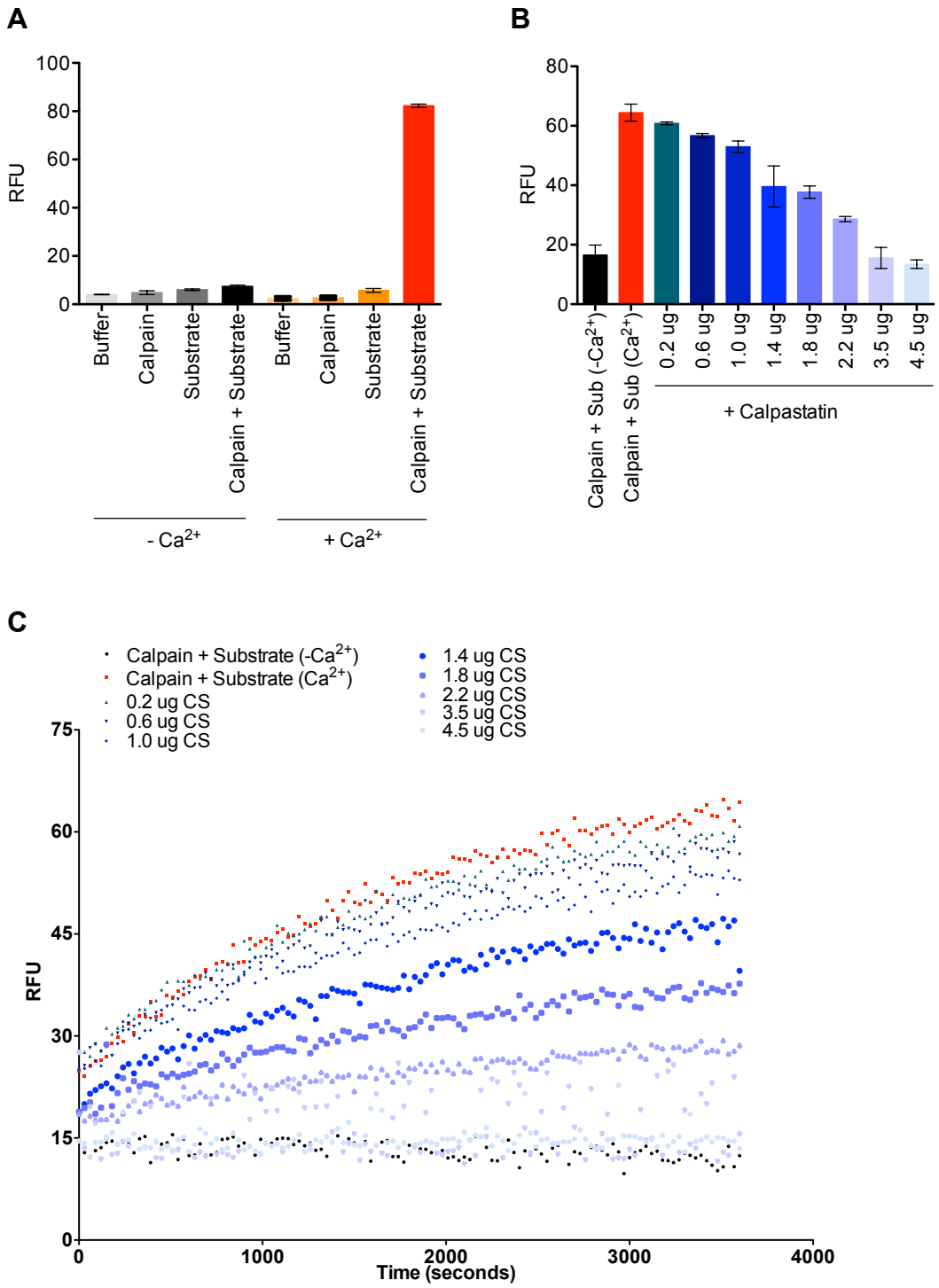

Figure 6.24 Calpain activity assay

A, Calpain I activity was measured in calcium free and calcium containing buffers, as described in *Materials and Methods*. Mean data and SEM of three independent experiments is shown. ***B and C,*** Dose dependent inhibition of calpain activity by 0.2 µg to 4.5 µg of WT calpastatin. ***C*** is real time calpain activity, as measured by fluorescence over an hour. Experiments were performed in triplicate. Mean fluorescence values are plotted against time.

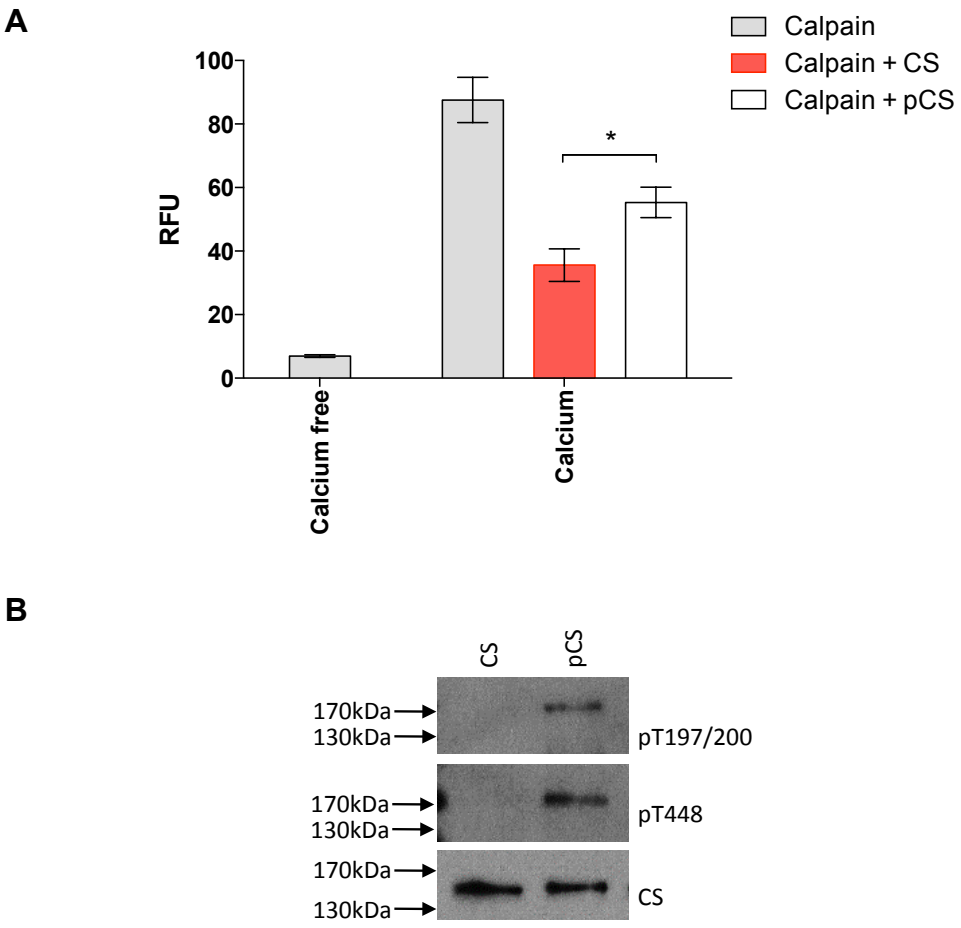

Figure 6.25 Effect of phosphorylation of calpastatin on calpain inhibition

A, Mean data and SEM of three independent experiments showing calpain activity in calcium free buffer or 3 mM calcium buffer -/+ calpastatin. Calpastatin was incubated with non-active and MKK6EE-activated p38γ prior to incubation in calpain reactions, as described in *Materials and Methods*. Phosphorylated calpastatin is less effective at inhibiting calpain. Data was analysed using one-way ANOVA (non-repeated measures) followed by Tukey post-hoc multiple comparisons test using Graphpad Prism v6.04. * denotes p<00.5. ***B,*** Representative SDS-PAGE/Western blot analysis of calpastatin *in vitro* kinase assays used in A.

6.4 Discussion

6.4.1 Summary

The aim of the experiments described above was to validate zfp260, LDB3 and calpastatin as cardiac substrates of p38γ. Whilst in our hands zfp260 did not undergo phosphorylation by p38γ, LDB3 and calpastatin were determined to be true substrates of p38γ *in vitro*. Additionally, both LDB3 and calpastatin were also found to be *in vitro* substrates of p38α. Independent mass spectrometry analysis of LDB3 and calpastatin phosphorylation sites confirmed the p38γ phosphorylation sites detected by the Shokat screen (LDB3: Ser^{98} and Ser^{240} and calpastatin: Thr^{197}/Ser^{200} and Thr^{448}). Furthermore, phospho-specific antibodies, raised against these sites, detected phosphorylation of WT proteins but not alanine mutant proteins. This confirms that p38γ targets LDB3 sites Ser^{98} and Ser^{240} and calpastatin sites Thr^{197}/Ser^{200} and Thr^{448} for phosphorylation *in vitro*. Further experiments to establish if LDB3 and calpastatin phosphorylation occurs at their respective sites *in vivo* are covered in the next chapter.

So far, *in vitro* calpain assays using a synthetic substrate have been used to assess the effect of calpastatin phosphorylation on its ability to inhibit calpain. Phosphorylation of calpastatin by p38γ reduces its ability to inhibit calpain.

6.4.2 Physiological role of LDB3 phosphorylation

p38γ is unique from its family members as it posses a carboxy-terminal PDZ interacting motif (Hasegawa et al. 1999). Therefore discovery of LDB3 as an interacting partner and substrate of p38γ is intriguing. Whilst the phosphorylation by p38γ *in vitro* does not require the PDZ interaction, physiologically it is likely to be an important characteristic. A co pull-down study using carboxy-terminal truncated p38γ could be used to probe this interaction further. Previous studies have also successfully utilised a cell permeable Tat fusion peptide to disrupt the PDZ interaction to study the interaction of p38γ with other PDZ domain containing substrates and subsequent phosphorylation in cells (Sabio et al. 2004).

Data presented in the following chapter shows that basal p38γ staining of cardiac tissue is cytoplasmic and concentrated at the intercalated disc of cardiomyocytes. LDB3 is localised to both the Z-disc and intercalated disc of cardiomyocytes (Bennett 2012, Zhou et al. 1999). Furthermore, it is also a substrate of PKC (Zhou et al. 1999) and PKA (Lin et al. 2013). Therefore LDB3 is a crucial scaffolding protein that modulates and/or is modulated by several signalling pathways. Given its role as a scaffold, an obvious thought is that phosphorylation regulates binding of LDB3 to other proteins. Assessment of the location of the p38γ phosphorylation sites does not immediately suggest that p38γ phosphorylation may interfere with the interaction of LDB3 with p38γ or any of its known binding partners. The residues do not fall within any of the protein-protein interaction domains. However, it is still a possibility that phosphorylation of LDB3 modulates its interaction with its binding partners. As LDB3 couples to multiple signalling pathways, phosphorylation may be a tool to modulate its coupling to different pathways. In addition to uncoupling/coupling of signalling proteins, LDB3 phosphorylation could effect its subcellular localisation. As it is basally localised to the Z-disc or intercalated disc via its interaction with α-actinin, phosphorylation of LDB3 could trigger dissociation from α-actinin, releasing LDB3 from its basal location. This scenario is observed upon p38γ-mediated phosphorylation of SAP97. Phosphorylated SAP97 no longer interacts with GKAP, causing its release from the cytoskeleton (Sabio et al. 2005). This could occur in isolation, as for SAP97, or with its interacting proteins bound. In this sense phosphorylation could cause shuttling of LDB3 with its associated kinases upon stimulation. Immunocytochemistry and fractionation of cells could be used to assess co-translocation of p38γ and LDB3.

6.4.3 Physiological role of calpastatin phosphorylation

The *in vitro* assessment of calpastatin phosphorylation, by means of a calpain functional assay, showed that phosphorylation of calpastatin by p38γ reduces its ability to inhibit calpain. This is in concert with previously reported findings on the effect of calpastatin phosphorylation. Furthermore this finding is exciting, as it may be a mechanism that explains the reduced hypertrophic response

observed in p38γ KO mice, in comparison to WT mice, in response to pressure overload hypertrophy. Further work is required to establish if this effect is translates *in vivo* and this is attempted in the following chapter. There are also other aspects of calpastatin signalling that phosphorylation could regulate and this is the only aspect assessed so far. Below is a brief discussion of other regulatory aspects that phosphorylation of calpastatin could effect.

As discussed previously, there are already some studies that have examined how phosphorylation of calpastatin affects it function. For example, phosphorylation of rat skeletal muscle calpastatin has been suggested to switch its inhibitory preference towards a particular calpain (Pontremoli et al. 1992, Salamino et al. 1994). The current calpain assay can be modified to assess this. Currently, only inhibition of purified native calpain I from porcine erythrocytes is assessed. The assay could be extended to assess the inhibition of calpain 2 by calpastatin.

It is reported that in its phosphorylated form, a higher concentration of calcium is needed for calpastatin interaction with calpain, in comparison to its non-phosphorylated form (Averna et al. 1999). If this is the case and to assess this, the assay conditions used in this study could be modified to asses this. Currently all assays are performed at a calcium concentration of 3 mM. In future assays, calpain assays with non-phosphorylated and phosphorylated calpastatin would need to be performed in the presence of different concentrations of calcium. This would reveal if the calcium sensitivity of the calpastatin-calpain interaction were altered upon calpastatin phosphorylation.

There is also further scope to investigate calpastatin phosphorylation *in vivo*. For example, some studies report that phosphorylation of calpastatin affects its cellular location. Analysis of calpastatin in human hematopoietic HUT-102 cells found that non-phosphorylated calpastatin was found mainly in the cytosolic fraction whereas 30% of phosphorylated calpastatin was found in the membrane fraction (Adachi et al. 1991). Phosphorylation of calpastatin has also been shown to alter its localisation in human neuroblastoma LAN-5 cells visually. In its phosphorylated form calpastatin is localised in aggregates close to the nucleus and dephosphorylation of calpastatin results in its redistribution

as a soluble inhibitor (Averna et al. 2001). Whilst myocyte calpastatin distribution can be examined without great difficulty, the challenges lie in determining if calpastatin is phosphorylated at the residues detected in this study and if this is mediated by p38γ. A comparison of hearts from WT and p38γ KO mice, by immunohistochemistry and SDS-PAGE/Western blotting using custom phospho-calpastatin antibodies, could be used to probe this. Additionally, the assessment of calpain activity in WT and p38γ KO mice hearts would also assist, albeit indirectly, in elucidating the effect of p38γ phosphorylation on the calpastatin-calpain system *in vivo*.

6.4.4 Isoform substrate selectivity

The results from this study show that the substrate specificity of p38 MAPK isoforms overlaps. For example, both p38α and p38γ isoforms are shown to phosphorylate ATF2, α1-syntrophin, LDB3 and calpastatin. However, whilst p38α could phosphorylate all p38γ substrates, p38γ could not mediate phosphorylation of TAB1. All experiments in this study have observed p38-MAPK substrate phosphorylation *in vitro*. Whilst important for advancing our understanding of signalling events, such experiments are not indicative of the true cellular scenario. It is likely that within the context of a cell, localisation of kinases and their respective substrates plays a crucial role in substrate specificity. Similarly, the PDZ interaction may be necessary within a cell to increase the affinity of p38γ for substrates such as α1-syntrophin or LDB3 as others have described (Sabio et al. 2004).

Kinase assays performed in this study also do not take into account the rate of phosphorylation of the substrates by the two isoforms. A static assessment of substrate phosphorylation was simply carried out after a 30 min kinase assay. Studying the rate of substrate phosphorylation by the two isoforms would provide further information on the selectivity of the isoforms towards different substrates.

Whilst the p38α and p38γ isoforms may share substrates, the data presented here highlights the different extent of phosphorylation by the kinases. For example, Phos-tag^{TM} SDS-PAGE analysis of LDB3 and calpastatin reveals that

the stoichiometry of phosphorylation differs between the isoforms. In addition, mass spectrometry analysis of LDB3 phosphorylation sites reveals that it is phosphorylated at a different subset of residues by each of the two kinases. Physiologically this could be important and suggests that isoforms of a kinase family are not functionally redundant. If a substrate is phosphorylated by both kinases *in vivo,* phosphorylation at different residues may have collaborative or possibly even opposing outcomes. Further work is required to determine if differential phosphorylation by kinase isoforms *in vivo* behaves as a molecular mechanism that fine tunes substrate function.

7 PHYSIOLOGICAL EFFECTS OF p38γ KNOCKOUT

7.1 Introduction

A preliminary study has shown that p38γ/δ$^{-/-}$ (double knock out) mice show markedly reduced cardiac dysfunction and develop less left ventricular hypertrophy, in comparison to congenic WT controls, following suprarenal aortic constriction (Tilgner et al. 2012). Although the mice were double knock out, it was assumed that the phenotype observed is most likely to be as a result of p38γ knock down owing to the relative abundance of each isoform in the heart. To confirm this, the development of hypertrophy following abdominal aortic banding was assessed in p38γ single knock out mice in this study. In addition to the physiological measurements, biochemical assays were carried out using WT and p38γ/δ$^{-/-}$ heart tissue to elucidate the signalling pathway of p38γ in the hypertrophic response. This also included an assessment of LDB3 and calpastatin as physiological substrates of p38γ and their role, if any, in the hypertrophic response.

7.1.1 Suprarenal aortic constriction as an *in vivo* model of pathological cardiac hypertrophy

Pathological cardiac hypertrophy can experimentally be induced in animals via several different experimental methodologies. Commonly used methods include chronic infusion of chemicals such as isoprenaline and angiotensin II or via constriction of the aorta (Berry et al. 2007). Amongst these models, aortic constriction is probably the most widely used strategy to induce left ventricular hypertrophy in mice. First described by Rockman et al. (1991), it causes left ventricular hypertrophy by generating pressure overload. Increase in afterload results in a smaller stroke volume and therefore an increase in end diastolic volume. To offset the increase in pressure, the left ventricular wall of the heart thickens (concentric hypertrophy) to generate a higher systolic blood pressure in order to eject an adequate stroke volume (Berry et al. 2007). However over time, with the continuous stress, the phase of compensation is followed by ventricular insufficiency and cardiac failure (Gomes et al. 2013).

There are a few versions of the technique, which differ in the anatomical location of the constriction. Constrictions can be a) thoracic; in the ascending portion of the aorta or in the aortic arch between the first and second trunks or b) abdominal; below or above the renal arteries (Gomes et al. 2013). The site of constriction affects the timeline of disease progression. Thoracic aortic constrictions result in a rapid and extreme afterload on the left ventricle and as such cardiac changes manifest within a shorter time frame. A 40% increase in left ventricle to body weight ratio is achieved within 7 days of surgery (Rockman et al. 1991). In contrast, abdominal aortic constrictions display a more gradual rise in pressure and hence result in cardiac changes over a longer time frame (deAlmeida et al. 2010, Gomes et al. 2013 and Sankaran et al. 2014). The preferred method in our laboratory is suprarenal aortic constriction, between the coeliac and superior mesenteric arteries. This method is preferred for several reasons. Firstly a slower and prolonged time frame of disease progression enables comprehensive and expansive investigation of biochemical changes associated with the development of hypertrophy. An additional benefit of constricting the aorta at the abdominal level is the reduced complexity of the procedure. Unlike thoracic constrictions, there is no breach of plural space and therefore does not necessitate intubation or ventilation of subjects. Owing to this, the procedure is less traumatic and perioperative mortality of abdominal constrictions is lower in contrast to thoracic constrictions (Grieve et al. 2006 and Sankaran et al. 2014).

7.2 Specific Methods

All animal studies were performed in accordance with regulations outlined in the Home Office Guidance provided on the Operation of the Animals (Scientific Procedures) Act 1986 and amendments in 2012, HMSO (London).

7.2.1 Generation of mice

Mice lacking both p38 γ and δ isoforms (p38γ/δ$^{-/-}$) were generated by, and obtained from, Dr Simon Arthur (University of Dundee, see Sabio et al. 2005). Mice were maintained in the Biological Services Animal Care facility of King's College London.

Homozygous p38γ$^{-/-}$ single KO mice generation was initiated by cross breeding p38γ/δ$^{-/-}$ and WT colonies from the same source. All offspring from mating of these colonies were heterozygous p38γ/δ$^{+/-}$ mice. Heterozygous offspring were mated with WT colonies to give heterozygous p38γ/δ$^{+/-}$, heterozygous p38γ$^{+/-}$, heterozygous p38δ$^{+/-}$ and WT offspring. Mating pairs of heterozygous p38γ$^{+/-}$ littermates were established to produce mixed litters of homozygous p38γ$^{-/-}$ single KO mice, heterozygous p38γ$^{+/-}$ mice and WT mice for experiments (homozygous p38γ$^{-/-}$ single KO and WT mice) and future breeding (heterozygous p38γ$^{+/-}$ mice).

7.2.2 Genotyping

The genomic DNA of the offspring of heterozygous p38γ$^{+/-}$ and heterozygous p38γ$^{+/-}$ mice was analysed by PCR to confirm genotype before any studies were undertaken. 5 mM tail clips or double ear punches were sampled from mice and processed using the REDExtract-N-Amp™ Tissue PCR Kit (Sigma) according to manufacturer's instructions with some modifications. All reagents were provided in the kit. 50 µL of tissue extraction solution and 12.5 µL of tissue preparation solution were added to each tissue sample. Tissue samples were vortexed for 10 s and incubated at 55°C for 10 min. Samples were then incubated at 95°C for 3 min before addition of 50 µL of neutralisation solution. Extracted DNA was then used as template in PCR reactions. Each reaction contained 10 µL of REDExtract-N-Amp PCR Reaction Mix, 4 µL of DNA template, 0.4 µM of each primer and H_20 up to 20 µL. Primers were designed by Sabio et al. 2005. PCR reactions were analysed by agarose gel electrophoresis as described in Section 2.6.

Table 7.1 Primers and PCR conditions used for genotyping mice. Primers were designed by Sabio et al. 2005.

Primer	Primer Sequence (5' to 3')
P1 F (WT)	CCTGAGGTTTAGATAGGCTGTATGTCTCACTCACAC
P2 R (targeted)	CACTTCGCCCAATAGCAGCCAGTCCCTTCC
P3 R (WT)	GAATTCCCAGTAGGTCATTCCTGGGACCATCC

PCR conditions

Step	Temperature	Time	Cycle
Initial Denaturation	94°C	3 min	1
Denaturation	94°C	30 s	30
Annealing	66°C	1 min	
Extension	72°C	1.5 min	
Final Extension	72°C	10 min	1

7.2.3 Transthoracic Echocardiography

Mice were weighed and anaesthetised using 4% isoflurane (100% O_2, 1 mL/min) in an anaesthetic chamber. After anaesthesia was confirmed by lack of pain response, mice were transferred onto a physiological bench in a supine position and anaesthesia maintained via nose cone to snout with 1-2% isoflurane (100% O_2, 0.5 mL/min). Mice paws were coated with conducting gel and secured to copper electrodes to allow respiration and heart rate to be monitored. A rectal thermistor was inserted to allow core body temperature to be monitored. Mice chest area was shaved and fur removed using depilatory cream (Veet™). Pre-warmed (37 ºC) ultrasound gel (Leonhard Lang Medical) was then placed over the chest of the mouse in preparation for ultrasound. The ultrasound probe (RMV 707B 30 MHz, Visual Sonics 770, Toronto) was gently lowered into the gel and ultrasound images of the heart were obtained in parasternal long and short axis views in two-dimensional B-mode. ECG-gated Kilo-Hertz Visualisation (EKV) recordings were taken during B-mode in both axes. Two-dimensionally guided M-mode echocardiograms were taken at the level of the posterior papillary muscle. Once all measurements were taken mice were cleaned of ultrasound gel, paws detached from electrodes and rectal probe removed. Mice were allowed to recover from anaesthesia on physiological bench and returned to stock upon confirmation of recovery.

7.2.4 Suprarenal Aortic Constriction

Mice (approximately 10 weeks old) were weighed and anaesthetised using 4% isoflurane (100% O_2, 1 mL/min) in an anaesthetic chamber. After anaesthesia was confirmed mice were transferred onto a homoeothermic mat on their right flank and anaesthesia maintained via nose cone to snout with 1-2% isoflurane (100% O_2, 0.5 mL/min). A rectal thermistor was inserted to allow core body temperature to be monitored with a custom homeothermic blanket system (Clark/Bell, KCL). Mice were secured into position using dermatological tape and 0.02 g/kg body weight Buprenorphine (Vetgesic™, Ceva Animal Health Ltd) analgesic was administered subcutaneously. The left abdominal area below the ribs was shaved and fur removed using depilatory cream. Skin in the operating area was cleaned using Videne™ antiseptic solution.

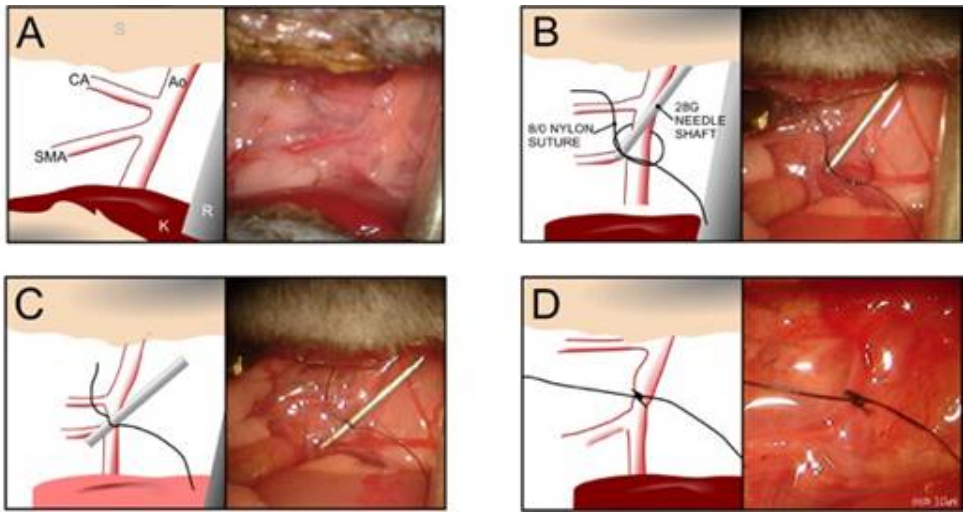

Figure 7.1 Suprarenal Aortic Constriction

Visual representation of suprarenal aortic constriction. ***A,*** Location of aortic constriction is between the coeliac (CA) and superior mesenteric arteries (SMA). ***B – C,*** After cleaning of aorta, a nylon suture is inserted under the aorta. A 28 bluntened gauge needle (≈6mm) is placed parallel to the aorta in the region of the suture and a double throw surgeons knot is made over the aorta and the needle. ***D,*** The constriction is secured by a second single throw knot and the needle is removed. Diagram and images courtesy of Dr James Clark, King's College London.

A laparotomy was performed on the left lateral wall of the abdomen. Retractors were used to expose the descending portion of the aorta between the coeliac and superior mesenteric arteries (Figure 7.1). The aorta in this region was cleaned of fatty and connective tissue by blunt dissection and a 2 cm length of 8-0 monofilament silk suture (Ethilon™, Johnson & Johnson Medical) was inserted under the aorta between the coeliac and superior mesenteric arteries. A short length of 28 gauge blunted needle (≈6 mm long) was placed parallel to the aorta over the suture and a double throw surgeons knot was made over both the aorta and needle. Full occlusion of the aorta was confirmed by observed blanching of the left kidney. The suture was secured with a second single throw knot and the needle was removed leaving a ligature around the aorta and resulting in a reproducible constriction. The site of the operation was cleaned and retractors removed.

Both abdominal muscle and skin layers were sequentially closed with 5-0 silk sutures and a curved cutting needle (Ethicon™, Johnson & Johnson Medical). The skin around the wound was cleaned using Videne™, rectal probe carefully removed and mouse unsecured. The mouse was recovered from anaesthesia

on the operating mat and returned to an isolation cage upon confirmation of recovery. Mice in isolation cages were maintained at 28°C for at least 18 hr following surgery to enable full recovery. Once recovered, mice were returned to stock and monitored daily. Transthoracic echocardiography was performed on a weekly basis to monitor cardiac phenotype throughout the duration of the study.

7.2.5 Heart Excision

Mice were anaesthetised by intraperitoneal injection of sodium pentobarbital (200 mg/kg). Mice were also co-administered 150 I.U. of heparin anti-coagulant to aid flushing of blood from the heart. Upon confirmation of anaesthesia mice were secured in supine position and a mid-line abdominal incision and thoracotomy was performed to access the heart. An incision was made in the right atria using fine scissors and the heart was flushed with approximately 2 mL of cold heparinised (10 IU/mL) saline via injection into the left ventricle at the apex. The heart was then excised, dried on tissue, weighed and snap frozen in liquid nitrogen. Hearts were stored at -80 °C until required.

7.2.6 Cryosectioning

To obtain sections of heart tissue for immunohistochemistry, hearts were removed as described in Section 7.2.5 but following excision a 1.5 inch, 28-gauge needle was inserted into the apex of the heart towards the base and hearts were rolled in Optimal Cutting Temperature (OCT) embedding medium. Once coated, the hearts were attached at the base to a 1.5 cm diameter circular corkboard (Electron Microscopy Sciences) using the tip of the needle. Corkboard attached hearts were immersed into iso-pentane pre-cooled to -160°C over liquid nitrogen. Once frozen, the needle was removed and hearts were stored in foil at -80°C. For cryosectioning, corkboard mounted hearts were cut into 20 µM thick sections using a cryostat (Bright 5030 Microtome Cryostat) at -20°C. Heart slices were placed on polylysine coated microscopy slides (VWR International, Belgium) and stored at -20°C until staining was carried out as detailed below.

7.2.7 Immunohistochemistry

Microscopy slides were removed from -20°C and defrosted briefly at room temperature. Wax circles were drawn around each heart section using a Dako pen (Dako, Agilent Technologies, USA) to aid multiple staining on each slide. Slides were washed in PBS for 5 min at room temperature and then heart sections were permeabilised with PBS with 0.1% (v/v) Triton X for 30 min at room temperature. Following permeabilisation, slides were washed three times with PBS for 5 min and incubated with primary antibodies in PBS with 1% (w/v) BSA overnight at 4°C. The following morning slides were washed three times with PBS for 5 min. Sections were then incubated with the relevant secondary antibodies (1:1000) in PBS with 1% (w/v) BSA for 2 h in the dark at room temperature. At this time, if samples were to be stained with wheat germ agglutinin (WGA, Thermo Scientific), this was added to the secondary antibody solution at a dilution of 1:2000. Three further PBS washes were carried out for 5 min at room temperature after which mounting medium (Vectashield Hard Set mounting medium with DAPI (4', 6-diamidino-2-phenylindole), Vector Laboratories, USA) was dropped onto slides. Heart sections were covered with a cover slip and dried in the dark for 1 h at 4°C before analysis by confocal microscopy (Leica TCS SP5). Antibodies and conditions used to stain heart tissue are given in Table 7.2.

7.2.8 Western Blotting

Excised hearts were prepared for Western blotting analysis as described in Section 2.8 and Western blotting analysis carried out as described in Section 2.13. Antibodies and conditions used to probe heart tissue are given in Table 7.3.

Table 7.2 Antibodies used for immunohistochemistry

Antibody	Primary antibody	Secondary antibody
p38γ	1:200 (R&D Systems)	1:200 anti-rabbit DyLight 652 (Jackson Immunoresearch Labs)
β-MHC	1:200 (Sigma)	1:200 anti-mouse Cy3 (Jackson Immunoresearch Labs)
α-actinin	1:400 (Sigma)	1:200 anti-mouse Cy3 (Jackson Immunoresearch Labs)
α1-syntrophin	1:200 (Abcam)	1:200 anti-rabbit DyLight 652 (Jackson Immunoresearch Labs)
Calpastatin	1:200 (Cell signalling)	1:200 anti-rabbit DyLight 652 (Jackson Immunoresearch Labs)

Table 7.3 Antibodies used for Western Blot analysis

Antibody	Blocking reagent	Primary antibody	Secondary antibody
p38γ (R&D Systems)	0.3% BSA 1.2% milk	1:1000 1% BSA	1:2000 in TBS-0.1% Tween HRP-conjugated rabbit
pp38 (Cell signalling)	0.3% BSA 1.2% milk	1:1000 1% BSA	1:2000 in TBS-0.1% Tween HRP-conjugated rabbit
p38T (Cell signalling)	0.3% BSA 1.2% milk	1:1000 1% BSA	1:2000 in TBS-0.1% Tween HRP-conjugated rabbit
β-MHC (Sigma)	0.3% BSA 1.2% milk	1:1000 5% milk	1:2000 in TBS-0.1% Tween HRP-conjugated mouse
PDLIM5 (Abnova)	0.3% BSA 1.2% milk	1:1000 5% milk	1:2000 in TBS-0.1% Tween HRP-conjugated mouse
Calpastatin (Cell signalling)	0.3% BSA 1.2% milk	1:1000 1% BSA	1:2000 in TBS-0.1% Tween HRP-conjugated rabbit

7.2.9 Statistical Analysis

Physiological data were compared using Two-way repeated measures ANOVA where TIME and GENOTYPE were dependent variables using Graphpad Prism v6.04 (Graphpad, USA). Post-hoc multiple comparisons using Tukey test was carried out for pair-wise analysis of differences between genotypes at each time point and between times within the same genotype. Data are presented as means ± SEM.

7.3 Results

7.3.1 Morphological and functional analysis of pressure overload hypertrophy in WT and p38γ$^{-/-}$ mice

Transthoracic echocardiography was used to assess morphological and functional changes of mice hearts following constriction of the suprarenal aorta. The data consists of 8 WT and 5 p38γ KO mice owing to the time taken to generate the single knock out mouse line. The parameters measured are shown in Figure 7.2.

Five weeks following surgery, cardiac function decreases in WT and KO mice as there is a decrease from baseline in ejection fraction, fractional shortening and fractional area change of the endocardium. However only WT mice display a decline in function that is significantly different from cardiac function prior to surgery. Furthermore, a significant difference was observed in ejection fraction and endocardial fractional area change between WT and KO mice.

Supporting the augmented decline in cardiac function of WT mice in comparison to KO mice, thickness of the left ventricular (LV) posterior wall and LV internal dimensions at systole and diastole were also significantly increased from baseline in WT mice. In contrast whilst KO mice did show thickening of the LV posterior wall and increases in LV internal dimensions, changes were not measured as significantly different to baseline. There was also a significant difference in LV internal dimension during systole between the two cohorts.

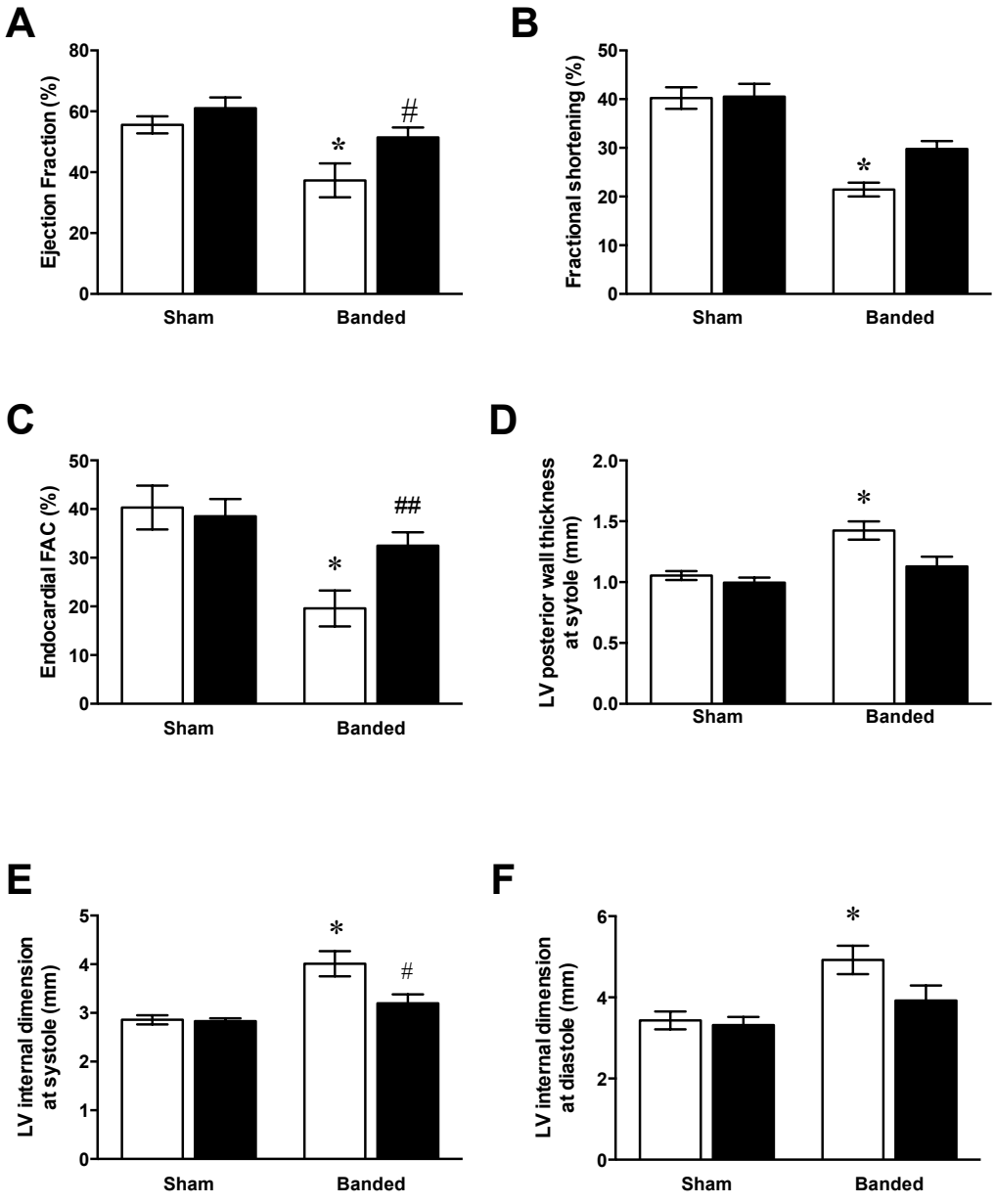

Figure 7.2 Cardiac morphometric and functional analysis of banded WT and p38γ KO mice by transthoracic echocardiography

Parameters assessed by cardiac ultrasound in age and sex-matched WT (open bars) and p38γ KO (black bars) 5 weeks following abdominal aortic banding (banded) or sham surgery. ***A,*** Ejection fraction ***B***, Fractional shortening ***C,*** Endocardial fractional area change (FAC%), ***D,*** Left ventriclular (LV) posterior wall thickness at systole ***E,*** LV internal dimension at systole ***E,*** LV internal dimension at diastole. All parameters measured indicate preserved cardiac function in p38γ KO mice in contrast to WT mice. Data are shown as mean ± SD of n=5-8 per group. *, P<0.05 vs control. #, P<0.05 vs corresponding WT control.

A decline in LV function can cause congestion at the pulmonary level (Lu et al. 2010). Therefore in addition to the cardiac parameters measured above, wet and dry lung weights of WT and p38γ KO mice were taken, to assess the extent of pulmonary oedema. There was no significant difference in the lung wet:dry weight ratio of sham operated WT and p38γ KO mice. Suprarenal aortic constriction resulted in an significant increase in the lung wet:dry weight ratio of the WT mice, but not in the p38γ KO mice. There was also a significant difference in the lung wet:dry weight ratio between the WT and KO cohort, suggesting that the KO mice develop less pulmonary oedema. This finding mirrors the difference in the extent of cardiac dysfunction described above between the two cohorts.

Given the literature concerning the various roles of p38γ in skeletal muscle (described in Chapter 1), it was also investigated if the growth of the p38γ KO mice was affected by p38γ gene knock out. Body mass measurements were taken to assess growth. From Figure 7.4 it can be seen that the mean body mass of p38γ KO mice was generally smaller than WT mice at each of the time points measured. The difference in body mass of the two cohorts is more apparent in juvenile p38γ KO mice (5 to 10 weeks). However, during adulthood (after 10 weeks) there is little difference in the mean body masses of the two cohorts. Hence, at the time of aortic constriction (10 weeks) there was little difference in the body masses of the mice used in the study.

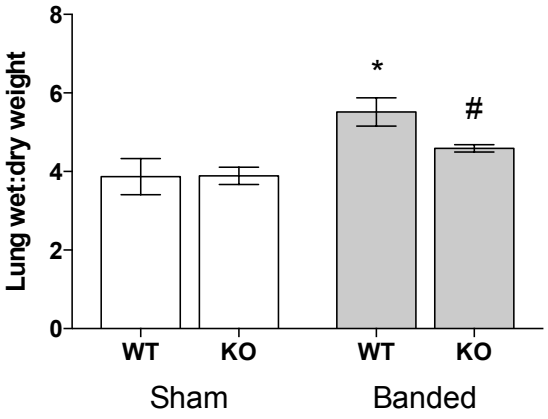

Figure 7.3 Comparison of pulmonary oedema in WT and p38γ KO mice

WT and p38γ KO mice wet and dry lung weights were obtained following mice euthanasia to assess extent of pulmonary oedema. p38γ KO mice develop significantly less pulmonary oedema than WT mice following suprarenal aortic constriction. Data are shown as mean ± SD of n=5-8 per group. *, P<0.05 vs control. #, P<0.05 vs corresponding WT control.

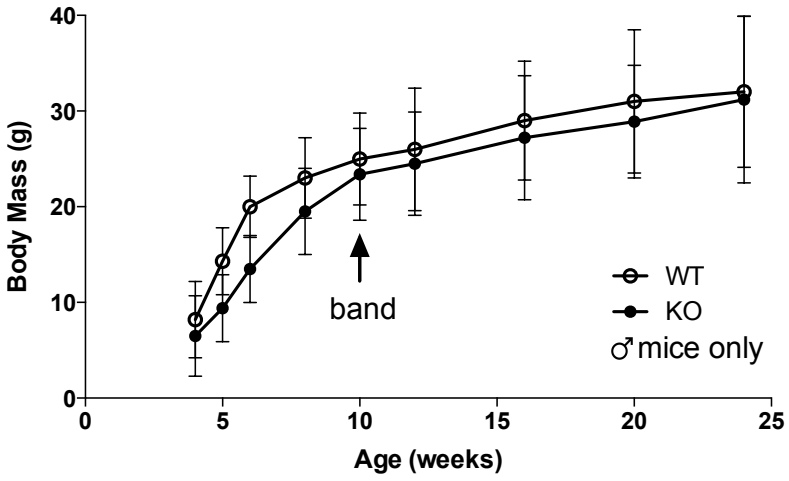

Figure 7.4 Comparison of the body mass of WT and p38γ KO mice

WT and p38γ KO mice were weighed for a period of 6 months to monitor differences in growth in the two cohorts. Mean body mass of p38γ KO mice was generally smaller than WT mice at each of the time points measured, but at week 10 this difference is minimal. Mice were weaned at 4 weeks. n=8 for each group.

7.3.2 Biochemical analysis of pressure overload hypertrophy in WT and p38γ$^{-/-}$ mice

7.3.2.1 Immunohistochemistry

The expression and localisation of several cardiac proteins was assessed by immunohistochemistry in WT sham and pressure overload hypertrophy induced hearts. Firstly expression for β-MHC was tested, as shown in Figure 7.5. Sham surgery of mice does not cause an increase in expression of β-MHC, as there is a similar level of staining in the control samples. There is however increased expression of β-MHC in banded samples in comparison to hearts of time-matched sham operated mice or control mice, which is expected in murine cardiac failure (Krenz and Robbins, 2004). Another observation is that there are fewer cells in the field of view of banded heart samples compared to sham or control hearts. Cells of banded hearts are visually larger, indicative of cardiomyocyte hypertrophy.

Next, the localisation of p38γ was examined. In sham-operated hearts, p38γ staining is localised to the cytoplasm and intercalated discs of cardiomyocytes (Figure 7.6). However, during the development of pressure overload hypertrophy (banded hearts; weeks 2 and 4), there is translocation of p38γ to the nucleus. This can be seen as an increase in the co-localisation of p38γ (green) with DAPI (blue) in banded mice hearts. Quantification of the percentage p38γ positive nuclei in heart sections, revealed that there was a significant increase in nuclear co-localisation of p38γ in 2 week (13.6 ± 1.7, $p<0.01$) and 4 week (15.75± 6.9, $p<0.05$) banded hearts, compared to sham operated controls (5.9± 2.2).

Localisation of p38γ substrates, examined previously in this study, was also studied. As expected, α1-syntrophin was found localised at the cell membrane of cardiomyocytes (Figure 7.7). Closer inspection also reveals α1-syntrophin striated staining within the cell. However, a comparison of α1-syntrophin localisation in the control and banded hearts does not reveal any differences in localisation. Lastly an attempt was made to examine calpastatin localisation (Figure 7.8). Unfortunately this experiment was largely unsuccessful as staining

of calpastatin was poor and undefined. Therefore changes in calpastatin localisation during cardiac hypertrophy could not be examined. LDB3 localisation could also not be investigated, due to the lack of suitable specific antibodies for immunohistochemistry.

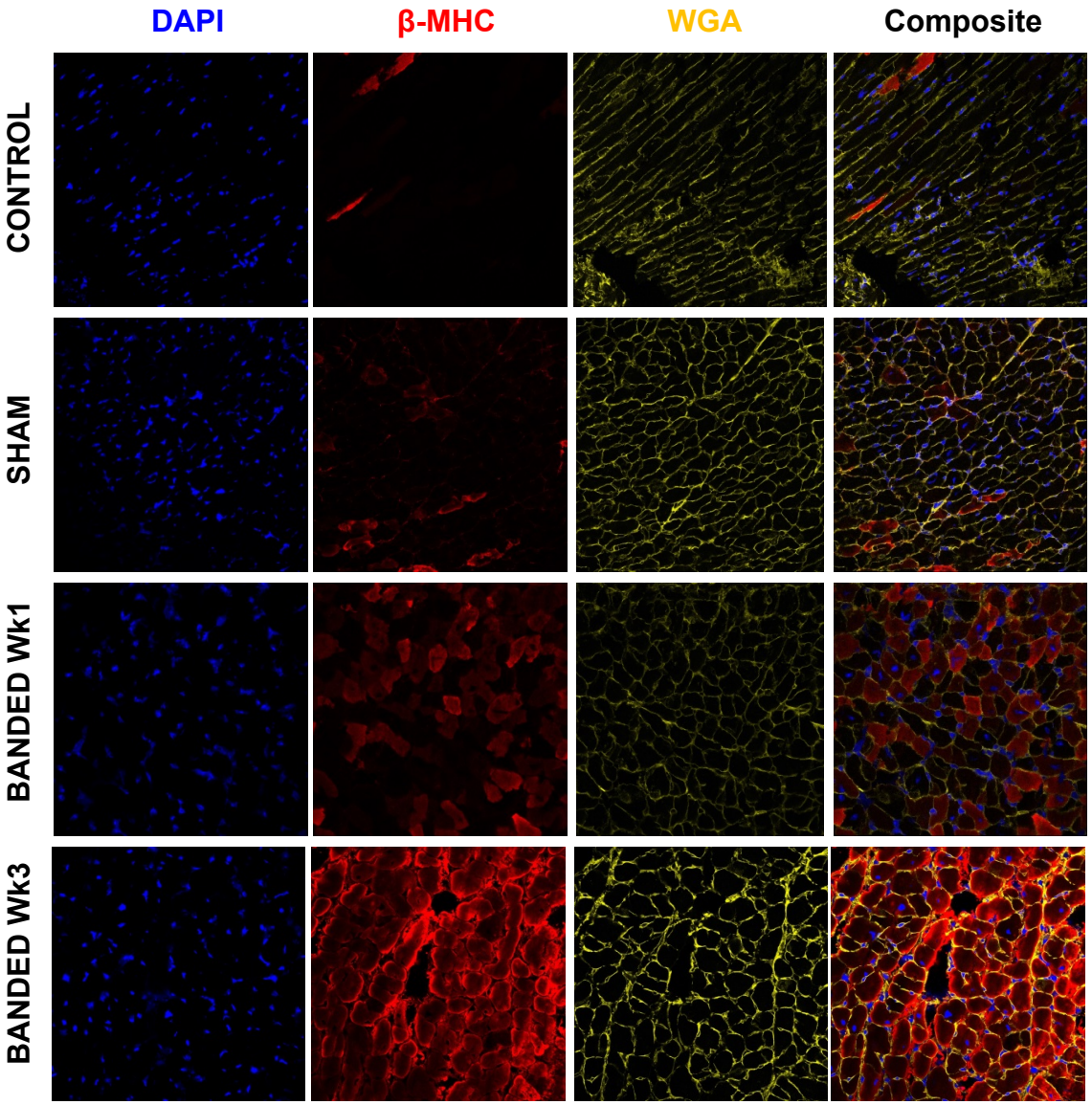

Figure 7.5 Expression of β-MHC in WT sham and pressure overload hypertrophy induced heart sections

Sections of cardiac tissue (20 μM) from WT sham and suprarenal aortic constricted WT mice were immunostained for DAPI (nuclei), β-MHC and wheat germ agglutinin (WGA, cell membrane). There is increased expression of β-MHC in banded samples in comparison to hearts of time-matched sham operated mice or control mice. Cells from banded hearts are visibly larger and there are fewer cells in the field of view in contrast to sham or control hearts.

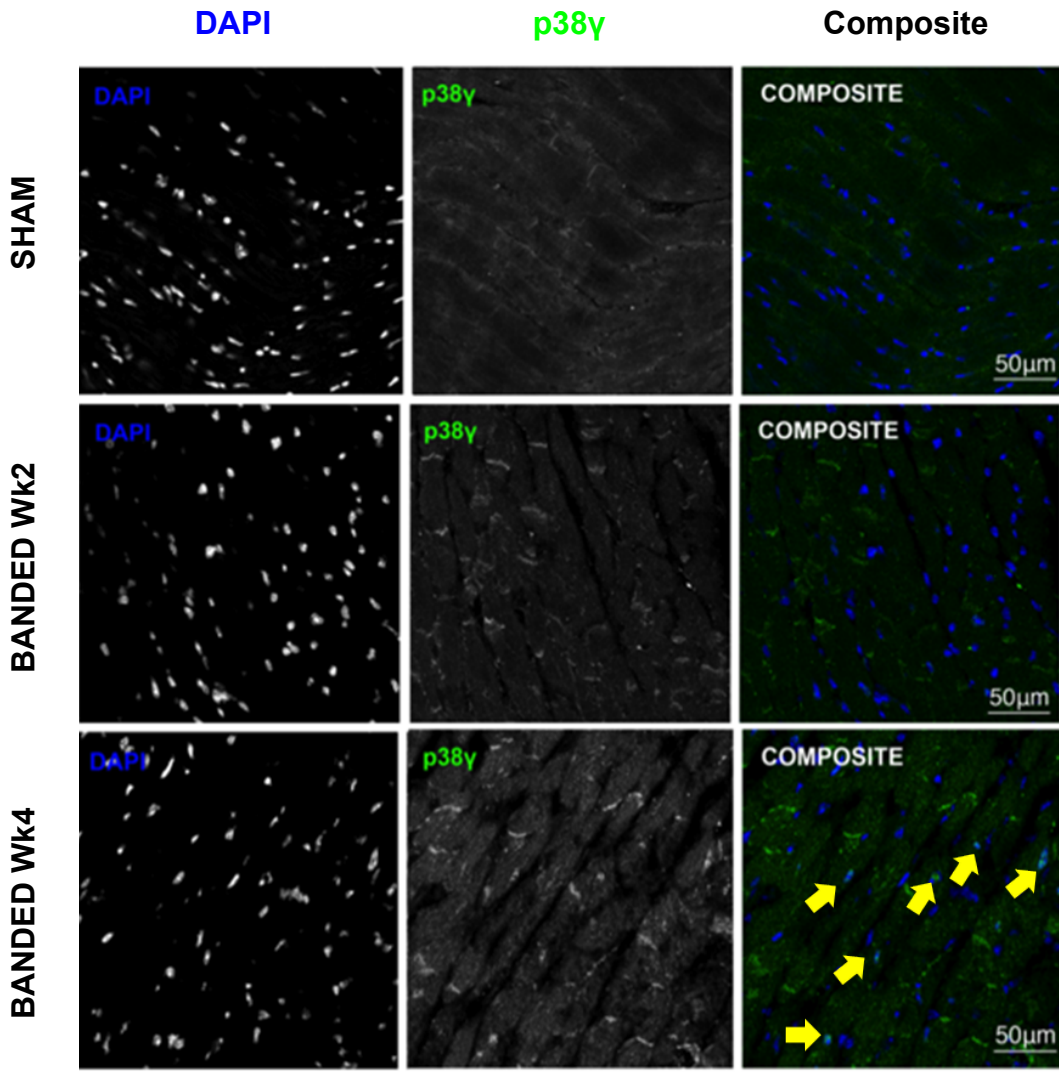

Figure 7.6 Localisation of p38γ in WT sham and pressure overload hypertrophy induced heart sections

Sections of cardiac tissue (20 μM) from WT sham and suprarenal aortic constricted WT mice were immunostained for DAPI (nuclei) and p38γ. In sham hearts p38γ staining is mainly cytosolic and at the intercalated discs of myocytes. Following banding, there is increased co-localisation of p38γ with DAPI (indicated by the yellow arrows).

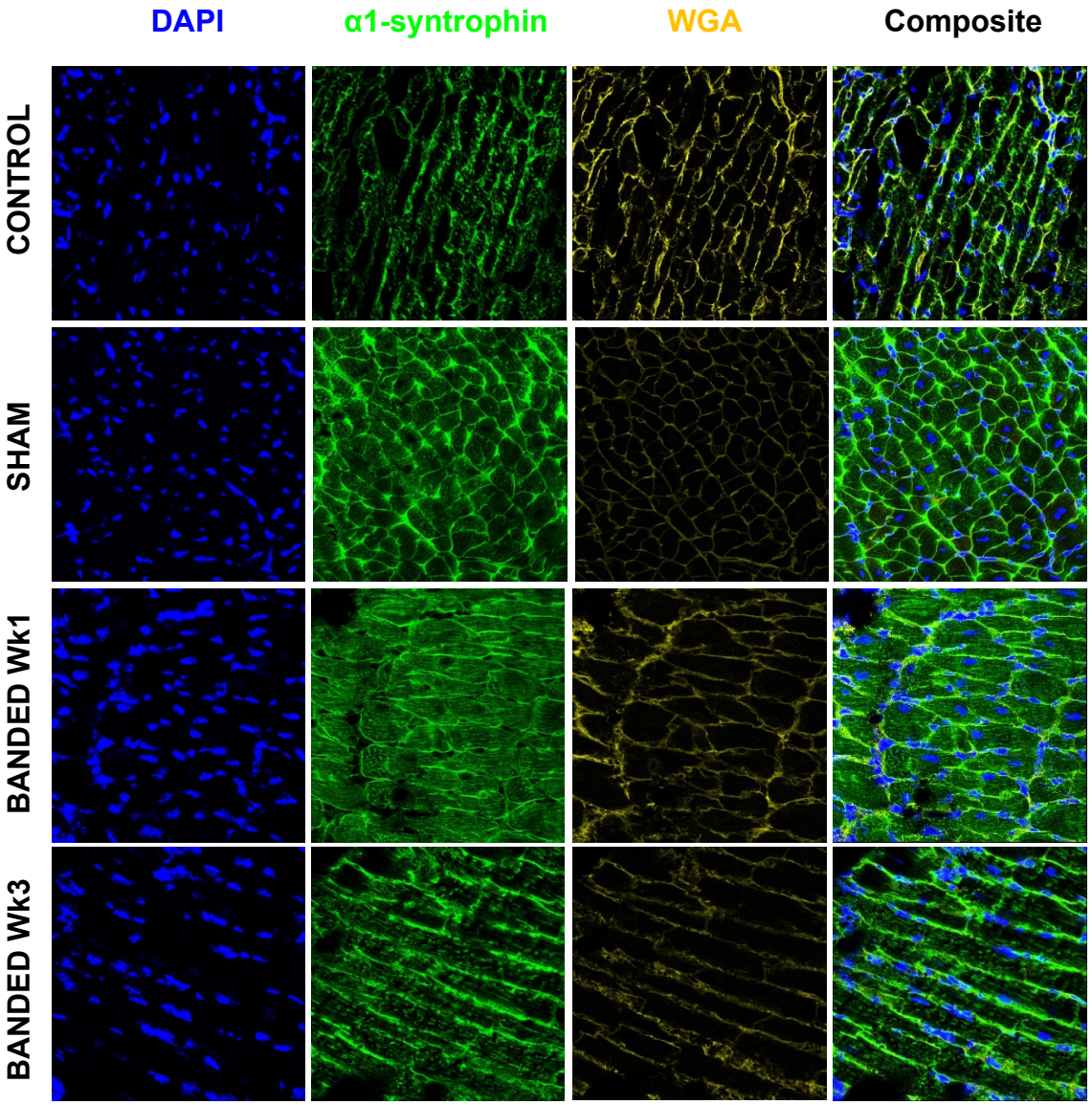

Figure 7.7 Localisation of α1-syntrophin in WT sham and pressure overload hypertrophy induced heart sections

Sections of cardiac tissue (20 μM) from WT sham and suprarenal aortic constricted WT mice were immunostained for DAPI (nuclei) and α1-syntrophin. α1-syntrophin staining is found at the cell membrane. There are no differences in α1-syntrophin staining of banded hearts in comparison to sham or control hearts.

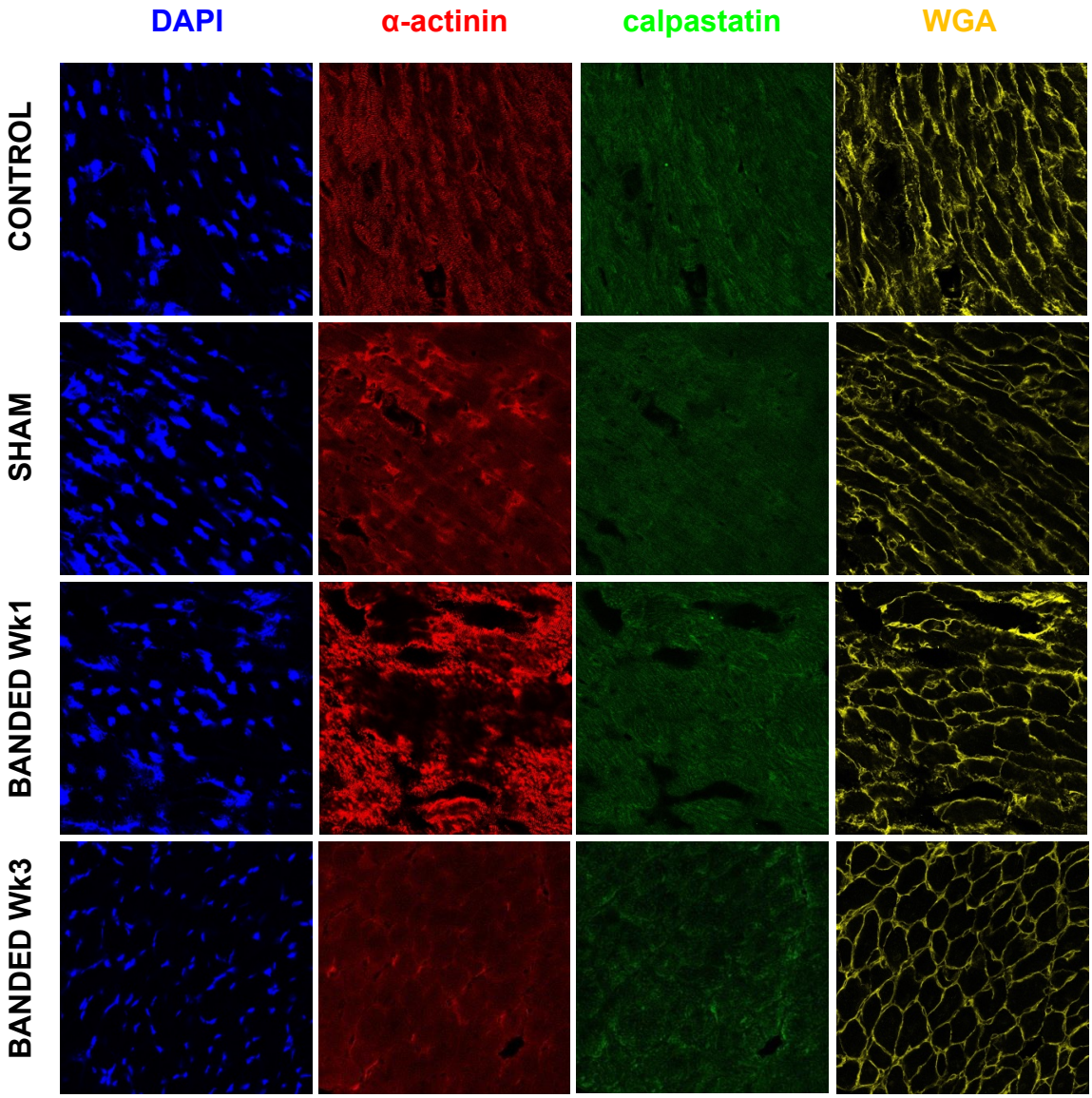

Figure 7.8 Localisation of calpastatin in WT sham and pressure overload hypertrophy induced heart sections

Sections of cardiac tissue (20 μM) from WT sham and suprarenal aortic constricted WT mice were immunostained for DAPI (nuclei), α-actinin, calpastatin and WGA. Calpastatin staining is poor and undefined.

7.3.2.2 Phosphorylation of LDB3 and calpastatin in vivo

From the *in vitro* characterisations of substrates in Chapter 6, it was found that p38γ targets LDB3 sites Ser^{98} and Ser^{240} and calpastatin sites Thr^{197}/Ser^{200} and Thr^{448} for phosphorylation. Therefore, the next question was to address if these sites are phosphorylated *in vivo*, in the context of pathological cardiac hypertrophy. In order to examine this, firstly it was established if both substrates could be detected in heart samples using their respective total antibodies. To avoid loss of limited heart sample from the physiological study of WT and p38γ$^{-/-}$ mice (described here), optimisations of substrate antibodies was carried out on heart samples from the previous p38γ/δ$^{-/-}$ (double knock out) study.

Western blotting analysis of WT and p38γ/δ$^{-/-}$ sham and 4 week banded heart samples for LDB3 are shown in Figure 7.9. The LDB3 antibody detects endogenous cardiac LDB3 at ~100 kDa. As expected, the migration of the recombinant LDB3 control is slightly retarded in comparison due to the presence of the His and V5 tags. A longer exposure of the membrane to film reveals several other bands detected by the LDB3 antibody. These likely correspond to splice variants and other members of the Enigma family (enigma, enigma homolog and LDB3) of proteins, which the antibody has been previously shown to detect (Cheng et al. 2010). The total calpastatin probe of heart samples is shown in Figure 7.10. The calpastatin antibody is highly specific and detects a doublet at ~130 kDa corresponding to the endogenous protein. The appearance of a doublet is attributable to different calpastatin isoforms (Goll et al. 2003). Again as expected the recombinant calpastatin sample is at a higher molecular weight compared to the endogenous protein due to the presence of the GST tag. Both LDB3 and calpastatin are expressed basally and during hypertrophy, at least at the 4-week time point. At this point, no interpretation can be made regarding change in expression of proteins following suprarenal aortic constriction, as samples were not equalised for protein concentration. Samples from this study were chosen for this analysis in the event that proteins were not basally expressed.

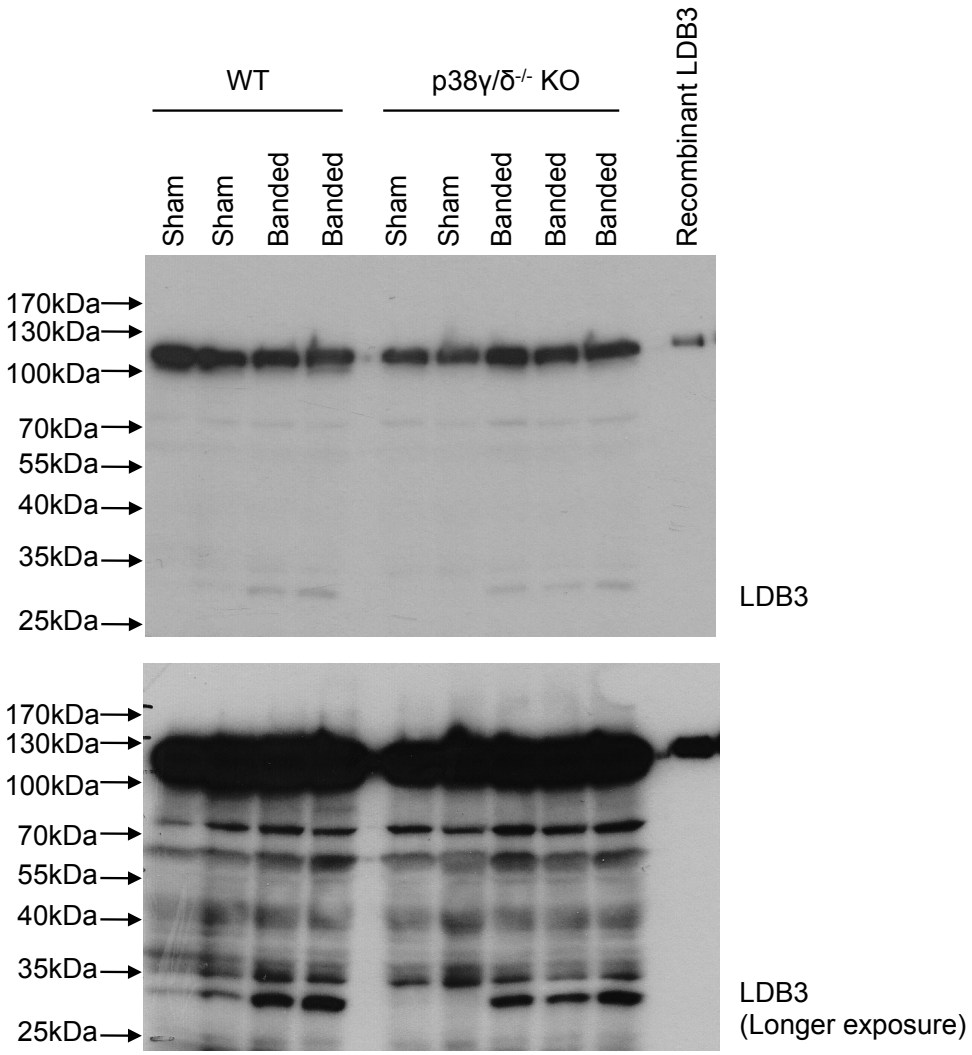

Figure 7.9 Detection of LDB3 in heart samples

Immunoblot analysis of total LDB3 in sham and 4-week banded WT and p38γ/δ$^{-/-}$ hearts. Endogenous LDB3 is expressed basally and during hypertrophy. A longer exposure of film to membrane reveals several other bands detected by the LDB3 antibody (splice variants or Enigma family proteins). Samples were resolved by 10% SDS-PAGE, as described in *Materials and Methods*.

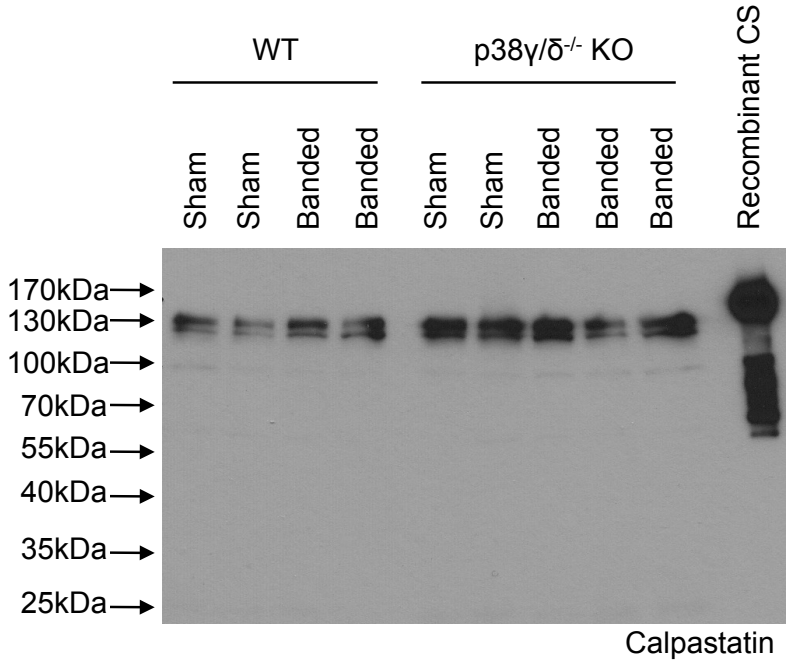

Figure 7.10 Detection of calpastatin in heart samples

Immunoblot analysis of total calpastatin in sham and 4-week banded WT and p38γ/δ$^{-/-}$ hearts. Endogenous calpastatin is expressed basally and during hypertrophy. A doublet is detected corresponding to the two isoforms of calpastatin. Samples were resolved by 10% SDS-PAGE, as described in *Materials and Methods*.

As the molecular weight of the endogenous substrates was now established, the subsequent experiment was to probe samples using the phospho-specific LDB3 and calpastatin antibodies. In chapter 6 the same phospho-specific antibodies were successfully used to validate p38γ phosphorylation sites of substrates *in vitro*. The results of the phospho-LDB3 probes are shown in Figure 7.11. Unfortunately, under the current conditions no clear bands are detected at the molecular weight of LDB3 using the phospho-Ser^{98} or phospho-Ser^{240} antibodies. An unsuccessful result is also encountered with the probe of heart samples with the phospho-calpastatin antibodies (Figure 7.12). There is no detection of bands at ~130 kDa with the phospho-Thr^{197}/Ser^{200} or phospho-Thr^{448} antibodies. The phospho-Thr^{197}/Ser^{200} detects a higher molecular weight dominant band (>170kDa) and the phospho-Thr^{448} antibody detects a dominant band at 70 kDa. Currently it cannot be said that these sites are not phosphorylated *in vivo,* as the antibodies may not be suitable for detection of phospho-sites in complex tissue samples.

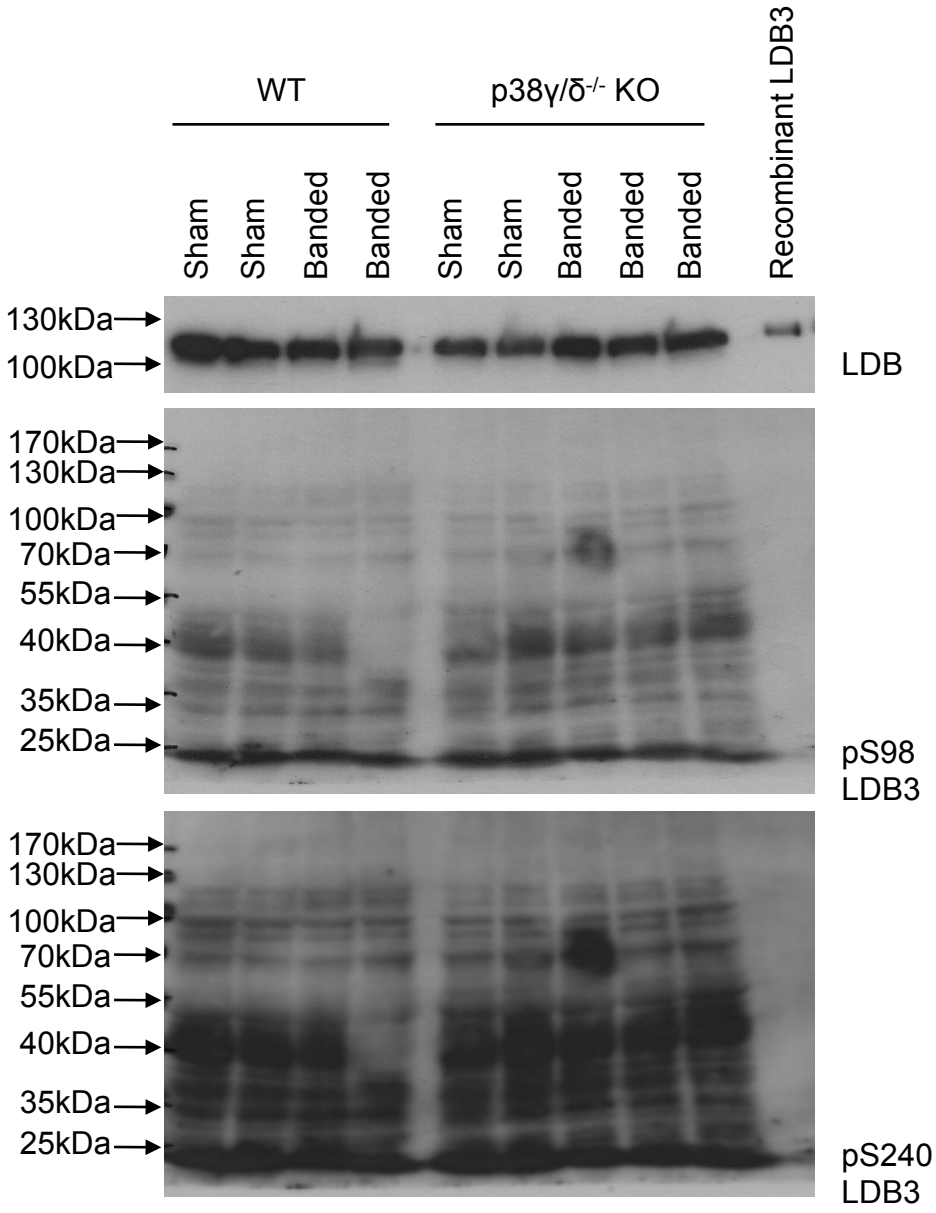

Figure 7.11 Probe of cardiac samples for phospho-LDB3

Immunoblot analysis of phosphorylated LDB3 in sham and 4-week banded WT and p38γ/δ$^{-/-}$ hearts using custom phospho-specific antibodies towards Ser^{98} and Ser^{240}. No bands at the correct molecular weight are detected with the phospho-LDB3 antibodies. Samples were resolved by 10% SDS-PAGE, as described in *Materials and Methods*.

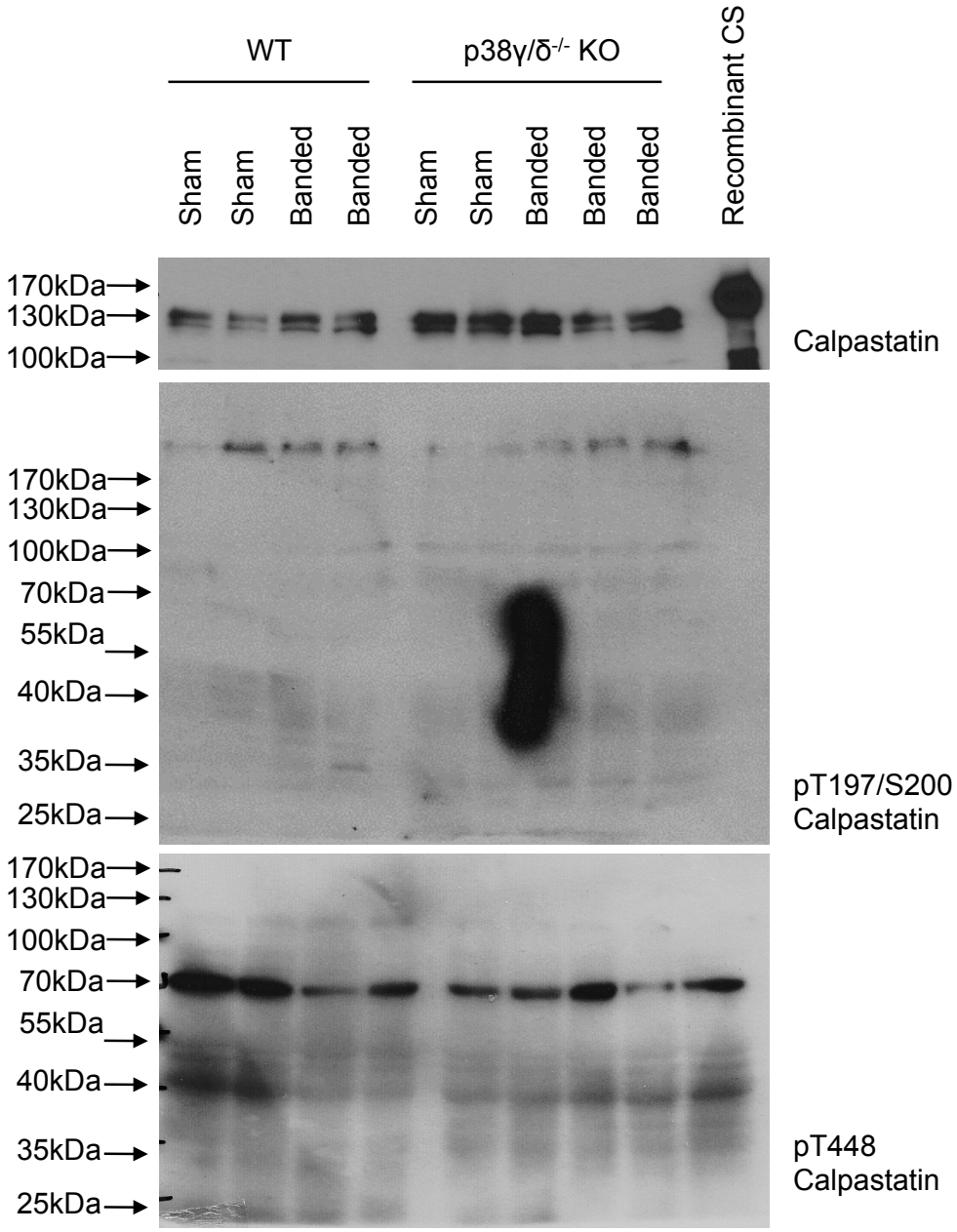

Figure 7.12 Probe of cardiac samples for phospho-calpastatin

Immunoblot analysis of phosphorylated calpastatin in sham and 4-week banded WT and p38γ/δ$^{-/-}$ hearts using custom phospho-specific antibodies towards Thr^{197}/Ser^{200} and Thr^{448}. No bands at the correct molecular weight are detected with the phospho-calpastatin antibodies. Samples were resolved by 10% SDS-PAGE, as described in *Materials and Methods*.

7.4 Discussion

7.4.1 Summary

Data presented in this chapter confirms the pro-hypertrophic role of p38γ in the myocardium. Global p38γ KO mice are less susceptible to the effects of pressure overload hypertrophy in comparison to their WT controls. Despite the roles of this isoform described in skeletal muscle development and maintenance, blunted growth of p38γ KO mice was not a confounding factor in this study. Although there was a slight difference in the body mass of juvenile WT and p38γ KO mice, overall the body mass of p38γ KO mice increased with age similar to that of WT mice.

Immunohistochemistry of WT control, sham and banded mice hearts revealed an increase in the expression of β-MHC and translocation of p38γ to the nucleus in banded hearts. Both of these observations have previously been reported in published studies of pressure overload hypertrophy (Kehat, Molkentin 2010, Barry, Davidson & Townsend 2008, Court et al. 2002). α1-syntrophin staining is observed predominantly at the cell membrane with some cytoplasmic staining and remains unchanged after banding. In WT hearts staining for calpastatin was unsuccesful and could not be used to define its localisation basally or after banding. LDB3 staining of cardiac tissue could not be attempted due to the lack of a specific LDB3 antibody for immunohistochemistry.

LDB3 and calpastatin were successfully detected in heart tissue of control and banded WT and p38γ/$\delta^{-/-}$ mice. Detecting phosphorylation of LDB3 and calpastatin *in vivo,* at the sites characterised from previous experiments, presented a major challenge. The custom phospho-antibodies, generated against Ser^{98} and Ser^{240} of LDB3 and Thr^{197}/Ser^{200} and Thr^{448} of calpastatin, did not detect bands at the expected molecular weight in control or banded WT and p38γ/$\delta^{-/-}$ mice heart samples.

7.4.2 The pro-hypertrophic role of p38γ

The effects of pressure overload hypertrophy, caused by suprarenal aortic constriction, manifested within a few weeks of surgery. The LV of WT mice gradually increased in mass and contraction of the LV was impaired, as indicated by an increase in the internal diameter of the LV during contraction. The change in endocardial area between diastole and systole (% FAC) also reduced over time. This also suggests impairment of LV contraction and function. Impaired function of the LV adversely affects the pulmonary circuit, leading to accumulation of fluid within the lungs. Whilst this is an incomplete study, the data so far shows that all of these changes are blunted in mice that lack the p38γ isoform. So how does p38γ mediate its pro-hypertrophic role?

7.4.2.1 Nuclear translocation of p38γ

Studies on cardiac function of p38γ are scarce. It has previously been shown that, in the established phase of pressure overload hypertrophy (7-28 days after surgery), p38γ immunoreactivity accumulates in the nucleus (Dingar et al. 2010). Results from this study corroborate this finding. Mechanistically it is not known what effect this translocation has on p38γ signalling. Given that many of the known substrates of MAPKs are located in the nucleus (Turjanski, Vaque & Gutkind 2007), an obvious notion is that p38γ mediates its hypertrophic actions via phosphorylation of a transcription factor. MEF2 transcription factors are pro-hypertrophic and phosphorylated by p38γ *in vitro* (Akazawa, Komuro 2003). However, it has also been shown that p38α and p38β isoforms more potently phosphorylate MEF2 transcription factors than p38γ (Han, Molkentin 2000). Examining the MEF2 phosphorylation profile during hypertrophy in the WT and p38γ KO would help establish if p38γ is mediating its hypertrophic effects via MEF2 transcription factors *in vivo*. With regards to this study, few transcription factors were identified in the Shokat approach. A pro-hypertrophic cardiac transcription factor identified was zfp260 (Debrus et al. 2005, Komati et al. 2011). Unfortunately, as shown in chapter 6, subsequent experiments to verify its phosphorylation by p38γ revealed that it is not a true substrate.

As a kinase, it is likely that p38γ is mediating its pro-hypertrophic effects via phosphorylation of a substrate. However, as it contains a carboxy-terminal PDZ interacting motif (Hasegawa et al. 1999), it is also a possibility that p38γ could mediate the effects of hypertrophy in a kinase independent manner. An example of regulation by p38γ in this manner has previously been described for SAP97 and PSF (Sabio et al. 2010). Translocation of p38γ to the nucleus under osmotic stress conditions causes displacement of SAP97 from PSF and an increase in p38γ- SAP97 association (Sabio et al. 2010). Similarly, during the development of pathological hypertrophy, translocation of p38γ to the nucleus could cause a rearrangement of protein interactions that lead to changes in gene transcription.

7.4.2.2 Cytoplasmic targets of p38γ

In addition to any nuclear targets, p38γ may also mediate its hypertrophic actions via proteins in the cytoplasm or at the intercalated disc. α1-syntrophin is a known substrate of p38γ. Additionally, data obtained in this study shows that endogenous cardiac α1-syntrophin interacts specifically with p38γ. α1-syntrophin is a molecular scaffold that contains many protein interaction motifs. In the heart it has been shown to scaffold nitric oxide synthase-1 (NOS-1) and plasma membrane calcium ATPase isoform 4b (PMCA) (Williams et al. 2006). Although the dominant role of the PMCA is to extrude calcium from the cell cytosol, it is also a modulator of signal transduction pathways. In this instance, it acts synergistically with α1-syntrophin to negatively regulate NOS-1 activity, resulting in a decrease of NO production and cGMP (Williams et al. 2006). α1-syntrophin also links the cardiac sodium channel SCN5A to the aforementioned complex (Ueda et al. 2008). Furthermore a missense mutation of α1-syntrophin, found in patients with long QT syndrome, disrupts the complex and releases inhibition of NOS-1. This is proposed to cause S-nitrosylation of SCN5A, which results in increased late sodium current (Ueda et al. 2008).

Given its importance in cardiac physiology, it is worthwhile exploring the functional significance of p38γ interaction and phosphorylation of α1-syntrophin. Immunohistochemistry of α1-syntrophin in WT hearts showed that it is localised

at the plasma membrane, as expected, and banding does not alter its location within the cell. It would be also worthwile examining α1-syntrophin localisation in the hearts of sham and banded p38γ/δ$^{-/-}$ mice. This study also did not characterise the α1-syntrophin sites targeted for phosphorylation by p38γ or assess α1-syntrophin phoshorylation in hearts from the physiological study. This would provide further insight into p38γ and α1-syntrophin signalling during cardiac hypertrophy.

Two novel substrates of p38γ identified in this study are LDB3 and calpastatin. A review of the literature (see chapter 6 for summary) reveals the involvement of both substrates in cardiac hypertrophy. Unfortunately successful staining for the two substrates in cardiac sections could not be obtained due to the lack of appropriate antibodies. And whilst extensive characterisation of the proteins and their p38γ phosphorylation sites has been carried out *in vitro*, it could not be determined if these sites are (patho)physiological targets *in vivo*. Again this is due to the problems associated with the lack of suitable antibodies for use with whole heart homogenates or histological sections. The custom phospho-antibodies generated against the novel phosphorylation sites identified in this study were shown to be somewhat effective *in vitro* with recombinant proteins. However a probe of complex samples, such as heart homogenate, does not identify phospho-bands at the correct molecular weight. Both LDB3 and calpastatin are expressed well in the heart as determined by the respective total antibody probes.

At this juncture, the following scenarios are possible; it may be the case that the sites could potentially be phosphorylated, but the antibodies are ineffective or antibody conditions need optimisation. It could also be the case that sites are not detected as the wrong timeframe of hypertrophy is being examined. Alternatively, it may be the case that the sites are not phosphorylated *in vivo*. If further analysis of different time points of hypertrophy or optimisation of conditions does not yield any progress, alternative antibodies with high affinity for the phospho-proteins need to be sourced. However, the generation of new custom antibodies is costly and there is no certainty that an alternative antibody will have the specificity or affinity required.

An alternative method is to analyse heart tissue samples by LC-MS/MS. However, as discussed previously in chapter 4, LC-MS/MS detection of phospho-proteins also has limitations. Detection of phospho-peptides is difficult; therefore to increase the chances of site detection, the endogenous protein will probably need to be enriched by immunoprecipitation prior to LC-MS/MS. This approach is comparable to the Shokat approach taken in this study. With the Shokat approach, detection of phospho-peptides by LC-MS/MS, was dependent on successful enrichment of phospho-peptides by a covalent capture protocol.

7.4.2.3 Activation profile of p38γ during pathological cardiac hypertrophy

An assumption made in this study is that p38γ is active during the development of pathological hypertrophy. To date, the activation profile of p38γ during the development of hypertrophy has not been characterised and attempts to do so have not been successful. Again this is due to the limitation associated with the specificity of phospho-antibodies. An alternative method to assess activation is the use of Phos-tag™ SDS-PAGE technology. This would enable the use of the total p38γ antibody, which is specific to this isoform. Phos-tag™ SDS-PAGE of complex tissue samples is also difficult. It is both time consuming and has been shown to be unreliable in our laboratory. Nonetheless establishing the activaiton profile of p38γ following banding is key to elucidating its signalling pathway. For example, it would inform of the right timeframe for assessing downstream substrate phosphorylation. The time points currently used in this study may not be appropriate to probe for phospho-sites and could also explain why phosphorylation sites of LDB3 and calpastatin are not detected *in vivo*.

8 FINAL SUMMARY AND DISCUSSION

The aims of the study were to:

- Identify the endogenous substrates of the p38γ isoform in the myocardium.
- Identify any interacting proteins of p38γ via its carboxy-terminal PDZ interacting domain in the heart.
- Elucidate the signalling pathway in which p38γ is integrated in the heart.
- Determine the involvement of p38γ in the development of pathological cardiac hypertrophy.

The physiological data presented in this Thesis confirms our hypothesis that p38γ plays a pro-hypertrophic role in the myocardium following pressure overload. Mice that globally lack the p38γ isoform were less susceptible to the effects of pressure overload hypertrophy induced by suprarenal aortic banding (Figure 7.2, page 222). Immunohistochemistry of p38γ showed that it is basally localised in the cytoplasm and intercalated discs of cardiomyocytes and, that during cardiac hypertrophy, there was nuclear translocation of p38γ. This is likely to underlie the pro-hypertrophic role of p38γ in the myocardium (Dingar et al. 2010).

To elucidate its signalling pathway, a Shokat *in vitro* chemical genetic approach was utilised to identify putative substrates of cardiac p38γ, through which it may mediate its pro-hypertrophic effect. This involved the generation of a mutant 'analogue sensitive' p38γ kinase. The mutant AS kinase was able to accommodate unorthogonal expanded ATP analogues, which WT kinases were unable to utilise. The ATP analogues also contained a tag on the γ-phosphate that was transferred to the substrate, allowing subsequent purification and identification by LC-MS/MS. This overcomes the problems usually associated with identifying specific substrates of a kinase, particularly when no specific inhibitors are available (Bain et al. 2007). This has lead to the identification of 86 proteins, which could potentially be substrates of p38γ (Table 4.1, page 105).

Unique from its family members, p38γ also possess a carboxy-terminal PDZ domain consensus motif (Hasegawa et al. 1999). Therefore a co pull-down experiment was carried out to identify interacting partners of p38γ. In the first instance this led to the co-capture of endogenous cardiac α1-syntrophin with p38γ (Figure 5.7, page 134), which is a known substrate of this kinase (Hasegawa et al. 1999). Further analysis also identified 20 proteins that were specifically pulled down with p38γ, presumably through their interaction with the PDZ binding domain (Table 5.1, page 139 and Table 5.2, page 140). Following analysis of the proteins identified by the two approaches and a supporting literature review, zfp260, LDB3 and calpastatin were chosen for validation as potential p38γ substrates in the heart.

Subsequently, it was found that zfp260 did not undergo phosphorylation by p38γ *in vitro* (Figure 6.10, page 183), whereas LDB3 and calpastatin both successfully underwent phosphorylation *in vitro* and were determined to be true kinase substrates of p38γ. The sites targeted for phosphorylation were also determined by LC-MS/MS analysis and validated through the generation of phospho-mutants with phospho-specific antibodies (Figure 6.17, page 193 and Figure 6.23, page 202).

LDB3 was phosphorylated by p38γ at Ser^{98} and Ser^{240} *in vitro*. Calpastatin was phosphorylated by p38γ at Thr^{197}/Ser^{200} and Thr^{448} *in vitro*. Whilst the functional effect of LDB3 phosphorylation has not yet been examined, an attempt was made to assess the effect of calpastatin phosphorylation. As the endogenous inhibitor of calpain proteases, it was hypothesised that calpastatin phosphorylation may affect its inhibitory function (Salamino et al. 1997, Averna et al. 1999). As anticipated, p38γ mediated phosphorylation of calpastatin by p38γ reduced the efficiency of calpastatin at inhibiting calpain *in vitro* (Figure 6.25, page 205).

The association of LDB3 and calpastatin with p38γ in hypertrophy was next assessed *in vivo*. Both proteins were detected in WT and p38γ/$\delta^{-/-}$ mice heart tissue, basally and at the 4-week hypertrophy time point. But detection of the specific phospho-sites of LDB3 and calpastatin, using custom generated phospho-protein targeted antibodies, proved to be more challenging. Further

characterisation work is required to determine if these sites are phosphorylated *in vivo*. This is likely to require the optimisation of the custom phospho-antibodies and/or assessment of cardiac tissue from different time points of the hypertrophy study.

8.1 Implications of current findings

Cardiac hypertrophy and remodelling is an independent risk factor for poor outcome in cardiac disease (Levy et al. 1990). It is an adverse event that is common to several cardiac disease triggers such as arterial hypertension, myocardial infarction, chronic ischaemia and valvular disease (Bisping et al. 2014). Therefore, preventing or reducing the extent of left ventricular hypertrophy is a key goal to improve patient outcome. Much research is focused on elucidating the signalling mechanisms that underlie the development of pathological hypertrophy in order to identify new targets for its prevention/reduction.

Physiological data attained in this study provides clear evidence of a role of p38γ in the development of pathological cardiac hypertrophy, following pressure overload. This suggests that inhibition of p38γ activity could prevent the extent of hypertrophic development and the transition to heart failure. However, there are no specific inhibitors available for p38γ. The high homology of the active sites of protein kinases prevents specific inhibitor design. Consequently, few selective inhibitors are available for a given kinase, that do not have off target effects on other kinase signalling pathways (Bain et al. 2007). Whilst structural features common to all four p38-MAPK isoforms, such as the DFG motif, have enabled the design of potent and more specific inhibitors for p38-MAPKs, there are few regions of low homology that could be targeted for specific inhibition of p38γ (Marber, Rose & Wang 2011). Disappointingly, pirfenidone, a reported p38γ inhibitor (Blatt, Ozes 5005) tested in this study, did not result in inhibition of p38γ under the *in vitro* conditions tested. Moreover, due to the multiple functions of kinases in other tissues, targeting a kinase directly is not a feasible goal for therapy. Instead, the elucidation of the downstream signalling pathway of p38γ in the myocardium could provide alternative targets for treatment.

As such, a key aim of this study was to elucidate the signalling of p38γ in the myocardium. The Shokat approach enabled identification of novel substrates of p38γ and a parallel co pull-down study identified specific cardiac interacting proteins of p38γ. This led to the validation of LDB3 and calpastatin as novel substrates of p38γ, at least *in vitro*. However, further work is required to establish if these substrates are phosphorylated *in vivo*, if phosphorylation of substrates is altered during pathological cardiac hypertrophy and what the functional significance of this phosphorylation is.

So far, the calpastatin data *in vitro* is promising. If phosphorylation of calpastatin at the target sites cannot be determined *in vivo*, due to the limitations of antibodies, there are opportunities to explore this mechanism further. For example, calpain activity could be measured in sham and banded WT and KO p38γ hearts using the fluorescent probe or by measuring accumulation of target protein breakdown products. This would help delineate if calpastatin phosphorylation is the mechanism by which p38γ is mediating its pro-hypertrophic role. If LDB3 or calpastatin phosphorylation by p38γ aggravates cardiac hypertrophy, they may present as alternative therapeutic targets for the prevention or reduction of cardiac hypertrophy. Furthermore, if p38γ phosphorylation of LDB3 is dependent on the PDZ domain interaction, there is the potential for this to be specifically targeted as a therapy.

A complete understanding of p38γ signalling in the myocardium needs to be established before therapeutic outcomes related to this kinase can be realised. Ultimately, if the phosphorylation of LDB3 and calpastatin does not yield promising results *in vivo*, other candidate proteins detected in the Shokat approach could be re-examined for their involvement in p38γ signalling and the development of cardiac hypertrophy.

REFERENCE LIST

ADACHI, Y., ISHIDA-TAKAHASHI, A., TAKAHASHI, C., TAKANO, E., MURACHI, T. and HATANAKA, M., 1991. Phosphorylation and subcellular distribution of calpastatin in human hematopoietic system cells. *The Journal of biological chemistry,* **266**(6), pp. 3968-3972.

AKAZAWA, H. and KOMURO, I., 2003. Roles of cardiac transcription factors in cardiac hypertrophy. *Circulation research,* **92**(10), pp. 1079-1088.

ALLEN, J.J., LAZERWITH, S.E. and SHOKAT, K.M., 2005. Bio-orthogonal affinity purification of direct kinase substrates. *Journal of the American Chemical Society,* **127**(15), pp. 5288-5289.

ALLEN, J.J., LI, M., BRINKWORTH, C.S., PAULSON, J.L., WANG, D., HUBNER, A., CHOU, W.H., DAVIS, R.J., BURLINGAME, A.L., MESSING, R.O., KATAYAMA, C.D., HEDRICK, S.M. and SHOKAT, K.M., 2007. A semisynthetic epitope for kinase substrates. *Nature methods,* **4**(6), pp. 511-516.

ASKARI, N., DISKIN, R., AVITZOUR, M., CAPONE, R., LIVNAH, O. and ENGELBERG, D., 2007. Hyperactive variants of p38alpha induce, whereas hyperactive variants of p38gamma suppress, activating protein 1-mediated transcription. *The Journal of biological chemistry,* **282**(1), pp. 91-99.

AVERNA, M., DE TULLIO, R., PASSALACQUA, M., SALAMINO, F., PONTREMOLI, S. and MELLONI, E., 2001. Changes in intracellular calpastatin localization are mediated by reversible phosphorylation. *The Biochemical journal,* **354**(Pt 1), pp. 25-30.

AVERNA, M., DE TULLIO, R., SALAMINO, F., MELLONI, E. and PONTREMOLI, S., 1999. Phosphorylation of rat brain calpastatins by protein kinase C. *FEBS letters,* **450**(1-2), pp. 13-16.

BAIN, J., PLATER, L., ELLIOTT, M., SHPIRO, N., HASTIE, C.J., MCLAUCHLAN, H., KLEVERNIC, I., ARTHUR, J.S., ALESSI, D.R. and COHEN, P., 2007. The selectivity of protein kinase inhibitors: a further update. *The Biochemical journal,* **408**(3), pp. 297-315.

BARRY, S.P., DAVIDSON, S.M. and TOWNSEND, P.A., 2008. Molecular regulation of cardiac hypertrophy. *The international journal of biochemistry & cell biology,* **40**(10), pp. 2023-2039.

BEAUSOLEIL, S.A., VILLEN, J., GERBER, S.A., RUSH, J. and GYGI, S.P., 2006. A probability-based approach for high-throughput protein phosphorylation analysis and site localization. *Nature biotechnology,* **24**(10), pp. 1285-1292.

BENNETT, P.M., 2012. From myofibril to membrane; the transitional junction at the intercalated disc. *Frontiers in bioscience (Landmark edition),* **17**, pp. 1035-1050.

BERRY, J.M., NASEEM, R.H., ROTHERMEL, B.A. and HILL, J.A., 2007. Models of cardiac hypertrophy and transition to heart failure . *Drug Discovery Today: Disease Models,* **4**(4), pp. 197-206.

BHAT, H.F., ADAMS, M.E. and KHANDAY, F.A., 2013. Syntrophin proteins as Santa Claus: role(s) in cell signal transduction. *Cellular and molecular life sciences : CMLS,* **70**(14), pp. 2533-2554.

BISHOP, A., BUZKO, O., HEYECK-DUMAS, S., JUNG, I., KRAYBILL, B., LIU, Y., SHAH, K., ULRICH, S., WITUCKI, L., YANG, F., ZHANG, C. and SHOKAT, K.M., 2000. Unnatural ligands

for engineered proteins: new tools for chemical genetics. *Annual Review of Biophysics and Biomolecular Structure,* **29**, pp. 577-606.

BISHOP, A.C., SHAH, K., LIU, Y., WITUCKI, L., KUNG, C. and SHOKAT, K.M., 1998. Design of allele-specific inhibitors to probe protein kinase signaling. *Current biology : CB,* **8**(5), pp. 257-266.

BISHOP, A.C., UBERSAX, J.A., PETSCH, D.T., MATHEOS, D.P., GRAY, N.S., BLETHROW, J., SHIMIZU, E., TSIEN, J.Z., SCHULTZ, P.G., ROSE, M.D., WOOD, J.L., MORGAN, D.O. and SHOKAT, K.M., 2000. A chemical switch for inhibitor-sensitive alleles of any protein kinase. *Nature,* **407**(6802), pp. 395-401.

BISPING, E., WAKULA, P., POTESER, M. and HEINZEL, F.R., 2014. Targeting cardiac hypertrophy: toward a causal heart failure therapy. *Journal of cardiovascular pharmacology,* **64**(4), pp. 293-305.

BLATT, L.M. and OZES, O.N., 2005. *Use of pirfenidone in therapeutic regimens .* US7407973 edn. US: WO 2005040758 A2.

BLETHROW, J.D., GLAVY, J.S., MORGAN, D.O. and SHOKAT, K.M., 2008. Covalent capture of kinase-specific phosphopeptides reveals Cdk1-cyclin B substrates. *Proceedings of the National Academy of Sciences of the United States of America,* **105**(5), pp. 1442-1447.

BLOTTIERE, L., APIOU, F., FERBUS, D., GUENZI, C., DUTRILLAUX, B., PROSPERI, M.T. and GOUBIN, G., 1999. Cloning, characterization, and chromosome assignment of Zfp146 the mouse ortholog of human ZNF146, a gene amplified and overexpressed in pancreatic cancer, and Zfp260 a closely related gene. *Cytogenetics and cell genetics,* **85**(3-4), pp. 297-300.

BOPPART, M.D., ASP, S., WOJTASZEWSKI, J.F., FIELDING, R.A., MOHR, T. and GOODYEAR, L.J., 2000. Marathon running transiently increases c-Jun NH2-terminal kinase and p38 activities in human skeletal muscle. *The Journal of physiology,* **526 Pt 3**, pp. 663-669.

BRADFORD, M.M., 1976. A rapid and sensitive method for the quantitation of microgram quantities of protein utilizing the principle of protein-dye binding. *Analytical Biochemistry,* **72**, pp. 248-254.

BUENO, O.F., DE WINDT, L.J., TYMITZ, K.M., WITT, S.A., KIMBALL, T.R., KLEVITSKY, R., HEWETT, T.E., JONES, S.P., LEFER, D.J., PENG, C.F., KITSIS, R.N. and MOLKENTIN, J.D., 2000. The MEK1-ERK1/2 signaling pathway promotes compensated cardiac hypertrophy in transgenic mice. *The EMBO journal,* **19**(23), pp. 6341-6350.

BURKARD, N., BECHER, J., HEINDL, C., NEYSES, L., SCHUH, K. and RITTER, O., 2005. Targeted proteolysis sustains calcineurin activation. *Circulation,* **111**(8), pp. 1045-1053.

CAMPBELL, R.L. and DAVIES, P.L., 2012. Structure-function relationships in calpains. *The Biochemical journal,* **447**(3), pp. 335-351.

CARR, D.W., STOFKO-HAHN, R.E., FRASER, I.D., BISHOP, S.M., ACOTT, T.S., BRENNAN, R.G. and SCOTT, J.D., 1991. Interaction of the regulatory subunit (RII) of cAMP-dependent protein kinase with RII-anchoring proteins occurs through an amphipathic helix binding motif. *The Journal of biological chemistry,* **266**(22), pp. 14188-14192.

CHANG, W., GRUBER, D., CHARI, S., KITAZAWA, H., HAMAZUMI, Y., HISANAGA, S. and BULINSKI, J.C., 2001. Phosphorylation of MAP4 affects microtubule properties and cell cycle progression. *Journal of cell science,* **114**(Pt 15), pp. 2879-2887.

CHENG, G., IIJIMA, Y., ISHIBASHI, Y., KUPPUSWAMY, D. and COOPER, G.,4TH, 2002. Inhibition of G protein-coupled receptor trafficking in neuroblastoma cells by MAP 4

decoration of microtubules. *American journal of physiology.Heart and circulatory physiology,* **283**(6), pp. H2379-88.

CHENG, G., QIAO, F., GALLIEN, T.N., KUPPUSWAMY, D. and COOPER, G.,4TH, 2005. Inhibition of beta-adrenergic receptor trafficking in adult cardiocytes by MAP4 decoration of microtubules. *American journal of physiology.Heart and circulatory physiology,* **288**(3), pp. H1193-202.

CHENG, G., TAKAHASHI, M., SHUNMUGAVEL, A., WALLENBORN, J.G., DEPAOLI-ROACH, A.A., GERGS, U., NEUMANN, J., KUPPUSWAMY, D., MENICK, D.R. and COOPER, G.,4TH, 2010. Basis for MAP4 dephosphorylation-related microtubule network densification in pressure overload cardiac hypertrophy. *The Journal of biological chemistry,* **285**(49), pp. 38125-38140.

CHENG, H., KIMURA, K., PETER, A.K., CUI, L., OUYANG, K., SHEN, T., LIU, Y., GU, Y., DALTON, N.D., EVANS, S.M., KNOWLTON, K.U., PETERSON, K.L. and CHEN, J., 2010. Loss of enigma homolog protein results in dilated cardiomyopathy. *Circulation research,* **107**(3), pp. 348-356.

CHENG, X.W., SHI, G.P., KUZUYA, M., SASAKI, T., OKUMURA, K. and MUROHARA, T., 2012. Role for cysteine protease cathepsins in heart disease: focus on biology and mechanisms with clinical implication. *Circulation,* **125**(12), pp. 1551-1562.

CLELAND, J., DARGIE, H., HARDMAN, S., MCDONAGH, T. and MITCHELL, P., 2013. *National Heart Failure Audit April 2012 - March 2013.* 6. London, UK: National Institute for Cardiovascular Outcomes Research (NICOR).

COLOMER, J.M., MAO, L., ROCKMAN, H.A. and MEANS, A.R., 2003. Pressure overload selectively up-regulates Ca2+/calmodulin-dependent protein kinase II in vivo. *Molecular endocrinology (Baltimore, Md.),* **17**(2), pp. 183-192.

COURT, N.W., DOS REMEDIOS, C.G., CORDELL, J. and BOGOYEVITCH, M.A., 2002. Cardiac expression and subcellular localization of the p38 mitogen-activated protein kinase member, stress-activated protein kinase-3 (SAPK3). *Journal of Molecular and Cellular Cardiology,* **34**(4), pp. 413-426.

CUADRADO, A. and NEBREDA, A.R., 2010. Mechanisms and functions of p38 MAPK signalling. *The Biochemical journal,* **429**(3), pp. 403-417.

CUENDA, A., COHEN, P., BUEE-SCHERRER, V. and GOEDERT, M., 1997. Activation of stress-activated protein kinase-3 (SAPK3) by cytokines and cellular stresses is mediated via SAPKK3 (MKK6); comparison of the specificities of SAPK3 and SAPK2 (RK/p38). *The EMBO journal,* **16**(2), pp. 295-305.

CUENDA, A. and ROUSSEAU, S., 2007. p38 MAP-kinases pathway regulation, function and role in human diseases. *Biochimica et biophysica acta,* **1773**(8), pp. 1358-1375.

DE NICOLA, G.F., MARTIN, E.D., CHAIKUAD, A., BASSI, R., CLARK, J., MARTINO, L., VERMA, S., SICARD, P., TATA, R., ATKINSON, R.A., KNAPP, S., CONTE, M.R. and MARBER, M.S., 2013. Mechanism and consequence of the autoactivation of p38alpha mitogen-activated protein kinase promoted by TAB1. *Nature structural & molecular biology,* **20**(10), pp. 1182-1190.

DEALMEIDA, A.C., VAN OORT, R.J. and WEHRENS, X.H., 2010. Transverse aortic constriction in mice. *Journal of visualized experiments : JoVE,* **(38). pii: 1729. doi**(38), pp. 10.3791/1729.

DEBRUS, S., RAHBANI, L., MARTTILA, M., DELORME, B., PARADIS, P. and NEMER, M., 2005. The zinc finger-only protein Zfp260 is a novel cardiac regulator and a nuclear effector of alpha1-adrenergic signaling. *Molecular and cellular biology,* **25**(19), pp. 8669-8682.

DENISE MARTIN, E., DE NICOLA, G.F. and MARBER, M.S., 2012. New therapeutic targets in cardiology: p38 alpha mitogen-activated protein kinase for ischemic heart disease. *Circulation,* **126**(3), pp. 357-368.

DINGAR, D., MERLEN, C., GRANDY, S., GILLIS, M.A., VILLENEUVE, L.R., MAMARBACHI, A.M., FISET, C. and ALLEN, B.G., 2010. Effect of pressure overload-induced hypertrophy on the expression and localization of p38 MAP kinase isoforms in the mouse heart. *Cellular signalling,* **22**(11), pp. 1634-1644.

DORN, G.W.,2ND, 2009. Apoptotic and non-apoptotic programmed cardiomyocyte death in ventricular remodelling. *Cardiovascular research,* **81**(3), pp. 465-473.

ELPHICK, L.M., LEE, S.E., CHILD, E.S., PRASAD, A., PIGNOCCHI, C., THIBAUDEAU, S., ANDERSON, A.A., BONNAC, L., GOUVERNEUR, V. and MANN, D.J., 2009. A quantitative comparison of wild-type and gatekeeper mutant cdk2 for chemical genetic studies with ATP analogues. *Chembiochem : a European journal of chemical biology,* **10**(9), pp. 1519-1526.

ELPHICK, L.M., LEE, S.E., GOUVERNEUR, V. and MANN, D.J., 2007. Using chemical genetics and ATP analogues to dissect protein kinase function. *ACS chemical biology,* **2**(5), pp. 299-314.

ENGEL, K., SCHULTZ, H., MARTIN, F., KOTLYAROV, A., PLATH, K., HAHN, M., HEINEMANN, U. and GAESTEL, M., 1995. Constitutive activation of mitogen-activated protein kinase-activated protein kinase 2 by mutation of phosphorylation sites and an A-helix motif. *The Journal of biological chemistry,* **270**(45), pp. 27213-27221.

EYERS, P.A., CRAXTON, M., MORRICE, N., COHEN, P. and GOEDERT, M., 1998. Conversion of SB 203580-insensitive MAP kinase family members to drug-sensitive forms by a single amino-acid substitution. *Chemistry & biology,* **5**(6), pp. 321-328.

FASSETT, J.T., XU, X., HU, X., ZHU, G., FRENCH, J., CHEN, Y. and BACHE, R.J., 2009. Adenosine regulation of microtubule dynamics in cardiac hypertrophy. *American journal of physiology.Heart and circulatory physiology,* **297**(2), pp. H523-32.

FAULKNER, G., PALLAVICINI, A., FORMENTIN, E., COMELLI, A., IEVOLELLA, C., TREVISAN, S., BORTOLETTO, G., SCANNAPIECO, P., SALAMON, M., MOULY, V., VALLE, G. and LANFRANCHI, G., 1999. ZASP: a new Z-band alternatively spliced PDZ-motif protein. *The Journal of cell biology,* **146**(2), pp. 465-475.

FOSTER, W.H., TIDBALL, J.G. and WANG, Y., 2012. P38gamma Activity is Required for Maintenance of Slow Skeletal Muscle Size. *Muscle & nerve,* **45**(2), pp. 266-273.

GARDNER, D.G., 2003. Natriuretic peptides: markers or modulators of cardiac hypertrophy? *Trends in endocrinology and metabolism: TEM,* **14**(9), pp. 411-416.

GILLESPIE, M.A., LE GRAND, F., SCIME, A., KUANG, S., VON MALTZAHN, J., SEALE, V., CUENDA, A., RANISH, J.A. and RUDNICKI, M.A., 2009. P38-{Gamma}-Dependent Gene Silencing Restricts Entry into the Myogenic Differentiation Program. *The Journal of cell biology,* **187**(7), pp. 991-1005.

GOEDERT, M., HASEGAWA, M., JAKES, R., LAWLER, S., CUENDA, A. and COHEN, P., 1997. Phosphorylation of microtubule-associated protein tau by stress-activated protein kinases. *FEBS letters,* **409**(1), pp. 57-62.

GOLL, D.E., THOMPSON, V.F., LI, H., WEI, W. and CONG, J., 2003. The calpain system. *Physiological Reviews,* **83**(3), pp. 731-801.

GOMES, A.C., FALCAO-PIRES, I., PIRES, A.L., BRAS-SILVA, C. and LEITE-MOREIRA, A.F., 2013. Rodent models of heart failure: an updated review. *Heart failure reviews,* **18**(2), pp. 219-249.

GOOD, M.C., ZALATAN, J.G. and LIM, W.A., 2011. Scaffold proteins: hubs for controlling the flow of cellular information. *Science (New York, N.Y.),* **332**(6030), pp. 680-686.

GORDON, J.W., SHAW, J.A. and KIRSHENBAUM, L.A., 2011. Multiple facets of NF-kappaB in the heart: to be or not to NF-kappaB. *Circulation research,* **108**(9), pp. 1122-1132.

GRIEVE, D.J., CAVE, A.C. and SHAH, A.M., 2006. Cardiac Hypertrophy. In: Q. XU, ed, *A Handbook of Mouse Models of Cardiovascular Disease.* West Sussex, England: John Wiley & Sons, Ltd, pp. 220.

HAN, J. and MOLKENTIN, J.D., 2000. Regulation of MEF2 by p38 MAPK and its implication in cardiomyocyte biology. *Trends in cardiovascular medicine,* **10**(1), pp. 19-22.

HAN, Y., WEINMAN, S., BOLDOGH, I., WALKER, R.K. and BRASIER, A.R., 1999. Tumor necrosis factor-alpha-inducible IkappaBalpha proteolysis mediated by cytosolic m-calpain. A mechanism parallel to the ubiquitin-proteasome pathway for nuclear factor-kappab activation. *The Journal of biological chemistry,* **274**(2), pp. 787-794.

HANNA, R.A., CAMPBELL, R.L. and DAVIES, P.L., 2008. Calcium-bound structure of calpain and its mechanism of inhibition by calpastatin. *Nature,* **456**(7220), pp. 409-412.

HASEGAWA, M., CUENDA, A., SPILLANTINI, M.G., THOMAS, G.M., BUEE-SCHERRER, V., COHEN, P. and GOEDERT, M., 1999. Stress-activated protein kinase-3 interacts with the PDZ domain of alpha1-syntrophin. A mechanism for specific substrate recognition. *The Journal of biological chemistry,* **274**(18), pp. 12626-12631.

HEINEKE, J. and MOLKENTIN, J.D., 2006. Regulation of cardiac hypertrophy by intracellular signalling pathways. *Nature reviews.Molecular cell biology,* **7**(8), pp. 589-600.

HERTZ, N.T., WANG, B.T., ALLEN, J.J., ZHANG, C., DAR, A.C., BURLINGAME, A.L. and SHOKAT, K.M., 2010. Chemical genetic approach for kinase-substrate mapping by covalent capture of thiophosphopeptides and analysis by mass spectrometry. *Current protocols in chemical biology,* **2**(1), pp. 15-36.

HILL, J.A. and OLSON, E.N., 2008. Cardiac plasticity. *The New England journal of medicine,* **358**(13), pp. 1370-1380.

HO, R.C., ALCAZAR, O., FUJII, N., HIRSHMAN, M.F. and GOODYEAR, L.J., 2004. p38gamma MAPK regulation of glucose transporter expression and glucose uptake in L6 myotubes and mouse skeletal muscle. *American journal of physiology.Regulatory, integrative and comparative physiology,* **286**(2), pp. R342-9.

HODGSON, D.R. and SCHRODER, M., 2011. Chemical approaches towards unravelling kinase-mediated signalling pathways. *Chemical Society Reviews,* **40**(3), pp. 1211-1223.

HOSHIJIMA, M., 2006. Mechanical stress-strain sensors embedded in cardiac cytoskeleton: Z disk, titin, and associated structures. *American journal of physiology.Heart and circulatory physiology,* **290**(4), pp. H1313-25.

HOU, S., SURESH, P.S., QI, X., LEPP, A., MIRZA, S.P. and CHEN, G., 2012. p38gamma Mitogen-activated protein kinase signals through phosphorylating its phosphatase PTPH1 in

regulating ras protein oncogenesis and stress response. *The Journal of biological chemistry,* **287**(33), pp. 27895-27905.

HOU, S.W., ZHI, H.Y., POHL, N., LOESCH, M., QI, X.M., LI, R.S., BASIR, Z. and CHEN, G., 2010. PTPH1 dephosphorylates and cooperates with p38gamma MAPK to increase ras oncogenesis through PDZ-mediated interaction. *Cancer research,* **70**(7), pp. 2901-2910.

HU, J.Y., CHU, Z.G., HAN, J., DANG, Y.M., YAN, H., ZHANG, Q., LIANG, G.P. and HUANG, Y.S., 2010. The p38/MAPK pathway regulates microtubule polymerization through phosphorylation of MAP4 and Op18 in hypoxic cells. *Cellular and molecular life sciences : CMLS,* **67**(2), pp. 321-333.

HUANG, C., ZHOU, Q., LIANG, P., HOLLANDER, M.S., SHEIKH, F., LI, X., GREASER, M., SHELTON, G.D., EVANS, S. and CHEN, J., 2003. Characterization and in vivo functional analysis of splice variants of cypher. *The Journal of biological chemistry,* **278**(9), pp. 7360-7365.

HUANG, D., ZHOU, T., LAFLEUR, K., NEVADO, C. and CAFLISCH, A., 2010. Kinase selectivity potential for inhibitors targeting the ATP binding site: a network analysis. *Bioinformatics (Oxford, England),* **26**(2), pp. 198-204.

KEHAT, I. and MOLKENTIN, J.D., 2010. Molecular pathways underlying cardiac remodeling during pathophysiological stimulation. *Circulation,* **122**(25), pp. 2727-2735.

KERKELA, R. and FORCE, T., 2006. P38 Mitogen-Activated Protein Kinase: a Future Target for Heart Failure Therapy? *Journal of the American College of Cardiology,* **48**(3), pp. 556-558.

KIM, E. and SHENG, M., 2004. PDZ domain proteins of synapses. *Nature reviews.Neuroscience,* **5**(10), pp. 771-781.

KINOSHITA, E., KINOSHITA-KIKUTA, E., TAKIYAMA, K. and KOIKE, T., 2006. Phosphate-binding tag, a new tool to visualize phosphorylated proteins. *Molecular & cellular proteomics : MCP,* **5**(4), pp. 749-757.

KOMATI, H., MAHARSY, W., BEAUREGARD, J., HAYEK, S. and NEMER, M., 2011. ZFP260 is an inducer of cardiac hypertrophy and a nuclear mediator of endothelin-1 signaling. *The Journal of biological chemistry,* **286**(2), pp. 1508-1516.

KRENZ, M. and ROBBINS, J., 2004. Impact of beta-myosin heavy chain expression on cardiac function during stress. *Journal of the American College of Cardiology,* **44**(12), pp. 2390-2397.

KREUSSER, M.M. and BACKS, J., 2014. Integrated mechanisms of CaMKII-dependent ventricular remodeling. *Frontiers in pharmacology,* **5**, pp. 36.

KUMAR, S., MCDONNELL, P.C., GUM, R.J., HAND, A.T., LEE, J.C. and YOUNG, P.R., 1997. Novel homologues of CSBP/p38 MAP kinase: activation, substrate specificity and sensitivity to inhibition by pyridinyl imidazoles. *Biochemical and biophysical research communications,* **235**(3), pp. 533-538.

KWONG, J., HONG, L., LIAO, R., DENG, Q., HAN, J. and SUN, P., 2009. P38alpha and P38gamma Mediate Oncogenic Ras-Induced Senescence through Differential Mechanisms. *The Journal of biological chemistry,* **284**(17), pp. 11237-11246.

LAEMMLI, U.K., 1970. Cleavage of structural proteins during the assembly of the head of bacteriophage T4. *Nature,* **227**(5259), pp. 680-685.

LECHNER, C., ZAHALKA, M.A., GIOT, J.F., MOLLER, N.P. and ULLRICH, A., 1996. ERK6, a mitogen-activated protein kinase involved in C2C12 myoblast differentiation. *Proceedings of the National Academy of Sciences of the United States of America,* **93**(9), pp. 4355-4359.

LEE, H.J. and ZHENG, J.J., 2010. PDZ domains and their binding partners: structure, specificity, and modification. *Cell communication and signaling : CCS,* **8**, pp. 8-811X-8-8.

LETAVERNIER, E., PEREZ, J., BELLOCQ, A., MESNARD, L., DE CASTRO KELLER, A., HAYMANN, J.P. and BAUD, L., 2008. Targeting the calpain/calpastatin system as a new strategy to prevent cardiovascular remodeling in angiotensin II-induced hypertension. *Circulation research,* **102**(6), pp. 720-728.

LETAVERNIER, E., ZAFRANI, L., PEREZ, J., LETAVERNIER, B., HAYMANN, J.P. and BAUD, L., 2012. The role of calpains in myocardial remodelling and heart failure. *Cardiovascular research,* **96**(1), pp. 38-45.

LEVY, D., GARRISON, R.J., SAVAGE, D.D., KANNEL, W.B. and CASTELLI, W.P., 1990. Prognostic implications of echocardiographically determined left ventricular mass in the Framingham Heart Study. *The New England journal of medicine,* **322**(22), pp. 1561-1566.

LI, A., PONTEN, F. and DOS REMEDIOS, C.G., 2012. The interactome of LIM domain proteins: the contributions of LIM domain proteins to heart failure and heart development. *Proteomics,* **12**(2), pp. 203-225.

LI, Y., MA, J., ZHU, H., SINGH, M., HILL, D., GREER, P.A., ARNOLD, J.M., ABEL, E.D. and PENG, T., 2011. Targeted inhibition of calpain reduces myocardial hypertrophy and fibrosis in mouse models of type 1 diabetes. *Diabetes,* **60**(11), pp. 2985-2994.

LI, Z., JIANG, Y., ULEVITCH, R.J. and HAN, J., 1996. The primary structure of p38 gamma: a new member of p38 group of MAP kinases. *Biochemical and biophysical research communications,* **228**(2), pp. 334-340.

LIANG, Q. and MOLKENTIN, J.D., 2002. Divergent signaling pathways converge on GATA4 to regulate cardiac hypertrophic gene expression. *Journal of Molecular and Cellular Cardiology,* **34**(6), pp. 611-616.

LIN, C., GUO, X., LANGE, S., LIU, J., OUYANG, K., YIN, X., JIANG, L., CAI, Y., MU, Y., SHEIKH, F., YE, S., CHEN, J., KE, Y. and CHENG, H., 2013. Cypher/ZASP is a novel A-kinase anchoring protein. *The Journal of biological chemistry,* **288**(41), pp. 29403-29413.

LIU, X., RAMJIGANESH, T., CHEN, Y.H., CHUNG, S.W., HALL, S.R., SCHISSEL, S.L., PADERA, R.F.,JR, LIAO, R., ACKERMAN, K.G., KAJSTURA, J., LERI, A., ANVERSA, P., YET, S.F., LAYNE, M.D. and PERRELLA, M.A., 2009. Disruption of striated preferentially expressed gene locus leads to dilated cardiomyopathy in mice. *Circulation,* **119**(2), pp. 261-268.

LOPEZ-AYALA, J.M., ORTIZ-GENGA, M., GOMEZ-MILANES, I., LOPEZ-CUENCA, D., RUIZ-ESPEJO, F., SANCHEZ-MUNOZ, J.J., OLIVA-SANDOVAL, M.J., MONSERRAT, L. and GIMENO, J.R., 2014. A mutation in the Z-line Cypher/ZASP protein is associated with arrhythmogenic right ventricular cardiomyopathy. *Clinical genetics,* .

LU, Z., XU, X., HU, X., LEE, S., TRAVERSE, J.H., ZHU, G., FASSETT, J., TAO, Y., ZHANG, P., DOS REMEDIOS, C., PRITZKER, M., HALL, J.L., GARRY, D.J. and CHEN, Y., 2010. Oxidative stress regulates left ventricular PDE5 expression in the failing heart. *Circulation,* **121**(13), pp. 1474-1483.

MARBER, M.S., ROSE, B. and WANG, Y., 2011. The p38 mitogen-activated protein kinase pathway--a potential target for intervention in infarction, hypertrophy, and heart failure. *Journal of Molecular and Cellular Cardiology,* **51**(4), pp. 485-490.

MARTIN, J.L., AVKIRAN, M., QUINLAN, R.A., COHEN, P. and MARBER, M.S., 2001. Antiischemic effects of SB203580 are mediated through the inhibition of p38alpha mitogen-activated protein kinase: Evidence from ectopic expression of an inhibition-resistant kinase. *Circulation research,* **89**(9), pp. 750-752.

MEGGIO, F., DONELLA DEANA, A., RUZZENE, M., BRUNATI, A.M., CESARO, L., GUERRA, B., MEYER, T., METT, H., FABBRO, D. and FURET, P., 1995. Different susceptibility of protein kinases to staurosporine inhibition. Kinetic studies and molecular bases for the resistance of protein kinase CK2. *European journal of biochemistry / FEBS,* **234**(1), pp. 317-322.

MELLGREN, R.L., 2008. Structural biology: Enzyme knocked for a loop. *Nature,* **456**(7220), pp. 337-338.

MERTENS, S., CRAXTON, M. and GOEDERT, M., 1996. SAP kinase-3, a new member of the family of mammalian stress-activated protein kinases. *FEBS letters,* **383**(3), pp. 273-276.

MIHL, C., DASSEN, W.R. and KUIPERS, H., 2008. Cardiac remodelling: concentric versus eccentric hypertrophy in strength and endurance athletes. *Netherlands heart journal : monthly journal of the Netherlands Society of Cardiology and the Netherlands Heart Foundation,* **16**(4), pp. 129-133.

MOLDOVEANU, T., GEHRING, K. and GREEN, D.R., 2008. Concerted multi-pronged attack by calpastatin to occlude the catalytic cleft of heterodimeric calpains. *Nature,* **456**(7220), pp. 404-408.

MULLER, A.L. and DHALLA, N.S., 2012. Role of various proteases in cardiac remodeling and progression of heart failure. *Heart failure reviews,* **17**(3), pp. 395-409.

NOURRY, C., GRANT, S.G. and BORG, J.P., 2003. PDZ domain proteins: plug and play! *Science's STKE : signal transduction knowledge environment,* **2003**(179), pp. RE7.

PARKER, C.G., HUNT, J., DIENER, K., MCGINLEY, M., SORIANO, B., KEESLER, G.A., BRAY, J., YAO, Z., WANG, X.S., KOHNO, T. and LICHENSTEIN, H.S., 1998. Identification of stathmin as a novel substrate for p38 delta. *Biochemical and biophysical research communications,* **249**(3), pp. 791-796.

PARKER, L.L., SCHILLING, A.B., KRON, S.J. and KENT, S.B., 2005. Optimizing thiophosphorylation in the presence of competing phosphorylation with MALDI-TOF-MS detection. *Journal of proteome research,* **4**(5), pp. 1863-1866.

PATTERSON, C., PORTBURY, A.L., SCHISLER, J.C. and WILLIS, M.S., 2011. Tear me down: role of calpain in the development of cardiac ventricular hypertrophy. *Circulation research,* **109**(4), pp. 453-462.

PERDIGUERO, E., RUIZ-BONILLA, V., GRESH, L., HUI, L., BALLESTAR, E., SOUSA-VICTOR, P., BAEZA-RAJA, B., JARDI, M., BOSCH-COMAS, A., ESTELLER, M., CAELLES, C., SERRANO, A.L., WAGNER, E.F. and MUNOZ-CANOVES, P., 2007. Genetic analysis of p38 MAP kinases in myogenesis: fundamental role of p38alpha in abrogating myoblast proliferation. *The EMBO journal,* **26**(5), pp. 1245-1256.

PETRICH, B.G. and WANG, Y., 2004. Stress-activated MAP kinases in cardiac remodeling and heart failure; new insights from transgenic studies. *Trends in cardiovascular medicine,* **14**(2), pp. 50-55.

PONTREMOLI, S., VIOTTI, P.L., MICHETTI, M., SALAMINO, F., SPARATORE, B. and MELLONI, E., 1992. Modulation of inhibitory efficiency of rat skeletal muscle calpastatin by phosphorylation. *Biochemical and biophysical research communications,* **187**(2), pp. 751-759.

QI, X., HOU, S., LEPP, A., LI, R., BASIR, Z., LOU, Z. and CHEN, G., 2011. Phosphorylation and stabilization of topoisomerase IIalpha protein by p38gamma mitogen-activated protein kinase sensitize breast cancer cells to its poisons. *The Journal of biological chemistry,* **286**(41), pp. 35883-35890.

RABABA'H, A., SINGH, S., SURYAVANSHI, S.V., ALTARABSHEH, S.E., DEO, S.V. and MCCONNELL, B.K., 2014. Compartmentalization role of A-kinase anchoring proteins (AKAPs) in mediating protein kinase A (PKA) signaling and cardiomyocyte hypertrophy. *International journal of molecular sciences,* **16**(1), pp. 218-229.

ROCKMAN, H.A., ROSS, R.S., HARRIS, A.N., KNOWLTON, K.U., STEINHELPER, M.E., FIELD, L.J., ROSS, J.,JR and CHIEN, K.R., 1991. Segregation of atrial-specific and inducible expression of an atrial natriuretic factor transgene in an in vivo murine model of cardiac hypertrophy. *Proceedings of the National Academy of Sciences of the United States of America,* **88**(18), pp. 8277-8281.

RUWHOF, C. and VAN DER LAARSE, A., 2000. Mechanical stress-induced cardiac hypertrophy: mechanisms and signal transduction pathways. *Cardiovascular research,* **47**(1), pp. 23-37.

SABIO, G., ARTHUR, J.S., KUMA, Y., PEGGIE, M., CARR, J., MURRAY-TAIT, V., CENTENO, F., GOEDERT, M., MORRICE, N.A. and CUENDA, A., 2005. p38gamma regulates the localisation of SAP97 in the cytoskeleton by modulating its interaction with GKAP. *The EMBO journal,* **24**(6), pp. 1134-1145.

SABIO, G., CEREZO-GUISADO, M.I., DEL REINO, P., INESTA-VAQUERA, F.A., ROUSSEAU, S., ARTHUR, J.S., CAMPBELL, D.G., CENTENO, F. and CUENDA, A., 2010. p38gamma regulates interaction of nuclear PSF and RNA with the tumour-suppressor hDlg in response to osmotic shock. *Journal of cell science,* **123**(Pt 15), pp. 2596-2604.

SABIO, G., REUVER, S., FEIJOO, C., HASEGAWA, M., THOMAS, G.M., CENTENO, F., KUHLENDAHL, S., LEAL-ORTIZ, S., GOEDERT, M., GARNER, C. and CUENDA, A., 2004. Stress- and mitogen-induced phosphorylation of the synapse-associated protein SAP90/PSD-95 by activation of SAPK3/p38gamma and ERK1/ERK2. *The Biochemical journal,* **380**(Pt 1), pp. 19-30.

SALAMINO, F., AVERNA, M., TEDESCO, I., DE TULLIO, R., MELLONI, E. and PONTREMOLI, S., 1997. Modulation of rat brain calpastatin efficiency by post-translational modifications. *FEBS letters,* **412**(3), pp. 433-438.

SALAMINO, F., DE TULLIO, R., MENGOTTI, P., MELLONI, E. and PONTREMOLI, S., 1994. Differential regulation of mu- and m-calpain in rat hearts perfused with Ca2+ and cAMP. *Biochemical and biophysical research communications,* **202**(3), pp. 1197-1203.

SALAMINO, F., DE TULLIO, R., MICHETTI, M., MENGOTTI, P., MELLONI, E. and PONTREMOLI, S., 1994. Modulation of calpastatin specificity in rat tissues by reversible phosphorylation and dephosphorylation. *Biochemical and biophysical research communications,* **199**(3), pp. 1326-1332.

SANKARAN, S.K., KUMAR, A., RAJ, B. and RAJAGOPAL, R., 2014. Two different rat models for cardiac hypertrophy by constriction of ascending and abdominal aorta . *Journal of Laboratory Animal Science,* **2**(1), pp. 54-57.

SARAFRAZ, N., 2009. *Contribution of p38-MAPK Isotypes to Cardiac Physiology.* Doctor of Philosophy edn. University of London.

SAURIN, A.T., MARTIN, J.L., HEADS, R.J., FOLEY, C., MOCKRIDGE, J.W., WRIGHT, M.J., WANG, Y. and MARBER, M.S., 2000. The role of differential activation of p38-mitogen-activated protein kinase in preconditioned ventricular myocytes. *FASEB journal : official*

publication of the Federation of American Societies for Experimental Biology, **14**(14), pp. 2237-2246.

SHAH, K., LIU, Y., DEIRMENGIAN, C. and SHOKAT, K.M., 1997. Engineering unnatural nucleotide specificity for Rous sarcoma virus tyrosine kinase to uniquely label its direct substrates. *Proceedings of the National Academy of Sciences of the United States of America,* **94**(8), pp. 3565-3570.

SICARD, P., CLARK, J.E., JACQUET, S., MOHAMMADI, S., ARTHUR, J.S., O'KEEFE, S.J. and MARBER, M.S., 2010. The activation of p38 alpha, and not p38 beta, mitogen-activated protein kinase is required for ischemic preconditioning. *Journal of Molecular and Cellular Cardiology,* **48**(6), pp. 1324-1328.

SMITH, E., 2014. *A chemical genetic approach to finding substrates of p38alpha mitogen-activated protein kinase in the heart.* Doctor of Philosophy edn. King's College London.

SOONPAA, M.H. and FIELD, L.J., 1994. Assessment of cardiomyocyte DNA synthesis during hypertrophy in adult mice. *The American Journal of Physiology,* **266**(4 Pt 2), pp. H1439-45.

SPINALE, F.G., COKER, M.L., HEUNG, L.J., BOND, B.R., GUNASINGHE, H.R., ETOH, T., GOLDBERG, A.T., ZELLNER, J.L. and CRUMBLEY, A.J., 2000. A matrix metalloproteinase induction/activation system exists in the human left ventricular myocardium and is upregulated in heart failure. *Circulation,* **102**(16), pp. 1944-1949.

STORR, S.J., CARRAGHER, N.O., FRAME, M.C., PARR, T. and MARTIN, S.G., 2011. The calpain system and cancer. *Nature reviews.Cancer,* **11**(5), pp. 364-374.

TAMAOKI, T., 1991. Use and specificity of staurosporine, UCN-01, and calphostin C as protein kinase inhibitors. *Methods in enzymology,* **201**, pp. 340-347.

TANG, J., QI, X., MERCOLA, D., HAN, J. and CHEN, G., 2005. Essential role of p38gamma in K-Ras transformation independent of phosphorylation. *The Journal of biological chemistry,* **280**(25), pp. 23910-23917.

TANNO, M., BASSI, R., GOROG, D.A., SAURIN, A.T., JIANG, J., HEADS, R.J., MARTIN, J.L., DAVIS, R.J., FLAVELL, R.A. and MARBER, M.S., 2003. Diverse mechanisms of myocardial p38 mitogen-activated protein kinase activation: evidence for MKK-independent activation by a TAB1-associated mechanism contributing to injury during myocardial ischemia. *Circulation research,* **93**(3), pp. 254-261.

TILGNER, K.D., LOONAT, A.A., MARBER, M.S. and CLARK, J.E., 2012. Ablation of p38γ-MAPK reduces cardiac remodelling following pressure overload, *Biomedical Basis of Elite Performance*, 19/03/12 2012.

TORTORELLA, L.L., LIN, C.B. and PILCH, P.F., 2003. ERK6 is expressed in a developmentally regulated manner in rodent skeletal muscle. *Biochemical and biophysical research communications,* **306**(1), pp. 163-168.

TURJANSKI, A.G., VAQUE, J.P. and GUTKIND, J.S., 2007. MAP kinases and the control of nuclear events. *Oncogene,* **26**(22), pp. 3240-3253.

UEDA, K., VALDIVIA, C., MEDEIROS-DOMINGO, A., TESTER, D.J., VATTA, M., FARRUGIA, G., ACKERMAN, M.J. and MAKIELSKI, J.C., 2008. Syntrophin mutation associated with long QT syndrome through activation of the nNOS-SCN5A macromolecular complex. *Proceedings of the National Academy of Sciences of the United States of America,* **105**(27), pp. 9355-9360.

VAN DER HEIDEN, K., CUHLMANN, S., LUONG LE, A., ZAKKAR, M. and EVANS, P.C., 2010. Role of nuclear factor kappaB in cardiovascular health and disease. *Clinical science (London, England : 1979),* **118**(10), pp. 593-605.

VATTA, M., MOHAPATRA, B., JIMENEZ, S., SANCHEZ, X., FAULKNER, G., PERLES, Z., SINAGRA, G., LIN, J.H., VU, T.M., ZHOU, Q., BOWLES, K.R., DI LENARDA, A., SCHIMMENTI, L., FOX, M., CHRISCO, M.A., MURPHY, R.T., MCKENNA, W., ELLIOTT, P., BOWLES, N.E., CHEN, J., VALLE, G. and TOWBIN, J.A., 2003. Mutations in Cypher/ZASP in patients with dilated cardiomyopathy and left ventricular non-compaction. *Journal of the American College of Cardiology,* **42**(11), pp. 2014-2027.

WANG, Y., 2007. Mitogen-activated protein kinases in heart development and diseases. *Circulation,* **116**(12), pp. 1413-1423.

WEEKS, K.L. and MCMULLEN, J.R., 2011. The athlete's heart vs. the failing heart: can signaling explain the two distinct outcomes? *Physiology (Bethesda, Md.),* **26**(2), pp. 97-105.

WENDT, A., THOMPSON, V.F. and GOLL, D.E., 2004. Interaction of calpastatin with calpain: a review. *Biological chemistry,* **385**(6), pp. 465-472.

WILLIAMS, J.C., ARMESILLA, A.L., MOHAMED, T.M., HAGARTY, C.L., MCINTYRE, F.H., SCHOMBURG, S., ZAKI, A.O., OCEANDY, D., CARTWRIGHT, E.J., BUCH, M.H., EMERSON, M. and NEYSES, L., 2006. The sarcolemmal calcium pump, alpha-1 syntrophin, and neuronal nitric-oxide synthase are parts of a macromolecular protein complex. *The Journal of biological chemistry,* **281**(33), pp. 23341-23348.

WILSON, E.M. and SPINALE, F.G., 2001. Myocardial remodelling and matrix metalloproteinases in heart failure: turmoil within the interstitium. *Annals of Medicine,* **33**(9), pp. 623-634.

YANG, D., MA, S., TAN, Y., LI, D., TANG, B., ZHANG, X., SUN, M. and YANG, Y., 2010. Increased expression of calpain and elevated activity of calcineurin in the myocardium of patients with congestive heart failure. *International journal of molecular medicine,* **26**(1), pp. 159-164.

YE, T., WANG, Q., ZHANG, Y., SONG, X., YANG, D., LI, D., LI, D., SU, L., YANG, Y. and MA, S., 2015. Over-expression of calpastatin inhibits calpain activation and attenuates post-infarction myocardial remodeling. *PloS one,* **10**(3), pp. e0120178.

YOUNG, P.R., MCLAUGHLIN, M.M., KUMAR, S., KASSIS, S., DOYLE, M.L., MCNULTY, D., GALLAGHER, T.F., FISHER, S., MCDONNELL, P.C., CARR, S.A., HUDDLESTON, M.J., SEIBEL, G., PORTER, T.G., LIVI, G.P., ADAMS, J.L. and LEE, J.C., 1997. Pyridinyl imidazole inhibitors of p38 mitogen-activated protein kinase bind in the ATP site. *The Journal of biological chemistry,* **272**(18), pp. 12116-12121.

ZARUBIN, T. and HAN, J., 2005. Activation and signaling of the p38 MAP kinase pathway. *Cell research,* **15**(1), pp. 11-18.

ZHENG, M., CHENG, H., LI, X., ZHANG, J., CUI, L., OUYANG, K., HAN, L., ZHAO, T., GU, Y., DALTON, N.D., BANG, M.L., PETERSON, K.L. and CHEN, J., 2009. Cardiac-specific ablation of Cypher leads to a severe form of dilated cardiomyopathy with premature death. *Human molecular genetics,* **18**(4), pp. 701-713.

ZHOU, Q., CHU, P.H., HUANG, C., CHENG, C.F., MARTONE, M.E., KNOLL, G., SHELTON, G.D., EVANS, S. and CHEN, J., 2001. Ablation of Cypher, a PDZ-LIM domain Z-line protein, causes a severe form of congenital myopathy. *The Journal of cell biology,* **155**(4), pp. 605-612.

ZHOU, Q., RUIZ-LOZANO, P., MARTONE, M.E. and CHEN, J., 1999. Cypher, a striated muscle-restricted PDZ and LIM domain-containing protein, binds to alpha-actinin-2 and protein kinase C. *The Journal of biological chemistry,* **274**(28), pp. 19807-19813.